THE DISSOLUTION RATE OF UNIRRATIATED UO_2 UNDER REPOSITORY CONDITIONS: THE INFLUENCE OF FUEL AND WATER CHEMISTRY, DISSOLVED OXYGEN, AND TEMPERATURE

A Dissertation

Presented to

the Faculty of the Graduate School

University of Missouri-Columbia

In Partial Fulfillment

of the Requirements for the Degree

Doctor of Philosophy

By

AMANDA J. CASELLA

DECEMBER 2008

Dr. William H. Miller — Dissertation Supervisors

Dr. Brady D. Hanson

The undersigned, appointed by the Dean of the Graduate School, have examined the dissertation entitled

THE DISSOLUTION RATE OF UNIRRATIATED UO_2 UNDER REPOSITORY CONDITIONS: THE INFLUENCE OF FUEL AND WATER CHEMISTRY, DISSOLVED OXYGEN, AND TEMPERATURE

Presented by AMANDA J. CASELLA

a candidate for the degree of Doctor of Philosophy in Nuclear Engineering

and hereby certify that in their opinion it is worthy of acceptance.

_____
Dr. William H. Miller

_____
Dr. Brady D. Hanson

_____
Dr. Sudarshan K. Loyalka

_____
Dr. Tushar K. Ghosh

_____
Dr. Truman S. Storvick

ACKNOWLEDGEMENTS

This research was performed under appointment of the Office of Civilian Radioactive Waste Management Graduate Fellowship Program administered by Oak Ridge Institute for Science and Education under a contract between the U.S. Department of Energy and Oak Ridge Associated Universities. This work was sponsored in part through the Source Term Strategic Thrust Area of the Office of the Chief Scientist within the U.S. Department of Energy Office of Civilian Radioactive Waste Management. Additional assistance was provided by a G. Ellsworth Huggins Fellowship from the University of Missouri and an American Nuclear Society Scholarship. I am very grateful to my advisor Dr. Miller at the University of Missouri-Columbia and my mentor Dr. Hanson at Pacific Northwest National Laboratory (PNNL) for all of their efforts and guidance during this research. Without them, my committee members, and fellow coworkers at PNNL this work would not have been possible. Throughout this research I received immense support from my family and friends and for that I will always be thankful. To my husband, Andy, who always provided an understanding ear and endless encouragement I will be eternally grateful.

TABLE OF CONTENTS

TABLE OF CONTENTS CONTINUED

LIST OF FIGURES

LIST OF TABLES

ABSTRACT

The dissolution rate of both unirradiated UO_2 and spent fuel has been studied by numerous countries as part of the performance assessments of proposed geologic repositories. The effects of variables such as temperature, dissolved oxygen, and water and fuel chemistry on the dissolution rates of the fuel are necessary to provide a quantitative estimate of the potential dose over geologic time frames. The primary objective of this research was to determine the influence these parameters have on the dissolution rate of unirradiated UO_2 under Yucca Mountain repository conditions and compare them to the current Yucca Mountain Model.

Fuels containing between 0 and 8 wt% Gd_2O_3-doped UO_2 were tested in a single-pass flow-through setup. These tests have verified that in bicarbonate solutions as temperature increased the dissolution rate increased. However, the presence of silicate in the feedwater altered the system and lowered the dissolution rate at higher temperatures. Pure UO_2 samples exhibited a dependence on the dissolved oxygen concentration, which in the current experiments was varied from 3.0 to 8.7 ppm. The significance of this dissolved oxygen dependence increased with rising temperature. At 75ºC the powder samples had a maximum dependence of 0.7, although the fragment samples had a much larger dependence up to 2.2. For the case of the Gd_2O_3-doped samples, there was minimal oxygen dependence at any temperature. The Gd_2O_3-dopant stabilized the fuel matrix, which lowered the dissolution rates by over an order of magnitude at the higher dopant levels. This effect in lowering the dissolution rate was more pronounced at higher

temperatures, and additional dopant continued to decrease the dissolution rate up to the 4 wt% Gd_2O_3-doped UO_2 tested.

The dissolution rates for pure UO_2 compared reasonably well with the Yucca Mountain Model for tests performed at 50ºC and 75ºC, but were found to be approximately half the values predicted by the model at 25ºC. After long time periods when the radiolytic field has diminished, additional benefits in dissolution reduction should exist due to constituents, such as Gd_2O_3 being present in spent fuel and silicate being present in the groundwater. Thus, the durability of spent fuel in Yucca Mountain may be greater than previously modeled.

CHAPTER 1: INTRODUCTION

Introduction

A realistic understanding of the dissolution rate of commercial spent nuclear fuel is crucial to support the scientific basis for the containment of radionuclides in a geologic repository. Numerous factors are involved in an accurate evaluation of the dissolution rate of the fuel. These factors include temperature, dissolved O_2 concentrations, and fuel chemistry. In order to model dissolution rates over a range of potential conditions within a geologic repository, it is necessary to determine the dependence of the dissolution rate on these factors.

This research involved the testing of unirradiated UO_2 containing various concentrations of Gd_2O_3 as a surrogate for commercial spent nuclear fuel. The tests were designed to determine the effect on the dissolution rate of temperature, dissolved O_2 levels, and fuel chemistry. Unirradiated UO_2 samples containing Gd_2O_3 were crushed into either fragments or grain sized powders and tested utilizing single-pass flow-through methods. The dissolved O_2, temperature, pH, and carbonate levels were closely monitored throughout the experiment.

After the relatively short lived radionuclides in spent fuel have decayed and the effects of water radiolysis on fuel dissolution are greatly decreased, fuel chemistry may have a significant impact on the dissolution rate of the fuel. Instead of behavior similar to unirradiated UO_2, spent fuel may exhibit lower dissolution rates due to the changes in fuel chemistry that result from the fission products and higher actinides that are soluble in

the UO_2 matrix. This research provides data to refine the temperature, dissolved O_2 concentration, and fuel chemistry effects on the dissolution rate of spent fuel.

Yucca Mountain

The proposed long-term geologic repository for the United States is Yucca Mountain, located approximately 100 miles North of Las Vegas, Nevada. Yucca Mountain is composed of rock formed from compacted volcanic ash. The majority of the high-level radioactive material and transuranics that will be stored within the Yucca Mountain repository will be spent fuel from commercial nuclear power plants and waste generated by national defense programs. Yucca Mountain has a very dry climate, receiving approximately 7.5 inches of rain a year, 95% of which runs off, evaporates, or is taken up by vegetation.[1] The radioactive material inside Yucca Mountain would be stored 660 to 1,600 feet under the surface, but would still be 1,000 feet above the water table as shown in Figure 1.1.

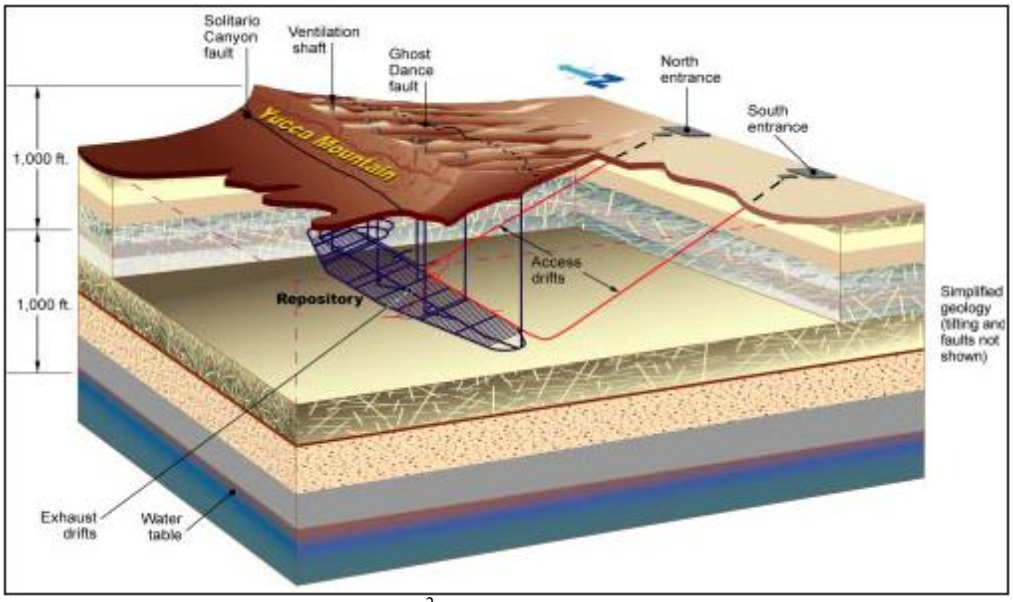

Figure 1.1. Yucca Mountain repository[2]

The spent fuel going into Yucca Mountain is from light water reactors, namely either pressurized water reactors or boiling water reactors. Current models for waste packages going into Yucca Mountain, as shown in Figure 1.2, consist of an outer cylinder of alloy 22 (a nickel based alloy) and an inner cylinder of stainless steel type 316NG. Another barrier of protection for the fuel is a titanium drip shield that covers the outermost packaging of the fuel. This shield serves two purposes: to prevent rock fall from hitting the waste package and damaging it and to prevent water from dripping onto the waste package. An overall view of the proposed configuration is shown in Figure 1.3.

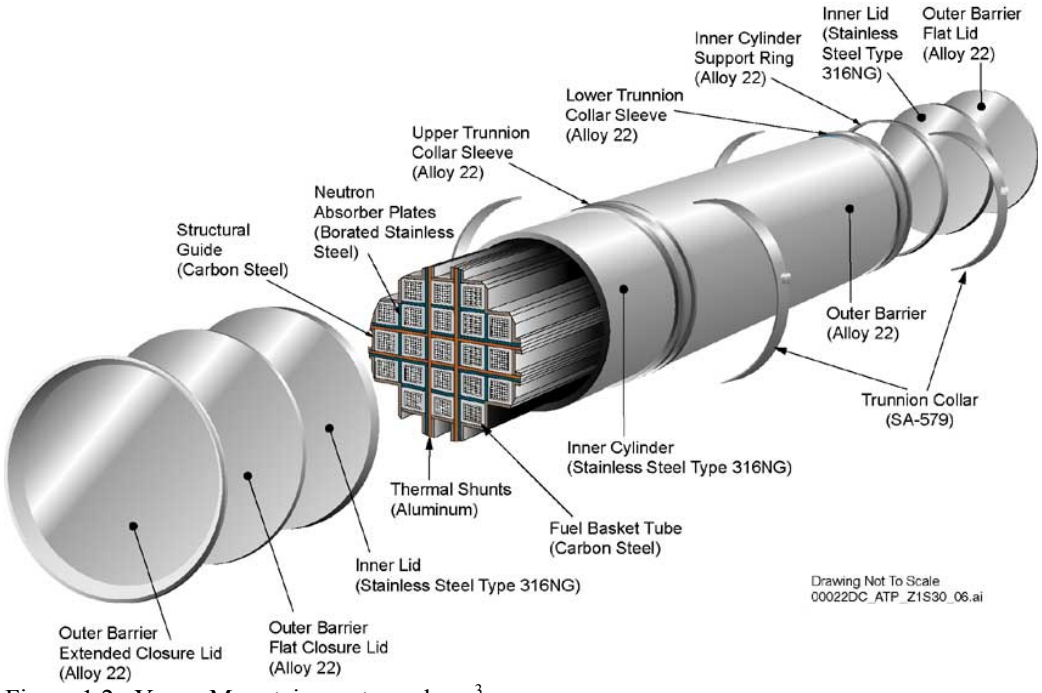

Figure 1.2. Yucca Mountain waste package[3]

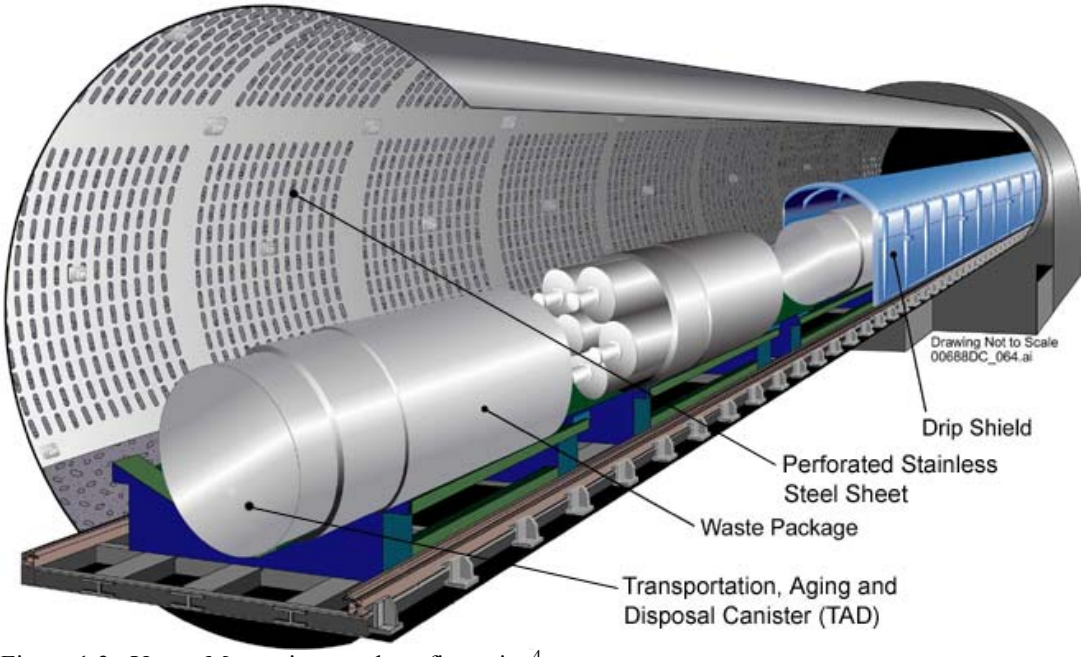

Figure 1.3. Yucca Mountain tunnel configuration[4]

In the scenario being simulated for this thesis, the drip shield, waste package, and cladding have been breached, as shown in Figure 1.4. Groundwater, which has seeped through the rock in Yucca Mountain, dissolving carbonate species in the process, has had sufficient time to equilibrate with the surrounding temperature and O_2 level in the atmosphere. The groundwater enters into the waste package, allowing for dissolution of the fuel and subsequent transport of dissolved radionuclides and colloids out of the engineered barrier system and into the unsaturated zone where they may be released into the surrounding environment. Sufficiently high water flow rates are assumed in order to maintain a forward rate of dissolution. This condition is a worst case scenario in that it prevents back reactions, which could cause secondary or alteration phases from forming that would lower the dissolution rate of the fuel. This work focuses on the dissolution rate of the fuel once it has come into contact with the groundwater, in order to quantify the release of radioactivity and degradation of the fuel.

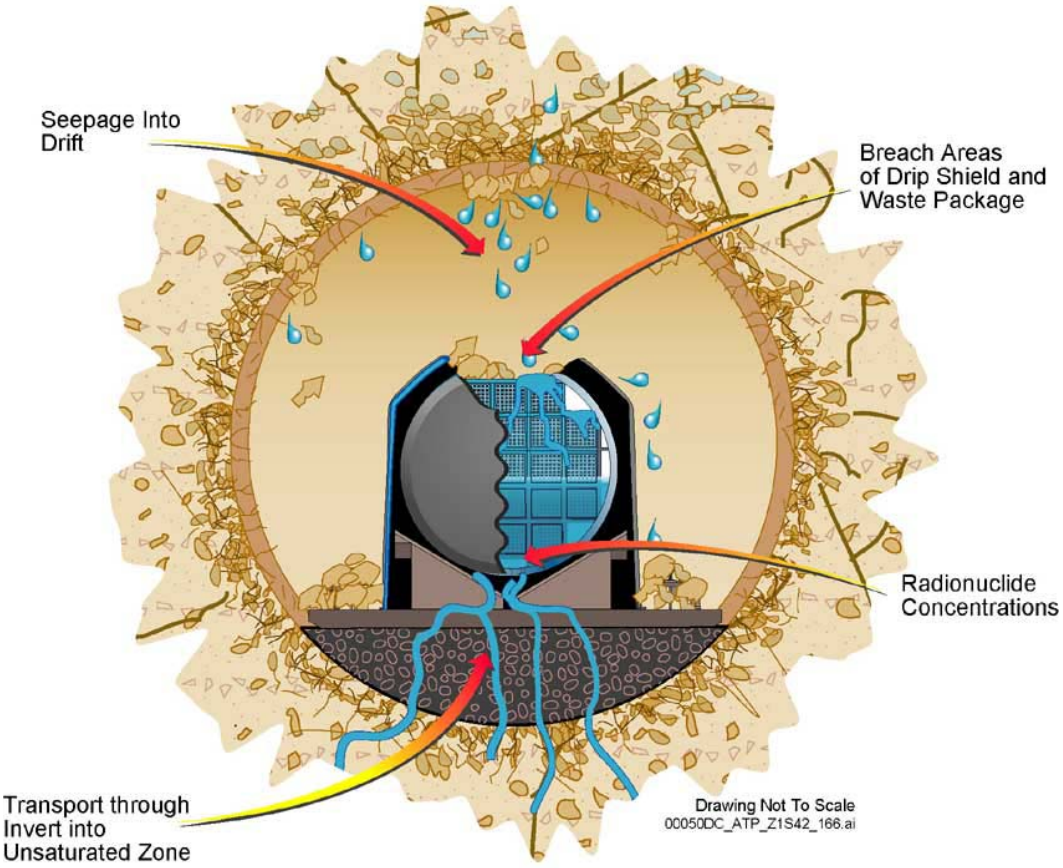

Figure 1.4. Breached spent fuel cask showing water infiltration into a waste package[3]

References

[1]U.S. Department of Energy Office of Civilian Radioactive Waste Management, "Yucca Mountain Preliminary Site Suitability Evaluation," DOE/RW-0540, (July 2001)

[2]U.S. Department of Energy Office of Civilian Radioactive Waste Management, "Yucca Mountain Site Characterization Project," http://www.ocrwm.doe.gov/info_library/program_docs/annualreports/00ar/00ar-c1.htm, (2008)

[3]U.S. Department of Energy Office of Civilian Radioactive Waste Management, "Yucca Mountain Science and Engineering Report," DOE/RW-0539, (July 2001)

[4]U.S. Department of Energy, "Repository Engineering and Design," http://www.ocrwm.doe.gov/ym_repository/studies/engdesign/index.shtml, (2008)

CHAPTER 2: OXIDATION AND DISSOLUTION OF UO_2 IN CARBONATE SOLUTIONS

Uranium dioxide forms cubic fluorite lattices as shown in Figure 2.1. When UO_2 fuel is fabricated, the actual chemical composition is UO_{2+x} where $x \leq 0.001$. This slight excess in oxygen produces ionization of U^{4+} to U^{5+} or U^{6+}. As a result, holes are formed in the U5f sub-band, which migrate through the UO_{2+x} lattice producing conductivity. UO_2 is highly insoluble, but as U^{4+} is oxidized and converted to U^{6+}, the solubility increases by orders of magnitude.[2,3]

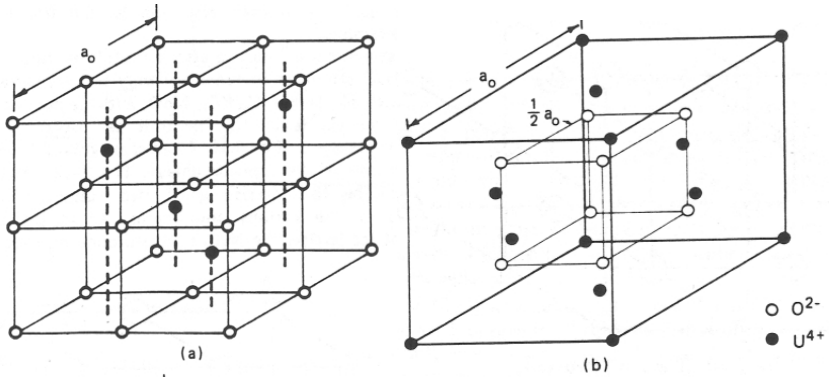

Figure 2.1. The fluorite structure (a) The sc structure of the anion sublattice (b) The fcc structure of the cation sublattice[1]

The aqueous oxidation of UO_2 has been shown to occur in two steps.[4] A thin layer on the surface of the fuel oxidizes until a stoichiometry of approximately $UO_{2.33}$ is achieved. This surface layer of $UO_{2.33}$ then further oxidizes to UO_2^{2+} or the U^{6+} state. This process is shown below in Figure 2.2. Once the uranium has reached the 6+ state it will either dissolve or, if the solution solubility limits are exceeded, form alteration phases on the surface of the fuel.

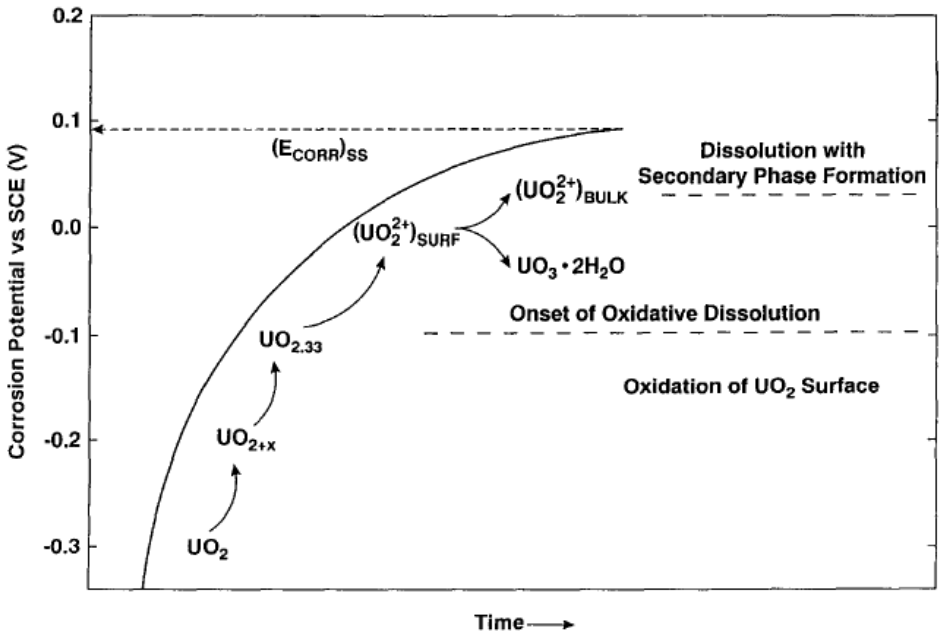

Figure 2.2. The behavior of the corrosion potential measured on UO_2 electrodes in 0.1 M $NaClO_4$ (approximately pH 9.5). The stages of oxidation and dissolution are also illustrated.[5]

When complexing agents such as carbonate are present, the dissolution rate for UO_2 increases greatly. This increase in dissolution is mostly attributed to the following main reactions:

$$UO_2^{2+} + 2CO_3^{2-} \Leftrightarrow UO_2CO_3(aq) \qquad \log K_1 = 9.5 \pm 0.4 \tag{2.1}$$

$$UO_2^{2+} + 2CO_3^{2-} \Leftrightarrow UO_2(CO_3)_2^{2-} \qquad \log \beta_2 = 16.6 \pm 0.3 \tag{2.2}$$

$$UO_2^{2+} + 3CO_3^{2-} \Leftrightarrow UO_2(CO_3)_3^{4-} \qquad \log \beta_3 = 21.6 \pm 0.6 \tag{2.3}$$

Shoesmith[2] studied the effect of various carbonate concentrations on UO_2 dissolution and concluded that when there is no carbonate in solution, surface complexes such as $UO_3 \cdot 2H_2O$ will form and inhibit dissolution. When carbonate is present at concentrations lower than 10^{-3} M, it will increase UO_2^{2+} solubility and prevent surface complexation. As

the concentration is increased to the range of 10^{-3} M to 10^{-1} M, the carbonate becomes kinetically involved in the dissolution process. When the carbonate concentration is greater than 10^{-1} M, phases such as UO_2CO_3 begin to form on the surface of the UO_2 and hinder dissolution.

In work by Peper et. al.[6], an investigation was performed on the effects bicarbonate had on dissolution. The purpose of this experiment was to optimize the dissolution for reprocessing purposes and, as part of the work, H_2O_2 was added as an oxidizer. As shown in Figure 2.3, the lowest concentration of carbonate, 0.25 M, produced the highest initial dissolution rate. This result is consistent with the previously stated trend that as carbonate concentrations are increased over 10^{-1} M, phases may form on the surface that begin to hinder the dissolution. As time progressed in Peper's experiment, the 0.5 M carbonate ended up achieving the highest total dissolution with over 90% of the UO_2 being dissolved. This was attributed to the hypothesis that although the carbonate aides in the solubility of the UO_2, at high concentrations the increased ionic strength of the solution and the degradation of the H_2O_2 caused by the carbonate will ultimately lower the dissolution rate.

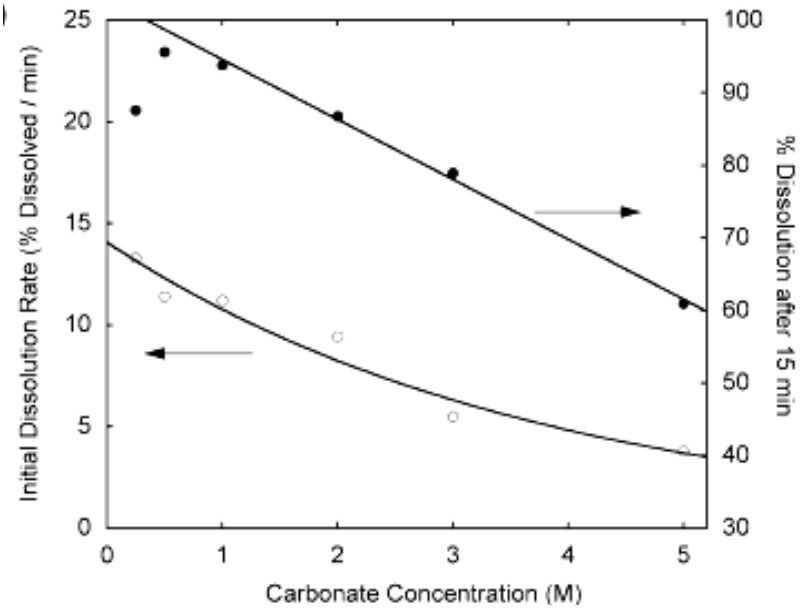

Figure 2.3. Dependence of the initial UO_2 dissolution rate and the dissolution capacity after 15 minutes in the carbonate concentration. Solid lines indicate exponential and linear trends in the data.[6]

In a report by Gimenez et. al.[7], much lower concentrations of carbonate were studied. The experiment was designed to examine bicarbonate concentrations in the range of 10^{-4} to 10^{-2} M. Part of the overall objective of the report was to achieve a better understanding of the rate of oxidation compared to that of dissolution, since previous work had suggested that the dissolution step in bicarbonate media is very fast and oxidation is the limiting step. To determine the oxidation step, the concentration of the oxygen in solution was measured with a dissolved oxygen meter, and the uranium concentration was determined using Inductively Coupled Plasma-Mass Spectroscopy (ICP-MS). The data from these measurements were used to determine the dissolution rate. The results of their experiment are plotted in Figure 2.4. It can be seen that at 10^{-4} M bicarbonate, the oxidation rate is faster than the dissolution rate by approximately 1.5 orders of magnitude. It is not until around a concentration of 10^{-2} M bicarbonate that the rates began to converge. An overall trend is seen in the range as bicarbonate at low

concentrations is increased as the dissolution rate increases. These trends also confirm Shoesmith's[2] conclusions that at low concentrations, the carbonate mostly influences the oxidation, but as the concentration is increased it also contributes to the dissolution of the UO_2.

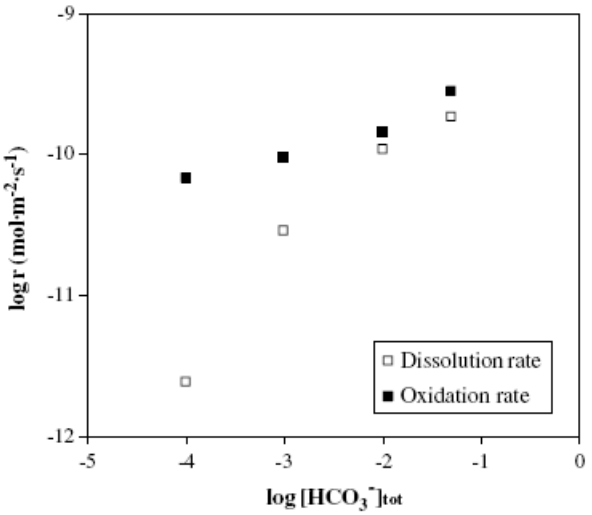

Figure 2.4. Uranium dissolution rate as a function of the bicarbonate concentration[7]

In this thesis the leachate solution will have 2×10^{-3} M bicarbonate in deionized water. This is the concentration present in J-13 water[8], which is taken from a well located near Yucca Mountain and assumed to have a similar composition as infiltrated groundwater in the mountain. Previous researchers have also used this concentration, which will allow for comparison to published data.

References

[1]Olander, D., "Fundamental Aspects of Nuclear Reactor Fuel Elements", TID-26711-P1, Energy Research and Development Administration (1976)

[2]Shoesmith, D.W., "Fuel Corrosion Processes under Waste Disposal Conditions," *Journal of Nuclear Materials*, **282**, 1-31 (2000)

[3]Shoesmith, D.W., Sunder, S., "The Prediction of Nuclear Fuel (UO_2) Dissolution Rate under Waste Disposal Conditions," *Journal of Nuclear Materials*, **190**, 20-35 (1992)

[4]Christensen, H., Sunder, S., "Current State of Knowledge of Water Radiolysis Effects on Spent Nuclear Fuel Corrosion," *Nuclear Technology*, **131**, 102-123 (2000)

[5]Christensen, H., Sunder, S., Shoesmith, D. W., "Oxidation of Nuclear Fuel (UO_2) by the Products of Water Radiolysis: Development of a Kinetic Model," *Journal of Alloys and Compounds*, **213/214**, 93-99 (1994)

[6]Peper, S., et. al., "Kinetic Study of the Oxidative Dissolution of UO_2 in Aqueous Carbonate Media," *Industrial & Engineering Chemistry Research*, **43**, 8188-8193 (2004)

[7]Giménez, J., et. al., "Oxidation and Dissolution of UO_2 in Bicarbonate Media: Implications for the Spent Nuclear Fuel Oxidative Dissolution Mechanism," *Journal of Nuclear Materials*, **345**, 232-238 (2005)

[8]Domski, P.S., "In-Package Chemistry Abstraction," ANL-EBS-MD-000037 (2007)

CHAPTER 3: EFFECT OF TEMPERATURE

Another factor to consider that can influence the dissolution rate of fuel in Yucca Mountain is the temperature. In Yucca Mountain, some of the variables that can affect temperature are the thermal output of the assemblies due to the decay heat, placement of the waste packages, initial heat load of the waste packages, the ability of the mountain to disperse the heat, and ventilation during the lifespan of the repository. Figure 3.1 shows one scenario of the temperature profile of the mountain defined in the Yucca Mountain Science and Engineering Report[1]. In this case, the repository is maintained below boiling conditions by active ventilation for the first 50 years and then natural ventilation for the rest of its lifespan. In this scenario, the temperature from the outside of the fuel cask through the drift wall varies from approximately 90ºC at five years to slightly above ambient temperature at 10,000 years.

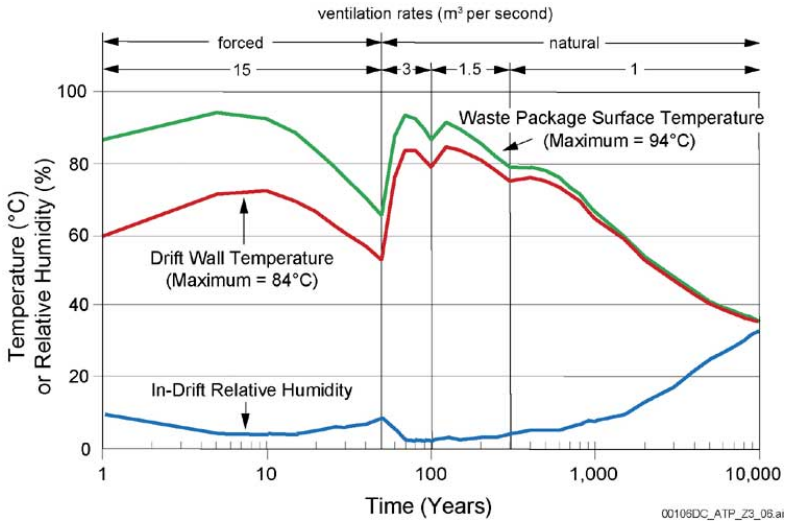

Figure 3.1. Waste package surface temperature, drift wall temperature, and in-drift relative humidity for an operational scenario in which drifts loaded at the end of emplacement operations at 1.45 kW/m are actively ventilated for 50 years and then naturally ventilated indefinitely[1]

Although repository temperatures may remain below 100ºC, the temperature of the fuel will be much higher. Inside a fuel bundle, temperatures may range from 100ºC to 320ºC over the first 1,000 years as shown in Figure 3.2. Therefore, if water were to come in close contact with this fuel it would be vaporized, preventing it from contacting the fuel as a liquid. This situation can create a humid air environment which also has corrosive properties.

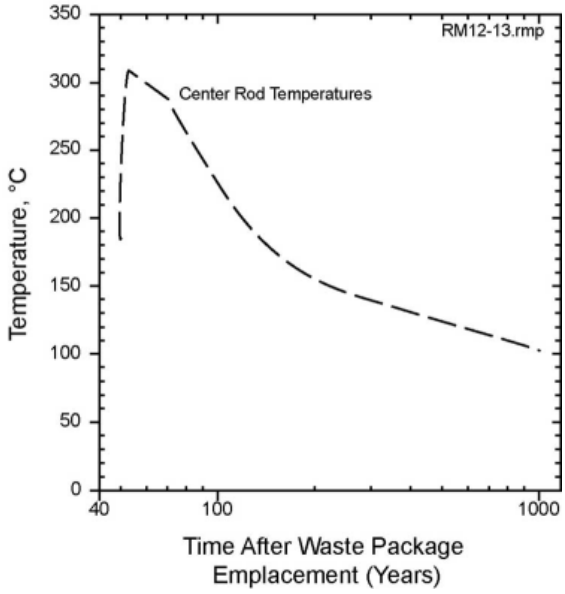

Figure 3.2. Expected temperature profile of fuel to be placed in Yucca Mountain[2]

One fuel dissolution study that incorporated the effects associated with temperature was performed by Gray et al.[3]. In this study, they used a single-pass flow-through method to measure the dissolution rate of both light water reactor fuel and unirradiated UO_2. In their tests, they varied the temperature, carbonate, and oxygen levels in the leachate solution. With experimental conditions including a 2×10^{-4} M carbonate concentration in the flow-through water that had been sparged with a gas containing 20% O_2, they noticed a significant increase in the dissolution rate of both the spent fuel and the UO_2 as the temperature increased. This observation is shown

quantitatively in Table 3.1. The dissolution rate of unirradiated UO_2 increased by a factor of approximately 4, while the dissolution rate of the spent fuel increased by over an order of magnitude. However, these differences may have been a result of the differences in surface area of the samples where the UO_2 had larger pieces (fragments of a fuel pellet) and the spent fuel was mostly grain sized powder. The larger fragments had a smaller specific area due to the surface area to volume ratio, and had a higher probability of the surface area changing over the course of the experiment, as is described further in Chapter 6.

Table 3.1. Comparison of dissolution rate of spent fuel and UO_2 in 2×10^{-4} M carbonate with a 20% O_2 sparge gas[3]

	U Dissolution Rate ($mg\ m^{-2}\ d^{-1}$)	
Temp (ºC)	Spent Fuel	UO_2
25	0.63	2.55
75	8.6	10.9

De Pablo et al.[4] also investigated the effect temperature had on dissolution. In their study, they placed one gram of unirradiated powdered UO_2 into a thin-film continuous flow-through reactor. The leachate used in the de Pablo experiment was water with varying amounts of bicarbonate for each sample. Separate tests were performed at 10ºC, 25ºC, 45ºC, and 60ºC to determine the effect of temperature on dissolution at different bicarbonate levels. The data produced from their experiments are shown in Figure 3.3. For all bicarbonate levels, as the temperature increased, the dissolution increased by upwards of 2 orders of magnitude between the 10ºC and 60ºC tests. Also, as the bicarbonate level increased, the temperature had a larger influence on the dissolution. This correlation had also been observed in a similar study by Steward

and Mones.[5] This effect may be a result of the increased kinetics of the carbonate reacting with the uranium, increasing the dissolution rate.

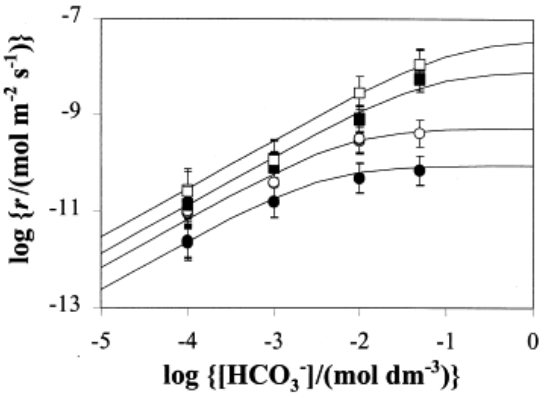

Figure 3.3. Dissolution rates as a function of bicarbonate concentration at various temperatures compared with the dissolution rates predicted by a developed model (solid lines) ● 10°C, ○ 25°C, ■ 45°C, □ 60°C[4]

Another area where temperature is important, in the case of spent fuel, is in the production of radiolytic species which will be discussed more in depth in Chapter 6. Elliot et al[6] looked at the effect that an increase in temperature had on the generation-values (G-values) for gamma irradiated water. In this study, they were testing the temperature range of 25ºC to 300ºC, with applications pertaining to the reactor core. In the experiment, they heated and irradiated the samples in an autoclave. Only hydrogen was directly measured, using a gas chromatograph. The concentrations of other species were calculated based on this measurement. They determined that only when temperatures over 200°C were achieved that significant changes began occurring in the G-values. In the range of 250ºC to 300ºC, the G-values became approximately 50% greater for H, H_2, H_2O_2, OH, and e_{aq}^- than those at room temperature. Therefore, when radiolysis is a factor in dissolution (at temperatures lower than 95ºC, which is the boiling

point of water at the elevation of Yucca Mountain), the G-values should remain relatively constant.

Although dissolution increases with temperature, when high temperatures are reached a negative effect can begin to be observed. At high temperatures, hydrogen peroxide, which is produced during radiolysis and is highly oxidizing to UO_2, begins to decompose. Štefanić and LaVerne[7] investigated this phenomenon and developed a reaction rate constant to model the decomposition.

Štefanić and LaVerne[7] purged each of their samples with helium and then placed them in an oven with a ^{60}Co source of 1.1, 3.9, or 19 krad/min. The temperature was varied from 25 to 150^{o}C and the peroxide was measured by the Ghormley tri-iodide method with KI. In this experiment, they found the temporal dependence of the formation of H_2O_2 by selectively scavenging the OH radical with methanol, ethanol or bromide. The OH was scavenged as it combined with itself to form a new H_2O_2 molecule, skewing the decomposition results. Other species, such as the hydrated electrons and hydrogen atoms, also need to be scavenged with sodium nitrate to prevent them from reacting with the H_2O_2. With the peroxide decomposition measured as a function of temperature, the following thermal decomposition rate equation was produced:

$$k_{decomp} = 6.5\,(\pm 0.2)\times 10^{5}\ \exp\left[\frac{-71\ \text{kJ/mol}}{RT}\right] \quad s^{-1} \tag{3.1}$$

where R is the ideal gas constant and T is the temperature. Therefore, if the temperature is increased, then less peroxide would be in solution oxidizing the fuel. But, this factor would become much less prominent as the fuel decays and less peroxide is created by radiolysis.

The temperature of the solution that may come in contact with the fuel in Yucca Mountain will be a factor of the time that has elapsed from placement in the mountain, ventilation of the mountain, initial heat load of the waste packages, and the spacing of the waste packages once inside the mountain. In this thesis, a range of temperatures below the boiling point of water will be investigated in order to simulate different time periods in the mountain where the solution may come into contact with the fuel. Since only unirradiated UO_2 will be used in these experiments, radiolysis should not play a major role and therefore peroxide decomposition should not influence the results of temperature-dependent experiments.

References

[1]U.S. Department of Energy Office of Civilian Radioactive Waste Management, "Yucca Mountain Science and Engineering Report," DOE/RW-0539, (July 2001)

[2]U.S. Department of Energy Office of Civilian Radioactive Waste Management, "Yucca Mountain Preliminary Site Suitability Evaluation," DOE/RW-0540, (July 2001)

[3]Gray, W.J., Thomas, L.E., "Initial Results from the Dissolution Testing of Various Air Oxidized Spent Fuels, Scientific Basis for Nuclear Waste Management XVII," *Materials Research Society Symposium Proceedings*, **257**, 353-360 (1994)

[4]de Pablo et. al., "The Oxidative Dissolution Mechanism of Uranium Dioxide. I. The Effect of Temperature in Hydrogen Carbonate Medium," *Geochimica et Cosmochimica Acta*, **63**, 3097-3103 (1999)

[5]Steward, S.A., Mones, E.T., "Comparison and Modeling of Aqueous Dissolution Rates of Various Uranium Oxides," *Materials Research Society Symposium Proceedings*, **465**, 557-564 (1994)

[6]Elliot, A. J., Chenier, M. P., Ouellette, D. C., "G-Values for γ-Irradiated Water as a Function of Temperature," *Canadian Journal of Chemistry*, **68**, 712-719 (1989)

[7]Štefanić, I., LaVerne, A., "Temperature Dependence of the Hydrogen Peroxide Production in the γ-Radiolysis of Water," *Journal of Physical Chemistry A*, 106, 447-452 (2002)

CHAPTER 4: EFFECT OF DISSOLVED O_2

Oxygen is a vital component to the oxidative dissolution of spent fuel. Unlike some proposed European repositories, Yucca Mountain may present an oxidizing environment throughout its entire lifetime. The composition of the atmosphere and the temperature of the groundwater inside the repository would be major controlling factors of the quantity of oxygen that would be present in the groundwater.

The equilibrium of dissolved O_2 in solution is established by Henry's Law when temperatures are below the boiling point. This correlation is defined by the equation:

$$[O_2] = k_H \times pp_{O_2} \tag{4.1}$$

where pp_{O_2} is the partial pressure of O_2 in equilibration with the solution and

$$k_H = k_H^o \times \exp\left(\frac{-\Delta_{soln}H}{R} \times \left(\frac{1}{T} - \frac{1}{T^o}\right)\right) \tag{4.2}$$

where T is the temperature of solution in Kelvins, $k_H^o = 1.3 \times 10^{-3}$ M, $T^o = 298.15$ K, and $\frac{-\Delta_{soln}H}{R} = 1500$ K. Henry's Law demonstrates that as the temperature increases the capacity of the water to hold dissolved O_2 decreases. Therefore, at higher temperatures in Yucca Mountain less dissolved O_2 would be present in the groundwater solutions to react with the fuel.

Christensen and Sunder[1] summarized research regarding the influence of dissolved O_2 on uranium dissolution. In their work, they compared several studies where the corrosion rate of UO_2 was measured or calculated at varying O_2 concentrations (which were performed at a pH of approximately 9). Figure 4.1 shows a comparison of an electrochemical model developed by Shoesmith and Sunder[2] and an experiment performed by Casas et al.[3] Casas's results agree with the trend of Shoesmith and Sunder relatively well for the range in which they were performed, where every order of magnitude increase in dissolved oxygen concentration results in an increase of the corrosion rate by approximately one order of magnitude. Although, in Shoesmith and Sunder's model for O_2 concentrations less than 10^{-4} M (approximately 3.2 ppm O_2) the trend in not apparent and the dissolution rates varied around 2 orders of magnitude at the same O_2 concentrations.

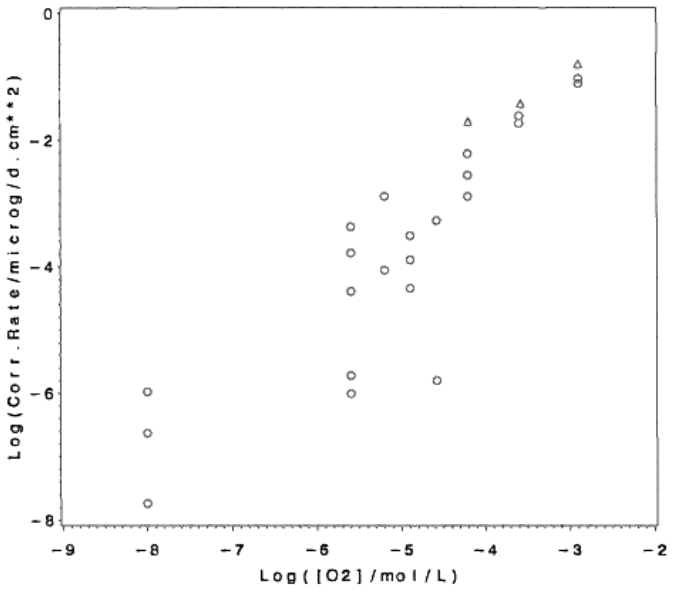

Figure 4.1. Corrosion rates (in units of μg/cm^2/d) for UO_2 as a function of dissolved oxygen concentration: ○ Shoesmith and Sunder[2]; Δ Casas et al.[3] The results of Shoesmith and Sunder were obtained from corrosion potential measurements, and those of Casas et al. are from the measurements of uranium concentrations in solutions.[1]

Oversby[4] also reviewed published data on UO_2 dissolution rates and in it presented the results of Steward and Weed[5] shown in Figures 4.2 and 4.3. Steward and Weed's tests used polycrystalline UO_2 composed of 1 to 2 cm diameter fragments that had low-angle grain boundaries. In Figures 4.2 and 4.3 on all of the tests, except the 25°C with 2×10^{-4} M carbonate, duplicates were run for the case in which the sparge gas of the leachate solution had an O_2 partial pressure of 0.2. In the results presented it was difficult to draw any conclusions as to the influence the oxygen levels had on the dissolution rate as there was no apparent trend in oxygen dependence for temperature or carbonate levels. One conclusion that was presented in the work of Steward and Weed[5] was that the reaction rate of the O_2 was approximately $[O_2]^{0.5}$ based upon the regression of the data.

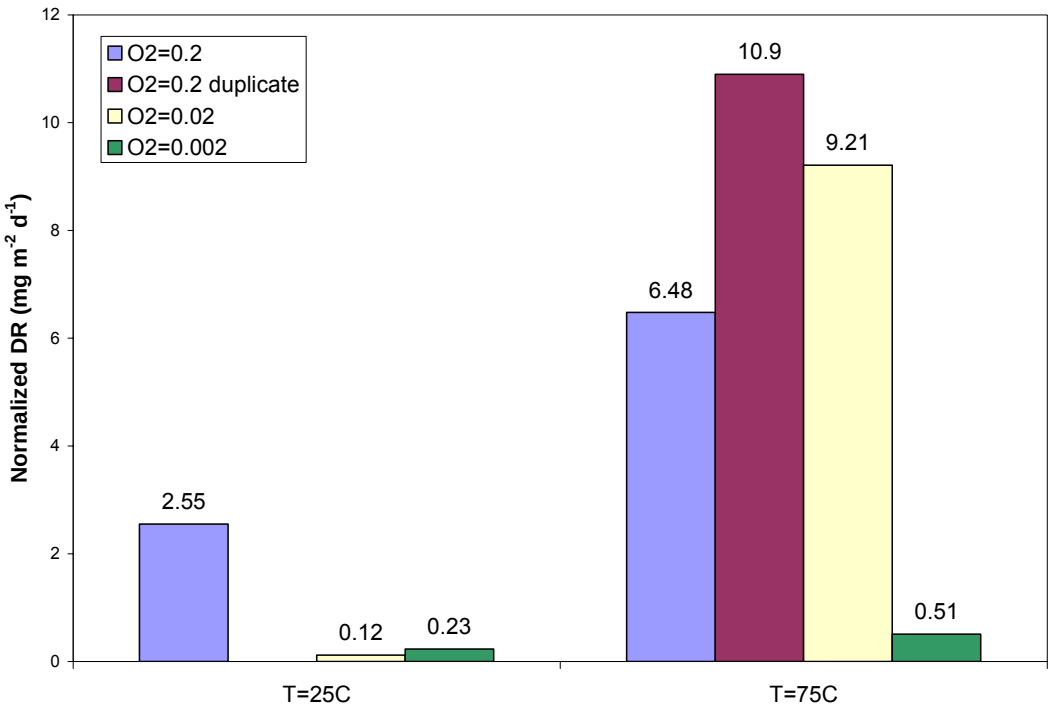

Figure 4.2. Comparison of dissolution rates of unirradiated UO_2 with O_2 partial pressures in the sparge gas between 0.002 and 0.2. Tests were run at both 25°C and 75°C with a pH between 7.8 and 10.3 and with 2×10^{-4} M carbonate in DIW as the leachate solution.[5]

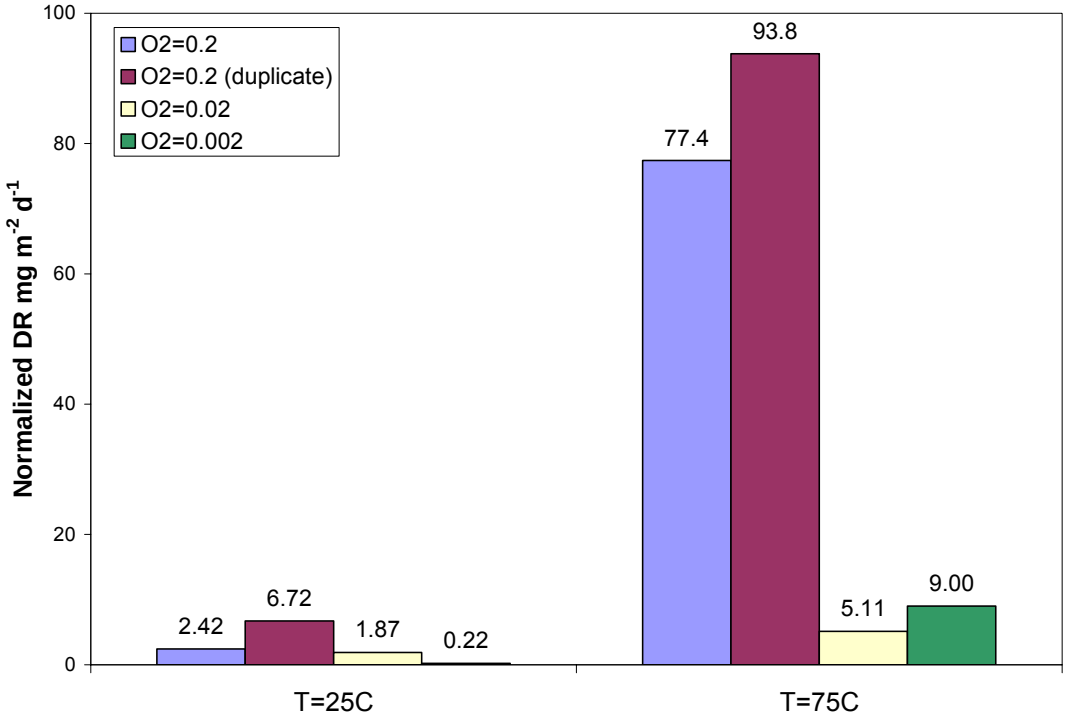

Figure 4.3. Comparison of dissolution rates of unirradiated UO_2 with O_2 partial pressures in the sparge gas between 0.002 and 0.2. Tests were run at both 25°C and 75°C with a pH between 7.8 and 10.3 and with 2×10^{-2} M carbonate in DIW as the leachate solution.[5]

Oversby[4] also reviewed data published by Nguyen et al.[6] They tested conditions similar to Steward and Weed[5] only these tests were performed on unirradiated UO_2 pellets. In these tests the trend of the data, shown in Table 4.1, was for the dissolution rate to increase as the oxygen content was decreased, which was contrary to the previous research by Christensen and Sunder[1].

Table 4.1. Normalized dissolution rates at 25ºC for unirradiated UO_2 pellets for 2×10^{-2} M and 2×10^{-4} M carbonate solutions with sparge gasses containing O_2 partial pressures from 0.0002 to 0.2[4]

$Na_2CO_3 + NaHCO_3$	pp O_2	pH	Dissolution Rate (mg m^{-2} d^{-1})
2×10^{-2} M	0.2	8.16	0.80
	0.002	8.06	2.33
2×10^{-4} M	0.2	9.7	0.24
	0.0002	9.82	1.02

Torrero et al.[7] investigated the influence pH and O_2 had on the dissolution of UO_2 powder. Samples in this experiment were one gram, containing particles ranging from 100 to 300 μm, and were tested in a flow-through apparatus. These tests looked at the difference between 5%, 21% and 100% O_2 gasses sparged in the leachate. The results from this experiment are shown in Figure 4.4. It can be seen that for high pH values the amount of dissolved O_2 had little influence on the dissolution rate, but as the pH became more acidic the dissolved oxygen had a greater influence on the dissolution. Once around a pH of 6, the dissolution rate approximately tripled from 5% to 100% O_2. As pH decreased further the O_2 became more significant and around a pH of 4 the dissolution rate of the 100 % O_2 case was over 2 orders of magnitude larger than the 5% O_2 case. These trends may be a result of a change in the rate determining step. In the case of low pH, dissolution has shown to be very fast and in a review by Shoesmith[8] at pH ≤ 5 an $UO_{2.33}$ layer was not observed on the surface of the fuel. At high pH values the dissolution is slower and the surface oxidizes to $UO_{2.33}$, thus this layer must either dissolve or diffuse O_2 through that layer to oxidize fuel beneath it.

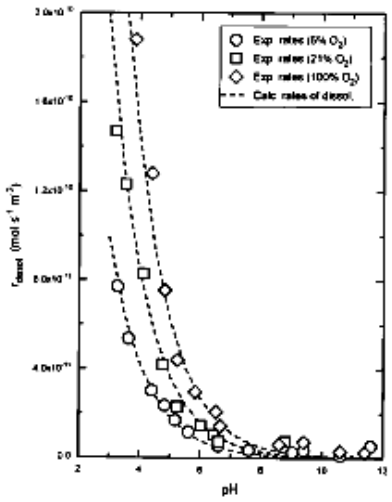

Figure 4.4. Dissolution rates for UO_2 as a function of pH and oxygen concentration. The symbols represent the experimental data and the dashed lines represent the mathematical model. ◊=5% O_2, □=21% O_2, ○=100% O_2[4]

Based upon the oxidation of UO_2, described in Chapter 2, due to the low solubility of UO_2, O_2 is needed in the leachate in order for the oxidation and dissolution to proceed. From previous research it is unclear how varying levels of dissolved O_2 will influence upon the dissolution rate. This thesis will investigate different O_2 levels that may be applicable to Yucca Mountain conditions in order to help determine this dependence. The dissolved O_2 levels in this thesis ranged from 3.0 to 4.2 ppm representing an atmospheric temperature range below boiling correlated through Henry's Law.

References

[1]Christensen, H., Sunder, S., "Current State of Knowledge of Water Radiolysis Effects on Spent Nuclear Fuel Corrosion," Nuclear Technology, **131**, 102-123 (2000)

[2]Shoesmith, D., Sunder, S., "An Electrochemistry-Based Model for the Dissolution of UO2," AECL-10488, Atomic Energy of Canada Limited; also SKB Technical Report 91-63, SKB, Stockholm (1991)

[3]Casas, I., et al., "The Dissolution of UO_2 in $MgCl_2$-Brines under Different Redox Conditions," Scientific Basis for Nuclear Waste Management XVI, C.G. INTERRANTE and R. T. PABALAN, Eds., Material Research Society Symposium Proceedings, **294**, 67 (1993)

[4]Oversby, V.M., "Uranium Dioxide, SIMFUEL, and Spent Fuel Dissolution Rates-A Review of Published Data," Technical Report TR-99-22, Svensk Kärnbränslehantering AB, Swedish Nuclear Fuel and Waste Management Company (October 1999)

[5]Steward, S.A., Weed, H.C., "Modeling of UO_2 Aqueous Dissolution over a Wide Range of Conditions," *Material Research Society Symposium Proceedings*, **333**, 409-416 (1994)

[6]Nguyen, S.N., et al., "Dissolution Kinetics of UO_2. I. Flow-Through Tests on $UO_{2.00}$ Pellets and Polycrystalline Schoepite Samples in Oxygenated, Carbonate/Bicarbonate Buffer Solutions at 25°C," *Material Research Society Symposium Proceedings*, **257**, 339-344 (1992)

[7]Torrero, M., et al., "Kinetics of Corrosion and Dissolution of Uranium Dioxide as a Function of pH," *International Journal of Chemical Kinetics*, **29**, 261-267 (1997)

[8]Shoesmith, D.W., "Fuel Corrosion Processes under Waste Disposal Conditions," *Journal of Nuclear Materials*, **282**, 1-31 (2000)

CHAPTER 5: EFFECT OF UO_2 DOPANTS

The fuel matrix composition may have a significant influence on the dissolution rate of nuclear fuel. Uranium dioxide has often been used to simulate spent fuel when measuring the dissolution rate at long time periods after the radiolysis effect has diminished. The justification for this is that spent fuel with a burnup of 50 MWd/kgM has a composition of approximately 94% UO_2. Although spent fuel is mostly UO_2, some of the remaining portion that has been incorporated into the UO_2 matrix can alter the oxidation and dissolution rates. Modifications to the UO_2 matrix, such as the presence of fission products and higher actinides, may advantageously stabilize the matrix and slow the oxidation and/or dissolution rate. Therefore, at long time periods when radiolytic production of oxidants is greatly reduced relative to fresh spent fuel, spent fuel may have a lower dissolution rate than pure UO_2.

Grandstaff[1] investigated the effect of composition on the dissolution of natural uraninite. Table 5.1 lists the compositions of the tested materials. The testing utilized a 500 mL reaction cell with a fritted glass disc at the base that allowed the leachate solution to be pulled from the sample without removal of the fuel. After samples were taken they were acidified and reacted with ion-exchange papers. The uranium content was then analyzed by a Norelco Universal Vacuum Spectrograph.

Table 5.1. Chemical analysis of uraninites used by Grandstaff[1]

	Weight Percent					
	NC	M	N	W	BR	VR
UO_2	75.5	29.3	30.8	50.0	22.7	23.2
UO_3	12.3	59.8	51.0	20.1	42.6	46.9
ThO_2	2.0	3.2	4.1	15.3	6.1	3.9
CeO_2	0.2	0.3	0.4	0.8	1.0	1.1
PbO	5.8	5.5	10.9	13.9	22.6	21.0
La_2O_3	0.0	0.0	0.0	0.1	0.1	0.6
Y_2O_3	1.5	1.4	1.6	0.0	1.9	0.2
CaO	0.2	0.2	1.9	0.1	0.7	1.1
FeO	0.1	0.1	0.1	0.1	0.1	0.2
S	0.0	0.0	0.0	0.0	0.9	1.1

NC, M, N, W=Pegmatic uraninite
BR=Uraniferous conglomerate from Blind River-Elliot Lake, Ontario, Canada
VR=Uraniferous conglomerate from Vaal Reefs West Mine, South Africa

One of the species specifically examined in this study was ThO_2, which had previously shown resistance to dissolution[2,3]. The effect of the ThO_2 on the dissolution rate can be seen in Figure 2.1. As the ThO_2 content was increased up to 5 wt% an exponential dependence was observed in the normalized dissolution rate. Although between 5 and 15 wt% a minimal drop was seen relative to the previous change, leading to a possible threshold effect of dopants. Therefore, the addition of ThO_2 to the UO_2 matrix may lower the dissolution rate to a point, but any further addition may not prove beneficial in this respect. Although as the ThO_2 content is largely increased there may be a concentration where the fuel properties tend more towards those of pure ThO_2 and less of the mixture, which may display different dissolution properties.

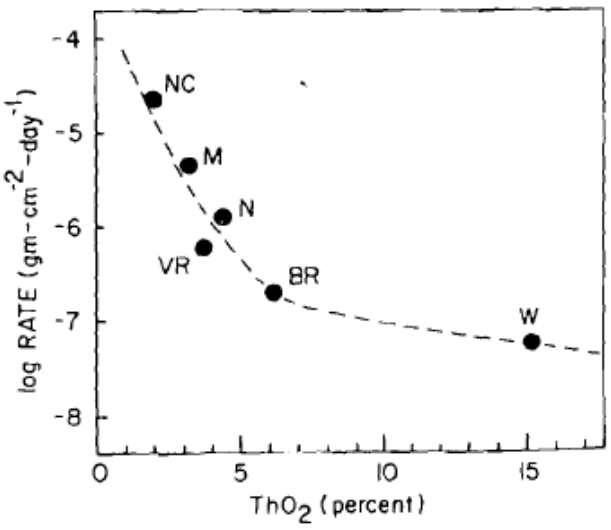

Figure 5.1. Rate of uraninite dissolution as a function of uraninite ThO_2 content (T=23°C, ambient air, distilled water)[1]

On a molecular scale, the Th is assumed to be incorporated into the UO_2 matrix by substituting Th 4+ for U 4+. Uranium dioxide forms cubic fluorite lattices as shown in Figure 5.2. The presence of a dopant atom in one of these cubic lattices may have an effect on the solubility properties of the matrix, but it may be possible that saturating the matrix greater than a certain amount does not further affect the solubility. In the cubic fluorite lattice structure each U atom has 12 nearest U neighbors, but when one dopant atom is present in a UO_2 unit cell the 8 surrounding unit cells may be influenced due to a semi-conductor electron transfer effect[1]. Therefore a possible threshold effect may be seen at concentrations lower than one non-uranium ion per UO_2 unit cell and instead may be observed when all cells are affected. Theoretically, for homogeneously mixed ThO_2-doped UO_2 at 20 wt%, every UO_2 unit cell will contain one Th atom. If each Th atom has the ability to affect all of its nearest neighbors, then at 3 wt% ThO_2, every UO_2 unit cell will be affected. Differences are seen in Figure 5.1 between the 3 and 5 wt% ThO_2 samples with the threshold not being seen until sometime after 5 wt%. Although this is

higher than with every UO_2 unit cell being affected, attributes such as sample inhomogeneity may result in an increase in the threshold value.

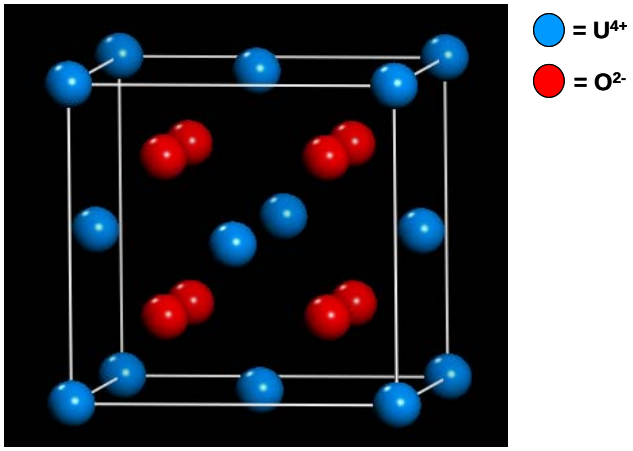

Figure 5.2. UO_2 unit cell; picture provided by Dr. Frannie Skomurski

Grandstaff produced a second graph to compare all non-uranium species as opposed to just ThO_2, which can be seen in Figure 5.3. Similar to the result in Figure 5.1 the NC, M, N, and W samples all showed decreasing dissolution rates as the mole fraction of non-uranium cations was increased. The same trend was also seen in the VR and the BR samples, although they did not correlate to the others. The explanation given for this trend is the distribution of the non-uranium cation dispersion in the samples where NC, M, N, and W samples were relatively homogenous, but VR and BR were heterogeneous. In these graphs no threshold effect was observed, although the data may be insufficient to display one, as with the exclusion of W the trend might be beginning to appear.

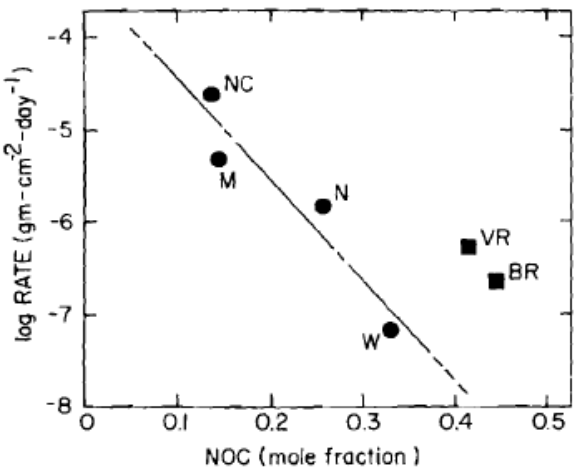

Figure 5.3. Rate of uraninite dissolution as a function of non-uranium cation mole fraction (NOC) content (T=23°C, ambient air, distilled water)[2]

Demkowicz et al.[4], also did a study on the effects of Th in the UO_2 matrix. In their study they investigated the advantages of using $(U,Th)O_2$ pellets in a reactor and their benefits as a wasteform. The fuels used in this study were powders and fragments of $(U_yTh_{1-y})O_2$ where y ranged from 0.05 to 0.5, which correlates to 95 to 50 wt% ThO_2. The experimental setup was a batch dissolution system where the dissolved O_2 concentration was approximately 8 ppm and the pH was between 8 and 8.6. The leachate used was simulated J-13 well water and tests were run at both room temperature and 90ºC.

The results from the work of Demkowicz et al.[4] can be seen in Figure 5.4. These graphs show the dissolved uranium per square meter of powder surface area (mg/m^2). The pure UO_2 had the highest dissolution rate being approximately an order of magnitude above that of the y=0.05 sample. In the case of the 90 to 250 μm powders an increase in the dissolution was seen between the y=0.05 sample (almost entirely ThO_2) and the other ThO_2 doped samples, but there was minimal difference between the other doped samples.

Therefore, for midrange compositions for mixtures may be similar, but when Th is the majority of the cation constituents, the matrix may shift to its properties.

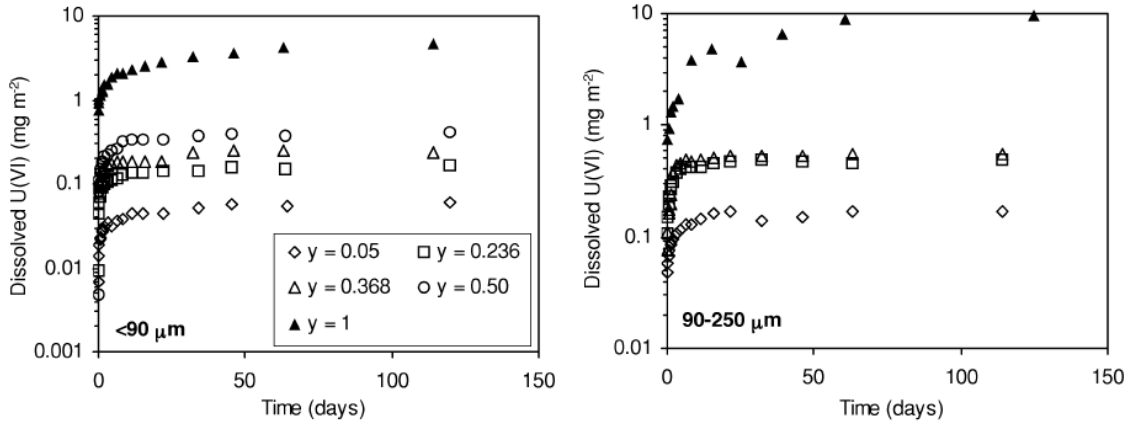

Figure 5.4. Dissolved uranium per square meter of powder surface area for < 90 μm (left) and 90 to 250 μm (right) crushed and sieved unirradiated $(U_yTh_{1-y})O_2$ pellets[4]

The results from the unirradiated whole pellets can be seen in Figure 5.5. As was seen in the case of the powders again the pure UO_2 pellets had the highest normalized dissolution rate by approximately an order of magnitude. However, in these there was statistically no difference seen between the y=0.368 and the y=0.50 samples.

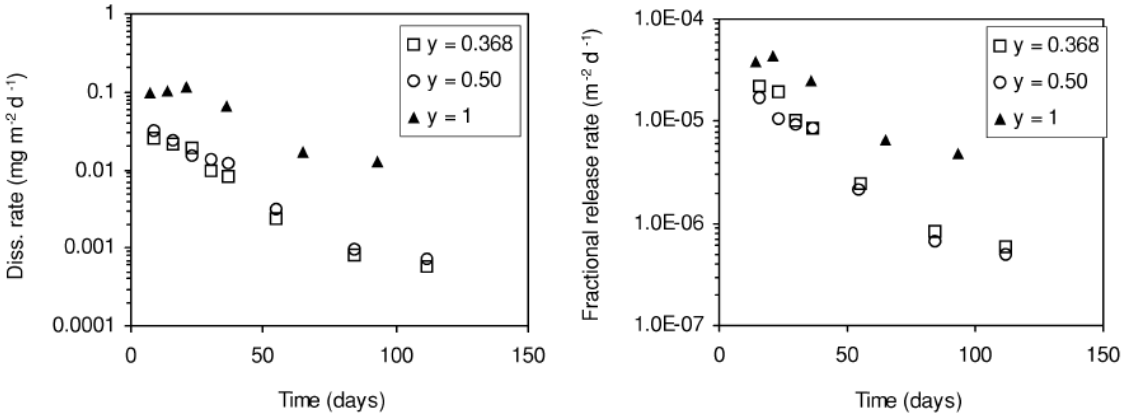

Figure 5.5. Dissolution rates (left) and surface area normalized fractional release rates (right) of unirradiated whole $(U_yTh_{1-y})O_2$ pellets in J=13 water at 90ºC[4]

The normalized dissolution rate (mg m^{-2} d^{-1}) for the powder samples can be seen in Figure 5.6. As before, the pure UO_2 had the highest dissolution rate and the largest

doped sample (almost entirely ThO_2) had the lowest by one to two orders of magnitude. An interesting trend in this data is that as time proceeded the dissolution rate continued to decrease, which may be a result of the changing surface area, as will be discussed in Chapter 6. This trend may also result from the changing surface chemistry. When the U is oxidized and dissolved Th remains behind, thus increasing its concentration on the surface. As more Th is present, fewer effective sites are available for U oxidation and dissolution.

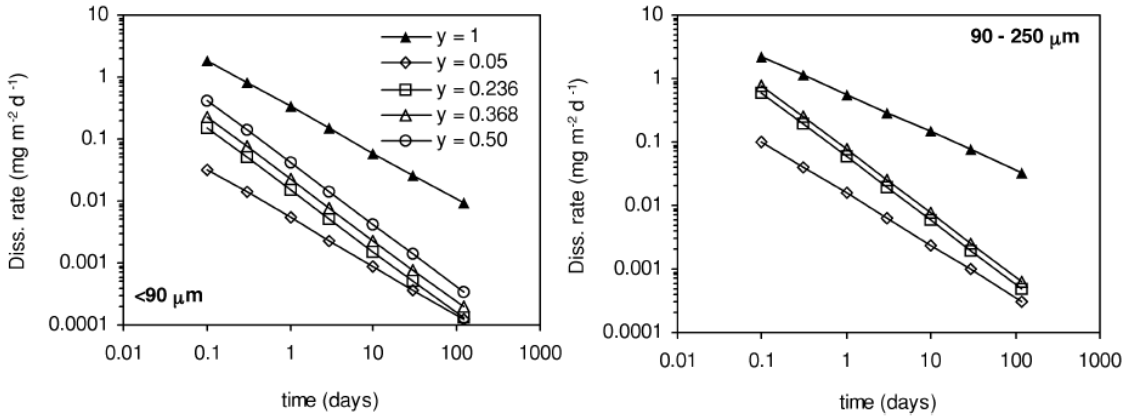

Figure 5.6. Surface area normalized fractional uranium release rates for crushed and sieved unirradiated $(U_yTh_{1-y})O_2$ pellets[4]

Another dopant used in UO_2 fuel is gadolinia, which has often been studied because it is a common burnable poison applied to fuels prior to irradiation. In the same theory that was describe for the ThO_2, Gd_2O_3 behaves similarly where at 15 wt% all UO_2 unit cells will contain one Gd atom, but at 2 wt% all unit cells are affected in part by the different oxidation state[1]. Kim et al.[5] studied the effect Gd^{3+} had on oxidation. In these experiments thermogravimetric measurements, batch oxidation and phase characterization were run on Gd_2O_3-doped UO_2. The dopant levels, in these samples,

ranged from 0 to 0.29 for y where $(U_{1-y}Gd_y)O_{2.00}$, which correlates to a maximum doping of around 21 wt% Gd_2O_3.

The tests indicated that as the dopant level was increased the lattice parameter was linearly decreased, and that a fluorite lattice was maintained over the range. In the oxidation tests it was observed that as $(U_{1-y}Gd_y)O_2$ went to $(U_{1-y}Gd_y)_4O_9$ the gradient of the oxidation kinetic curves decreased as the Gd levels were increased, but the reaction to $(U_{1-y}Gd_y)_3O_8$ was more gradual, therefore the Gd seemed to have more of an impact on reducing the dissolution rate in the first stage of the oxidation. No threshold effect was seen in these results, which may be an indicator of a separate role of Gd in the dissolution.

Scheele et al.[6] studied the air oxidation of Gd_2O_3-doped UO_2. They examined 0 to 10 wt% Gd_2O_3-doped UO_2 with < 50 μm diameters using thermogravimetric analysis and differential scanning calorimetry. This study showed that Gd_2O_3-doping increased the stability of the intermediary oxidation state ($UO_{2.33}$ discussed in Chapter 2), thus inhibiting the further stages of oxidation and thus dissolution of the surface. This is in contrast to the work of Kim et al.[5] which stated the initial stages of oxidation were inhibited. Although in both cases drops in the dissolution rate would be observed.

In the experiments where Gd_2O_3 and ThO_2 were added and incorporated into the UO_2 matrix, the oxidation and/or dissolution rates decreased. Therefore having dopants such as these present in the wasteform may assist in decreasing the rate at which spent fuel dissolves in a repository setting by possibly an order of magnitude. The experiments performed in this work will look at unirradiated UO_2 and Gd_2O_3-doped UO_2. The Gd_2O_3-doped UO_2 will be compared to the unirradiated UO_2 in order to measure any effects that

may modify the dissolution rate due to the altered fuel chemistry. Multiple levels of Gd_2O_3-doped UO_2 will be examined to observe possible trends regarding the dopant levels and to identify if any threshold effects result.

References

[1]Grandstaff, D. E., "A Kinetic Study of the Dissolution of Uraninite," *Economic Geology*, **71**, 1493-1506 (1976)

[2]Frondel, C., "Systematic Mineralogy of Uranium and Thorium," *U.S. Geological Survey Bulletin*, **1064**, 400 (1958)

[3]Davidson, C.F., "The Present State of the Witwatersrand Controversy," *Mining Magazine*, **102**, 84-95, 149-159, 222-229 (1960)

[4]Demkowicz, P.A., Jerden, J.L., Cunnane, J.C., Shibuya, N., Baney, R., Tulenko, J., "Aqueous Dissolution of Urania-Thoria Nuclear Fuel," *Nuclear Technology*, **147**, 157-**170** (2004)

[5]Kim, J.G., Ha, Y.K., Park, S.D., Jee, K.Y., Kim, W.H., "Effect of a Trivalent Dopant, Gd^{3+}, on the Oxidation of Uranium Dioxide," Journal of Nuclear Materials, **297**, 327-331 (2001)

[6]Scheele, R.D., Hanson, B.D., Cumblidge, S.E., Jenson, E.D., Kozelinsky, A.E., Sell, R.L., MacFarlan, P.J., Snow, L.A., "Effect of Gadolinium Doping on the Air Oxidation of Uranium Dioxide," *Materials Research Society Symposium Proceedings*, **208**, CC8.8 (2004)

CHAPTER 6: EFFECT OF OTHER FACTORS: RADIOLYSIS, H_2O_2, pH, AND SURFACE AREA

Radiolysis

Radiolysis is seen during many stages of the nuclear fuel cycle. During reactor operation, radiolysis can induce corrosion of the cladding and piping inside the reactor. After the fuel has been removed from the core, radiolysis is still a factor, such as when the fuel is destined for long-term repository storage where cask and cladding failure may occur. Radiolysis alters the chemistry of water that may leak into the package, accelerating the oxidation and dissolution of the spent fuel and potentially resulting in a release of radionuclides to the environment.

Radiolysis is the phenomenon of radiation cleaving the bonds of water molecules. The main species apparent in water as a result of radiolysis are shown in Table 6.1, with the notation that will be used in this thesis. The amount of each of these species produced by the radiation is dependent upon the type of radiation and dose given to the water. The constant for a given set of conditions used to measure the production of radiolytic species is the G-value, which is the number of molecules produced per 100 eV dose given to the water.

Table 6.1. Names and notation used for the species produced by radiolysis

Species	Name
H^+	Hydrogen Ion
OH^-	Hydroxide
H_2O_2	Hydrogen Peroxide
HO_2^-	Hydroperoxy Anion
e_{aq}^-	Solvated Electron
H	Hydrogen Radical
OH	Hydroxyl Radical
O^-	Oxygen Anion Radical
HO_2	Hydroperoxy Radical
O_2^-	Super Oxide Radical
O_2	Oxygen
H_2	Hydrogen
O_3^-	Ozone Anion Radical
O_3	Ozone
HO_3	Hydrotrioxyl Radical

Gamma radiation tends to produce more radicals than molecules. The G-values for gamma radiation are shown in Table 6.2, where both Christensen et al.[1] and Pastina et al.[2] values agree reasonably well. As seen in Table 6.2, OH, e_{aq}^-, and H^+ are the major species produced by gamma radiolysis. The values for beta radiolysis are assumed to be the same as for gamma radiolysis.[3] Therefore, when a mixed field of beta and gamma is present, a combined dose rate can be used with the G-values for gamma radiation.

Table 6.2. G-values for gamma radiation

	Christensen et al.[1]	Pastina et al.[2]
OH	2.67	2.7
e_{aq}^-	2.66	2.6
H^+	2.76	3.1
H	0.55	0.66
H_2	0.45	0.45
H_2O_2	0.72	0.7
OH^-	0.1	0.5
H_2O	-6.87	
O_2^-	0	
HO_2		0.02

Alpha radiation predominates after spent fuel has been outside of the reactor more than 500 years as shown in Figure 6.1. Therefore, when looking at possible fuel-water interaction in this time frame alpha radiation will be a larger factor than beta or gamma radiation. Table 6.3 shows a comparison of some G-values determined for alpha radiation. Again, Christensen and Pastina show similar results for the G-values. As displayed by the G-values, alpha radiation tends to produce more H_2O_2 and H_2 than other species. Peroxide will react with the UO_2 resulting in oxidation and dissolution, although H_2 is a strong reducer and can be key in preventing oxidation of the UO_2. However, because it is a gaseous species, it will diffuse rapidly away from the fuel, which is the heat source.

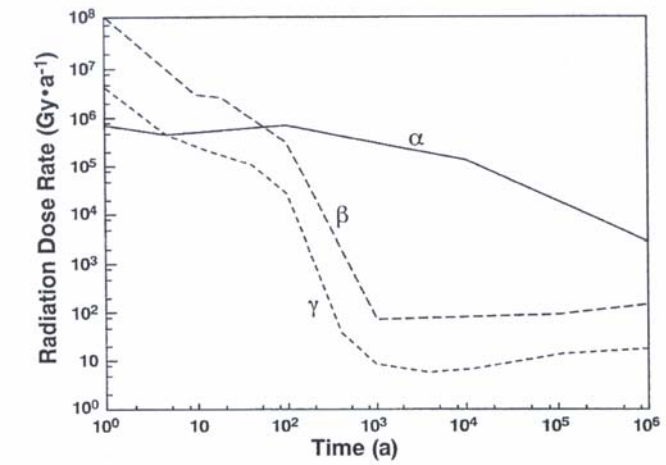

Figure 6.1. Alpha, beta, and gamma dose rates in the water layer in contact with a CANDU fuel bundle with a burnup of 721 GJ/kg U as a function of time[4]

Table 6.3. G-values for alpha radiation

	Christensen et al.[1]	Pastina et al.[2]
OH	0.24	0.35
e_{aq}^-	0.06	0.15
H^+	0.3	0.18
H	0.21	0.1
H_2	1.3	1.2
H_2O_2	0.985	1
OH^-	0.02	0.03
H_2O	-2.71	
O_2^-	0.22	
HO_2		0.1

One factor that is important when examining the dose given by spent fuel is the geometry of the fuel sample. Larger sample sizes, such as pellets compared to grains, will shield some radiation, thus reducing the dose that may reach the surrounding water. Miller et al.[5] developed a model to examine the change in dose to water due to these geometric differences. Figure 6.2 shows the dose to water from 23 year old spent fuel with a burnup of 41.2 MWd/kg crushed to a grain sized powder. Figure 6.3 utilizes the same fuel except in pellet form, and in all three radiation types there was a reduction in the dose due to the self shielding of the fuel.

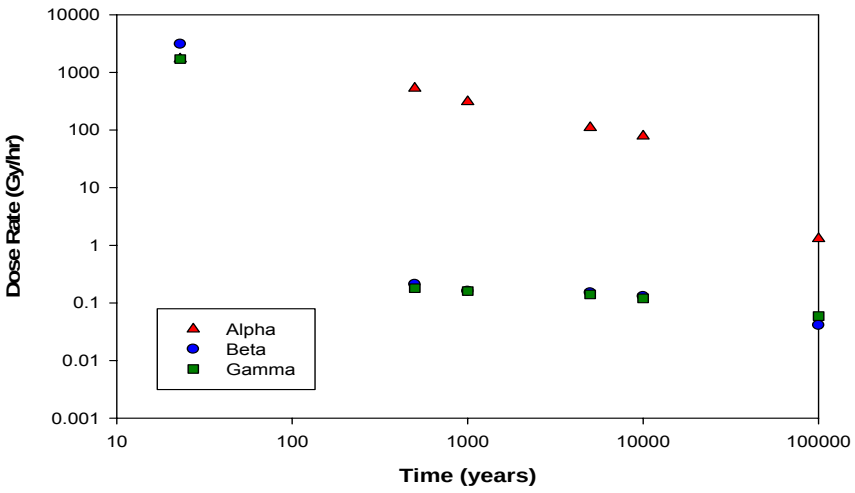

Figure 6.2. Dose to water (Gy/hr) as a function of time for a matrix of 15 μm diameter fuel grains[5]

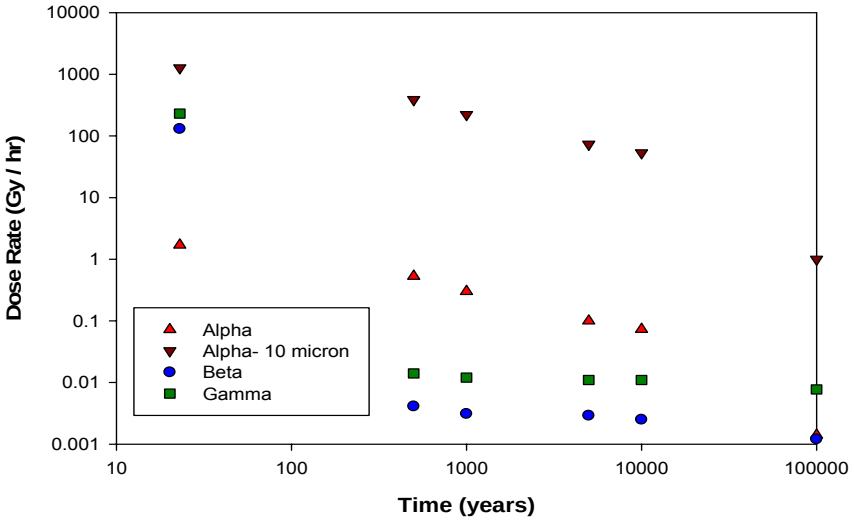

Figure 6.3. Dose to water (Gy/hr) as a function of time for a matrix of fuel pellets[5]

Peroxide can be a major contributor to the oxidation and dissolution of UO_2. It is involved in more than 20 different reactions in the aqueous solution ranging from interactions with other radiolytic products to direct interaction with UO_2. Even in an oxidizing environment it can influence the dissolution rate for spent fuel, as shown in the Modeling of UO_2 Radiolytic Products in the Appendix. In a study performed by Sunder et al.[6] the corrosion potential of standard CANDU UO_2 fuel pellets was measured at different levels of H_2O_2. It was determined that for concentrations of H_2O_2 lower than 10^{-4} mol/L the corrosion was directly proportional to the H_2O_2 concentration. When the concentration was between 10^{-4} and 10^{-2} mol/L the surface of the UO_2 was redox buffered by the H_2O_2 decomposition, and, at concentrations above this, the potential was again proportional to the H_2O_2 concentration. At the higher concentrations of peroxide, secondary phases may have begun forming on the surface, blocking the original interactions.

In a report by Amme[7], dissolution was tested with peroxide at 10^{-5}, 10^{-4}, 10^{-3}, and 10^{-2} M. In each test a pellet of depleted UO_2 was used as the solid phase and either

natural groundwater or deionized water (DIW) with the varying peroxide solutions was used as the contacting liquid phase. The tests were performed in scintillation vials where secondary phases could be formed given the right conditions. The results of their tests are shown in Figure 6.4. For concentrations of 10^{-5} M and 10^{-4} M peroxide, no yellow discoloration or visible alterations could be seen on the surface of the UO_2. For the 10^{-2} M solution in DI water a pale yellow discoloration produced by the formation of a secondary phase was observed. This discoloration was also seen in the 10^{-2} M sample in groundwater during the first three days, but disappeared afterwards. The same results were seen in the 10^{-3} M samples although they were much less pronounced.

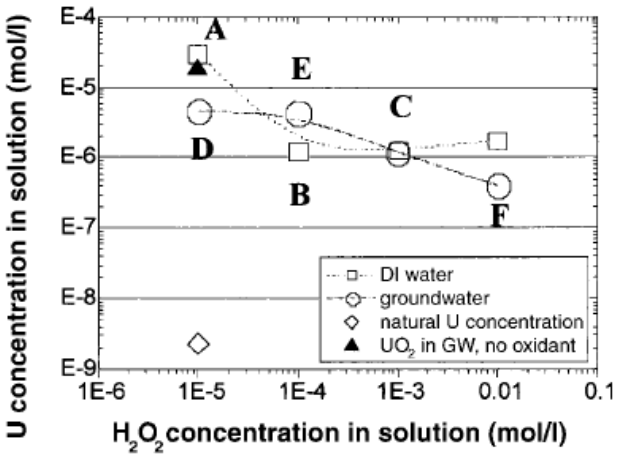

Figure 6.4. Concentrations of U in the leaching solutions after treatment with groundwater and DI water containing H_2O_2 for 1000 hours[7]

As shown in Figure 6.4, the uranium concentration was highest in the solutions with the lowest amount of peroxide. This may be attributed to the secondary phases seen on the UO_2 in the higher peroxide experiments. Another interesting phenomenon was that the uranium dissolution was higher in the DIW than it was in the groundwater. This is attributed to the H_2O_2 being de-activated by the groundwater. By looking at the

chemical reactions of ground water constituents with peroxide, it can be seen that different radicals can either promote or inhibit the dissolution. In the case of this experiment, Fe(II) is expected to oxidize to Fe(III) which has been found to decompose H_2O_2.[8]

Since after 500 years alpha radiation predominates, Pastina and LaVerne[2] looked at how different types of radiation and hydrogen added to the system affected the H_2O_2 concentration. Solutions used in the experiment had 0, 8, 80, and 300 μM dissolved H_2, which were then irradiated with either 2 MeV protons, 5 MeV protons, or 5 MeV helium ions. The results from the experiments are shown in Figure 6.5. As predicted by the G-values, the helium atom produced the largest concentrations of H_2O_2. Also, in all three experiments the added H_2 slightly increased the concentration of H_2O_2.

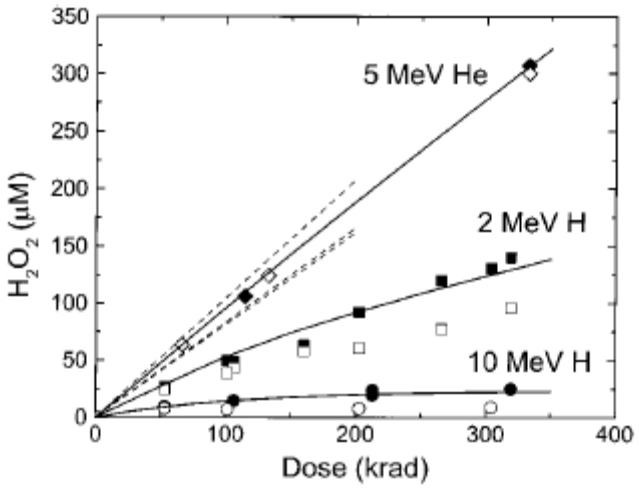

Figure 6.5. H_2O_2 concentration dependence on dose in the heavy ion radiolysis of water with no H_2 (filled symbols) and H_2 saturated (800 μM; open symbols): The solid lines are the homogeneous model predictions for solutions with no H_2, and the dashed lines are the estimated concentrations based on the escape yields.[2]

Radiolytically produced H_2O_2 expedites the dissolution of spent fuel and unirradiated UO_2. When high concentrations of peroxide are present secondary phases

begin to form, which may in turn inhibit the dissolution. So, low concentrations of H_2O_2 may be a worse scenario for dissolution kinetics than high or no H_2O_2. For flow-through tests, the flow rate of the solution passing the fuel sample can be varied to allow or inhibit the formation of secondary phases in order to obtain the desired conditions. When tests are run on powders, as opposed to fragments or pellets, H_2O_2 formation increases due to the lower self shielding ability of a small sample. Therefore, performing dissolution tests on powders with high radiolytic fields would produce larger dissolution rates than if the tests were run on pellets or fragments, which are expected in Yucca Mountain.

pH

Depending on the range, pH can play an important role in dissolution. Clarens et al.[9] studied the effects of pH on the oxidative dissolution of spent fuel. In their experiments they used a continuous flow-through reactor design to measure the influence of pH on the dissolution of unirradiated UO_2 with a particle size of 100-320 μm. The leachate solution was purged with nitrogen to eliminate the oxygen and carbonate, then circulated at 0.19 ± 0.02 cm^3/min in order to achieve steady state conditions. The pH was varied in the experiments over the range of 3.5 to 10.5, producing the results seen in Figure 6.6. As shown in the figure, pH has a significant effect on the dissolution for values lower than 6 and greater than 10. For these high and low pH values, the dissolution rate of the uranium increased by orders of magnitude. Over the pH range of 6 to 10 there appears to be little influence on the dissolution rate. This trend allows for a buffered zone between a pH of 6 and 10 where slight changes in the pH will not influence the dissolution experiment.

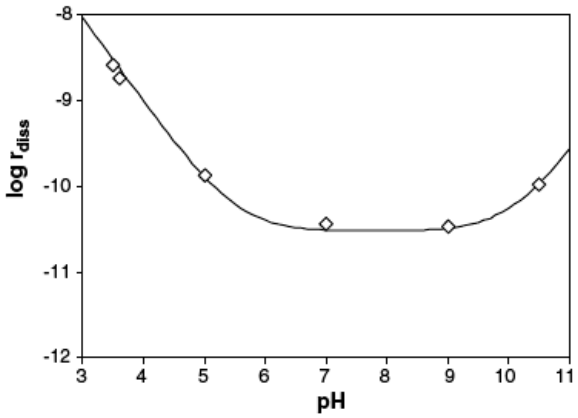

Figure 6.6. UO_2 dissolution rates (mol/(m^2 s)) as a function of pH. The diamonds represent experimental data and the solid line represents the theoretical model given by Equation (6.1).[9]

Along with the experiment, Clarens et al.[9] developed an empirical model to simulate this phenomenon. The model utilized the equation:

$$r_{diss} = k_H \cdot [H^+]^n + k_0 + k_{OH} \cdot [H^+]^m \qquad (6.1)$$

where the values for k_H, k_0, k_{OH}, n, and m that give the best correspondence to the experimental data are given in Table 6.4. This model is represented by the solid line in Figure 6.4 and fits well to the data only deviating at low pH values.

Table 6.4. Values of the parameter of Equation 6.1 fitted to the experimental data shown in Figure 6.4

k_H	$8 \pm 2 \times 10^{-6}$
k_0	$3 \pm 1 \times 10^{-11}$
k_{OH}	$4.0 \pm 0.5 \times 10^{-21}$
n	1.00 ± 0.04
m	-1.00 ± 0.04

Torrero et al.[10] also investigated the effects of pH on UO_2 dissolution, although unlike Clarens et al.[9], they allowed an O_2 environment in the leachate where trials were performed in equilibrium with 5%, 21%, and 100% oxygen. They also ran their experiments in a continuous flow-through reactor with a flow rate fast enough to ensure

steady state conditions. For the experiment, one gram of fabricated UO_2 powder with a particle size of 100 to 300 μm was placed in the reactor while water, which had been purged with either 5%, 21%, or 100% O_2, was used as the leachate. Once an experiment was performed at a specific pH, the pH was changed and the experiments run again.

The results from the Torrero et al.[10] experiments are shown in Figure 6.7. For each O_2 concentration in the experiment the dissolution greatly increased as the pH decreased to values less than 8. These results are similar to those of Clarens et al.[9] except that dissolution rates did not increase again at high pH values. Instead, Torrero's data appeared to level off for any pH values above 8. Torrero et al.[10] also developed a model to simulate their experimental results. In their model they used the equation:

$$r_{dissol} = k_{dissol} \cdot \left[H^+\right]^m \cdot \left[O_2\right]^n \qquad (6.2)$$

where m=0.37±0.01, n=0.31±0.02, and log k_{dissol}=-7.46±0.09. When this equation was compared to the data shown in Figure 6.2 it had a fit of r^2=0.98.

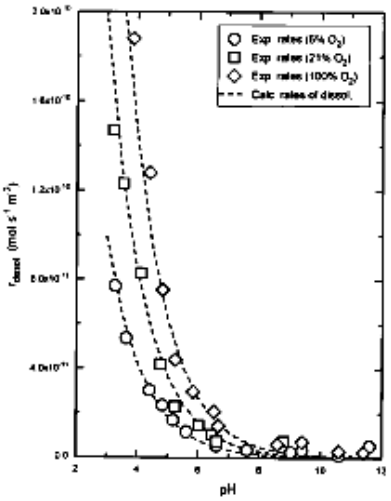

Figure 6.7. Dissolution rates for UO_2 as a function of pH and oxygen concentration. The symbols represent the experimental data and the dashed lines represent the mathematical model. ◊=5% O_2, □=21% O_2, ○=100% O_2[10]

As shown in both Clarens et al.[9] and Torrero's et al.[10] work, the pH can play an important role in the dissolution of UO_2. As the pH goes from neutral to highly acidic conditions the dissolution can increase by approximately two orders of magnitude. When going from neutral to basic conditions there is also evidence that dissolution may increase, although not as drastically as in acidic conditions. However, there appears to be a buffered region between a pH of 6 and 10 where the pH has little influence on dissolution.

Based upon these studies, the experiments performed in this thesis will use a pH of approximately 7 to 8. Clarens and Torrero showed that if the pH varies slightly between the tests, dissolution rates should not be affected. Therefore, extra measures will not be taken to keep all pH levels identical which could be detrimental to other significant areas, such as keeping carbonate levels constant or adding other variables to the system.

Surface Area

The amount of surface area on spent fuel will have a profound effect on how the fuel dissolves. The larger the surface area of the fuel, the more sites available for molecules or radicals to react with uranium leading to increased dissolution. Although this appears to be a straight forward relation, another factor must be taken into account when looking at the dissolution of spent fuel, the volume of the fuel. Alpha and beta particles are attenuated by the fuel, resulting in fewer radioactive particles making it to the fuel water interface as was previously discussed. With fewer particles reaching the surface, fewer radiolysis products will be created, decreasing the reactants in the

oxidation and dissolution processes. Therefore, when determining the dissolution rate, normalizing to the surface area may not produce accurate results, especially if the fuel size is larger than a grain.

The effect of the surface area was studied by Bruno et al.[11] In part of this study, the dissolution of a pellet was compared to that of a powder with particles on the order of 100-300 μm. In their work, test TS2 consisted of an 8.5 gram UO_2 pellet that was leached with $NaHCO_3$/NaCl. Test TS3 consisted of a 2.5 gram sample of UO_2 powder that was also leached with $NaHCO_3$/NaCl. The surface area to volume ratio for the pellet and powder was measured using the Brunauer, Emmett, Teller (BET) method and resulted in values of 13 m^{-1} and 226 m^{-1} respectively. Some of the results of their test can be seen in Figure 6.8. Although there is more UO_2 present in the TS2 sample than the TS3, there is approximately an order of magnitude more uranium dissolved in the leachate for the powdered sample. This shows that there is an effect based upon the surface area and that a linear relationship to the volume can not be made, therefore normalizing the dissolution rate to the surface area may deviate from the true dissolution rate.

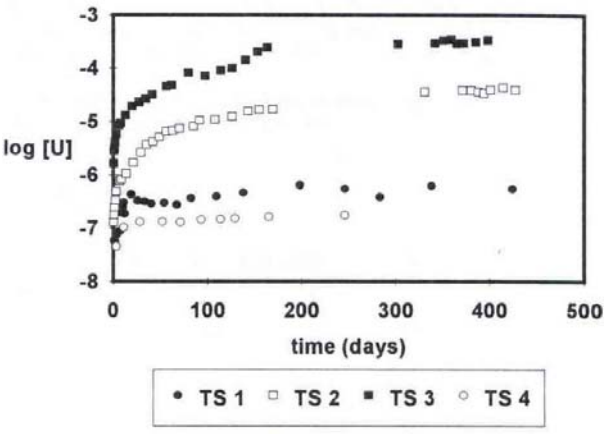

Figure 6.8. Uranium concentration versus cumulative time for the different experiments using the batch methodology[11]

One difficulty in normalizing to the surface area is in determining the true surface area of the fuel. The most common technique for measuring the surface area of powders is to use the Brenauer, Emmett, Teller (BET) method. In this method the surface area of the fuel is measured by the amount of nitrogen or krypton deposited on the surface of the fuel, when the gases containing these elements are brought to liquid nitrogen temperatures. As the sample is heated the nitrogen or krypton is release and measured. There has been some debate as to whether or not the nitrogen and krypton are able to penetrate pores and other areas that larger molecules such as water may not. Therefore, in this circumstance erroneously high surface areas would be predicted. In the case of fragments, often times the surface area is too low to be measured by the BET method and a geometric method is applied. In the geometric method the fragments are physically measured and a surface roughness is factored in, which leaves some question to the accuracy of measurements of a rigid object and a homogenously applicable roughness factor.

Another reason that normalizing to the surface area may cause inaccuracies in dissolution rates is that the surface area is not constant over the course of the dissolution study. Hanson and Stout[12] did a study of the different methods of calculating dissolution rates. In this study they discuss that the first thing to be penetrated, for tests on fragments, by the leaching solution is the grain boundaries, which may increase the surface area by a factor of five. In almost all of the tests studied the dissolution rate continued to decrease over time, even though the surface area may have been increasing. One possibility for this is the blockage of sites due to less soluble dopants as was discussed in Chapter 5. Alteration phases blocking oxidation sites was also discussed by

Hanson and Stout[12], where the surface area of the fuel decreased due to the secondary layer. Thus, normalizing the dissolution rate to the surface area may provide erroneous rates.

For the experiments carried out in this research, surface area will be measured via the BET method for the powders and geometrically for the fragments. Graphs and data presented will be displayed using both normalized dissolution rates and cumulative rates. The cumulative rates quantify total fuel released and exclude the surface area as a variable. The normalized dissolution rates allow the data to be compared to previous research and provide insight into validity of scaling factors or other effects causing variation in the rates. Although, the complication of surface area measurements should be considered when analyzing any normalized dissolution rate.

References

[1]Christensen, H., Sunder, S., "Current State of Knowledge of Water Radiolysis Effects on Spent Nuclear Fuel Corrosion," *Nuclear Technology*, **131**, 102-123 (2000)

[2]Pastina, B., LaVerne, J., "Effect of Molecular Hydrogen on Hydrogen Peroxide in Water Radiolysis," *Journal of Physical Chemistry A*, **105**, 9316-9322 (2001)

[3]Clarens, F., et al., "Influence of β Radiation on UO_2 Dissolution at Different pH Values," *Radiochimica Acta*, **93**, 533-538 (2005)

[4]Shoesmith, D. W., "Fuel Corrosion Processes under Waste Disposal Conditions," *Journal of Nuclear Materials*, **282**, 1-31 (2000)

[5]Miller, W.H., Kline, A.J., Hanson, B.D., "Dosimetry Modeling for Predicting Radiolytic Production at the Spent Fuel - Water Interface," *Proceedings of the 11th International High-Level Radioactive Waste Management Conference (IHLWM),* Las Vegas, NV, American Nuclear Society (2006)

[6]Sunder, S., Miller, N. H., Shoesmith, D. W., "Corrosion of Uranium Dioxide in Hydrogen Peroxide Solutions," *Corrosion Science*, **46**, 1095-1111 (2003)

[7]Amme, M., "Contrary Effects of the Water Radiolysis Product H_2O_2 upon the Dissolution of Nuclear Fuel in Natural Ground Water and Deionized Water," *Radiochimica Acta*, **90**, 399-406 (2002)

[8]Gmelin Handbook of Inorganic Chemistry, Oxygen. Verlag Chemie, Weinheim, 2353-2355 (1967)

[9]Clarens, F., et al., "The Oxidative Dissolution of Unirradiated UO2 by Hydrogen Peroxide as a Function of pH," *Journal of Nuclear Materials*, **345**, 225-231 (2005)

[10]Torrero, M., et al., "Kinetics of Corrosion and Dissolution of Uranium Dioxide as a Function of pH," *International Journal of Chemical Kinetics*, **29**, 261-267 (1997)

[11]Bruno, J., et. al., "Uranium (IV) Dioxide and SIMFUEL as chemical Analogues of Nuclear Spent Fuel Matrix Dissolution. A Comparison of Dissolution Results in a Standard NaCl/$NaHCO_3$ Solution," *Materials Research Society Symposium Proceedings*, **353**, 601-608 (1995)

[12]Hanson, B., Stout, R., "Reexamining the Dissolution of Spent Fuel: A Comparison of Different Methods for Calculating Rates," *Proceedings of the Materials Research Society Symposium*, **824**, 89-94

CHAPTER 7: SPENT FUEL AND UNIRRADIATED UO_2 DISSOLUTION TESTING

Two major studies on uranium dissolution were Gray and Wilson's[1] report for the United States repository program and Tait and Luht's[2] report for the Canadian repository program. These studies examined a variety of dissolution parameters which pertain to their particular repository program and compare to previous research performed. Some of the areas of their research include investigation into the effect of carbonate concentration, dissolved oxygen concentration, temperature, surface area, radiation dose, and solution flow rate on the dissolution rate of nuclear fuels that would be present in the repositories.

Work Performed in the U.S. by Gray and Wilson

Gray and Wilson[1] did an in-depth study looking at several aspects of spent fuel and unirradiated UO_2 dissolution. The main focuses of the report looked at the effect of different water chemistries on dissolution, how dissolution rates are influenced by preoxidation, and measuring gap and grain inventories of ^{137}Cs, ^{99}Tc, and ^{90}Sr. In this report supplementary studies were also performed that measured the dissolution of UO_2 in a solution containing a high concentration of uranium, and simultaneous changes in dissolution and streaming potential in response to changes in water chemistry.

In the experiments spent fuel was crushed to grain size pieces. After crushing, fines were removed through a washing process. This also removed some of the gap and grain boundary inventory, however this was not a major concern since the main focus was in measuring the matrix dissolution rate which was typically done by measuring the

uranium concentration in the leachate. In tests where unirradiated UO_2 was used, the UO_2 pellets came from Exxon Nuclear Company, Inc. In order to obtain powders, the pellets were crushed and sieved to grain sized particles and washed as before, then heated to 950^{o}C overnight in an Ar/8% H_2 atmosphere and cooled in dry He. All surface area measurements were made using either the Brenauer, Emmett, Teller (BET) method or a particle-size distribution (PSD) method. Normalized dissolution rates were calculated by measuring the dissolution rate and dividing by the surface area.

The tests utilized a flow-through experiment where approximately 200 mg of the sample was placed in a column, initially filled with the solution from the bottom to remove the air, then the column was turned over in order to allow the leachate to drip into the column. The tests ran with the flow-through system categorized into four areas: 1.) spent fuel grains; 2.) oxidized spent fuel; 3.) supplementary spent fuel tests; and 4.) unirradiated UO_2. In order to calculate the dissolution rate of the spent fuel matrix the following equation was used:

$$R = \frac{C_i F}{M A f_i} \tag{7.1}$$

where R is the dissolution rate of the spent fuel matrix based on the data for component i, C_i is the concentration of i in the column effluent, F is the flow rate, M is the initial mass of the sample, A is the specific surface area, and f_i is the concentration of component i in the fuel sample. An alternate equation was also used to calculate the dissolution rate of a specific component in the sample:

$$R_i = \frac{C_i F}{M A} \tag{7.2}$$

where R_i is the dissolution rate of component i.

One of the first tests performed was a measurement of the dissolution rate of ATM-103 fuel that had been crushed to grain sized particles. Approved Test Material (ATM) fuels were samples taken from LWR reactors with their properties shown in Table 7.1. The leachate solution consisted of DI water with 2×10^{-3} M $NaHCO_3/Na_2CO_3$ at a pH of 9. The solution was sparged with air containing 20% O_2, was maintained at a flow rate of approximately 0.2 mL/min, and was heated to 50ºC prior to contact with the fuel. (The solution being sparged was at room temperature.) Three tests were conducted under identical conditions in order to look at reproducibility; their results can be seen in Figure 7.1. These tests show that under these conditions the U dissolution rate remained between approximately 5 to 10 mg m^{-2} d^{-1}.

Table 7.1. Properties of ATM fuels[1]

Sample Number	Grain Size (μm)	Fission Gas Release (%)	U (fraction)	^{137}Cs (mCi/g)	^{99}Tc (mCi/g)	^{90}Sr (mCi/g)
ATM-101	6-10	0.21	0.845	57.5	0.0105	37.5
ATM-103	14-22	0.25	0.842	72.1	0.0114	47.2
ATM-104	9-14	1.1	0.831	97.7	0.0146	61.3
ATM-105	11-15	0.59	0.845	65.5	0.0110	44.9
ATM-106	Not Measured	18	0.825	105.6	0.0157	58.6

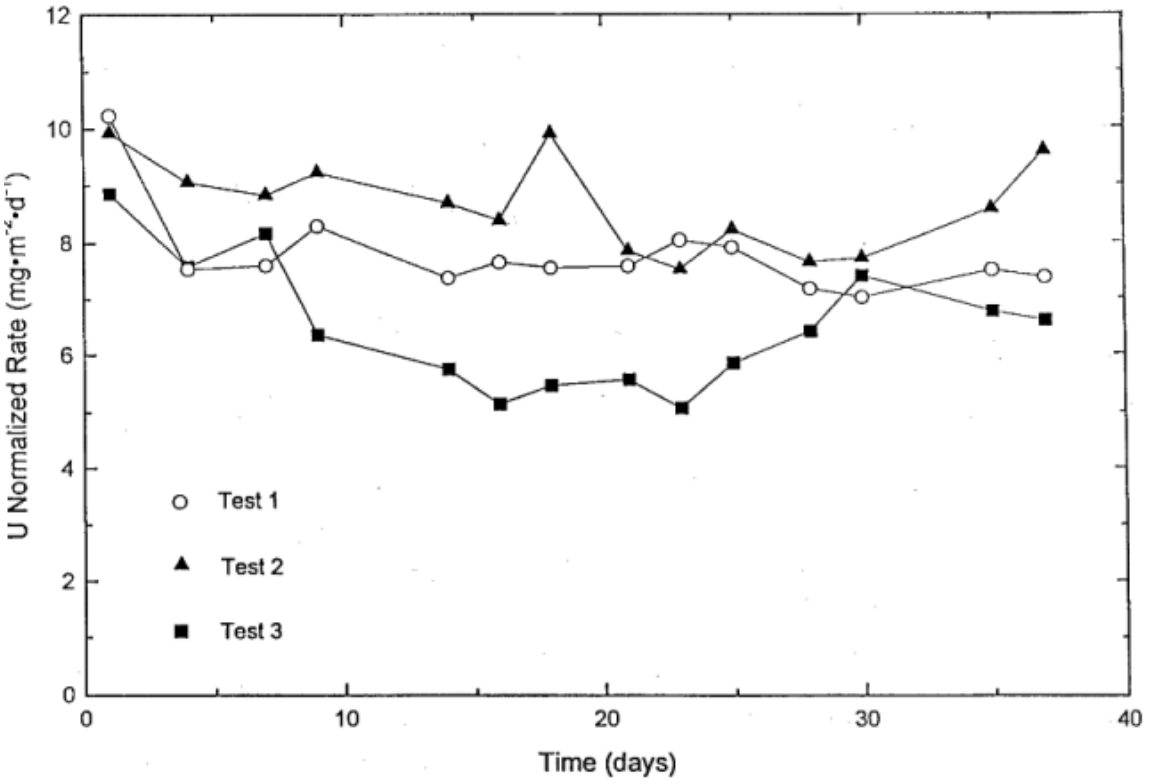

Figure 7.1. Tests 1, 2, and 3-Dissolution rates of ATM-103 fuel grains in 2×10^{-3} M $NaHCO_3/Na_2CO_3$, pH=9, O_2=0.2 atm, 50°C, Flow Rate= ~0.2 mL/min[1]

Gray and Wilson also looked at the effect that the flow rate had on dissolution, as shown in Figure 7.2. This test had the same carbonate concentration, pH, O_2 and temperature as the previous test, but the flow rate was varied between 0.2 and 0.04 mL/min. The first part of the tests was the data from Test 1 shown in Figure 7.1. After 37 days the flow rate was doubled, which resulted in a decrease in the dissolution rate followed by a return to the original dissolution rate. After this, the flow rate was decreased to 0.05 mL/min and the dissolution rate exhibited a decrease from approximately 7.5 mg m^{-2} d^{-1} to around 3 mg m^{-2} d^{-1}. Around day 53 the flow rate was increased to 0.15 mL/min and the dissolution rate increased. As the flow rate was then varied to 0.35 and 0.1 mL/min, the dissolution rate appeared to remain around

5 mg m^{-2} d^{-1}, until the flow rate was again decreased to 0.04 mL/min. Each time the flow rate was decreased to 0.05 mL/min or below, there was a significant drop in dissolution showing a strong correlation between flow rate and dissolution. But there was a much less dramatic change seen when the flow rate was above 0.1 mL/min and was increased.

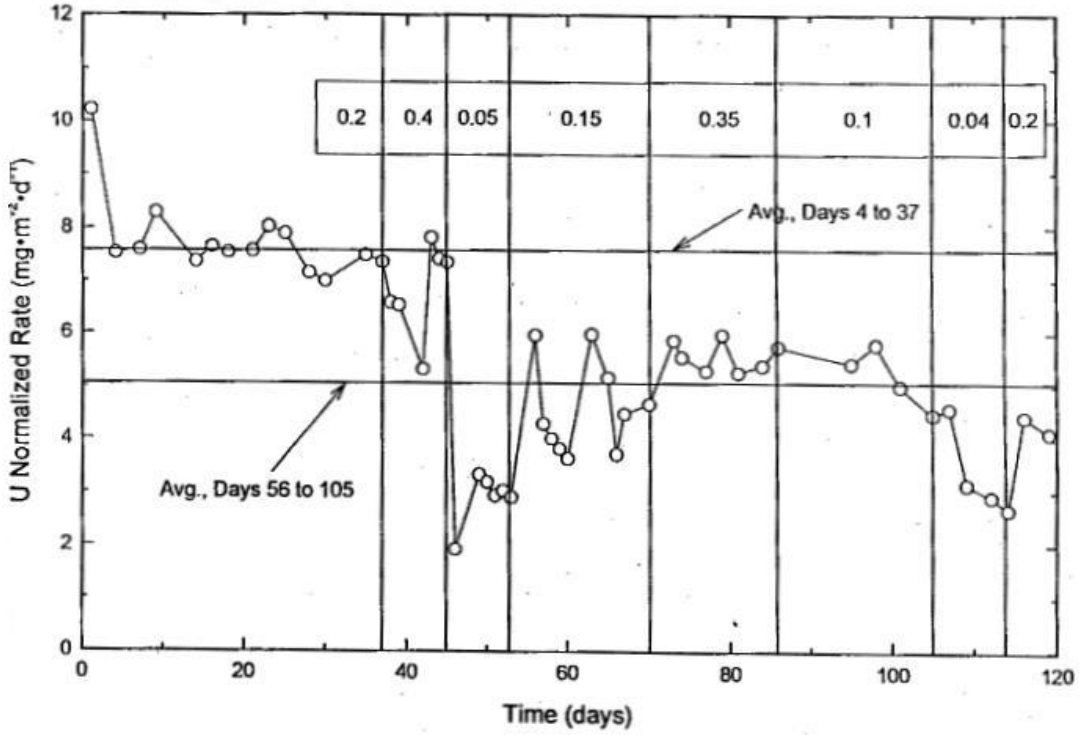

Figure 7.2. Tests 1-Dissolution rates of ATM-103 fuel grains in 2×10^{-3} M $NaHCO_3/Na_2CO_3$, pH=9, O_2=0.2 atm, 50ºC (Vertical lines divide regions of different approximate flow rates in mL/min, which are given by the numbers in the box)[1]

After the initial flow rate decrease, in Figure 7.2, to 0.05 mL/min the high rate of dissolution as achieved in the first 37 days was not observed. The flow rate measurements obtained using single-pass flow-through methods are only valid in measuring the forward rate of dissolution in the region where the dissolution rate is independent of the flow rate. Therefore, at low flow rates the U may exceed solubility and begin to form alteration phases. Once alteration phases cover the sample of the fuel the dissolution rate being measured is a function of those phases and not the pure fuel

sample, which would account for the lower overall dissolution rate after the flow rate was increased to previous levels.

Another test performed by Gray and Wilson looked at the influence dissolved O_2 content had on the dissolution rate, the results of which are shown in Figure 7.3. In this test, they sparged the solution with either 20% or 0.3% O_2. This test was performed at a higher pH and temperature than before and with a total carbonate concentration one order of magnitude less carbonate than the first test. The test showed that initially with a sparge gas containing 20% O_2 the dissolution rate was relatively constant holding slightly above 10 mg m^{-2} d^{-1}. When the O_2 concentration in the sparge gas was decreased to 0.3% there was a very dramatic decrease in the dissolution rate to approximately 0.1 mg m^{-2} d^{-1}. The O_2 was then cycled back to 20% and down to 0.3% with the same result. This showed that the dissolved O_2 has a very large effect on dissolution, but even with minimal dissolved O_2 there was still dissolution occurring. This test also measured the ^{137}Cs dissolution between days 80 and 150, which followed the same trend as the uranium dissolution.

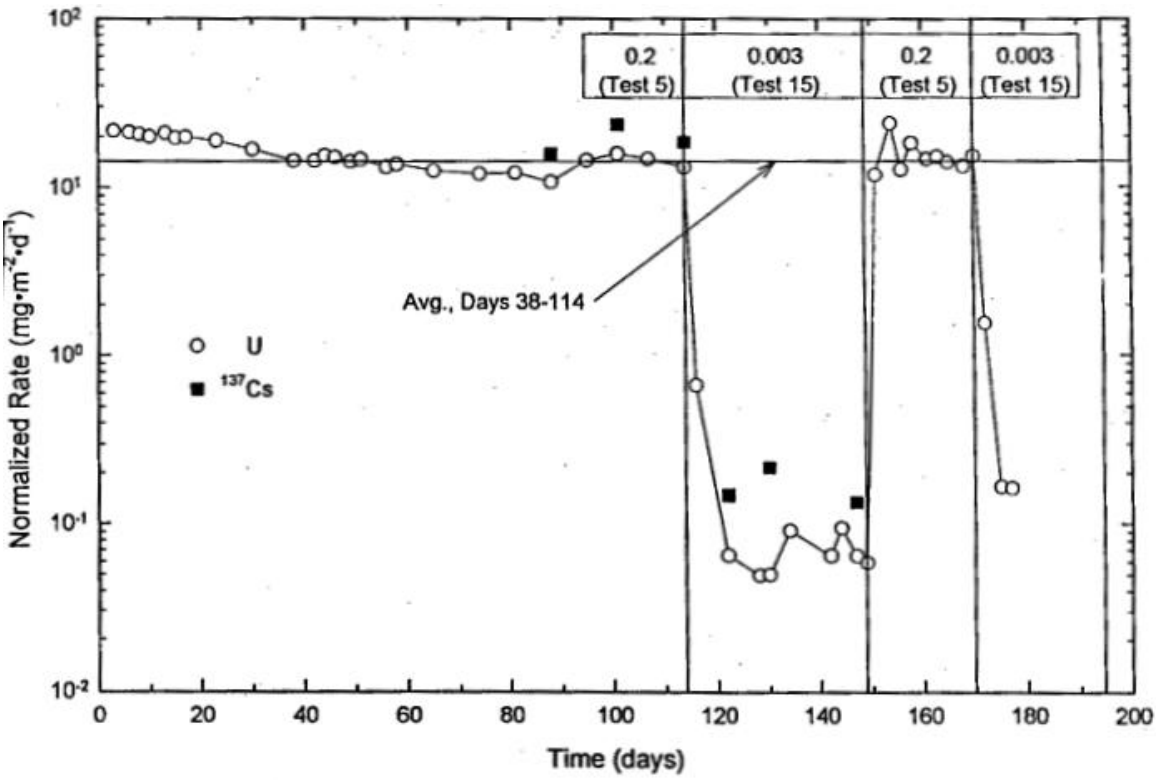

Figure 7.3. Dissolution Rates of ATM-103 fuel grains in 2×10^{-2} M $NaHCO_3/Na_2CO_3$, pH=10, 74°C (Vertical lines divide regions of different O_2 overpressures (atm), which are given by the numbers in the box)[1]

One factor to consider when measuring dissolution rate is the effect washing can have on the rate. Washing the fuel will remove fines and possibly some of the species residing on the gap and grain boundaries. Also, fresh fuel typically has a thin oxidized layer on the surface that will dissolve quickly upon initial contact with the leachate solution. Figure 7.4 shows the difference that these effects can make in the dissolution rate. The previously tested specimen has a low initial dissolution rate that increased to its steady state condition. However the fresh specimen had a high spike that dropped to its steady state condition, which can be attributed to the quick dissolution of the grain boundary and possibly fuel surface chemistry effects.

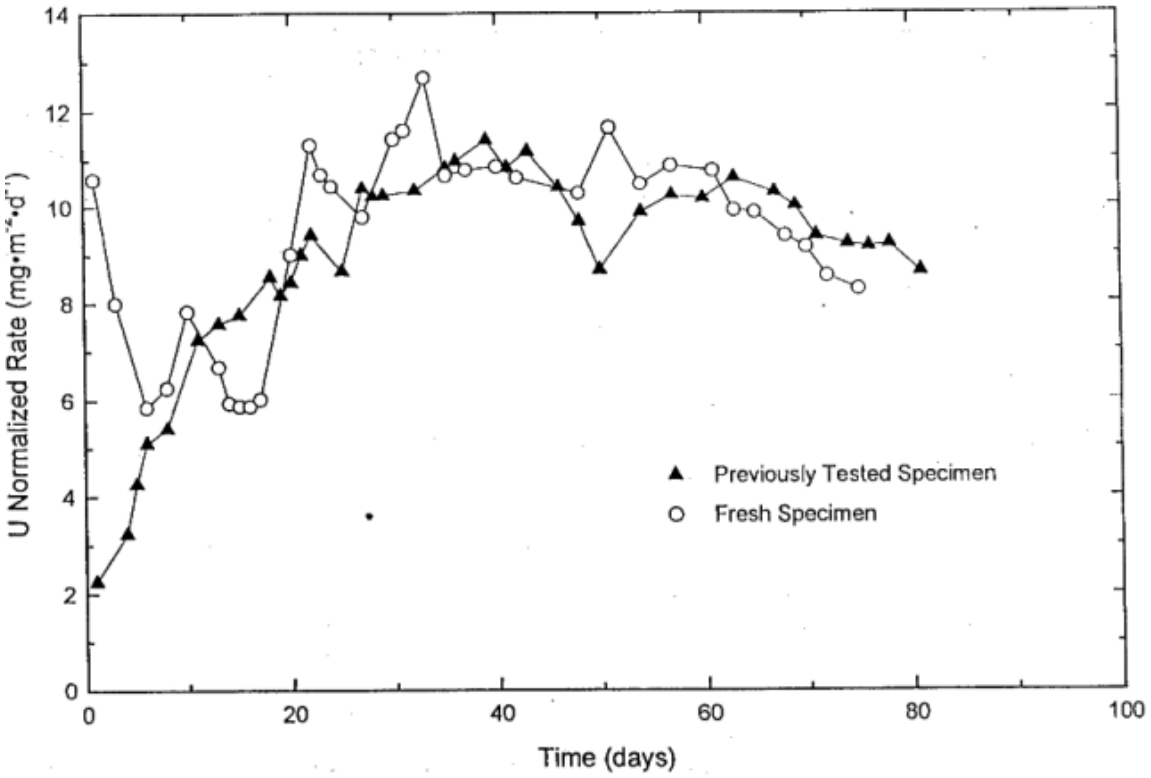

Figure 7.4. Dissolution Rates of ATM-103 fuel grains in 2×10^{-4} M $NaHCO_3/Na_2CO_3$, pH=8, O_2=0.2 atm, 74°C, Flow Rate= ~0.2 mL/min[1]

The isotopes of ^{137}Cs, ^{90}Sr, and ^{99}Tc were also measured along with the uranium dissolution. The results from these dissolutions are shown in Figure 7.5. Both ^{90}Sr and ^{99}Tc appear to have similar dissolution trends as uranium, but ^{137}Cs remains slightly higher. In this test the flow rate was also varied, but had minimal influence on the dissolution at the conditions tested.

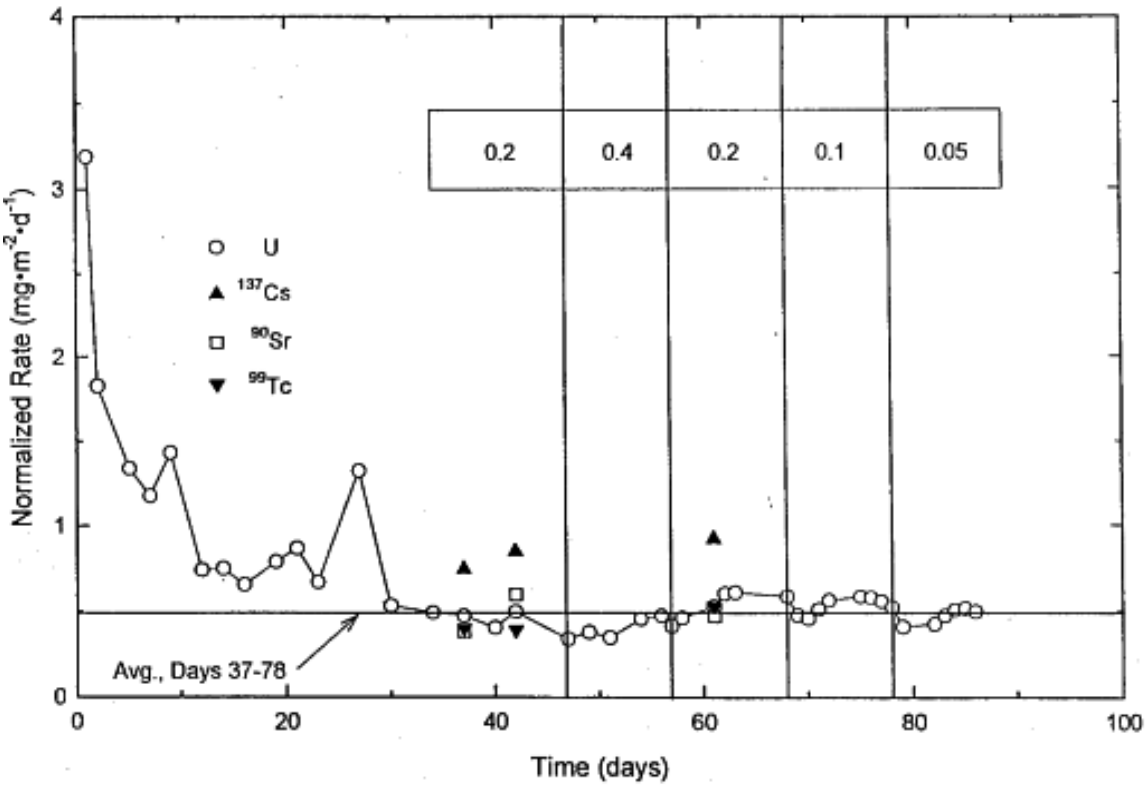

Figure 7.5. Dissolution rates of ATM-103 fuel grains in 2×10^{-4} M $NaHCO_3/Na_2CO_3$, pH=10, O_2=0.2 atm, 21°C (Vertical lines divide regions of different approximate flow rates in mL/min, which are given by the numbers in the box)[1]

Temperature also plays an important role in U dissolution. Figure 7.6 shows a test similar to 7.1, but with a pH of 10 and a temperature of 22°C. As compared with the dissolution rate in Figure 7.1 of 5 to 10 mg m^{-2} d^{-1} this lower temperature shows a dissolution rate of slightly below 2.5 mg m^{-2} d^{-1}. As discussed in detail in Chapter 6, a small increase of pH should not influence the dissolution.

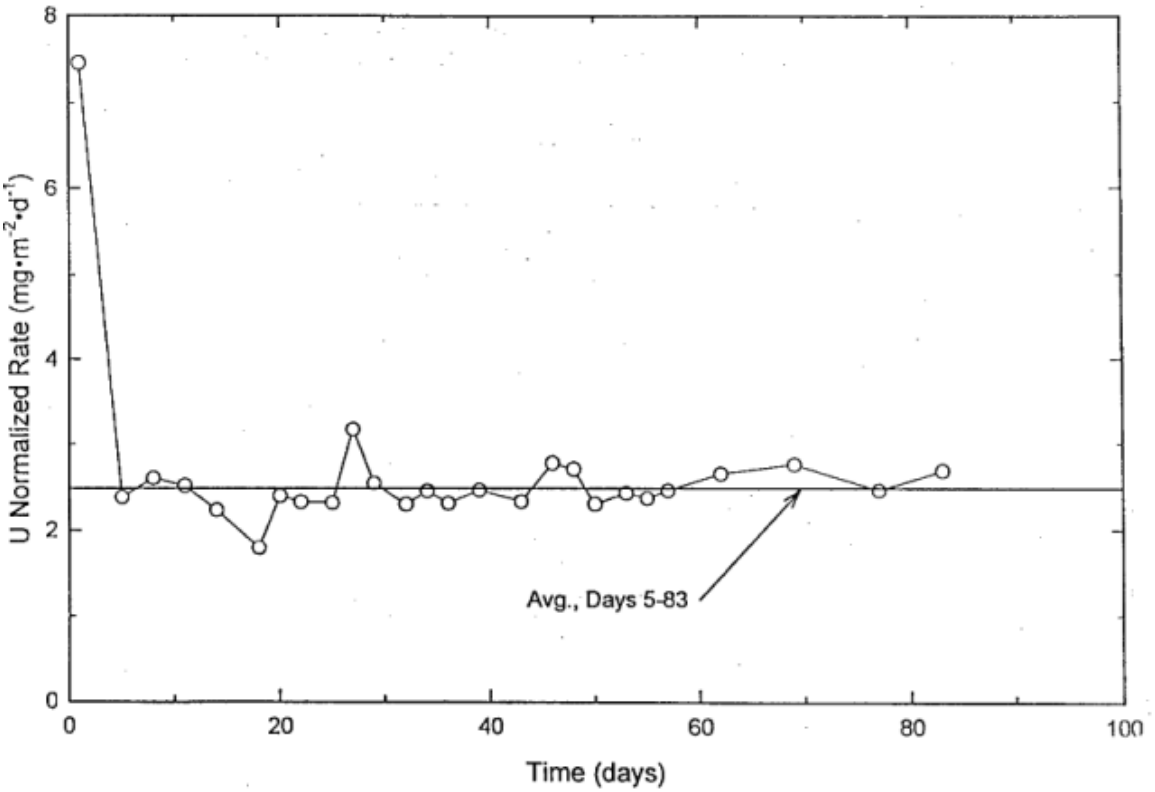

Figure 7.6. Dissolution rates of ATM-103 fuel grains in 2×10^{-3} M $NaHCO_3/Na_2CO_3$, pH=10, O_2=0.2 atm, 22°C, Flow Rate= ~0.2 mL/min[1]

When performing spent fuel dissolution tests, the size of the particle can greatly affect the results. The larger the particle, the more radiation is present. However, self-shielding, especially in the case of alpha radiation, will prevent it from being a linear relationship of dose to the water. Most dissolution rates are normalized to the surface area of and the samples and do not take into account any effects of radiolysis or self shielding. Figure 7.7 compares dissolution rates from both grains and fragments of spent fuel. The dissolution rates of the grains showed similar results for all of the isotopes measured and were around 10 mg m^{-2} d^{-1}. The particles showed U dissolution of around 20 mg m^{-2} d^{-1} with the ^{137}Cs, and ^{99}Tc at higher rates. These higher rates may be partly due to the dissolution from the gap and grain boundaries as opposed to the matrix dissolution, but factors such as normalization to the surface area and changing surface

areas also need to be considered (as was discussed in Chapter 6). In the case of spent fuel self shielding due to larger particles, which reduces the alpha and some beta dose to the water must also be taken into account as was discussed in the radiolysis section in Chapter 6.

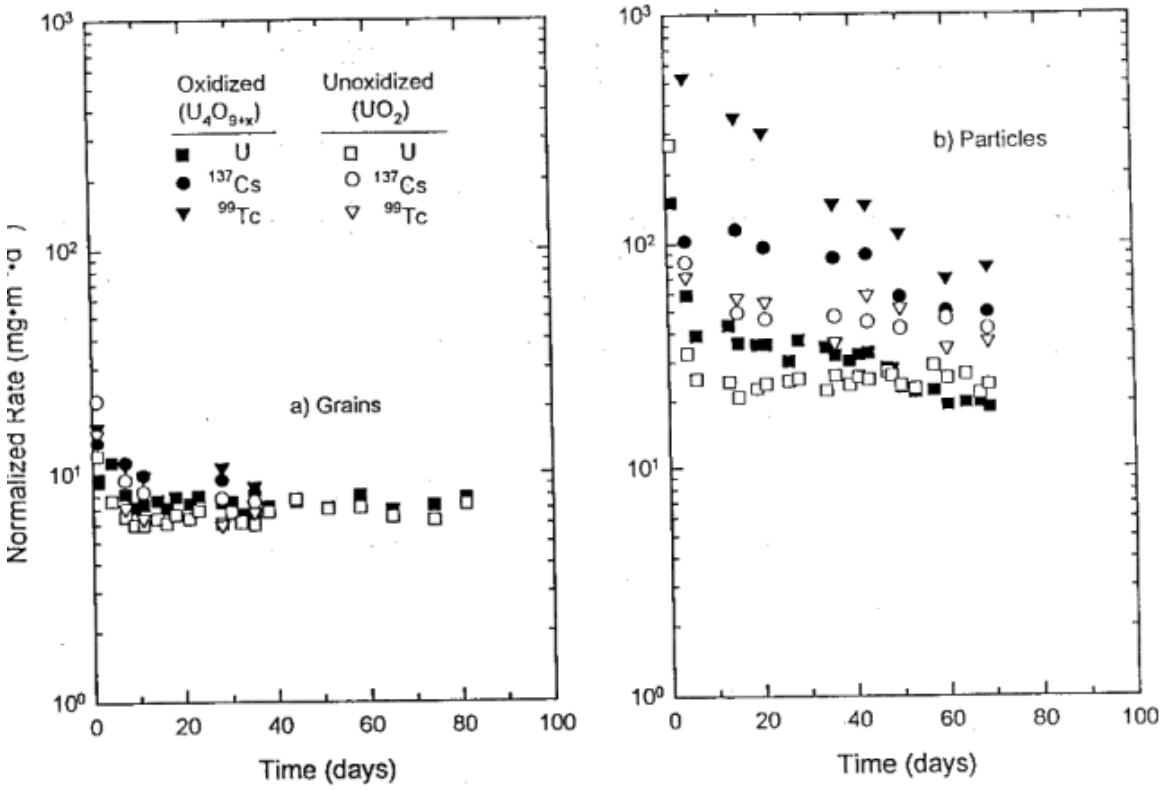

Figure 7.7. Dissolution rates of ATM-103 fuel grains in 2×10^{-3} M $NaHCO_3/Na_2CO_3$, pH=9, O_2=0.2 atm, 50°C, (Legend applies to both grains (7-20 μm) and particles (700-1700μm))[1]

Unirradiated UO_2 was tested as a surrogate for spent fuel at long time periods once the radiolytic field surrounding the fuel has greatly diminished. The results from one of the unirradiated UO_2 tests can be seen in Figure 7.8. Although the flow rate was varied during this experiment, it showed no clear effect on dissolution in the range tested, especially after 140 days. After 140 days the dissolution stabilized around 1.2 mg m^{-2} d^{-1} which was approximately four times lower than that of spent fuel run under similar

conditions that had a dissolution rate of 4.10 mg m^{-2} d^{-1}. This shows that the radiolytic field does significantly affect the oxidation and dissolution of spent fuel and after the field has diminished the dissolution rate should be much lower. But previous research by Gray has shown that this result may be specific to these conditions and Gray and Wilson's conclusion in their report is that there is no difference in rates between spent fuel and unirradiated UO_2.

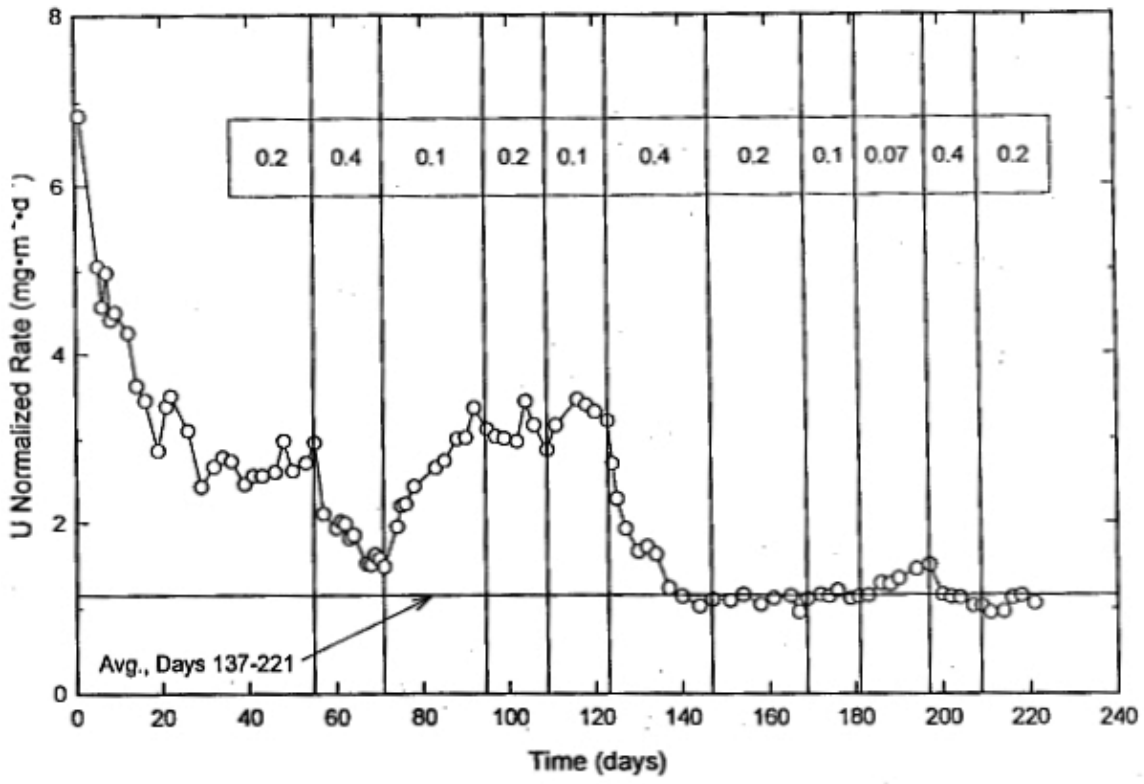

Figure 7.8. Dissolution rates of unirradiated UO_2 in 2×10^{-2} M $NaHCO_3/Na_2CO_3$, pH=8, O_2=0.2 atm, 22°C (Vertical lines divide regions of different approximate flow rates in mL/min, which are given by the numbers in the box)[1]

As was the case with spent fuel as shown in Figure 7.3, dissolved O_2 content has a large influence on the dissolution rates for unirradiated UO_2. Figure 7.9 shows the dissolution rate as the partial pressure of oxygen in the sparge gas was varied between 20% and 0.3%. Each time the O_2 content was dropped a definitive decrease was

observed in the dissolution rate. Correspondingly when the O_2 content was raised a spike could be seen in the dissolution rate.

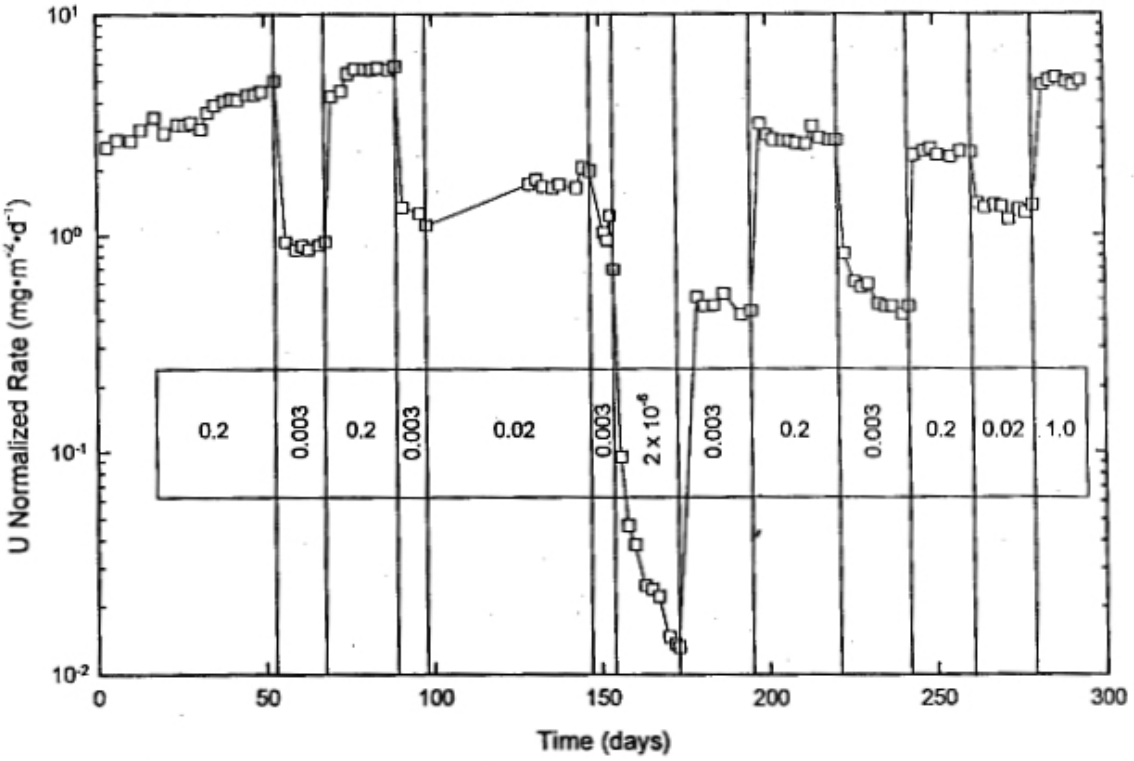

Figure 7.9. Dissolution rates of unirradiated UO_2 in 2×10^{-4} M $NaHCO_3/Na_2CO_3$, pH=10, 22°C (Vertical lines divide regions of different O_2 overpressures (atm), which are given by the numbers in the box)[1]

The results of Gray and Wilson's work showed that under their test conditions the dissolution rate of spent fuel and unirradiated UO_2 was between 0.5 and 20 mg m^{-2} d^{-1}. Gray and Wilson concluded that there was no discernable difference between the rates of spent fuel and unirradiated UO_2, therefore their range was grouped together. Their work showed that dissolved O_2, temperature, and carbonate concentrations all had a profound effect on the dissolution rate. The data regarding the influence the flow rate has on dissolution appeared inconclusive. Gray and Wilson developed an equation to represent their dissolution results:

$$\log(R) = 9.310 + 0.142 \times \log[CO_3] - 16.7 \times \log(P_{O_2}) + 0.140 \times \log[H] - \frac{2130}{T} + 6.81 \times \log(T) \times \log(P_{O_2}) \quad (7.3)$$

where the concentrations are in M, P_{O_2} is in atm, and T is in Kelvin. Applying equation 7.3 to the conditions of the experiment in this thesis work (2×10^{-3} M CO_3 and pH=8) predicts the dissolution rates shown in Table 7.2.

Table 7.2. Dissolution rates predicted by Gray and Wilson Model[1]

T (ºC)	O_2 (ppm)	P_{O_2} (atm)	DR (mg/m^2/d)
25	3.0	0.072	3.1
25	4.2	0.101	3.3
25	5.9	0.142	3.4
25	8.7	0.209	3.6
50	3.0	0.072	5.9
50	4.2	0.101	6.7
50	5.9	0.142	7.7
50	8.7	0.209	8.9
75	3.0	0.072	9.8
75	4.2	0.101	12.1
75	5.9	0.142	14.9
75	8.7	0.209	18.8

Work Performed in Canada

The Canadians have been investigating a repository that differs from Yucca Mountain. The prospective conditions for the Canadian repository will only be oxidizing until a few hundred years after it has been sealed. Therefore, when looking at times of predicted cask failure, reducing conditions may surround the fuel. Also, the current groundwater conditions expected are strongly saline, which is typical in the Canadian Shield.

Tait and Luht[2] have investigated a number of dissolution scenarios while working at Whiteshell Laboratories. Their tests were similar to those of Gray and Wilson[1], as they also utilized flow-through tests to inhibit secondary product formation. In Tait and

Luht's tests, they looked at the effects that temperature, radiation dose, and an O_2 rich versus an O_2 deficient environment would have on the dissolution. Along with these, additional experiments were performed to measure ^{137}Cs and ^{99}Tc release. They used three different leachate solutions: DIW, Standard Canadian Shield Saline Solution (SCSSS), and a standard carbonate (SC) solution. In this summarization of their work, only the results from the DIW and the SC solution will be presented in order to relate to the work being performed in the scope of this thesis.

The flow rate through Tait and Luht's apparatus was approximately 0.58 mL/min, which was determined sufficiently high to maintain a forward rate of reaction. In Tait and Luht's tests, where deoxygenated conditions were required, they purged the system with an Ar/2% H_2/0.02% CO_2 gas mixture. The tests used between 0.1 to 1.0 grams of UO_2 powder. One sample of the powder was prepared at PNNL in order to compare data between the laboratories. Fuels were washed to remove fines and heat treated to ensure an O/M ratio as close to 2.000 as possible. Particle size measurements estimate that the particles had a diameter between 20-105 μm. Along with UO_2 powder, spent fuel samples from CANDU fuel were also utilized, although not washed. For the external irradiation experiments an ^{192}Ir source was used with a dose rate of approximately 300 Gy/hr. Dissolution calculations were carried out in the same manner as Gray and Wilson, utilizing Equations 7.1 and 7.2.

Tait and Luht's first round of tests looked at the dissolution rate of unirradiated UO_2 in DIW and SC solution and their results can be seen in Figures 7.10 and 7.11. The dissolution rate was higher in the SC solution, 1.4 mg m^{-2} d^{-1}, than in the DI water, 5.7×10^{-2} mg m^{-2} d^{-1}. This effect has been seen in numerous experiments and is a result

of the carbonate/bicarbonate's ability to complex with the oxidized UO_2 as was discussed in Chapter 2.

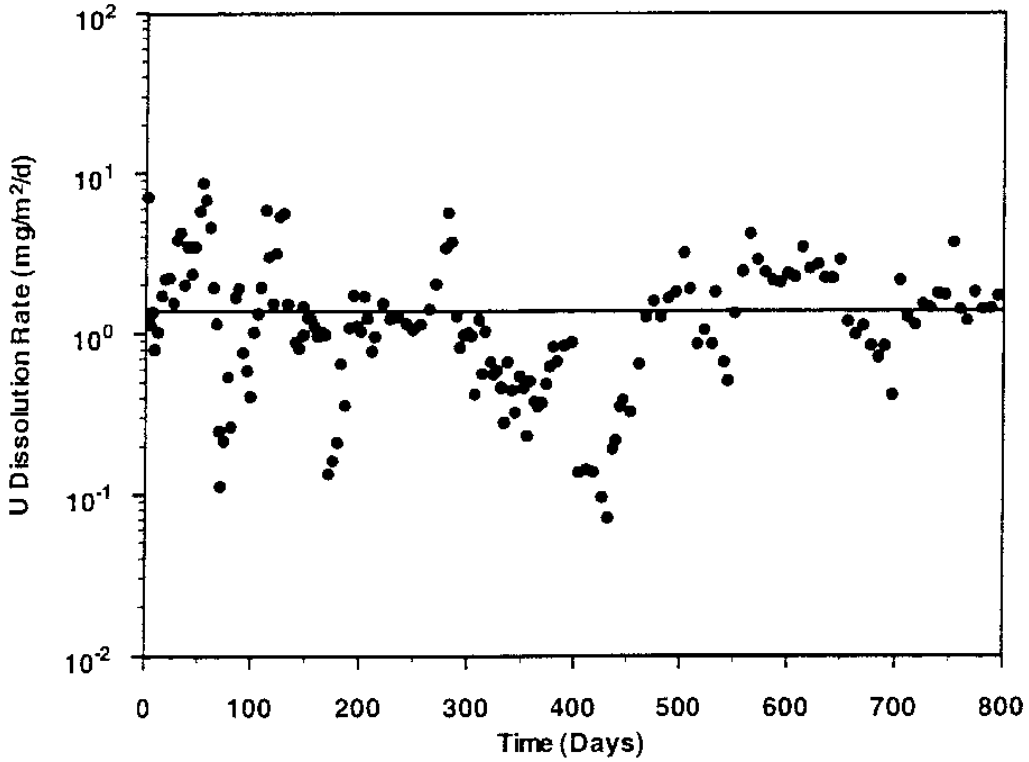

Figure 7.10. Uranium dissolution rate from UO_2 in aerated 0.01 M $NaHCO_3$/0.1 M NaCl (SC) solution at 25°C[2]

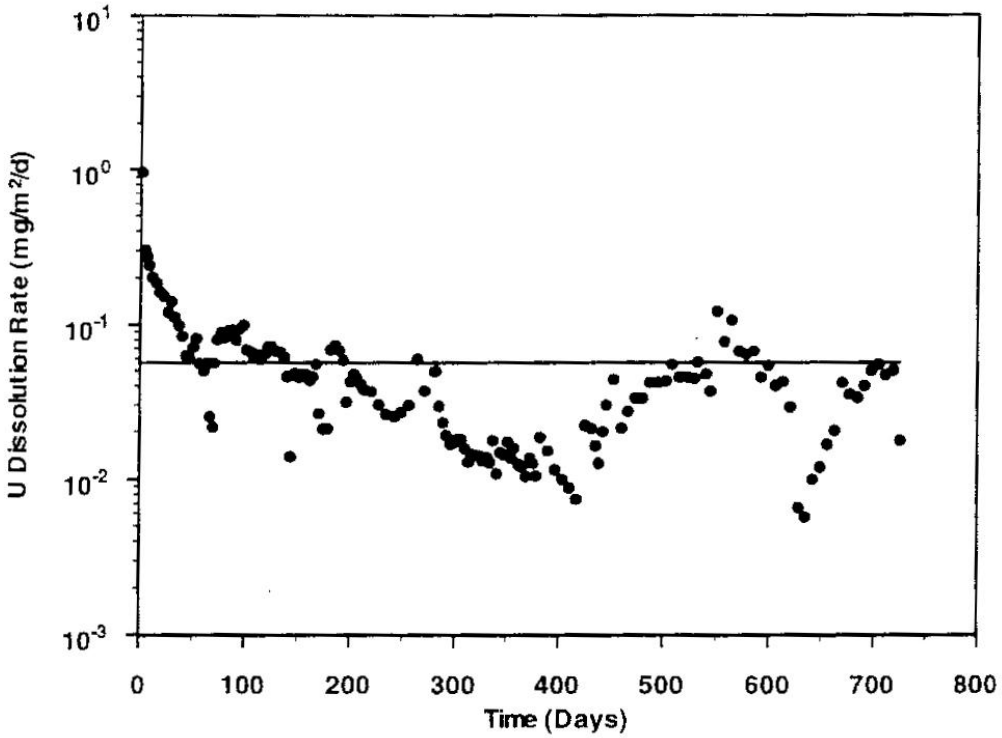

Figure 7.11. Uranium dissolution rate from UO_2 in aerated DIW at 25°C[2]

Tait and Luht investigated the effects of dissolved oxygen on the dissolution and compared their results with similar tests performed, shown in Figure 7.12. Tait and Luht tested two concentrations of dissolved O_2 in their solution, approximately 2 ppb and approximately 8 ppm. In both of their experiments, one with spent fuel and one with unirradiated UO_2, over one order of magnitude difference in the dissolution rate was observed. But, the effect on the dissolution was much more predominate in the unirradiated UO_2. This could be due to the radiation field creating additional oxidizers and therefore lessening the effect of the O_2.

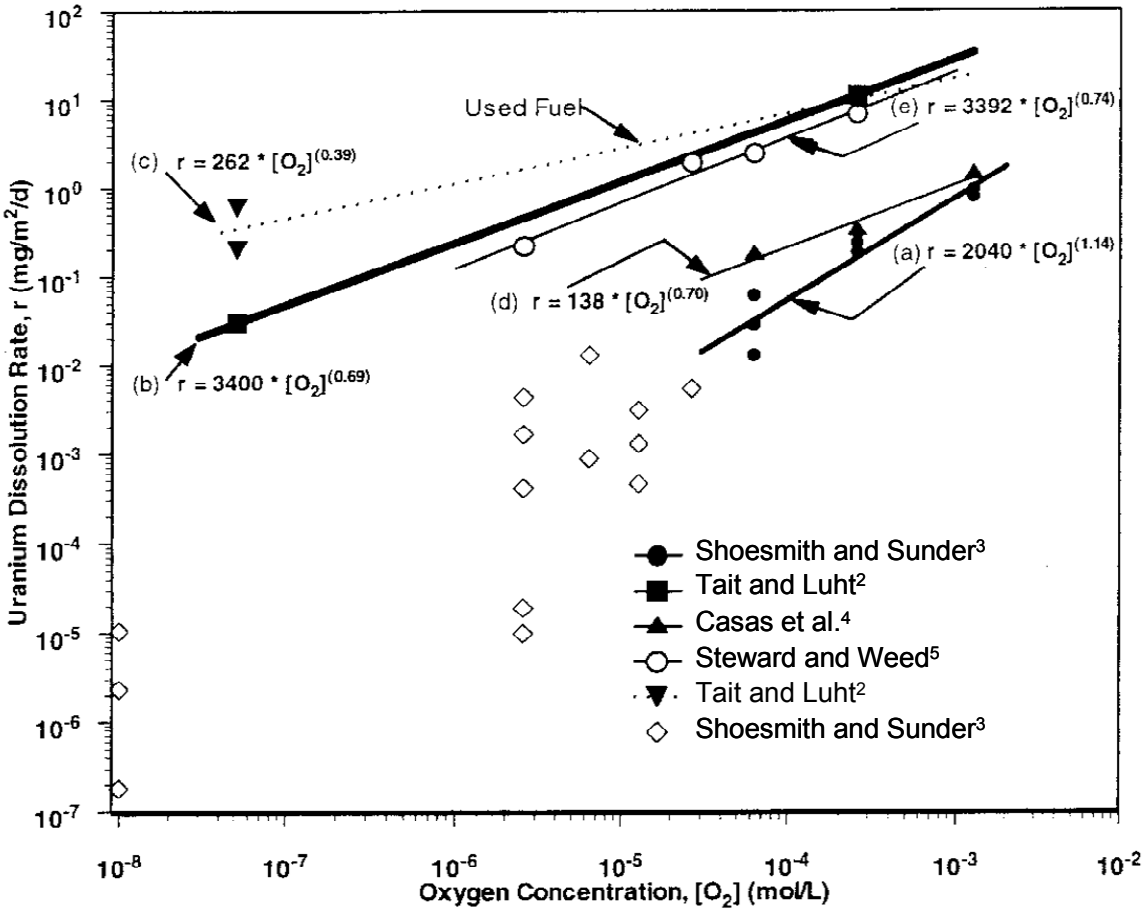

Figure 7.12. Dissolution rates of uranium from UO_2 and used fuel as a function of oxygen concentration at 25°C. Equations represent the best fit to the data.[2]

(a) (●,◇) predicted using the electrochemical model for oxygenated 0.1 M $NaClO_4$ (pH=9.5), Shoesmith and Sunder[3]

(b) (■) measured in SC solution (0.01 M $NaHCO_3$/0.1 M NaCl) (pH ~9) on UO_2, and (▼) used CANDU fuel, Tait and Luht[2]

(c) (▲) measured in oxygenated $MgCl_2$ brine (pH=4.5), Casas et al.[4]

(d) (○) measured in oxygenated 0.02 M $NaHCO_3$ (pH ~9), Steward and Weed[5]

The effect of the quantity of bicarbonate on dissolution was also studied by Tait and Luht. They tested a range of $NaHCO_3$ concentrations between 0.0005 and 0.1 M, with the resulting data shown in Figure 7.13. A large increase can be seen in the dissolution rate between 0.0005 M and 0.01 M solutions. There was much less variation when the solution was increased up to 0.1 M $NaHCO_3$, and each data point was within the uncertainty in the dissolution rate of the previous point. Based upon this data

$NaHCO_3$ helped increase dissolution, but once there was an abundance, minimal additional dissolution was observed.

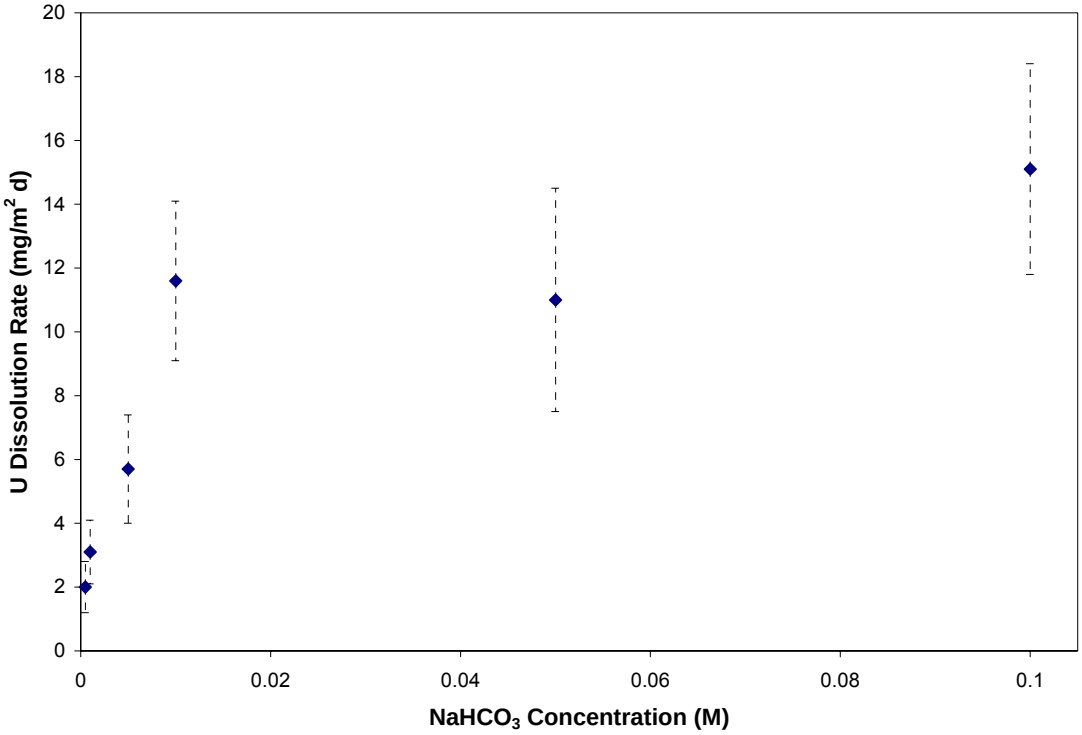

Figure 7.13. Uranium dissolution rate as a function of carbonate/bicarbonate concentration[2]

The results from the temperature variation experiments are shown in Figure 7.14. Tait and Luht tested CANDU spent fuel at 35ºC, 50ºC, and 75ºC. As in previous experiments, their tests showed that with an increase in temperature the U dissolution rate increased. In these tests, between 35ºC and 75ºC an order of magnitude increase in dissolution was observed. The tests also showed good reproducibility in alternating between the temperature levels.

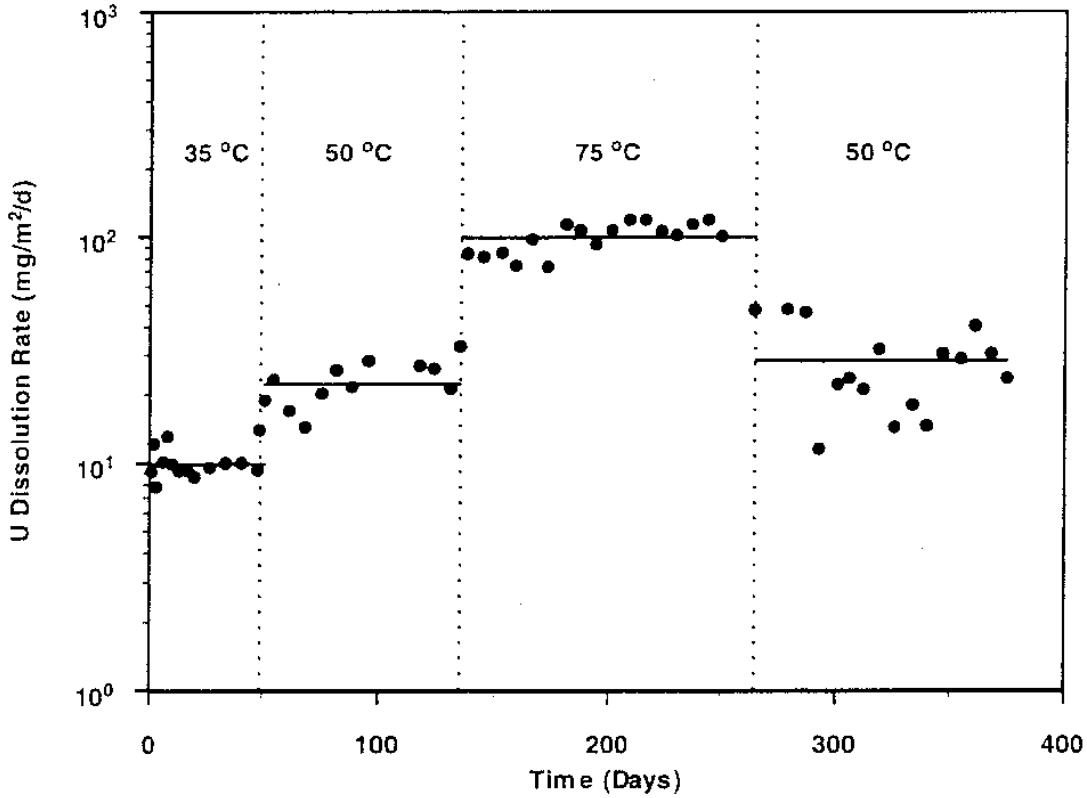

Figure 7.14. Uranium dissolution rate from CANDU UO_2 as a function of temperature in aerated SC solution[2]

The dose rate also showed a significant effect on dissolution, displayed in Figure 7.15. These experiments ranged in dose rate from 10^2 to 10^7 Rad/hr and the dissolution rate was increased by a half to a full order of magnitude for every order of magnitude increase in dose rate under all conditions tested. Again this shows that as spent nuclear fuel decays in a repository setting the potential dissolution rate should decrease.

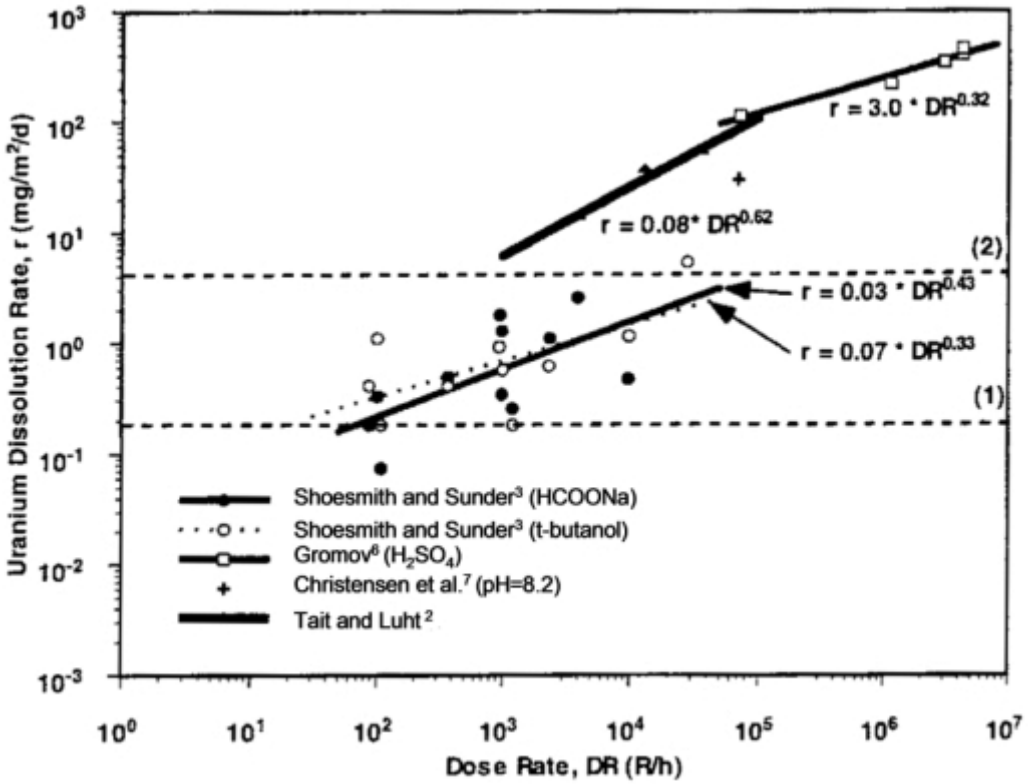

Figure 7.15. Uranium dissolution rate as a function of γ-dose rate at 25°C[2]

Along with measuring the uranium dissolution rate, Tait and Luht also looked at the rate of ^{137}Cs and ^{99}Tc dissolution. As shown in Figure 7.16, both the ^{137}Cs and ^{99}Tc dissolution followed the uranium dissolution. This indicates that they were dissolving from the UO_2 matrix as opposed to the grain boundaries. As before, an increase can also be seen between the dissolution rates in SC solution compared to DIW.

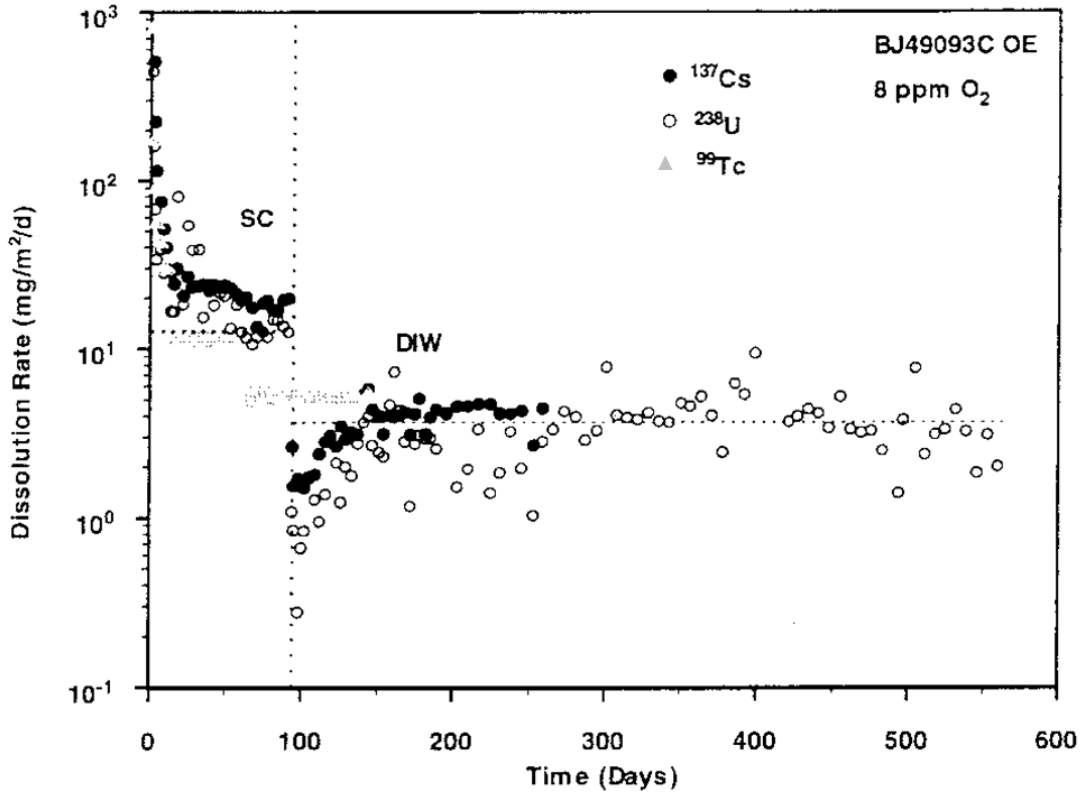

Figure 7.16. Uranium, ^{137}Cs, and ^{99}Tc dissolution rates from CANDU fuel BJ49093C in aerated SC solution and DIW at 25°C[2]

For similar test conditions Gray and Wilson and Tait and Luht's experiments produced comparable results. At approximately room temperature with carbonate on the order of 10^{-2} M and 0.2 atm partial pressure in the sparge gas, Gray and Wilson determined a dissolution rate of 1.2 mg m^{-2} d^{-1} while Tait and Luht concluded a dissolution rate of 1.4 mg m^{-2} d^{-1}. The comparisons of the data obtained from the spent fuel were more difficult due to the difference in radiation levels, as was displayed in Figure 7.15. Although, Gray and Wilson and Tait and Luht's experiments did show similar trends. In both tests, as the temperature decreased, the dissolution rates decreased. Also, it was seen that as the level of dissolved oxygen decreased the dissolution rate decreased.

References

[1]Gray, W., Wilson, C., "Spent Fuel Dissolution Studies FY 1991 to 1994," PNL-10540, December (1995)

[2]Tait, J. C., Luht, J. L., "Dissolution Rates of Uranium from Unirradiated UO_2 and Uranium and Radionuclides from Used CANDU Fuel Using the Single-Pass Flow-Through Apparatus," Atomic Energy of Canada Ltd., Whiteshell Laboratories, 06819-REP-01200-0006 R00, November (1997)

[3]Shoesmith, D., Sunder, S., "An Electrochemistry-Based Model for the Dissolution of UO2," AECL-10488, Atomic Energy of Canada Limited; also SKB Technical Report 91-63, SKB, Stockholm (1991)

[4]Casas, I., Gimenez, J., Pablo, J., Torrero, M. E., "Dissolution of UO_2(s) in MgCl2-brines under different redox conditions," Scientific Basis for Nuclear Waste Management XVI, *Proceedings of the Materials Research Society Symposium*, **294**, 67-72 (1993)

[5]Steward, S. A., Weed, H. C., "Modeling of UO_2 Aqueous Dissolution over a Wide Range of Conditions," Scientific Basis for Nuclear Waste Management XVII, Proceedings of the Materials Research Society Symposium, **333**, 409-416 (1994)

[6]Gromov, V., "Dissolution of Uranium Oxides in the Gamma-Radiation Field," *Radiation Physics and Chemistry*, **18**, 135-146 (1981)

[7]Christensen, H., Forsyth, R., Lundqvist, R., Werme, L. O., "Radiation Induced Dissolution of UO_2," Studsvik Report NS-90/85, Studsvik Energiteknik AB, Nykoping, Sweden (1990)

CHAPTER 8: YUCCA MOUNTAIN MODEL

The current model used to predict the dissolution rate for spent fuel in Yucca Mountain is based upon data collected from single-pass flow-through testing performed at Pacific Northwest National Laboratory and Lawrence Livermore National Laboratory.[1] This testing allows for measurement of the forward rate of reaction without the formation of secondary phases or alteration phases that would inhibit the oxidation and dissolution of the fuel and therefore lower the dissolution rate. The data for the model were obtained over the ranges shown in Table 8.1 and the model is only assumed applicable over these ranges. However, it is stated that the model should be applicable for temperatures up to 100ºC. The pH range tested was from 2 to 10.3 and two separate models were established; one for alkaline conditions (which is the focus of this work) and one for acidic conditions (which will not be discussed here). In the range of neutral pH conditions it has been shown[2,3] and was demonstrated in the development of this model that small variations in the pH have minimal effect on the dissolution rate and therefore this variable was not utilized in the final alkaline model.

Table 8.1. Range of applicability for the Yucca Mountain Model

Variable	Range
T	25ºC to 90ºC
ppO_2	0.002 atm to 0.2 atm
$[CO_3^-]$	0 to 2×10^{-2} M

The data used in the model is comprised from experiments on both unirradiated UO_2 and commercial spent nuclear fuel (CSNF). Initially, separate models were developed for both fuel types and then a combined model was developed from all of the

data which are shown in Tables 8.2 and 8.3. In these tables SA is the surface area, ppO_2 is the partial pressure of O_2 in the sparge gas, DR is the dissolution rate, and F is the fractional release per day.

Table 8.2. CSNF flow-through test dissolution data (alkaline conditions)[1] displaying the dissolution rate and fraction release of U over a range of conditions

Run #	SA (m^2/g)	T (ºC)	[CO_3] (M)	ppO_2	pH	DR (mg m^{-2} d^{-1})	St. Dev.	F (d^{-1})
1	0.0858	49	2.E-03	0.2	9.06	7.58	0.35	6.476E-04
2	0.0858	51	2.E-03	0.2	9.06	8.55	0.76	7.194E-04
3	0.0858	50	2.E-03	0.2	9.06	6.31	0.97	5.177E-04
4	0.0858	24	2.E-02	0.2	8.18	4.15	0.33	3.426E-04
5	0.0858	73	2.E-02	0.2	10.14	13.81	1.36	1.124E-03
5A	0.0858	77	2.E-02	0.2	10.03	21.38	2.39	1.878E-03
6	0.0858	75	2.E-04	0.2	8.13	10.52	1.60	9.265E-04
6A	0.0858	72	2.E-04	0.2	8.13	9.9	0.82	8.683E-04
7	0.0858	23	2.E-04	0.2	10.07	0.58	0.22	4.751E-05
7A	0.0858	20	2.E-04	0.2	10.02	1.08	0.29	8.653E-05
8	0.0858	24	2.E-02	0.2	9.12	3.52	0.31	2.755E-04
9	0.0858	24	2.E-03	0.2	10.11	2.47	0.25	2.128E-04
10	0.0858	27	2.E-04	0.02	8.00	2.12	0.16	1.819E-04
11	0.0858	78	2.E-04	0.02	9.86	1.77	0.15	1.552E-04
12	0.0858	26	2.E-02	0.02	10.04	2.46	0.21	2.082E-04
13	0.0858	77	2.E-02	0.02	8.10	3.57	0.34	3.027E-04
14	0.0858	23	2.E-02	0.002	8.25	2.94	0.09	2.494E-04
15	0.0858	75	2.E-02	0.002	10.12	0.95	0.32	8.624E-05
16	0.0858	76	2.E-04	0.002	8.00	1.41	0.15	1.225E-04
17	0.0858	20	2.E-04	0.002	10.00	0.76	0.19	6.042E-05
18	0.0858	50	2.E-02	0.002	10.05	1.2	0.16	1.076E-04
19	0.0858	22	2.E-03	0.002	8.97	1.95	0.33	1.808E-04
20	0.0858	74	2.E-02	0.02	10.11	5.65	1.05	4.569E-04
21	0.0984	50	2.E-03	0.2	9.05	6.61	0.54	6.578E-04
22	0.277	26	2.E-02	0.2	8.27	1.63	0.32	4.376E-04
23	0.0678	23	2.E-02	0.2	8.02	4.04	0.87	2.837E-04
24	0.0678	76	2.E-02	0.2	8.04	9.41	2.82	6.457E-04
25	0.0678	23	2.E-04	0.2	7.93	2.64	0.34	1.805E-04
26	0.0678	75	2.E-04	0.2	7.75	10.99	1.72	7.918E-04
27	0.136	23	2.E-02	0.2	8.27	3.62	0.64	4.453E-04
28	0.1023	25	2.E-02	0.2	8.30	3.83	0.22	3.873E-04
29	0.1023	76	2.E-02	0.2	8.30	6.9	1.04	6.939E-04
30	0.1023	25	2.E-04	0.2	7.56	2.85	0.56	2.737E-04
31	0.1023	74	2.E-04	0.2	7.56	9.45	1.37	9.902E-04
33	0.1023	75	2.E-02	0.002	8.06	1.35	0.36	1.552E-04
34	0.1023	27	2.E-04	0.002	7.76	2.03	0.20	2.071E-04
35	0.1023	74	2.E-04	0.002	7.74	3.5	0.46	3.612E-04
36	0.0837	27	2.E-02	0.2	8.02	3.24	0.54	2.739E-04
37	0.0837	76	2.E-02	0.2	7.96	11.94	3.97	9.558E-04
38	0.0837	27	2.E-04	0.2	7.62	3.74	0.47	3.050E-04
61	0.133	26	2.E-02	0.2	8.14	3.94	0.52	5.262E-04
62	0.133	76	2.E-02	0.2	8.12	5.61	1.56	7.769E-04
63	0.133	26	2.E-04	0.2	7.63	2.49	0.89	2.908E-04
64	0.133	76	2.E-04	0.2	7.16	6.77	1.49	9.008E-04
65	0.133	76	2.E-02	0.002	8.07	0.85	0.19	1.217E-04

Table 8.3. Unirradiated UO_2 flow-through test dissolution data (alkaline conditions)[1] displaying the dissolution rate of U over a range of conditions

Run #	T (ºC)	$[CO_3]$ (M)	ppO_2	pH	DR (mg m^{-2} d^{-1})
4	25	2.E-02	0.2	8.7	2.42
5	75	2.E-02	0.2	10.3	77.4
6	75	2.E-04	0.2	9.1	10.9
7	25	2.E-04	0.2	9	2.55
8	25	2.E-02	0.2	9.4	6.72
9	25	2.E-03	0.2	9.3	9.34
10	26	2.E-04	0.02	7.8	0.12
11	75	2.E-04	0.02	9.7	9.21
12	26	2.E-02	0.02	10.1	1.87
13	75	2.E-02	0.02	8.5	5.11
14	25	2.E-02	0.002	8	0.22
15	75	2.E-02	0.002	9.8	5.61
16	75	2.E-04	0.002	8.7	0.51
17	26	2.E-04	0.002	9.3	0.23
18	50	2.E-02	0.002	9.9	4.6
19	26	2.E-03	0.002	9	1.52
21	50	2.E-03	0.02	8.9	12.3
22	50	2.E-03	0.02	8.8	7.96
23	50	2.E-03	0.02	8.9	10.4
24	75	2.E-04	0.2	9.5	6.48
25	75	2.E-03	0.2	9.6	23.3
26	75	2.E-02	0.2	8.5	54

Three equations were generated to fit this data: an equation for commercial spent nuclear fuel (CSNF), one for unirradiated UO_2 and then a third equation was produced to combine the previous two equations in order to create a general case. The general equation for the models is:

$$\mathrm{Log}_{10}(\mathrm{DR}) = a_o + \frac{a_1}{T} + a_2 pO_2 + a_3 pCO_3 \tag{8.1}$$

where DR is the dissolution rate in $\frac{mg}{m^2 d}$, T is the temperature in Kelvin,

$$pO_2 = -\mathrm{Log}_{10}(ppO_2) \tag{8.2}$$

$$pCO_3 = -Log_{10}\left([HCO_3^-] + [CO_3^{2-}]\right) \quad (8.3)$$

ppO_2 is the partial pressure of O_2, and a_o, a_1, a_2, and a_3 are the model parameters defined in Table 8.4.

Table 8.4. Linear regression models for CSNF, UO_2, and Combined Model[1]

Model Term-CSNF	Parameter	Standard Error	Significance
a_0	3.424	0.508	<0.001
a_1	-776.683	157.894	<0.001
a_2	-0.279	0.0441	<0.001
a_3	-0.0378	0.0395	0.344
Model Term-UO_2	Parameter	Standard Error	Significance
a_0	7.618	1.313	<0.001
a_1	-1777.525	410.042	<0.001
a_2	-0.473	0.108	<0.001
a_3	-0.286	0.103	0.013
Model Term-Comb	Parameter	Standard Error	Significance
a_0	4.705	0.601	<0.001
a_1	-1093.826	186.829	<0.001
a_2	-0.338	0.0506	<0.001
a_3	-0.102	0.0471	0.034

These variables in Table 8.4 substituted into Equation 8.1 produce the equations below for modeling the dissolution rate of commercial spent nuclear fuel, UO_2, and a combined effect, respectively:

$$\begin{aligned} Log_{10}(\text{DR - CSNF}) = (3.424 \pm 0.508) - \frac{(776.683 \pm 157.894)}{T} \\ - (0.279 \pm 0.0441) \times pO_2 - (0.0378 \pm 0.0395) \times pCO_3 \end{aligned} \quad (8.4)$$

$$\mathrm{Log}_{10}\left(\mathrm{DR\text{-}UO_2}\right) = \left(7.618 \pm 1.313\right) - \frac{\left(1777.525 \pm 410.042\right)}{\mathrm{T}} - \left(0.473 \pm 0.108\right) \times \mathrm{pO_2} - \left(0.286 \pm 0.103\right) \times \mathrm{pCO_3} \quad (8.5)$$

$$\mathrm{Log}_{10}\left(\mathrm{DR\text{-}Comb}\right) = \left(4.705 \pm 0.601\right) - \frac{\left(1093.826 \pm 186.829\right)}{\mathrm{T}} - \left(0.338 \pm 0.0506\right) \times \mathrm{pO_2} - \left(0.102 \pm 0.0471\right) \times \mathrm{pCO_3} \quad (8.6)$$

For the condition where the sodium bicarbonate concentration is 2×10^{-3} M (sodium carbonate =0 M), Equation 8.3 becomes

$$\mathrm{pCO_3} = -\mathrm{Log}_{10}[2 \times 10^{-3}] = 2.699 \quad (8.7)$$

Substituting Equation 8.7 into Equations 8.4, 8.5, and 8.6 and propagating the error through the methods described in "Data Analysis" by Meyer[4], produces:

$$\mathrm{Log}_{10}\left(\mathrm{DR\text{-}CSNF}\right) = \left(3.322 \pm 0.519\right) - \frac{\left(776.683 \pm 157.894\right)}{\mathrm{T}} - \left(0.279 \pm 0.0441\right) \times \mathrm{pO_2} \quad (8.8)$$

$$\mathrm{Log}_{10}\left(\mathrm{DR\text{-}UO_2}\right) = \left(6.846 \pm 1.342\right) - \frac{\left(1777.525 \pm 410.042\right)}{\mathrm{T}} - \left(0.473 \pm 0.108\right) \times \mathrm{pO_2} \quad (8.9)$$

$$\mathrm{Log}_{10}\left(\mathrm{DR\text{-}Comb}\right) = \left(4.430 \pm 0.614\right) - \frac{\left(1093.826 \pm 186.829\right)}{\mathrm{T}} - \left(0.338 \pm 0.0506\right) \times \mathrm{pO_2} \quad (8.10)$$

In the development of the models derived above, all solutions were initially at room temperature and pO_2 represented the partial pressure of the sparge gas for the system. Therefore, for applicability to the models, when calculating pO_2, if the initial solutions are not at room temperature then the dissolved O_2 content at that temperature must be converted to the equivalent partial pressure needed at room temperature to achieve the same dissolved O_2 levels in solution. Looking at the cases of 3.0 ppm, 4.2 ppm, 5.9 ppm, and 8.7 ppm (which are the concentrations tested in this thesis that represent dissolved O_2 levels at slightly elevated temperatures) requires Henry's Law:

$$[O_2] = k_H \times pp_{O_2} \tag{8.11}$$

where pp_{O_2} is the partial pressure of O_2 being equilibrated through the solution and

$$k_H = k_H^o \times \exp\left(\frac{-\Delta_{soln}H}{R} \times \left(\frac{1}{T} - \frac{1}{T^o}\right)\right) \tag{8.12}$$

where T is the temperature of solution in Kelvins, $k_H^o = 1.3 \times 10^{-3}$ M, $T^o = 298.15$ K, and $\frac{-\Delta_{soln}H}{R} = 1500$ K. Table 8.5 shows the conversion of the dissolved gas concentration in parts per million to partial pressures and the pO_2 equivalent as calculated by Equation 8.2. Equations 8.8, 8.9, and 8.10 at each ppm level in Table 8.2. are shown over a range of temperatures in Figures 8.1 through 8.4.

Table 8.5. Conversion of ppm to ppO_2 and pO_2

ppm	ppO_2	pO_2
3.0	0.072	1.142
4.2	0.101	0.996
5.9	0.142	0.848
8.7	0.209	0.680

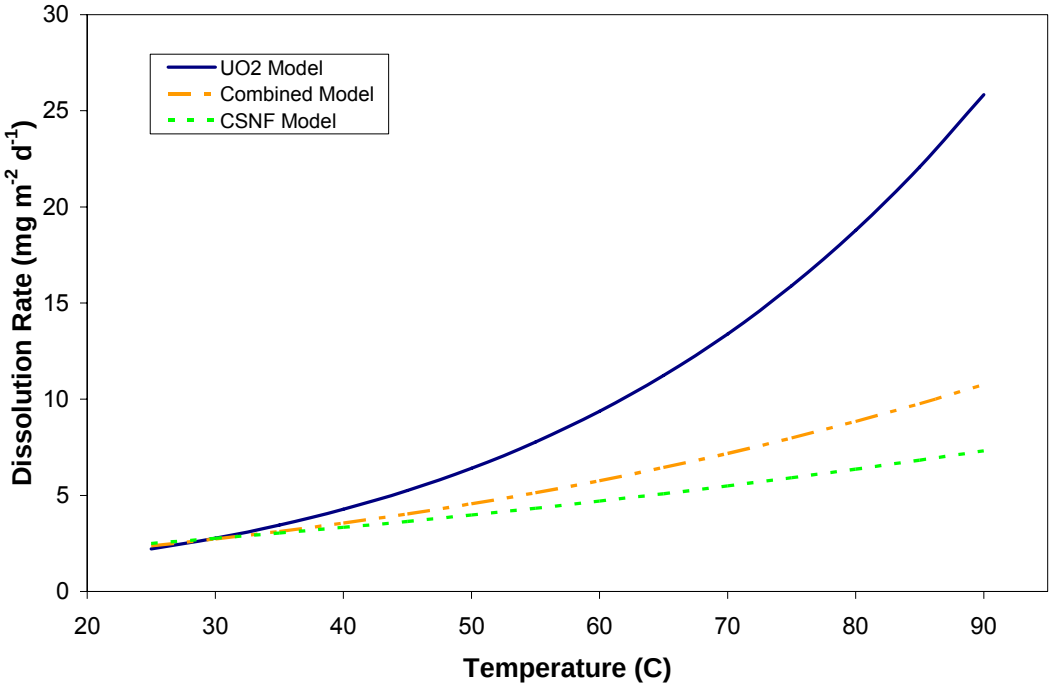

Figure 8.1. Yucca Mountain Model fit of 3.0 ppm dissolved O_2 content and 2×10^{-3} $NaHCO_3$

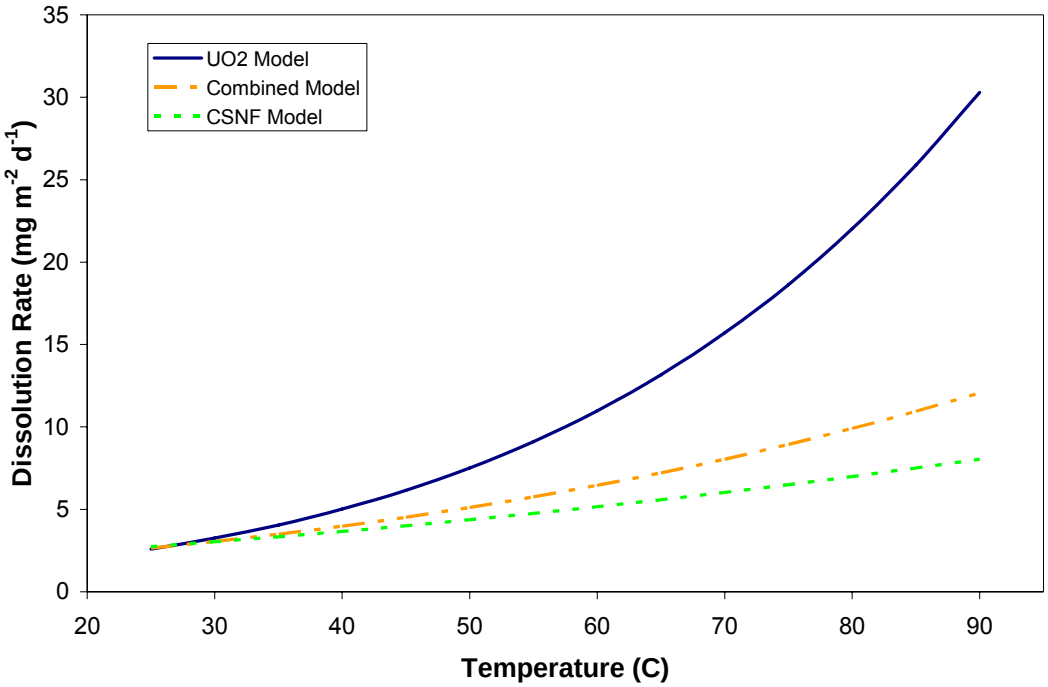

Figure 8.2. Yucca Mountain Model fit of 4.2 ppm dissolved O_2 content and 2×10^{-3} $NaHCO_3$

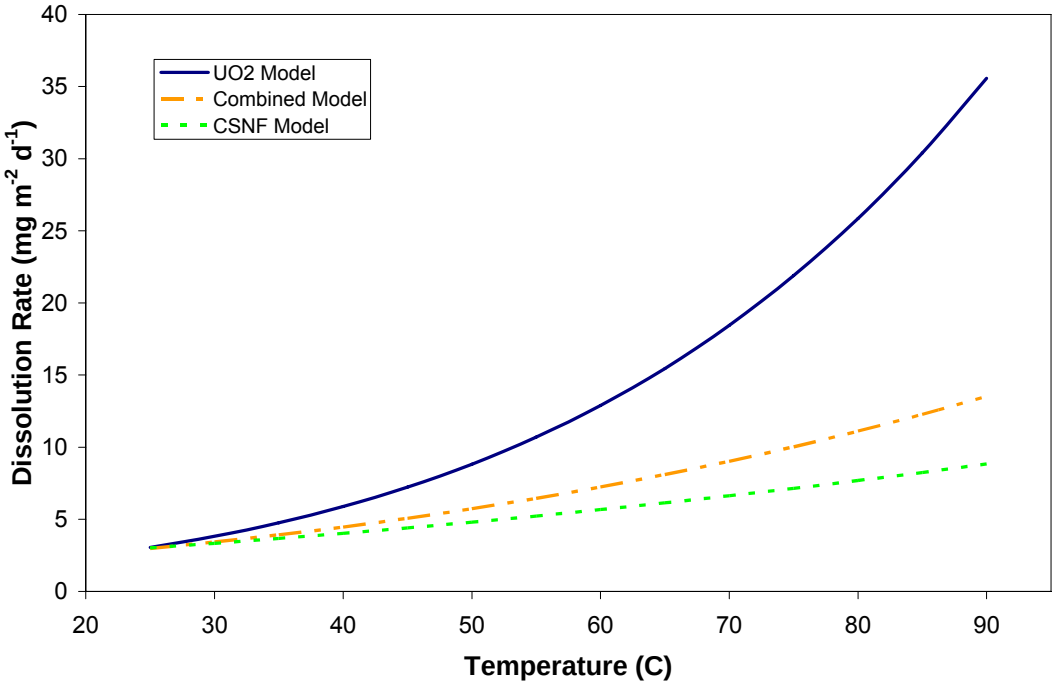

Figure 8.3. Yucca Mountain Model fit of 5.9 ppm dissolved O_2 content and 2×10^{-3} $NaHCO_3$

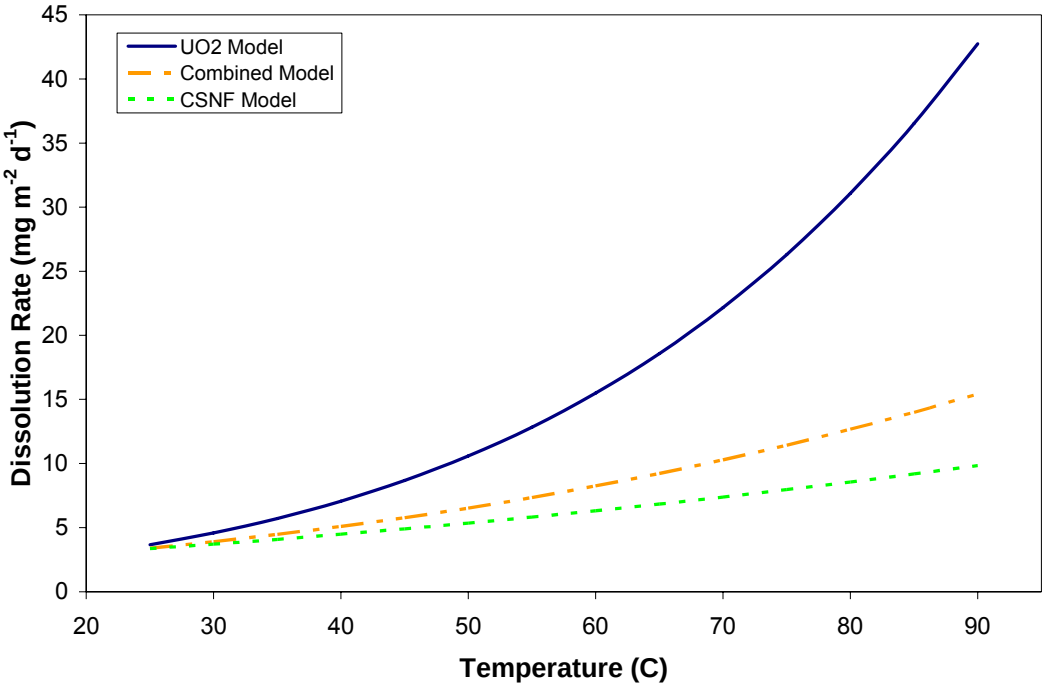

Figure 8.4. Yucca Mountain Model fit of 8.7 ppm dissolved O_2 content and 2×10^{-3} $NaHCO_3$

In Figures 8.1 through 8.4 the UO_2 model had a higher dissolution rate than the CSNF model, with the Combined Model falling in between the other two models. In these figures there was minimal dependence on dissolved O_2 in the CSNF model. Although large differences were observed between CSNF tests in Table 8.2 these O_2 concentrations spanned 3 orders of magnitude, while those graphed in Figures 8.1 through 8.4 ranged only between 3.0 and 8.7 ppm. The models predict the values in Table 8.6 for the conditions that were run in this research for each of the model types. In some cases, the error becomes large as a result of subtracting like numbers with sizeable uncertainties in Equations 8.8, 8.9, and 8.10.

Table 8.6. Predicted dissolution rates of the CSNF, UO_2, and Combined Model

Conditions		Predicted Dissolution Rate (mg m^{-2} d^{-1})					
ºC	ppm level	CSNF Model	error	UO_2 Model	error	Combined Model	error
25	3.0	2.5	4.3	2.2	9.8	2.4	4.8
25	4.2	2.7	4.7	2.6	11.5	2.7	5.4
25	5.9	3.0	5.2	3.0	13.5	3.0	6.0
25	8.7	3.4	5.8	3.7	16.2	3.4	6.9
50	3.0	4.0	6.5	6.4	27.3	4.6	8.9
50	4.2	4.4	7.2	7.5	32.0	5.1	9.9
50	5.9	4.8	7.9	8.8	37.5	5.7	11.1
50	8.7	5.4	8.8	10.6	45.1	6.5	12.7
75	3.0	5.9	9.4	15.9	65.5	8.0	15.0
75	4.2	6.5	10.3	18.6	76.8	8.9	16.8
75	5.9	7.1	11.4	21.9	90.1	10.0	18.9
75	8.7	8.0	12.7	26.3	108.3	11.4	21.5

In order to present a more generalized case pertaining to Yucca Mountain, a fragmented fuel geometry, resulting from the cracking due to thermal gradients, was estimated. This converted Equation 8.6 to show the fractional release of fuel per day.

$$\mathrm{Log}_{10}(\mathrm{F}) = \mathrm{Log}_{10}(\mathrm{A}) + a_o + \frac{a_1}{\mathrm{T}} + a_2 \mathrm{pO}_2 + a_3 \mathrm{pCO}_3 \qquad (8.13)$$

where F is the fractional matrix dissolution rate in d^{-1}, A is the fuel effective specific surface area in m^2/mg, and a_o, a_1, a_2, and a_3 are the model parameters defined in Table 8.7.

Table 8.7. Parameters for Fractional Release Model[1]

Fractional Release Model	Parameter	Standard Error
LOG(A)	-6.7	Triangular Distribution
a_0	4.705	0.601
a_1	-1093.826	186.829
a_2	-0.338	0.0506
a_3	-0.102	0.0471

*Distribution minimum = -7.3; distribution maximum = -5.4;
distribution apex = -6.7

Adding the terms into Equation 13 and the pCO_3 calculated in Equation 8.7 results in the equation:

$$\mathrm{Log}_{10}(\mathrm{FR}) = (-1.083 \pm 1.220) - \frac{(1093.826 \pm 186.829)}{\mathrm{T}} - (0.338 \pm 0.0506) \times \mathrm{pO}_2 \tag{8.14}$$

Figure 8.5 shows the results of Equation 8.14 plotted for 3.0, 4.2, 5.9, and 8.7 ppm over the temperature range of 25 to 90ºC. The results for the conditions that were run in this research are presented in Table 8.8.

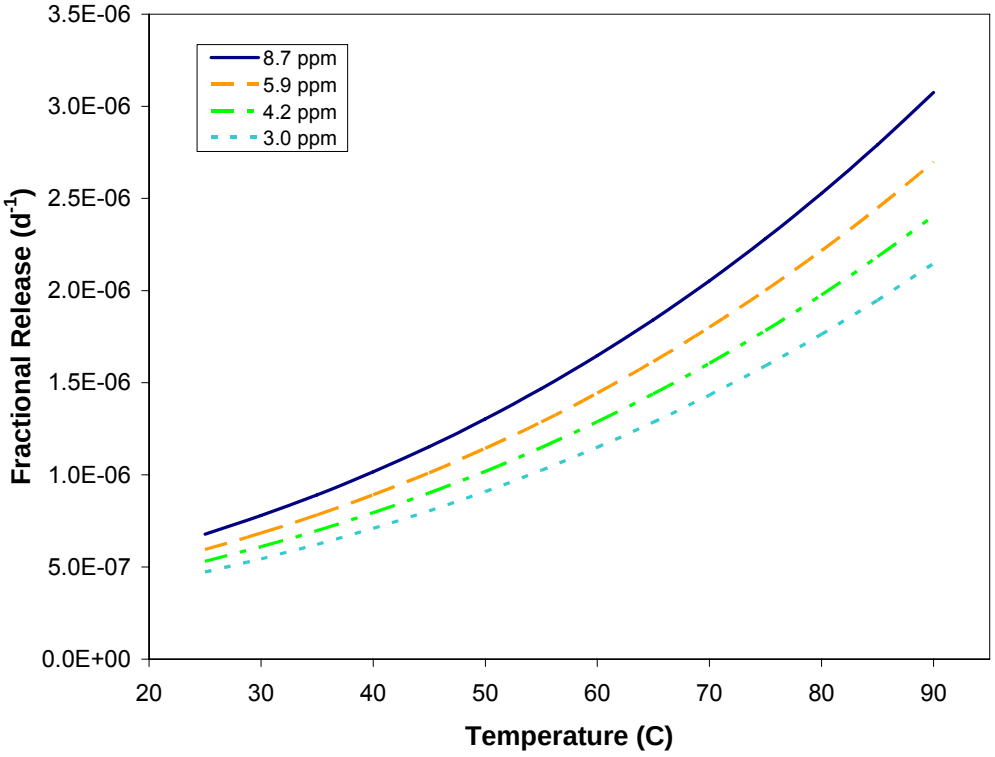

Figure 8.5. Fractional release rate as a function of temperature at 3.0, 4.2, 5.9, and 8.7 ppm as predicted by the Yucca Mountain Model

Table 8.8. Predicted results of Yucca Mountain Model for fractional release per day

Conditions		Fractional Release (d^{-1})		Conditions		Fractional Release (d^{-1})		Conditions		Fractional Release (d^{-1})	
ºC	ppm level	FR Model	error	ºC	ppm level	FR Model	error	ºC	ppm level	FR Model	error
25	3.0	4.732E-07	1.495E-06	50	3.0	9.096E-07	2.829E-06	75	3.0	1.592E-06	4.888E-06
25	4.2	5.302E-07	1.713E-06	50	4.2	1.019E-06	3.177E-06	75	4.2	1.784E-06	5.475E-06
25	5.9	5.947E-07	1.953E-06	50	5.9	1.143E-06	3.555E-06	75	5.9	2.001E-06	6.140E-06
25	8.7	6.781E-07	2.219E-06	50	8.7	1.304E-06	3.965E-06	75	8.7	2.281E-06	7.000E-06

References

[1]CSNF Waste Form Degradation: Summary Abstraction, ANL-EBS-MD-000015 Rev 02, (2004)

[2]Clarens, F., et al., "The Oxidative Dissolution of Unirradiated UO_2 by Hydrogen Peroxide as a Function of pH," *Journal of Nuclear Materials*, **345**, 225-231 (2005)

[3]Torrero, M., et al., "Kinetics of Corrosion and Dissolution of Uranium Dioxide as a Function of pH," *International Journal of Chemical Kinetics*, **29**, 261-267 (1997)

[4]Meyer, Stuart L., Data Analysis for Scientists and Engineers, John Wiley & Sons, Inc., New York, p. 40-41 (1975)

CHAPTER 9: EXPERIMENTAL SETUP

Preparation of Fuel

All initial fuel samples were unirradiated UO_2 pellets obtained from a commercial vendor, and all experiments were performed at Pacific Northwest National Laboratory. During preparation of the fuel samples the pellet was placed in a shearing device and broken to obtain approximately one gram per sample of fragment pieces. Once these were separated out the remaining pellet was crushed to a powder using a mortar and pestle. The powder was then placed in a shaker/tapper sieve system consisting of a 25 μm sieve, a 10 μm sieve, and a catch tray. After sieving for at least 18 hours the powder remaining between the 25 μm and 10 μm sieves was collected. In these tests the fuel was not washed in order to prevent oxidation of the surface prior to testing, but the sieving minimized fines in the powder. Once in powder form, approximately 200 mg samples were weighed out for each column.

Test Matrix

The test matrix for the experiments performed is in Table 9.1. All tests utilized $2\times10^{-3} \pm 2\times10^{-4}$ M sodium bicarbonate in deionized water that was maintained at a pH between 7 and 8.5. The sparge gas used was 20.9% O_2, 2000 ppm CO_2 with a balance of N_2 for Tests 1, 3, 4, and 5, and 10.3% O_2, 2000 ppm CO_2 with a balance of N_2 for Test 2. Test 1 baths were set to match the temperature of the corresponding ovens, while the temperatures of the baths in Tests 2 through 5 were adjusted to achieve the desired dissolved O_2 levels as determined by Henry's Law, discussed in Chapter 4. In Test 1 the

baths were at 25ºC, 50ºC, and 75ºC, while the temperatures of all of the baths for Tests 2, 3, 4, and 5 were 60ºC, 75ºC, 50ºC, 25ºC respectively. Test 2 temperature and O_2 conditions did not follow Henry's Law due to the sparge gas containing a lower partial pressure of O_2 than atmospheric conditions and the baths not being a closed system. Adjustments were made with the temperature in order to achieve 3.0 ppm with the 10.3% partial pressure of O_2 as verified by the inline O_2 probes. Test 1 examined three flow rates, approximately 0.10, 0.15, and 0.20 mL/min, for each type of powder sample and all fragment samples were run at approximately 0.20 mL/min. In Tests 2 through 5 all samples were run with a flow rate of approximately 0.20 mL/min.

Table 9.1. Test matrix of temperature and dissolved O_2 conditions for various fuel types

Test	Powders Tested	Fragments Tested	Temp (ºC)	Dissolved O_2 (ppm)
1	0, 4, 8 wt% Gd_2O_3	0, 7 wt% Gd_2O_3	25	8.7
			50	5.9
			75	4.2
2	0, 1.25, 2, 3, 4 wt% Gd_2O_3	0, 2, 3 wt% Gd2O3	25	3.0
			50	3.0
			75	3.0
3	0, 1.25, 2, 3, 4 wt% Gd_2O_3	0, 2, 3 wt% Gd_2O_3	25	4.2
			50	4.2
			75	4.2
4	0, 1.25, 2, 3, 4 wt% Gd_2O_3	0, 2, 3 wt% Gd_2O_3	25	5.9
			50	5.9
			75	5.9
5	0, 1.25, 2, 3, 4 wt% Gd_2O_3	0, 2, 3 wt% Gd_2O_3	25	8.7
			50	8.7
			75	8.7

SPFT Setup

Three identical set-ups were used in the single-pass flow-through (SPFT) testing, with each consisting of a bath system and pumps going to 8 columns inside an oven. The bath system consisted of an outer surrounding bath to maintain temperature and two tanks submerged in the bath, each with its own thermocouple. The feedwater tank pumped the solution to the columns in the oven, while a separate preequilibration tank allowed for the desired temperature and dissolved O_2 levels to be achieved prior to addition to the feedwater bath in order to minimize any shocks to the system. The solution in the feedwater bath was continuously circulated to maintain homogeneity. During the recirculation, the solution was monitored using in-line pH and O_2 sensors. A schematic of the bath set-up is shown in Figure 9.1 and a photograph of the system is shown in Figure 9.2.

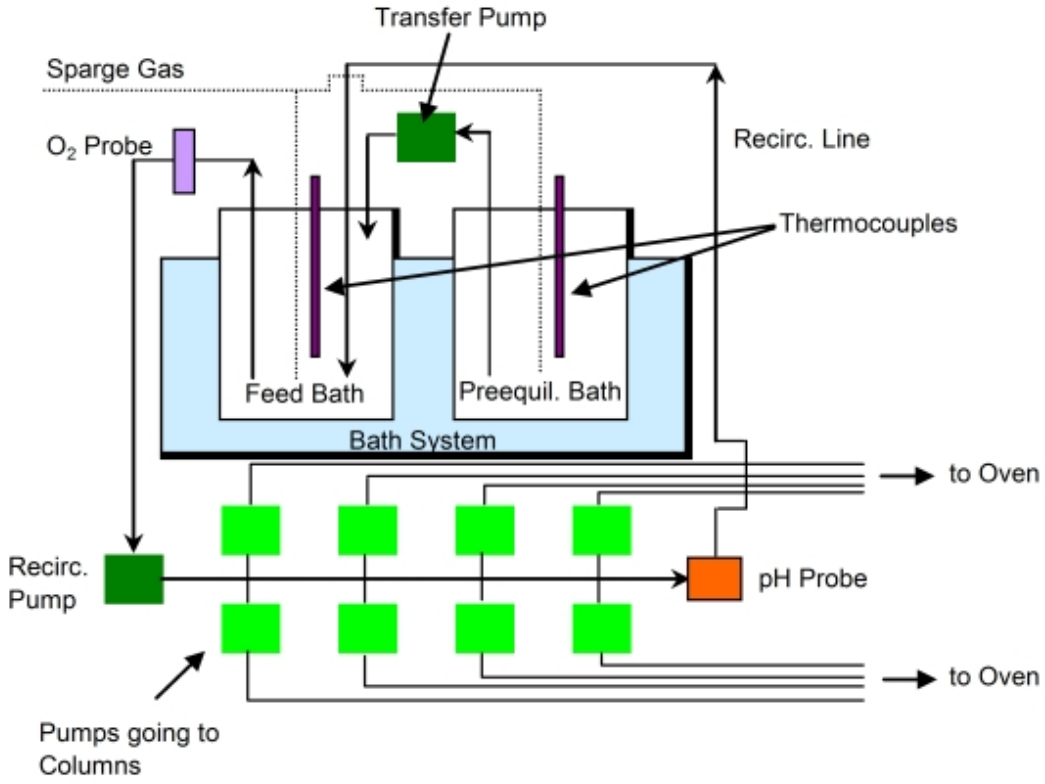

Figure 9.1. Bath system schematic

Figure 9.2. Bath system and pumps

Each set of solution feed lines coming from a bath system went into a separate oven, displayed in Figure 9.3, which was enclosed in a ventilated canopy, shown in Figure 9.4. Sixteenth inch diameter stainless steel tubing connected the pump to a column inside the oven and also extended from the column to the sample collection vial. Tubing was stainless steel in order to prevent gas diffusion (in or out) from influencing the dissolved O_2 concentration or pH (by uptake of CO_2). The lines between the baths and ovens were not heated and the solution cooled during transport, although in stainless steel lines, the properties of the water ($[O_2]$, $[CO_2]$, pH) should not be affected. Preliminary tests were run with O_2 monitors in the feedwater and after the sample collection and no significant change in O_2 levels were detected. Once the tubing entered the oven it coiled below the column containing the fuel, which allowed the solution to be heated to the test temperature before contact with the fuel, as shown in Figure 9.5. The

columns inside the oven that contained the fuel had a 0.25 inch inner diameter and were 2 inches long. The columns were made of stainless steel and capped at both ends by stainless steel frits. The frits had 0.5 μm openings to assure that only dissolved radionuclides or colloids (no particulates) exited the column. The solution entered through the bottom of the column and flowed in the up direction to prevent an air pocket from forming in the column and to obtain a more homogeneous contact with the fuel.

Figure 9.3. Oven used for SPFT test

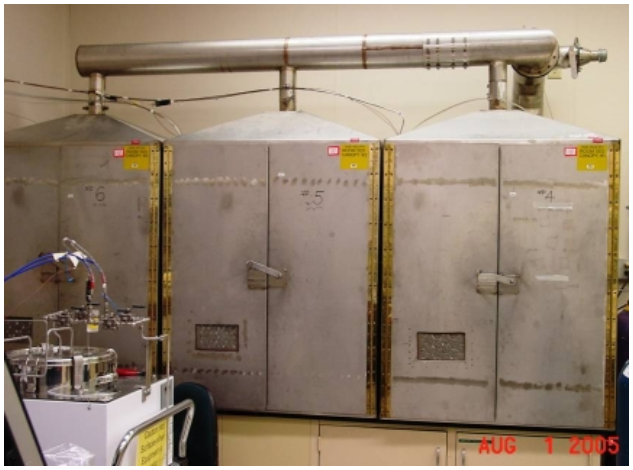

Figure 9.4. Canopies containing ovens

Figure 9.5. Columns inside oven

After the solution passed through the column containing the fuel it was piped out of the top of the oven by stainless steel tubing and directed to a three-way valve. The valve allowed for collection of the leachate, displayed in Figure 9.6, diversion to a waste stream, or for the line to be closed. During collection of the leachate the flow rate was measured by dividing the mass of the collected effluent by the time required to collect the sample. The flow rate was adjusted by changing the pump speed in order to maintain the desired value. A small amount, approximately 0.25 mL, of concentrated nitric acid was pipetted into all vials used to collect effluent samples for analysis to ensure that the uranium remained in solution rather than being deposited on the container walls. Also the addition of nitric acid acidified the carbonate solution for more accurate measurements during Kinetic Phosphorescence Analysis (KPA).

Figure 9.6. Collection vials on top of oven

When collections of the leachate were not being obtained, the solution went to a waste system. It was piped to ion-exchange columns containing AG MP-1M resin (50-100 mesh, chloride form) that stripped the solution of uranium, as shown in Figure 9.7. The remaining bicarbonate solution dripped into a heated round bottom flask. The evaporate (consisting of only DIW) was carried by a heated line to a fumehood where it cooled in a non-heated line and dripped into a stainless steel vessel on a hotplate. Here the deionized DIW was again evaporated and taken into the fumehood ventilation. This waste process allowed for a mass balance of the uranium through analysis of the ion-exchange columns and prevented mass quantities of a radioactive solution from accumulating.


Figure 9.7. Ion-exchange columns and heated round bottom flask

Analysis

Scanning electron microscopy (SEM) was performed on the powder samples prior to being added to the columns. In these tests visual examination of the fuel allowed for verification of the grain size and inspection of the amount of remaining fines. Some samples were also analyzed using Electron Dispersion Spectroscopy (EDS) that identified surface compositions of the fuels. Surface area measurements of the powder samples were obtained using the Brunauer, Emmett, Teller (BET) method. In the case of the fragments, geometric measurements were taken of the surface area and multiplied by 15 to account for surface roughness.

During the testing, dissolved uranium in the leachate was analyzed using KPA. After the testing was complete the solids were analyzed by X-ray diffraction to determine if any crystalline phases other than UO_2 were present. SEM and EDS analysis was also performed on the powders post-testing to determine altered surface composition, the

amount of grain boundary attack and cracking on sample fragments, and to examine the surface of samples for alteration phases (such as schoepite) that may form during testing.

CHAPTER 10: PRE-TEST ANALYSIS OF FUEL

Test 1

The fuels used in this study were initially pellets procured from a commercial vendor. The compositions, densities, and grain sizes of the fuels, as given by the vendor, used in Test 1 are listed in Table 10.1. The Gd_2O_3-dopant levels were the amount of additive combined with the UO_2 prior to pressing and sintering the pellet. These varying levels allow for investigation into the influence of fuel chemistry on dissolution. The nominal values of the Gd_2O_3 concentration listed in Table 10.1 will be referred to when comparing the effect on dissolution rates throughout this thesis.

Table 10.1. Composition, density, and grain size of the fuels used in Test 1

Fuel Label	Actual U-235 (%)	Nominal Gd_2O_3 (%)	Actual Gd_2O_3 (%)	% U	% Theoretical Density	Density (g/cc)	Grain Diameter (μm)
BDH-4	2.6048	7	7.1721	81.613	94.702	10.124	16
BDH-5	4.457	4	4.1145	84.386	95.031	10.266	14
BDH-10	0.7105	0	0	88.148	95.307	10.445	Not Given
BDH-11	4.5588	8	8.0255	80.784	95.322	10.158	13

As stated in Chapter 9, both powder and fragment samples were obtained by crushing and/or sieving the original pellets. The surface areas for all of the powders used in Tests 1 through 5 were measured via the BET method using a Quantachrome Monosorb Model MS-21 gas sorption analyzer which took single point measurements of the surface areas. The fragments were measured with calipers, and the surface area was calculated based upon these measurements. A surface roughness of 15 was then multiplied by the surface area to account for grain boundaries, pores, and other surface irregularities. The surface areas are listed in Table 10.2 along with the quantity and location of the loading.

Table 10.2. Surface area, geometry and distribution of fuels used in Test 1. In all tests oven A was kept at room temperature, oven B at 50ºC, and oven C was maintained at 75ºC.

Placement	Fuel Type	Geometry	# of Fragments	Surface Area (m^2/g)	Sample Size (g)
A1	BDH-10	Powder		2.68E-01	0.2009
A2	BDH-10	Powder		2.68E-01	0.1995
A3	BDH-10	Powder		2.68E-01	0.2077
A4	BDH-11	Powder		3.61E-01	0.2020
A5	BDH-11	Powder		3.61E-01	0.2001
A5-b	BDH-10	Fragments	2	2.49E-03	1.0553
A6	BDH-11	Powder		3.61E-01	0.1980
A7	BDH-5	Powder		3.54E-01	0.2003
A8	BDH-4	Fragments	2	1.62E-03	1.0258
B1	BDH-10	Powder		2.68E-01	0.2016
B2	BDH-10	Powder		2.68E-01	0.2086
B3	BDH-10	Powder		2.68E-01	0.1988
B4	BDH-11	Powder		3.61E-01	0.1973
B5	BDH-11	Powder		3.61E-01	0.1998
B5-b	BDH-10	Fragments	3	3.27E-03	0.9881
B6	BDH-11	Powder		3.61E-01	0.2010
B7	BDH-5	Powder		3.54E-01	0.2073
B8	BDH-4	Fragments	3	3.31E-03	1.0344
C1	BDH-10	Powder		2.68E-01	0.2011
C2	BDH-10	Powder		2.68E-01	0.2037
C3	BDH-10	Powder		2.68E-01	0.2051
C4	BDH-11	Powder		3.61E-01	0.1991
C5	BDH-11	Powder		3.61E-01	0.2050
C5-b	BDH-10	Fragments	3	2.29E-03	1.0286
C6	BDH-11	Powder		3.61E-01	0.2046
C7	BDH-5	Powder		3.54E-01	0.2030
C8	BDH-4	Fragments	3	2.17E-03	1.0057

In all tests, oven A was kept at room temperature while ovens B and C were maintained at 50ºC and 75ºC, respectively. The letter in the placement column in the table above depicts the oven in which the sample was run. In Test 1, samples with fragments contained 2 to 3 pieces per column. Initial testing began with columns 1 through 6, excluding 5b in each oven. Approximately 2 months later, columns with sample A7, B7, and C7 were inserted into the ovens and around 3 months after start-up, samples A8, B8, and C8 were added and the columns with samples A5, B5, and C5 were removed to allow for new columns with samples A5-b, B5-b, and C5-b to be run.

Figures 10.1 through 10.7 are SEM images of the 0, 4, and 8% Gd_2O_3-doped UO_2 powders and Figures 10.8 and 10.9 are pictures of the fragments (all taken before being loaded into the columns). The SEM used to produce these images was an Amray 1610T with a 200,000x magnification capability and resolution to 45 Angstroms. The SEM was equipped with an EDAX 9900 Light Element Detector and ANS Quantum System 4404 semi-quantitative analysis system. The BDH-10 (0% Gd_2O_3-doped UO_2) and BDH-11 (8% Gd_2O_3-doped UO_2) fuels were crushed and sieved first and had a noticeable quantity of fines on the grains. The BDH-5 fuel (4% Gd_2O_3-doped UO_2), as stated before, was added to the system after the other fuels had already been running. It had been observed that the large number of fines in the original fuels may have been clogging the frits, so these fuels were sieved for approximately 48 hours as opposed to 18 hours in order to remove a larger quantity of fines. From Figures 10.1 through 10.7 it can be seen that the grains were approximately the size reported by the vendor.

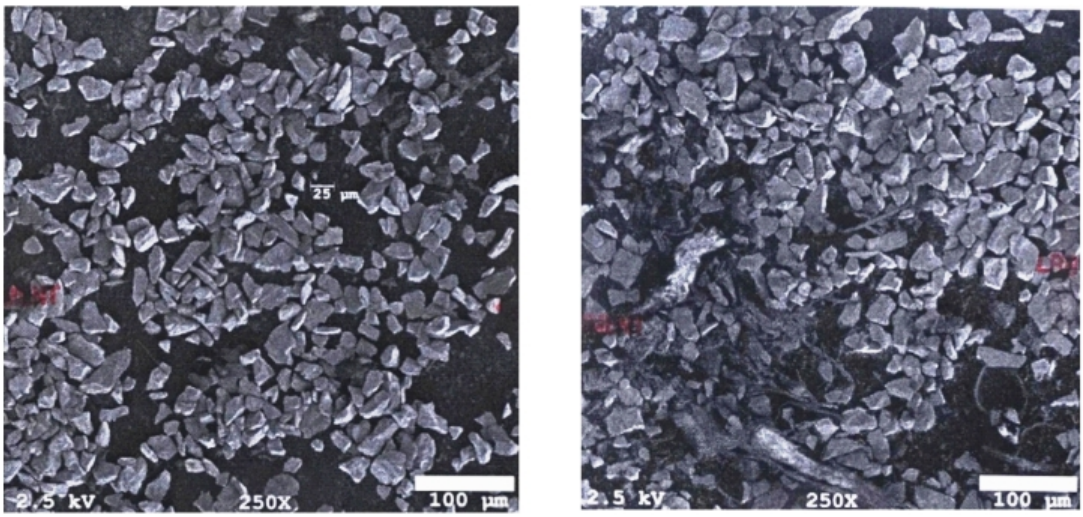

Figure 10.1. SEM image of BDH-5 (4% Gd_2O_3-doped UO_2) before SPFT testing with 250x magnification

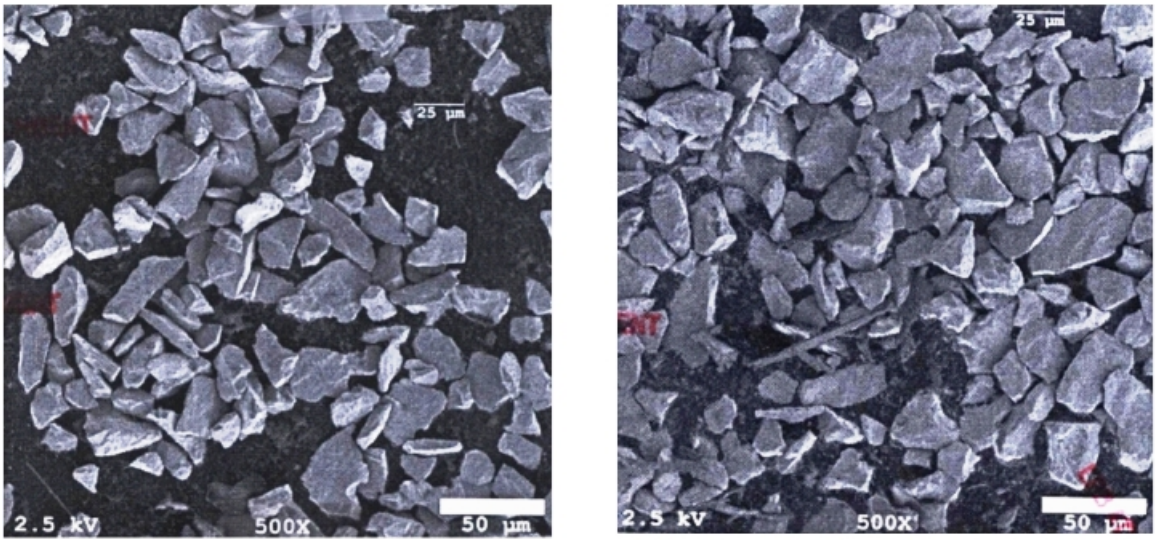

Figure 10.2. SEM image of BDH-5 (4% Gd_2O_3-doped UO_2) before SPFT testing with 500x magnification

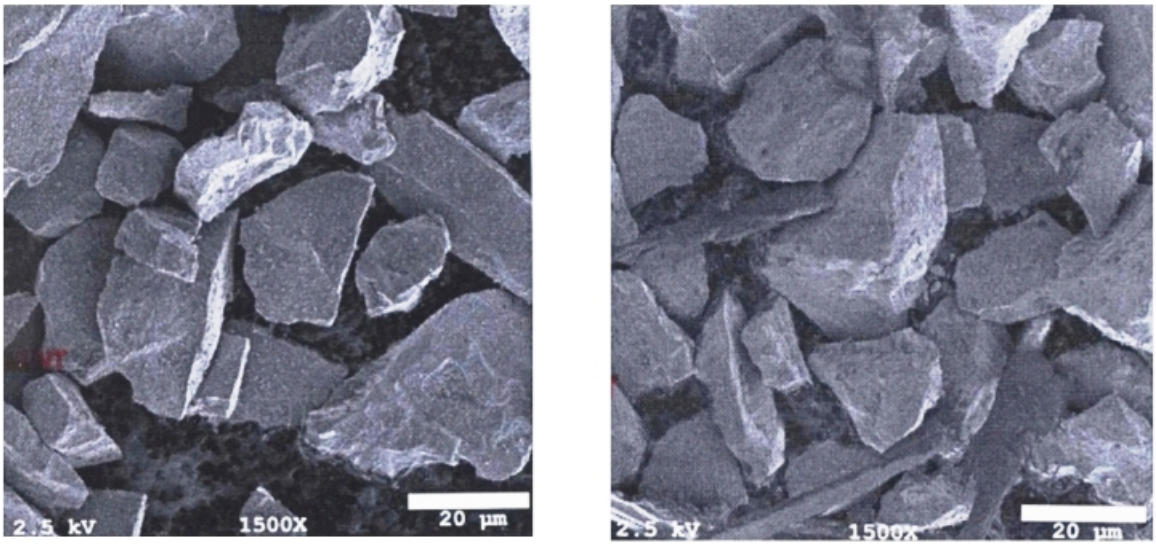

Figure 10.3. SEM image of BDH-5 (4% Gd_2O_3-doped UO_2) before SPFT testing with 1500x magnification

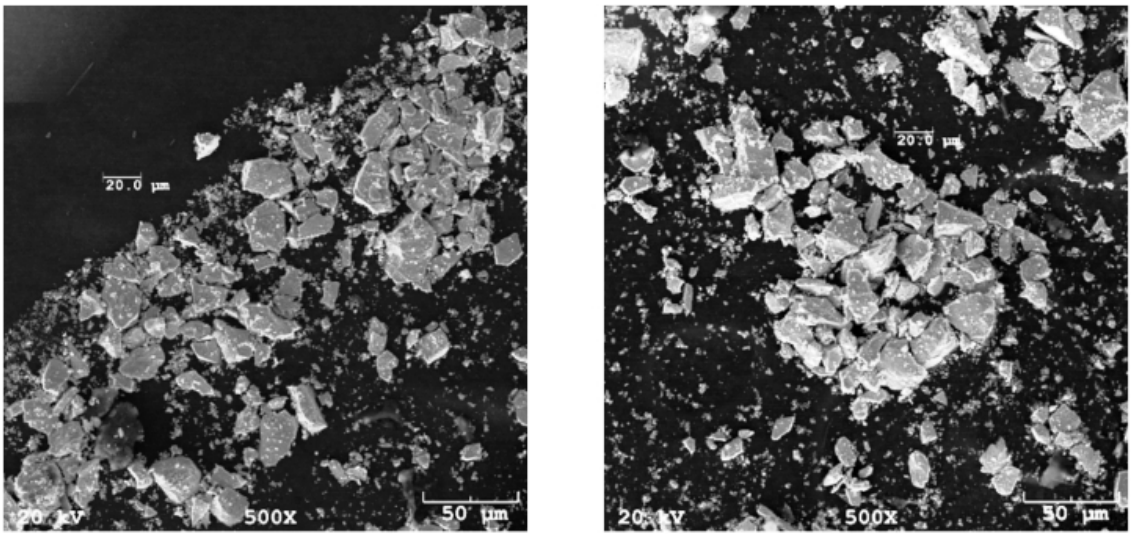

Figure 10.4. SEM image of BDH-10 (0% Gd_2O_3-doped UO_2) before SPFT testing with 500x magnification

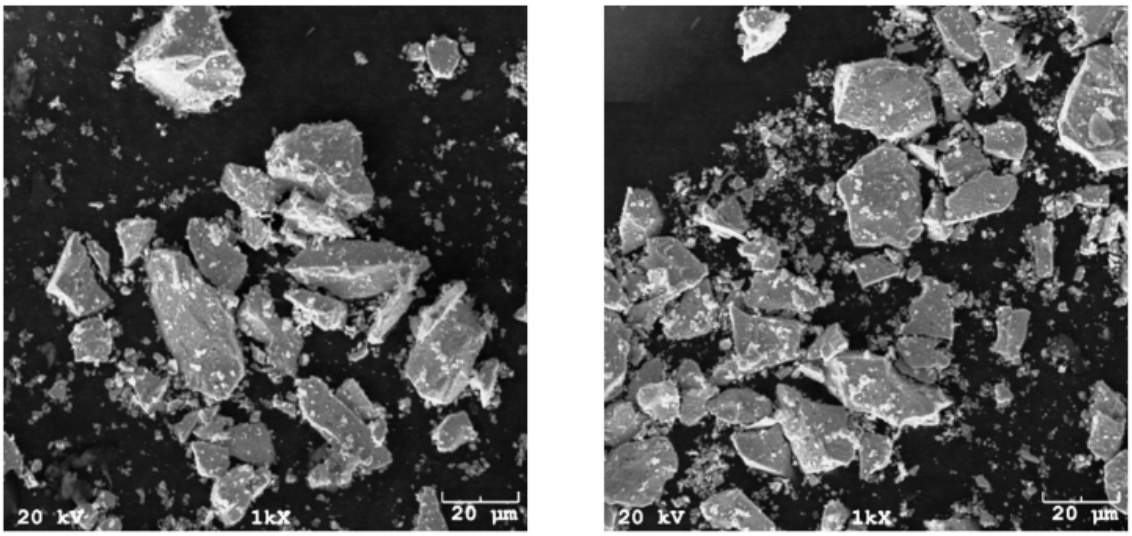

Figure 10.5. SEM image of BDH-10 (0% Gd_2O_3-doped UO_2) before SPFT testing with 1000x magnification

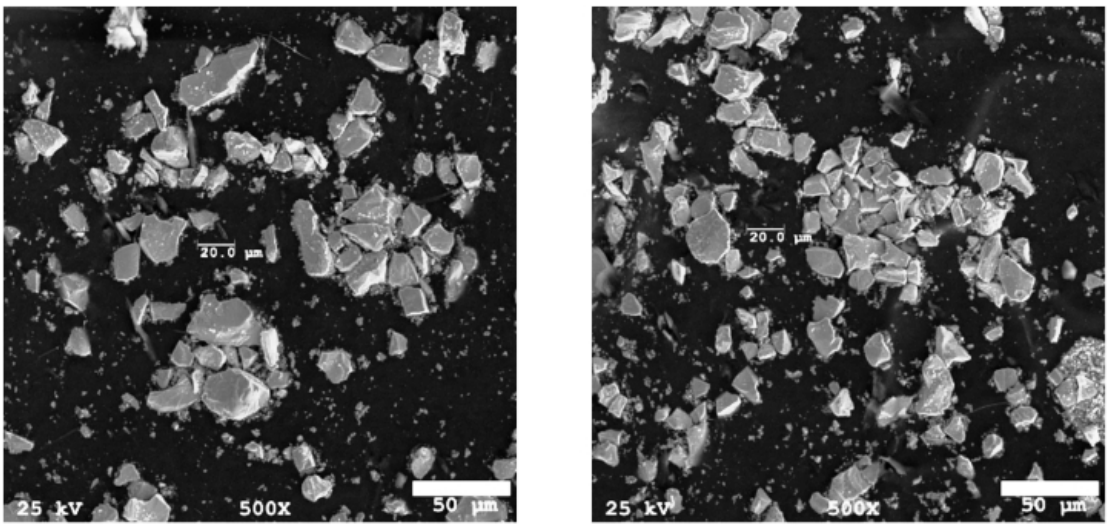

Figure 10.6. SEM image of BDH-11 (8% Gd_2O_3-doped UO_2) before SPFT testing with 500x magnification

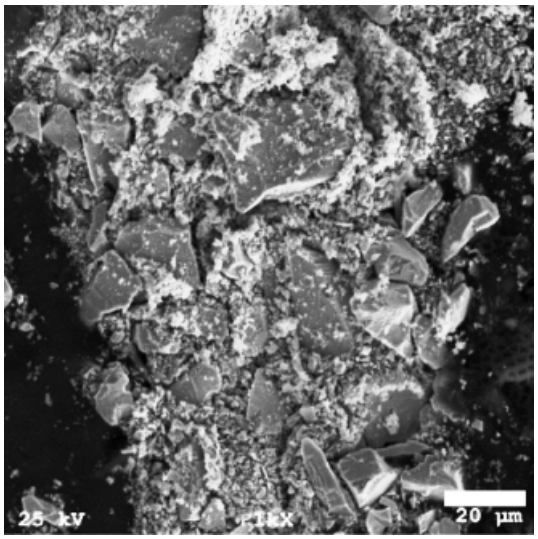

Figure 10.7. SEM image of BDH-11 (8% Gd_2O_3-doped UO_2) before SPFT testing with 1000x magnification

Figure 10.8. BDH-4 fragments (7% Gd_2O_3-doped UO_2) before SPFT testing

Figure 10.9. BDH-10 fragments (0% Gd_2O_3-doped UO_2) before SPFT testing

Tests 2-5

The composition, density, and grain size (as reported by the vendor) of the fuels used in tests 2 through 5 are shown in Table 10.3. These tests investigate a lower Gd_2O_3-dopant range with a maximum of 4%. The surface area, distribution, and geometry of the fuels can be seen in Table 10.4. In these tests, 5 of the samples in each oven were powders and 3 were fragments. Unlike before, placements 7 and 8 contained 4 to 5 fragments instead of the 2 to 3 fragments obtained in Test 1. This larger number was a result of how the pellet split during the shearing step of the procedure.

Table 10.3. Composition, density, and grain size of the fuels used in Tests 2-5

Fuel Label	Actual U-235 (%)	Nominal Gd_2O_3 (%)	Actual Gd_2O_3 (%)	% U	% Theoretical Density	Density (g/cc)	Grain Diameter (μm)
BDH-1	3.9727	1.25	1.2728	86.964	94.879	10.352	15
BDH-2	3.8035	3	3.0549	85.314	95.651	10.372	14
BDH-5	4.457	4	4.1145	84.386	95.031	10.266	14
BDH-6	0.7105	0	0	88.148	95.337	10.448	Not Given
BDH-8	4.8183	2	2.1068	86.199	95.292	10.366	12

Table 10.4. Surface area, geometry and distribution of fuels used in Tests 2-5. In all tests oven A was kept at room temperature, ovens B at 50ºC, and oven C was maintained at 75ºC.

Placement	Fuel Type	Geometry	# of Fragments	Surface Area (m^2/g)	Sample Size (g)
A1	BDH-6	powder		1.47E-01	0.1993
A2	BDH-1	powder		1.54E-01	0.2051
A3	BDH-8	powder		2.03E-01	0.2012
A4	BDH-2	powder		1.60E-01	0.2053
A5	BDH-5	powder		1.44E-01	0.1977
A6	BDH-6	fragments	2	2.93E-03	1.0089
A7	BDH-8	fragments	4	3.07E-03	0.9966
A8	BDH-2	fragments	5	5.35E-03	0.8911
B1	BDH-6	powder		1.47E-01	0.2070
B2	BDH-1	powder		1.54E-01	0.1976
B3	BDH-8	powder		2.03E-01	0.1979
B4	BDH-2	powder		1.60E-01	0.2076
B5	BDH-5	powder		1.44E-01	0.2048
B6	BDH-6	fragments	2	2.01E-03	1.0219
B7	BDH-8	fragments	4	3.06E-03	0.9402
B8	BDH-2	fragments	4	4.39E-03	0.8781
C1	BDH-6	powder		1.47E-01	0.2299
C2	BDH-1	powder		1.54E-01	0.2062
C3	BDH-8	powder		2.03E-01	0.2100
C4	BDH-2	powder		1.60E-01	0.2070
C5	BDH-5	powder		1.44E-01	0.2025
C6	BDH-6	fragments	2	3.23E-03	1.0222
C7	BDH-8	fragments	4	3.63E-03	0.9703
C8	BDH-2	fragments	5	6.10E-03	0.8946

The SEM images of the second set of fuels can be seen in Figures 10.10 through 10.14. As with BDH-5 (4% Gd_2O_3-doped UO_2) in Test 1, the fuels used in Tests 2 through 5 were sieved approximately 48 hours. Some high contrast areas can be seen in the SEM images, which may be a result of the application technique to the SEM mounts.

In this process wooden rod tips were dipped into the fuel and pressed onto the mount which may have allowed small splinters to be deposited. Overall the samples appeared to have minimal fines and the grains were of approximately the size provided by the vendor. Pictures of the fragments used in Tests 2 through 5 are shown in Figure 10.14. This picture was taken after SPFT testing was complete and 1 fragment from each sample had been removed for SEM-EDS analysis.

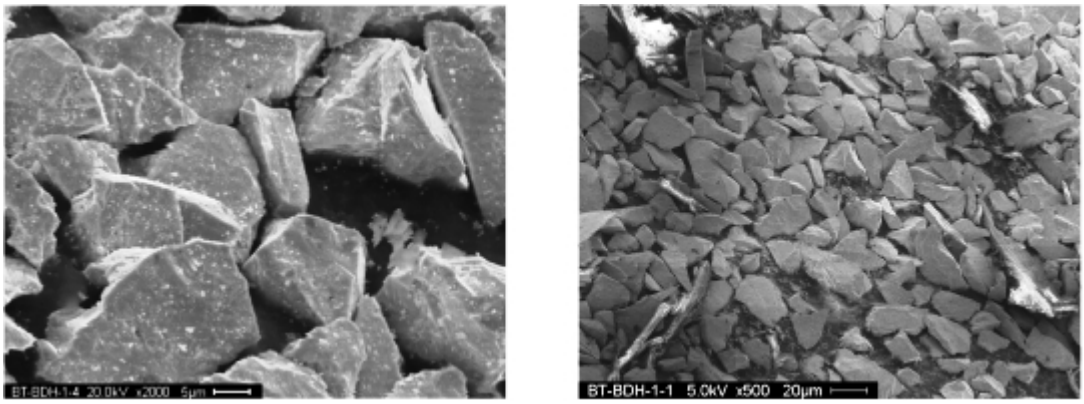

Figure 10.10. SEM image of BDH-1 (1.25% Gd_2O_3-doped UO_2) before SPFT testing

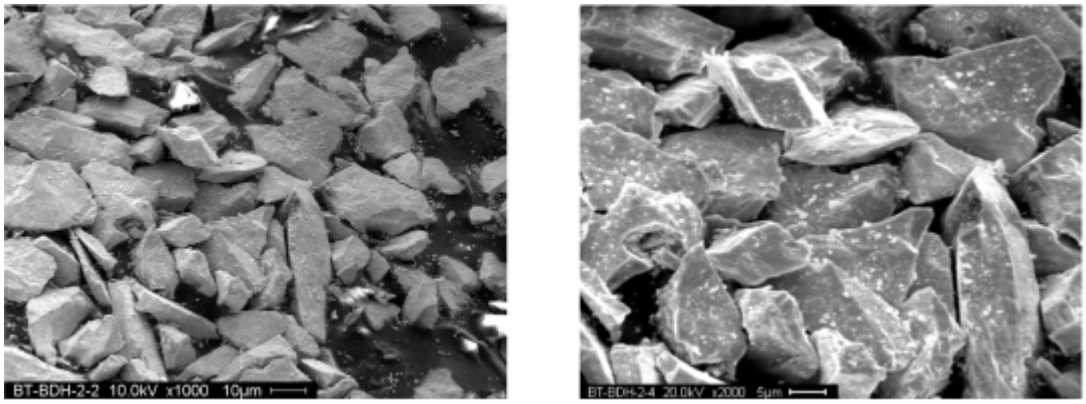

Figure 10.11. SEM image of BDH-2 (3% Gd_2O_3-doped UO_2) before SPFT testing

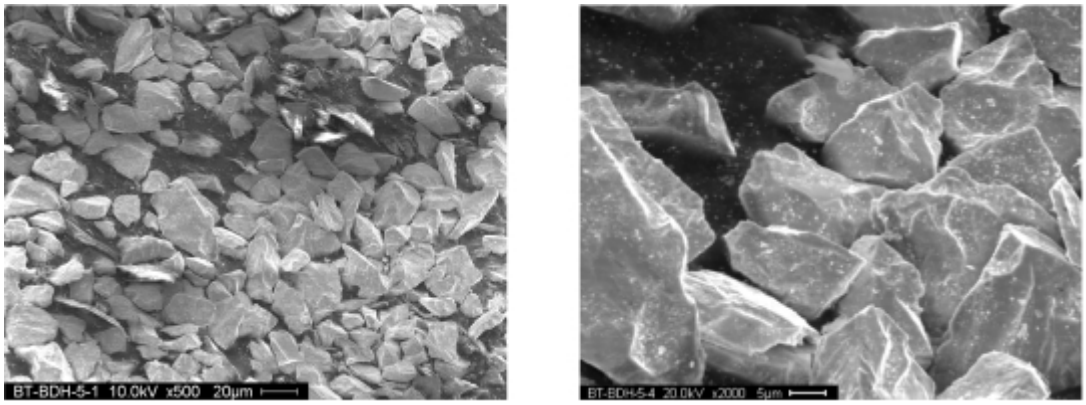

Figure 10.12. SEM image of BDH-5 (4% Gd_2O_3-doped UO_2) before SPFT testing

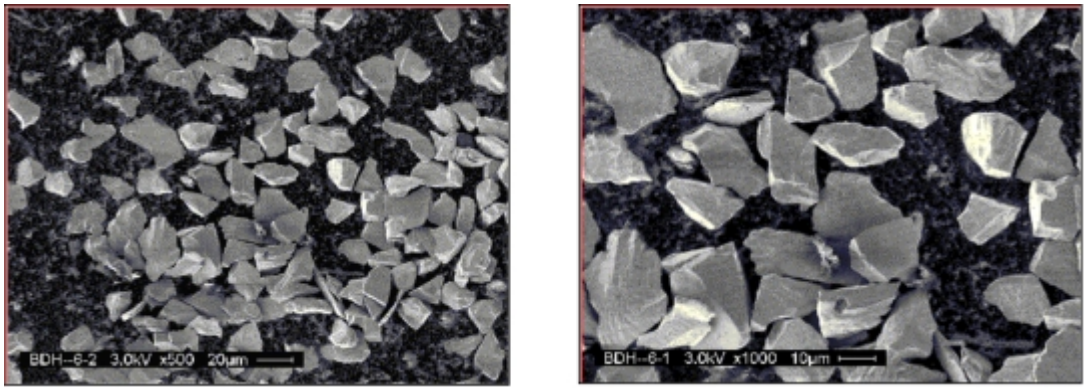

Figure 10.13. SEM image of BDH-6 (0% Gd_2O_3 doped UO_2) before SPFT testing

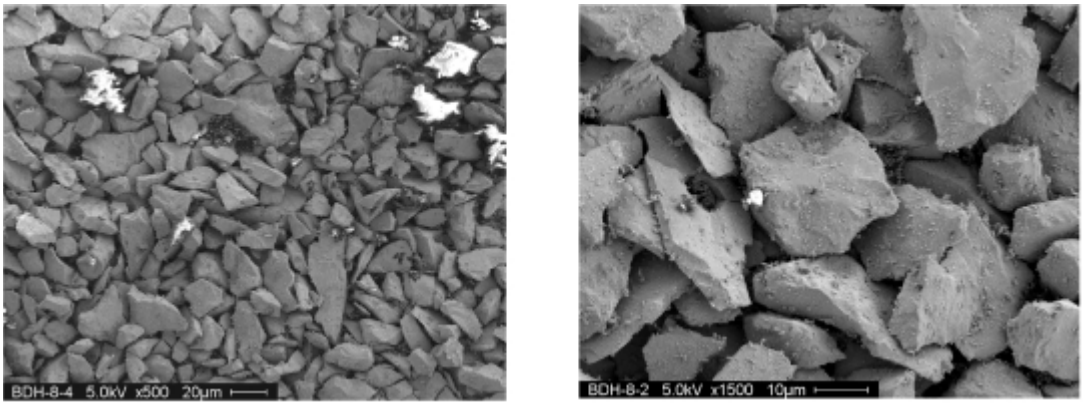

Figure 10.14. SEM image of BDH-8 (2% Gd_2O_3-doped UO_2) before SPFT testing

Figure 10.15. Fragments for Tests 2-5 after SPFT testing

Along with the SEM analysis, EDS was performed on these fuels and the results are given in Tables 10.5 through 10.9. The wt% measured by EDS is representative of only the Gd and the dopant levels indicated in Table 10.3 are listed as wt% Gd_2O_3. In order to compare these results to the levels given by the commercial vendor the Gd_2O_3 must be converted to Gd, with the results shown in Table 10.10. In these tests, analyses were performed in 4 separate areas in order to observe possible variations in the sample. As shown in the tables, the Gd distribution was not homogeneous throughout the fuel; the most extreme case observed was in Table 10.6 where the Gd ranged from 1.51 to 3.94%. An unexpected result produced in the EDS analysis was the presence of copper. As these fuels did not come into contact with copper during the crushing or sieving processes, if any copper were present it would have been in the initial fuel. A XRD analysis was performed on the fuel after the SPFT testing was complete and no copper was detected, therefore its presence may be an anomaly of peak overlap on the EDS that was erroneously detected as a constituent.

Table 10.5. EDS analysis of BDH-1 (1.47% Gd-doped UO_2) before SPFT testing

BDH-1 (Wt %)						
Element	Area 1	Area 2	Area 3	Area 4	Average	Deviation
C	5.16	5.43	7.84	5.80	6.06	1.22
O	16.02	16.88	17.03	17.67	16.90	0.68
U	72.90	73.13	67.18	72.67	71.47	2.87
Gd	1.45	1.87	1.83	1.57	1.68	0.20
Cu	4.46	2.69	6.12	2.29	3.89	1.76

Table 10.6. EDS analysis of BDH-2 (3.52% Gd-doped UO_2) before SPFT testing

BDH-2 (Wt %)						
Element	Area 1	Area 2	Area 3	Area 4	Average	Deviation
C	6.66	13.44	7.69	6.42	8.55	3.30
O	17.58	18.46	22.32	17.93	19.07	2.20
U	67.58	56.22	62.80	68.34	63.74	5.58
Gd	3.00	1.51	3.94	3.19	2.91	1.02
Cu	5.18	10.38	3.24	4.12	5.73	3.20

Table 10.7. EDS analysis of BDH-5 (4.72% Gd-doped UO_2) before SPFT testing

BDH-5 (Wt %)						
Element	Area 1	Area 2	Area 3	Area 4	Average	Deviation
C	8.09	8.24	10.79	5.76	8.22	2.06
O	24.30	23.30	16.06	15.85	19.88	4.55
U	62.35	62.63	61.35	71.30	64.41	4.63
Gd	3.81	3.58	3.32	4.42	3.78	0.47
Cu	1.44	2.25	8.47	2.67	3.71	3.22

Table 10.8. EDS analysis of BDH-6 (0% Gd-doped UO_2) before SPFT testing

BDH-6 (Wt %)						
Element	Area 1	Area 2	Area 3	Area 4	Average	Deviation
C	8.16	5.18	20.65	5.96	9.99	7.22
O	21.77	13.34	20.45	17.91	18.37	3.71
U	66.78	75.67	47.79	72.13	65.59	12.42
Gd	1.17	0.64	0.59	0.70	0.78	0.27
Cu	2.12	5.17	10.52	3.31	5.28	3.71

Table 10.9. EDS analysis of BDH-8 (2.44% Gd-doped UO_2) before SPFT testing

BDH-8 (Wt %)						
Element	Area 1	Area 2	Area 3	Area 4	Average	Deviation
C	18.20	13.62	23.89	30.74	21.61	7.39
O	37.68	32.25	43.81	29.39	35.78	6.36
U	43.10	53.75	31.48	26.75	38.77	12.12
Gd	1.02	0.39	0.83	0.49	0.68	0.29
Cu	0.00	0.00	0.00	12.64	3.16	6.32

Table 10.10. Conversion of wt% Gd_2O_3 to wt% Gd

nominal wt% Gd_2O_3	actual wt% Gd_2O_3	actual wt% Gd
0	0	0
1.25	1.27	1.47
2	2.11	2.44
3	3.05	3.52
4	4.11	4.72

CHAPTER 11: RESULTS

Test 1

Samples containing approximately 15 mL of the leachate solution after it had come into contact with the fuels were collected daily. The uranium (U) concentrations of the samples were measured using Kinetic Phosphorescence Analysis. The U concentration was then used to calculate the normalized dissolution rate (NDR) and the cumulative fraction (CF) of U released. The equations for these calculations are depicted in Equations 11.1, 11.2, and 11.3.

$$\mathrm{NDR} = \frac{(\text{Flow Rate}) \times (\text{U Concentration in Leachate})}{(\text{Fuel Sample Size}) \times \left(\frac{\text{grams U}}{\text{grams } UO_2 + \text{Gd}} \right) \times (\text{Specific SA})} \tag{11.1}$$

$$CF_x = (\text{U Frac}) \times (\text{Day}_x - \text{Day}_{x\text{-}1}) + CF_{x-1} \tag{11.2}$$

$$\text{U Frac} = \frac{(\text{Flow Rate}) \times (\text{U Concentration in Leachate})}{(\text{Fuel Sample Size}) \times \left(\frac{\text{grams U}}{\text{grams } UO_2 + \text{Gd}} \right)} \tag{11.3}$$

where U Frac is the fractional release of U over a given time period (usually a day), Day_x is the day number of the specific run, Day_{x-1} is the day prior to Day_x, and the (grams U)/(grams UO_2+Gd) is the specific fraction of U per sample which takes into account any Gd weight.

The normalized dissolution rates and cumulative releases from Test 1 are shown in Figures 11.1 through 11.8. Initially only powder samples containing 0 or 8% Gd_2O_3-doped UO_2 were studied. On day 71 of testing, the columns with the 4% Gd_2O_3-doped UO_2 samples were inserted into the ovens and on day 98, the fragment columns were placed in the ovens. On some of the following graphs, the samples are all shifted to begin at day zero in order to compare their release relative to the run length. Spikes are commonly seen in dissolution data that are the result of fines coming through during sampling or pitting of the fuel surface which results in a small piece of U breaking off. Typically, these spikes are only seen on one day and the rate returns to previous levels the following day. This occurrence will shift cumulative curves up, however the slope before and after remains constant. There was minimal difference between the trends displayed by the three flow rates, which was the result of the forward rate of reaction being maintained in all samples. This was further established by the absence of alteration phases on the surface of the fuels as shown in Chapter 12.

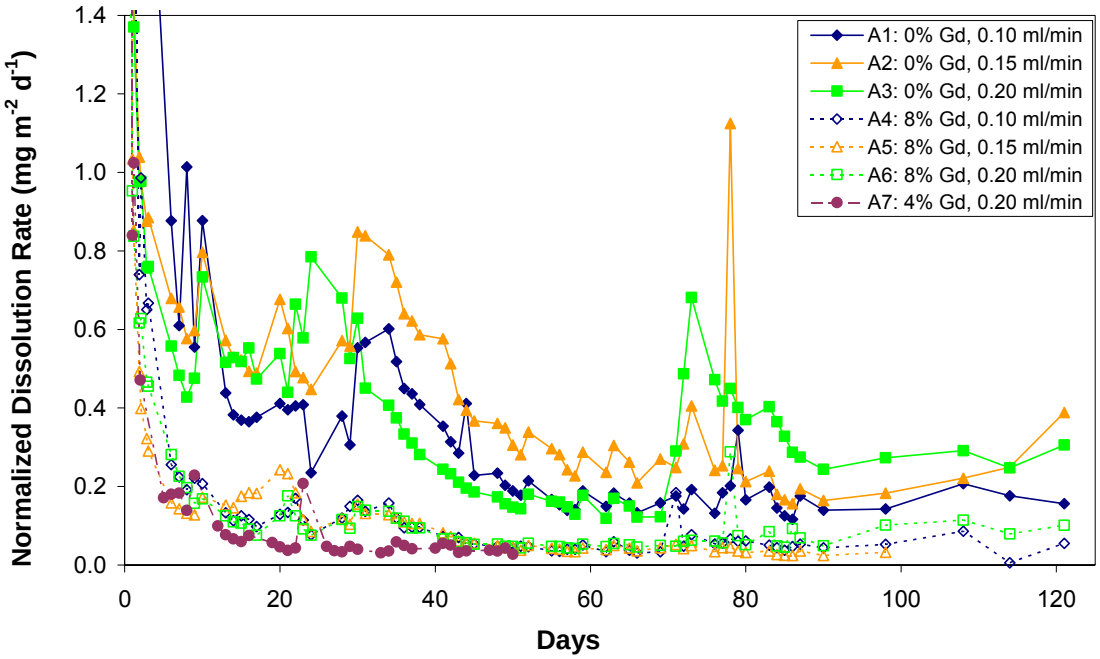

Figure 11.1. Normalized dissolution rates of powder unirradiated UO_2 samples with 0-8% Gd_2O_3-doping and flow rates from 0.10-0.20 mL/min run at 25ºC

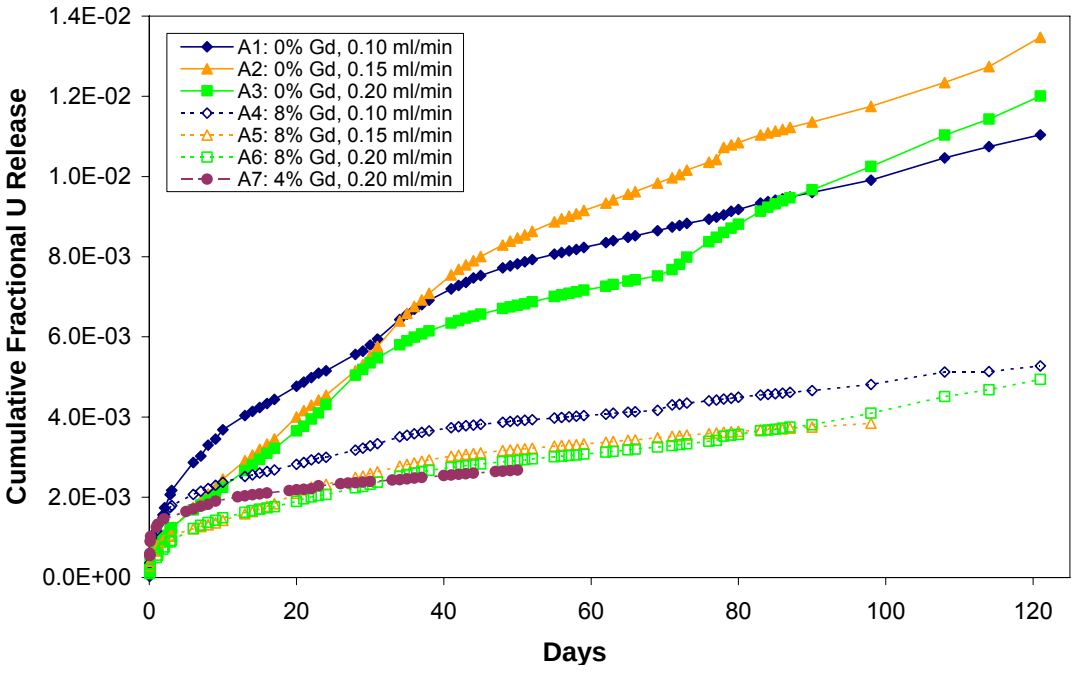

Figure 11.2. Cumulative fraction of uranium released from powder unirradiated UO_2 samples with 0-8% Gd_2O_3-doping and flow rates from 0.10-0.20 mL/min run at 25ºC

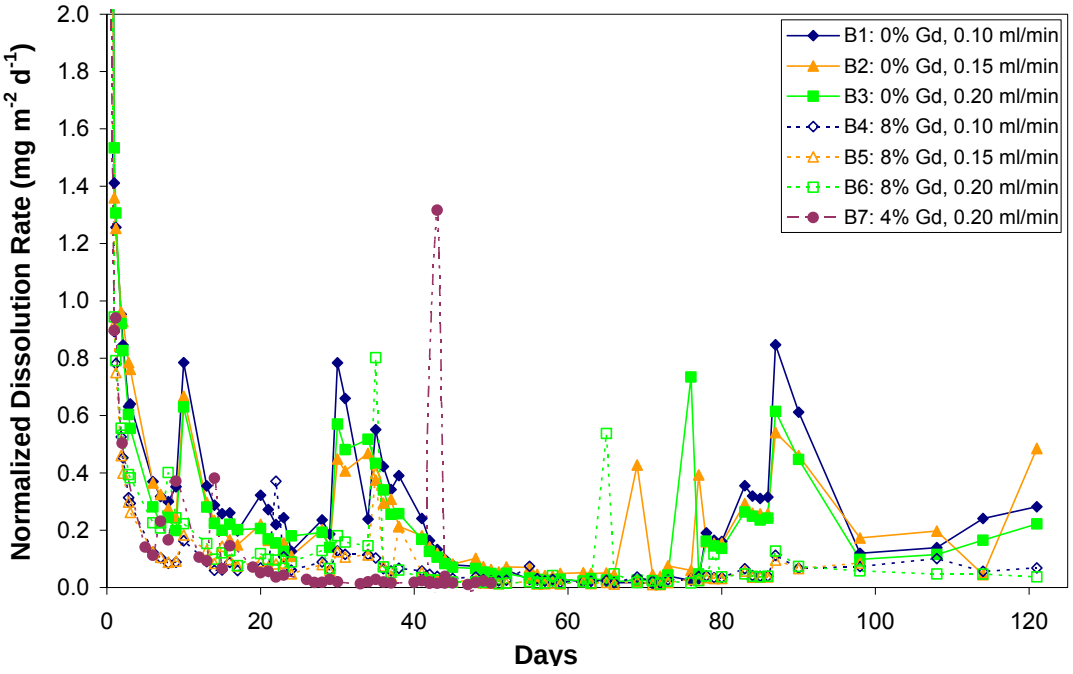

Figure 11.3. Normalized dissolution rates of powder unirradiated UO_2 samples with 0-8% Gd_2O_3-doping and flow rates from 0.10-0.20 mL/min run at 50ºC

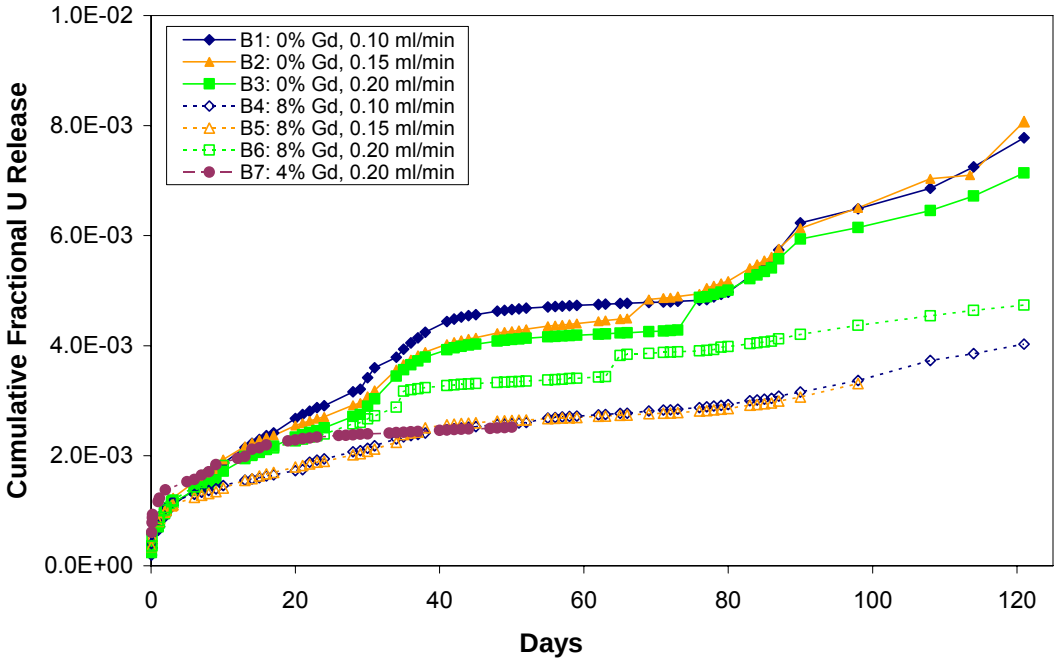

Figure 11.4. Cumulative fraction of uranium released from powder unirradiated UO_2 samples with 0-8% Gd_2O_3-doping and flow rates from 0.10-0.20 mL/min run at 50ºC

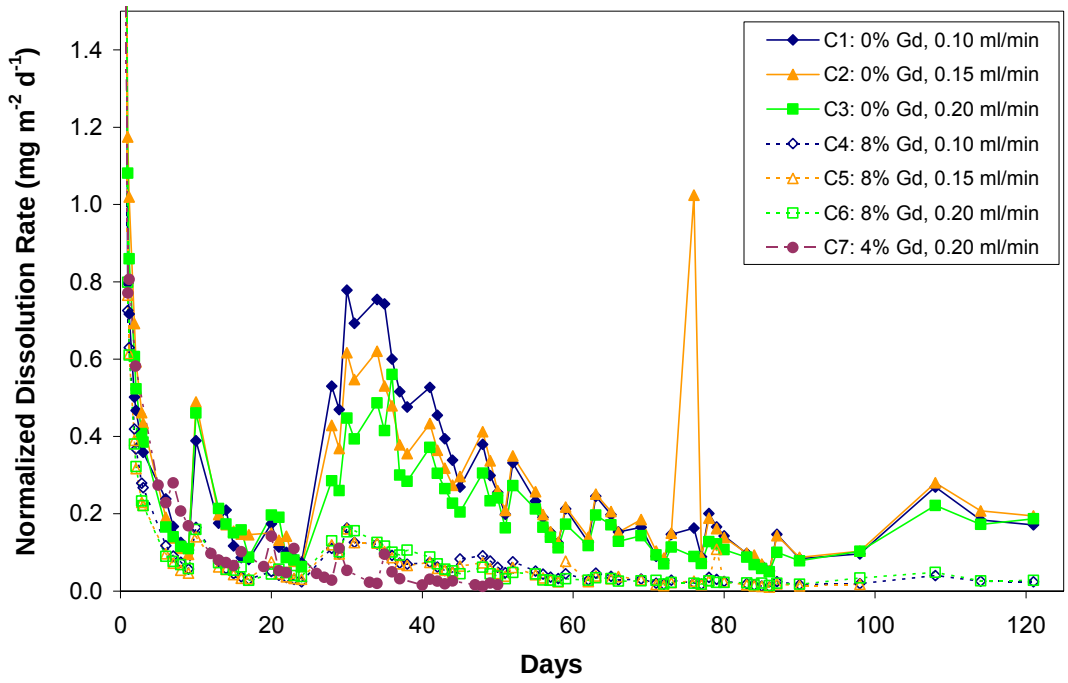

Figure 11.5. Normalized dissolution rates of powder unirradiated UO_2 samples with 0-8% Gd_2O_3-doping and flow rates from 0.10-0.20 mL/min run at 75ºC

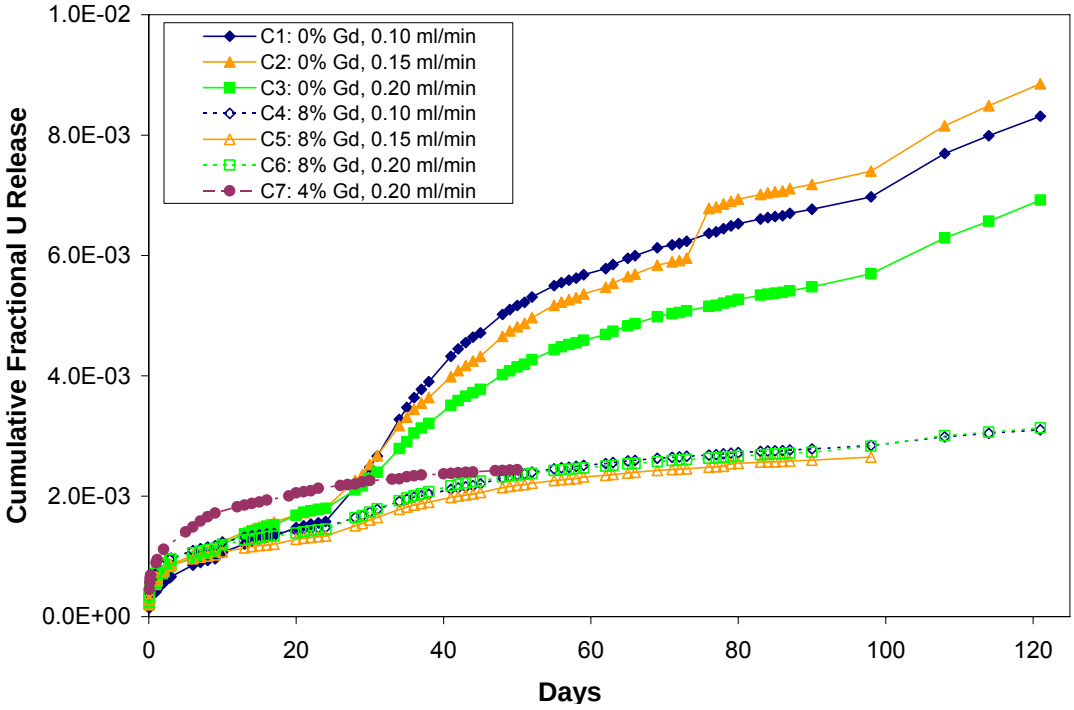

Figure 11.6. Cumulative fraction of uranium released from powder unirradiated UO_2 samples with 0-8% Gd_2O_3-doping and flow rates from 0.10-0.20 mL/min run at 75ºC

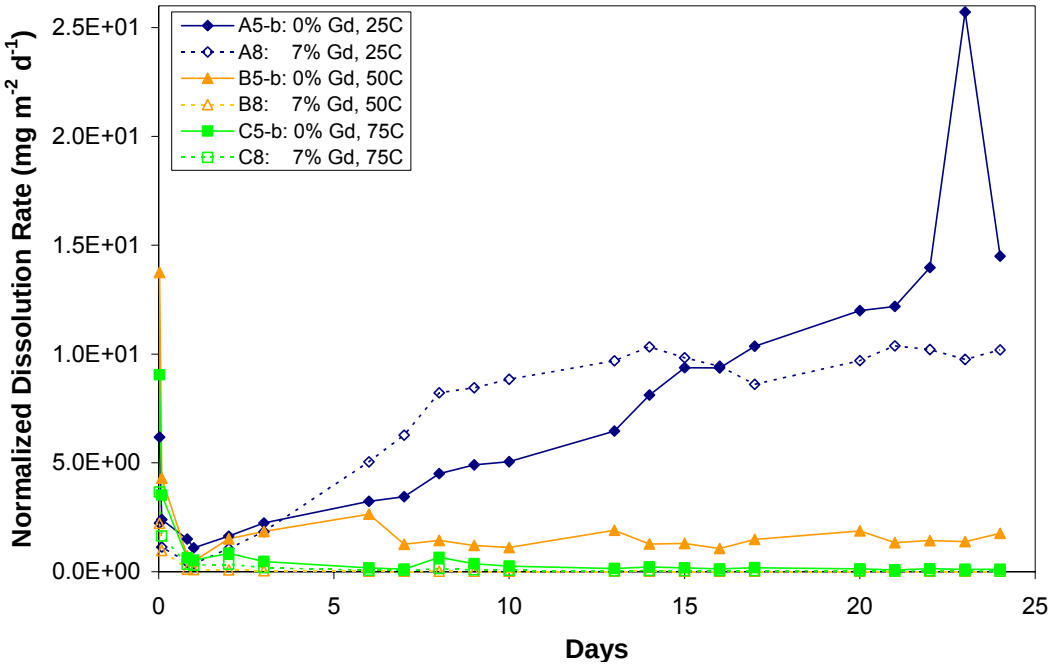

Figure 11.7. Normalized dissolution rates of fragmented unirradiated UO_2 samples with 0 and 7% Gd_2O_3-doping and flow rates of 0.20 mL/min run at 25ºC, 50ºC, and 75ºC

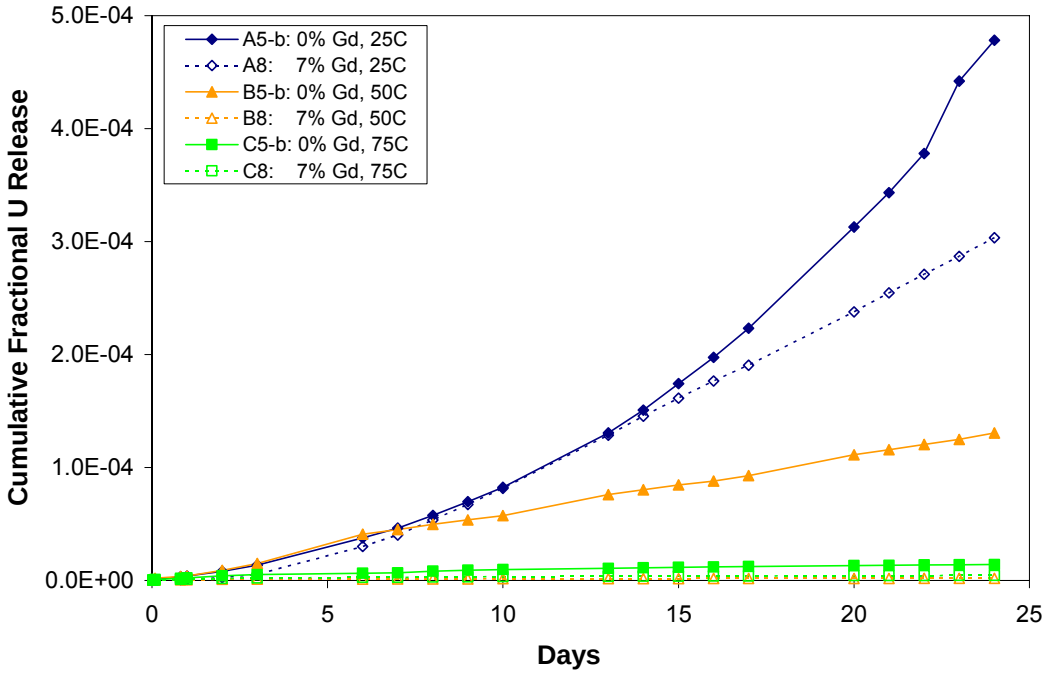

Figure 11.8. Cumulative fraction of uranium released from fragmented unirradiated UO_2 samples with 0 and 7% Gd_2O_3-doping and flow rates of 0.20 mL/min run at 25ºC, 50ºC, and 75ºC

In Figures 11.1, 11.3, and 11.5 an increase in the normalized dissolution rate was observed around day 31. The water used for the leachate solutions was obtained from a millipore filtration unit fed by a DIW system. On day 31 the conductivity dropped below acceptable levels and the filtration cartridges were exchanged. It was later discovered that the building DIW system feeding the millipore unit was not functioning properly for the entirety of Test 1. This resulted in higher levels of some contaminants entering the millipore unit which was only designed to filter minimal amounts. As a result, the ion exchange capacity of the filters was expended and higher levels of contaminant were allowed into the feedwater, although the conductivity was still acceptable. Analysis on the feedwaters was performed and will be presented in Chapter 13. This increase was not seen in the fragment data in Figure 11.7 because the fragments were inserted on day 98 of the original testing, which was after the filter replacement had occurred. This incident is described in Table 11.1 along with the other occurrences that happened during testing.

Table 11.1. Incidents during Test 1 and affected columns with days measured from the beginning of the initial test with 0 and 8% Gd_2O_3-doped UO_2 powders

Day	Affected Columns	Incident
7	B3	Tapped Column (after sampling)
9	A4, B5, B6	Tapped Column (after sampling)
14	A5, B3, B4, B5	Tapped Column (after sampling)
14	C set	Recirculation Pump Down for ~ 1hr (after sampling)
15	B3	Tapped Column (after sampling)
17	A5, B3, B4, C2, C3, C5, C6	Tapped Column (after sampling)
20	A5, C6	Tapped Column (after sampling)
21	A2, A3, A5, B2, B4, B5, C2, C3, C6	Tapped Column (after sampling)
31	All	Filters on Ultrapure Water System Changed
44	C4	Tapped Column (after sampling)
71	A3, A6	Tapped Column (after sampling)
73	A2	Tapped Column (after sampling)
77	B set	B Recirculation Pump Down for ~15 min, B Column Pumps Down for ~2.5 hr (before sampling)
78	All	Building Power Down for ~ 1 hr 15 min, Battery Back-ups Held for ~1 hr: All Systems Down for ~ 15 min (before sampling)
121	B6	Pump B6 off for ~1 hr before sampling
125	All	Wall Outlet Tripped: All A Column Pumps Down, B Recirculation Pump Down, C Bath Heater Down (All Down for 1 Day-C Bath Kept Down)
146	A and B sets	Bath A Temperature Changed from 25ºC to 75ºC; Bath B Temperature Changed from 50ºC to 25ºC
151	All	Hot Plate Failed Shutting Down All Pumps-Testing is Ended

Another major occurrence during testing was the clogging of frits due to the large amount of fines in the powders. Unlike some research, the fuels in this experiment were

not washed to remove fines. One reason for this decision was that there was not enough fuel to wash and still have the amount required for testing, because approximately half of the sample can be lost during the washing process. The second reason not to rinse the fuels was to prevent any surface reactions from occurring prior to testing. The complication this produced was that there were too many fines, some of which were greater in size than 0.5 microns (the size of the frit openings). This clogged the frits, causing the flow rate of the sample to decrease. During testing it was initially unknown that this was occurring and the pump speeds were continually increased to compensate until it was postulated, and later verified when the columns were removed and opened, that the fines were clogging the frits. Upon tapping the top and bottom of the columns near the frits with a wrench the flow rate would increase. In some of the ion-exchange columns, this resulted in a visible powder being deposited at the top of the column, but without the tapping the pumps could not handle the pressure build-up. The tappings occurred after daily sampling, and therefore would have less of an effect on the average dissolution rate. All columns inserted after this test were sieved for 48 hours instead of 18 hours to remove a larger amount of the fines. None of these columns, including those in tests 2 through 5, exhibited this behavior.

Another occurrence during this experiment was electrical outlet trips and power outages, which resulted in the pumps shutting down. When the column pumps were down the leachate solution in the columns was stagnant and the total dissolved U built-up. Therefore, when the pumps restarted, higher concentrations were seen than would have been present without the disturbance. Analysis of the fuel post testing revealed no

alteration phases formed on the surface of the fuel. Such phases are a concern when stagnant conditions are present.

One of the results obtained during testing and seen in Figures 11.1 through 11.8 is that the room temperature tests had higher dissolution rates than the 50ºC and 75ºC tests. The initial hypothesis was that this was due to the change in dissolved O_2 levels at the varying temperatures. In order to test this hypothesis, the plan was to shut off the temperature on the 75ºC bath, thereby increasing the dissolved O_2 from 4.2 to 8.7 ppm. On day 125 of the powder tests an electrical trip caused this to happen, therefore the bath was kept off to observe any changes. The result was an increase in the dissolution rates for the samples in oven C, as shown in Figure 11.9. In this graph, the C7 sample start day was shifted with respect to that of the other samples in order to see the corresponding effect. The electrical trip also caused the pumps to ovens A and B to go down which resulted in spikes in those systems.

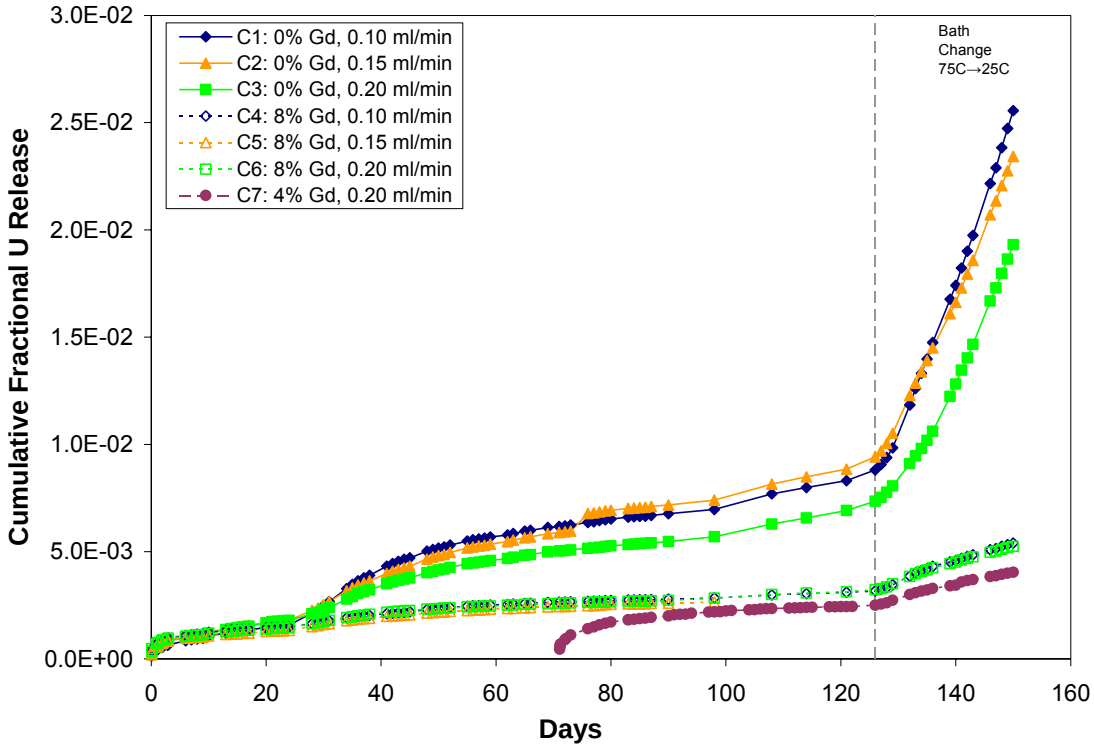

Figure 11.9. Cumulative fraction of uranium released from unirradiated UO_2 samples with 0-8% Gd_2O_3-doped UO_2 and flow rates from 0.10-0.20 mL/min ran in 75ºC oven. Temperature was changed on bath C from 75ºC to 25ºC.

Since increases were seen in all samples in oven C with the increase in dissolved O_2 levels, changes were made to baths A and B in order to see what influences temperature changes had on those systems. Bath A was raised from 25ºC to 75ºC and bath B was dropped from 50ºC to 25ºC, with the results shown in Figures 11.10 through 11.12. It appeared that the U release in system A dropped as the O_2 level was decreased and the release in system B increased as the O_2 level increased. As shown in Table 11.1 the system shut down on day 151 preventing more data from being collected during these secondary experiments.

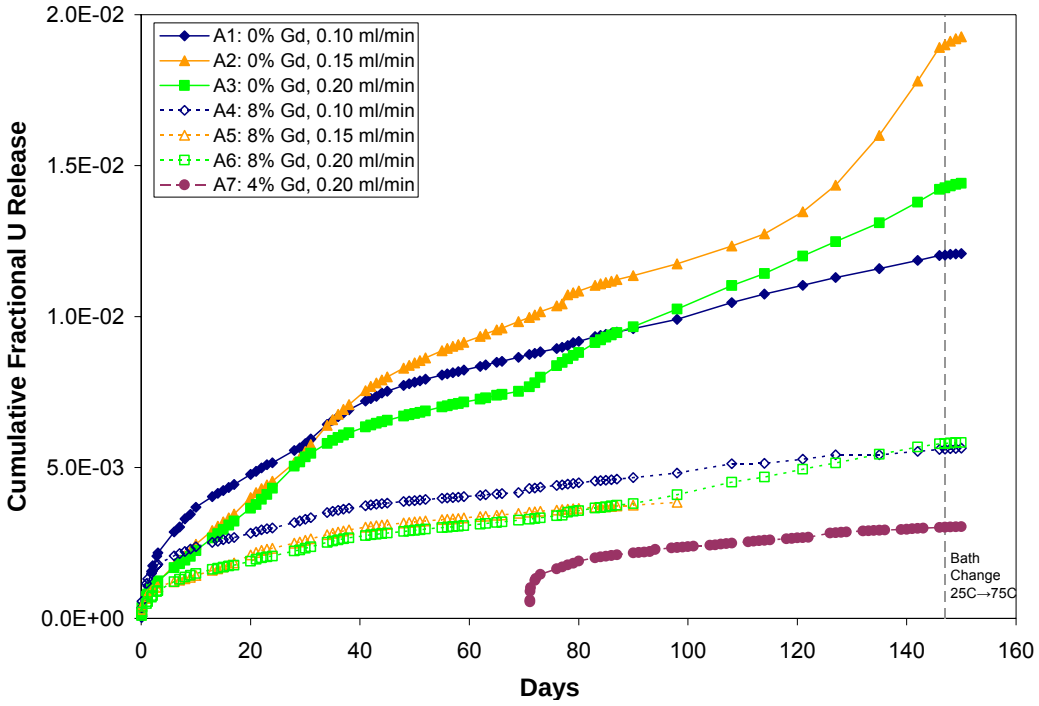

Figure 11.10. Cumulative fraction of uranium released from unirradiated UO_2 powder samples with 0-8% Gd_2O_3-doped UO_2 and flow rates from 0.10-0.20 mL/min ran in 25ºC oven. Temperature was changed on bath from 25ºC to 75ºC.

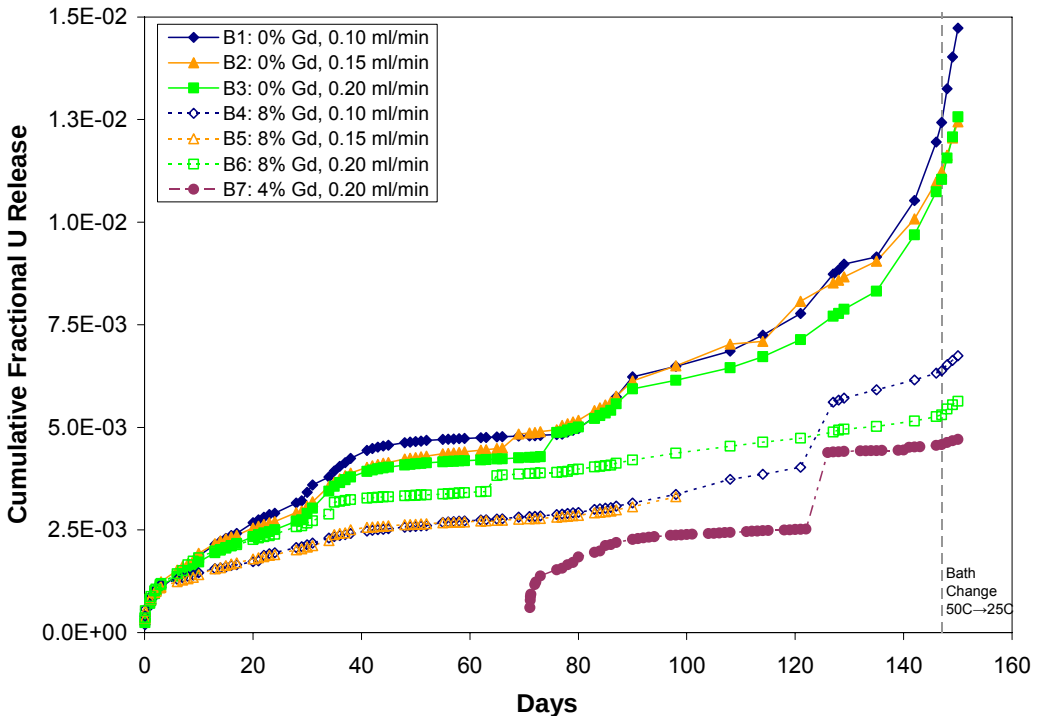

Figure 11.11. Cumulative fraction of uranium released from unirradiated UO_2 powder samples with 0-8% Gd_2O_3-doped UO_2 and flow rates from 0.10-0.20 mL/min ran in 50ºC oven. Temperature was changed on bath from 50ºC to 25ºC.

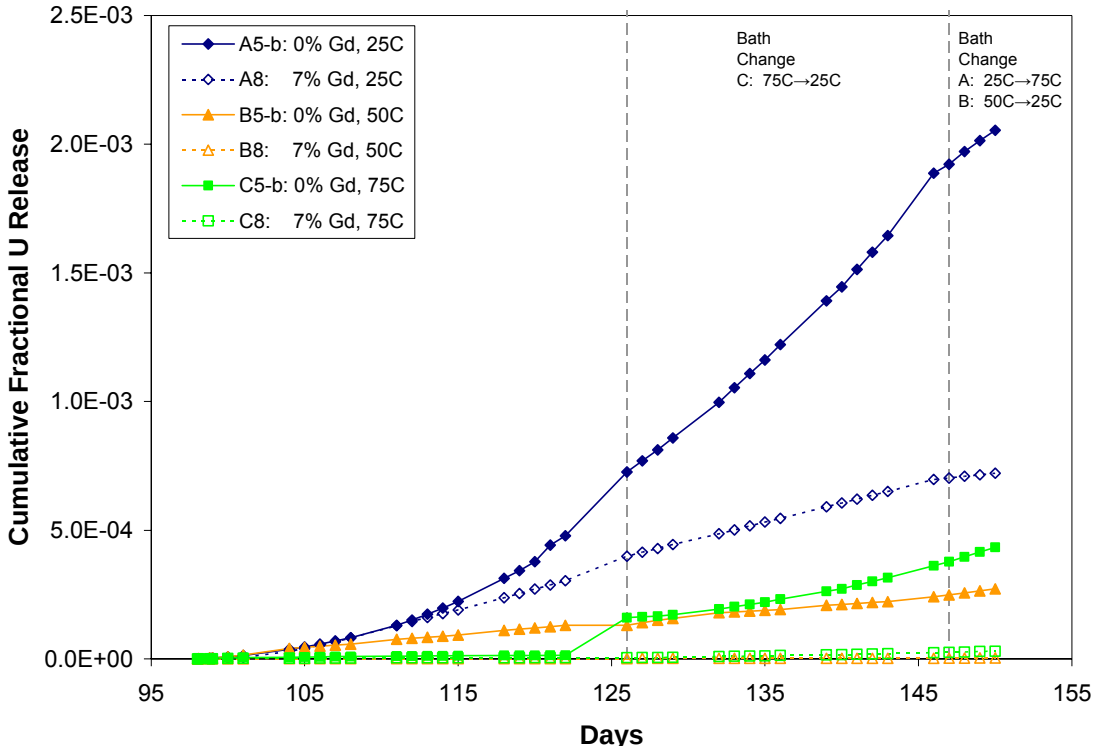

Figure 11.12. Temperature change effects of cumulative fraction of uranium released from unirradiated UO_2 fragment samples with 0 and 7% Gd_2O_3-doped UO_2 and a flow rate of 0.20 mL/min

Figure 11.13 shows the calculation of some of the slopes of the 0.20 mL/min powder samples. It was observed that the increase in release rates was 10 and 6 times higher for the 0 and 8% Gd_2O_3-doped UO_2 respectively, after approximately doubling the dissolved O_2 content. In the case of the reduced O_2 levels, both the doped and non-doped samples dropped by approximately a third. These results served as the basis for the remaining tests where O_2 levels were varied while keeping the ovens at the same temperature, thus examining the direct influence dissolved O_2 had on the dissolution rate.

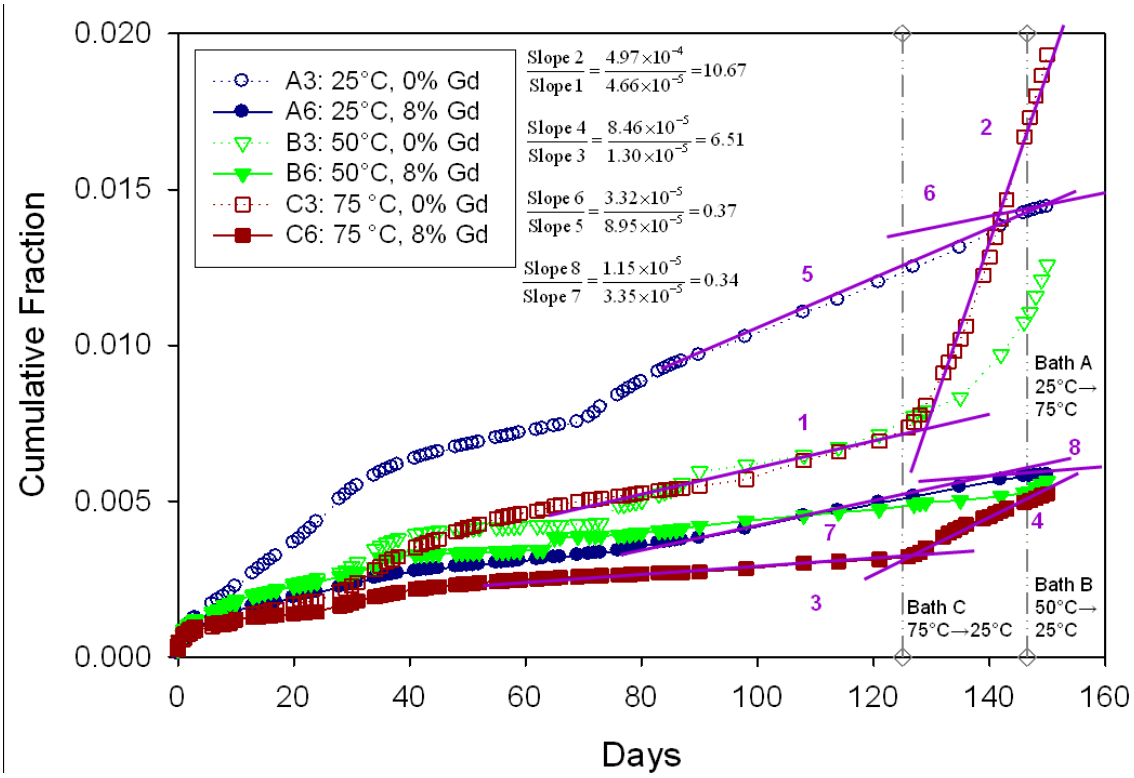

Figure 11.13. Temperature change effects of cumulative fraction of uranium released from unirradiated UO_2 powder samples with 0 and 8% Gd_2O_3-doped UO_2 and a flow rate of 0.20 mL/min

Tests 2-5

The data from Tests 2 though 5 are shown in Figures 11.14 through 11.21. In achieving the 4.2, 5.9, and 8.7 ppm dissolved O_2 levels, the baths were kept at 25, 50 and 75°C respectively and sparged with 20.9% O_2 as predicted by Henry's Law and verified by the inline O_2 probes. In order to achieve the 3.0 ppm O_2 level with 20.9% O_2, a temperature of 105°C would be required, which was not realistic since it is above the boiling point of water and exceeds the limitations of Henry's Law. Instead a 10.3% O_2 gas was utilized which predicted a bath temperature of 48°C necessary for 3.0 ppm O_2. This was not able to be achieved in our system, and may have been a result of atmospheric air surrounding the bath. It was discovered by the inline O_2 probes that if the bath temperature was raised to 60°C, the desired 3.0 ppm could be maintained.

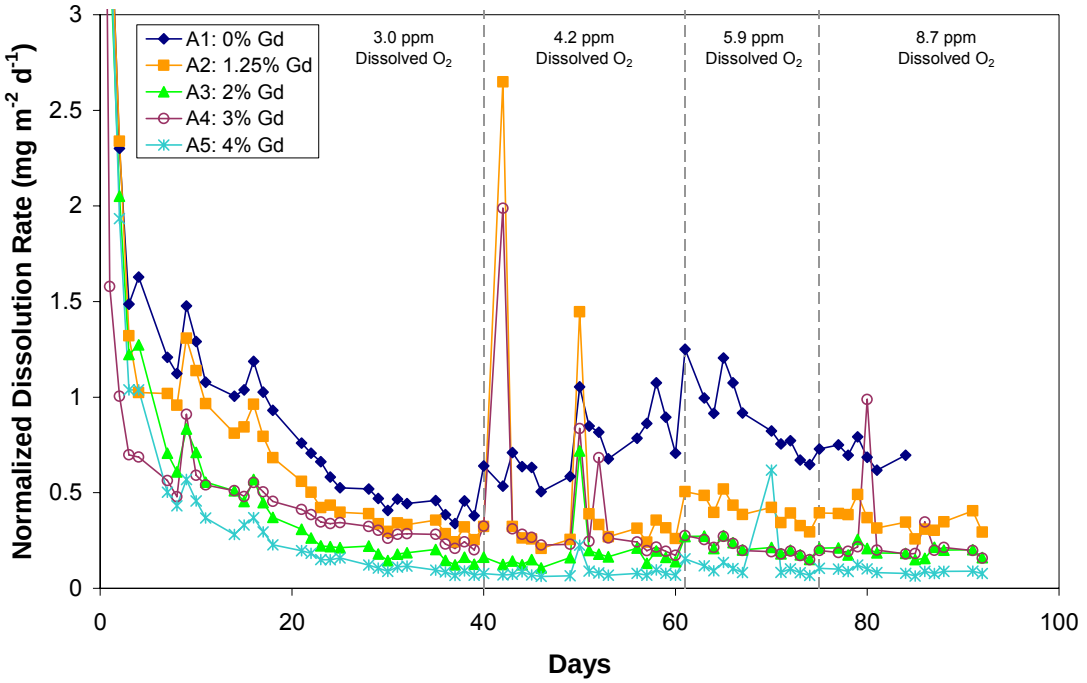

Figure 11.14. Normalized dissolution rate of unirradiated UO_2 powder samples ran at 25ºC with Gd_2O_3 dopant levels ranging from 0-4% over an O_2 range of 3.0 to 8.7 ppm

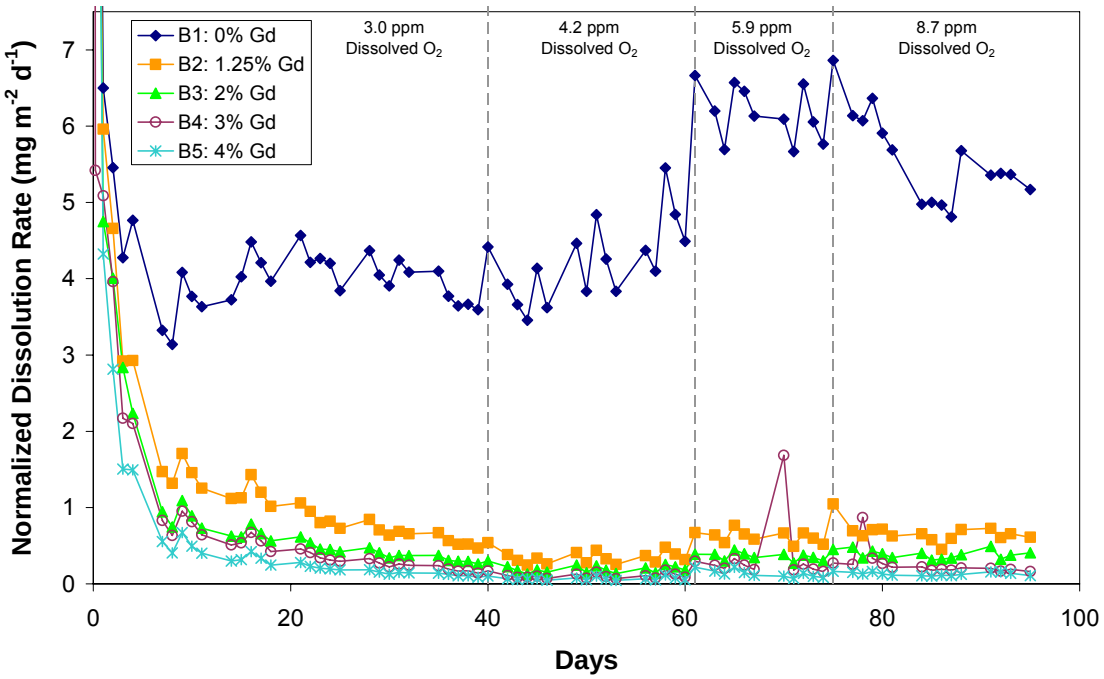

Figure 11.15. Normalized dissolution rate of unirradiated UO_2 powder samples ran at 50ºC with Gd_2O_3 dopant levels ranging from 0-4% over an O_2 range of 3.0 to 8.7 ppm

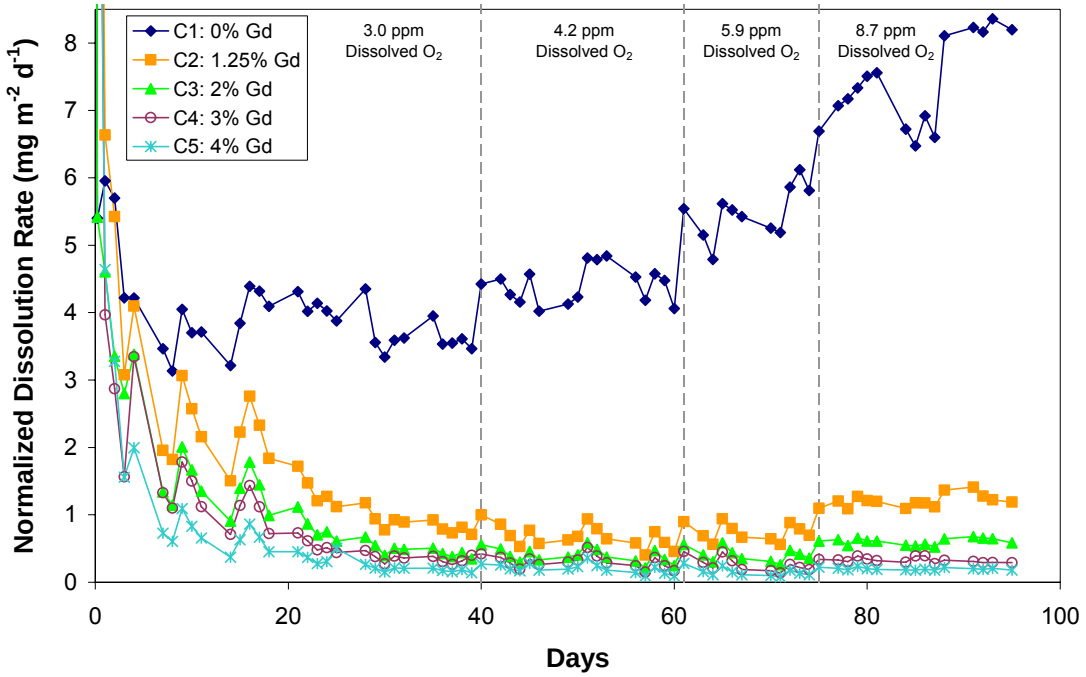

Figure 11.16. Normalized dissolution rate of unirradiated UO_2 powder samples ran at 75ºC with Gd_2O_3 dopant levels ranging from 0-4% over an O_2 range of 3.0 to 8.7 ppm

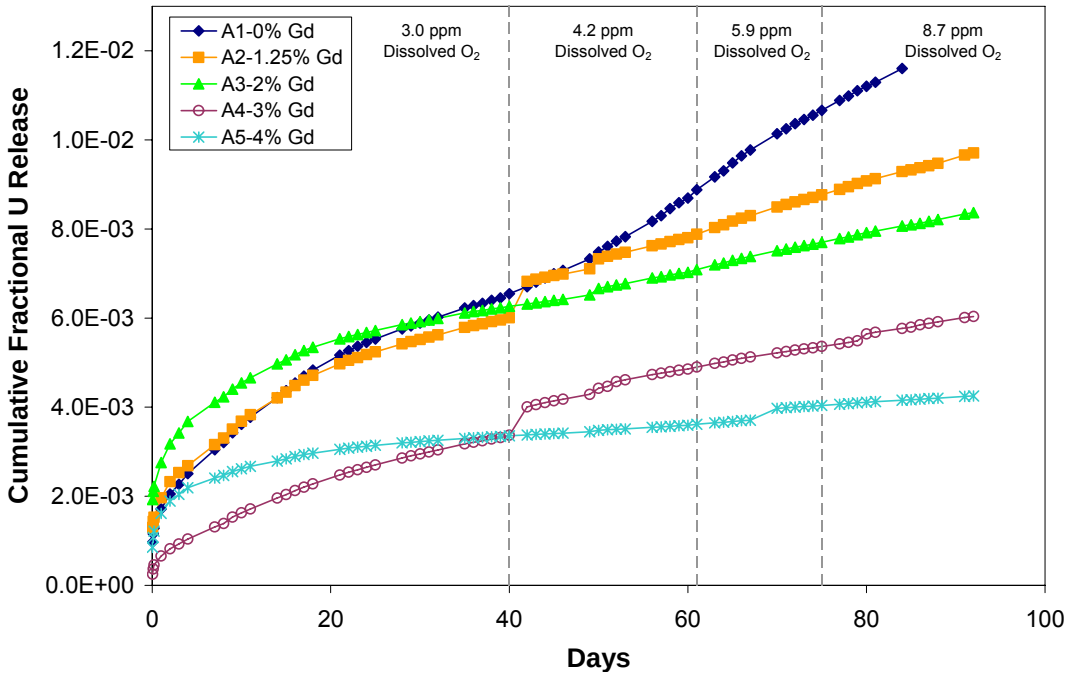

Figure 11.17. Cumulative fraction of uranium released from powder unirradiated UO_2 samples ran at 25ºC with Gd_2O_3 dopant levels ranging from 0-4% over an O_2 range of 3.0 to 8.7 ppm

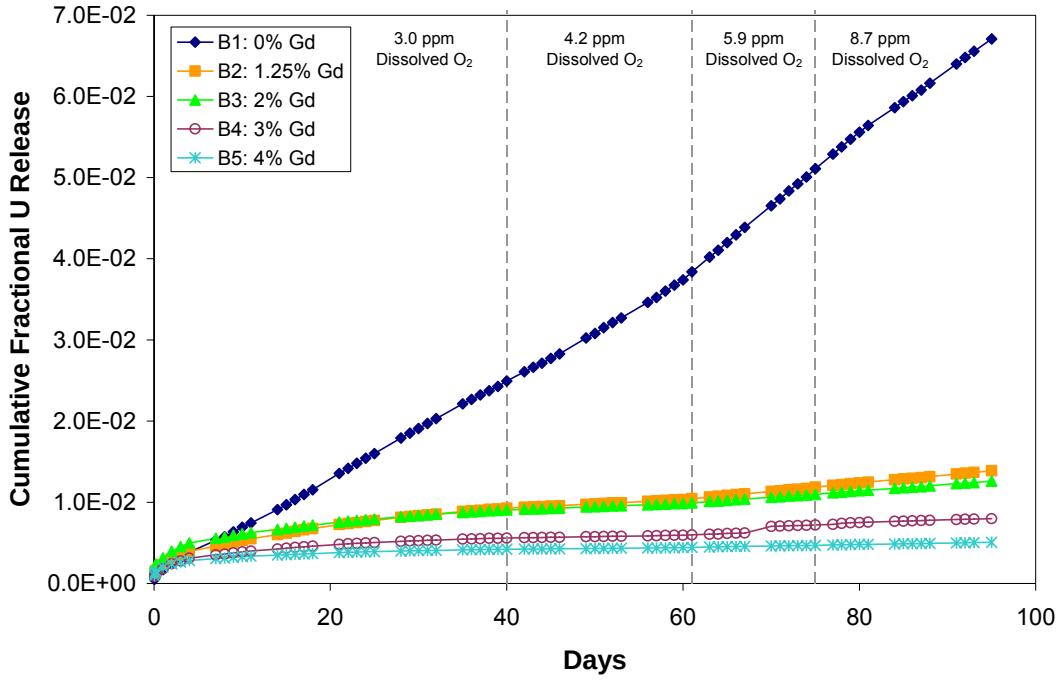

Figure 11.18. Cumulative fraction of uranium released from powder unirradiated UO_2 samples ran at 50ºC with Gd_2O_3 dopant levels ranging from 0-4% over an O_2 range of 3.0 to 8.7 ppm

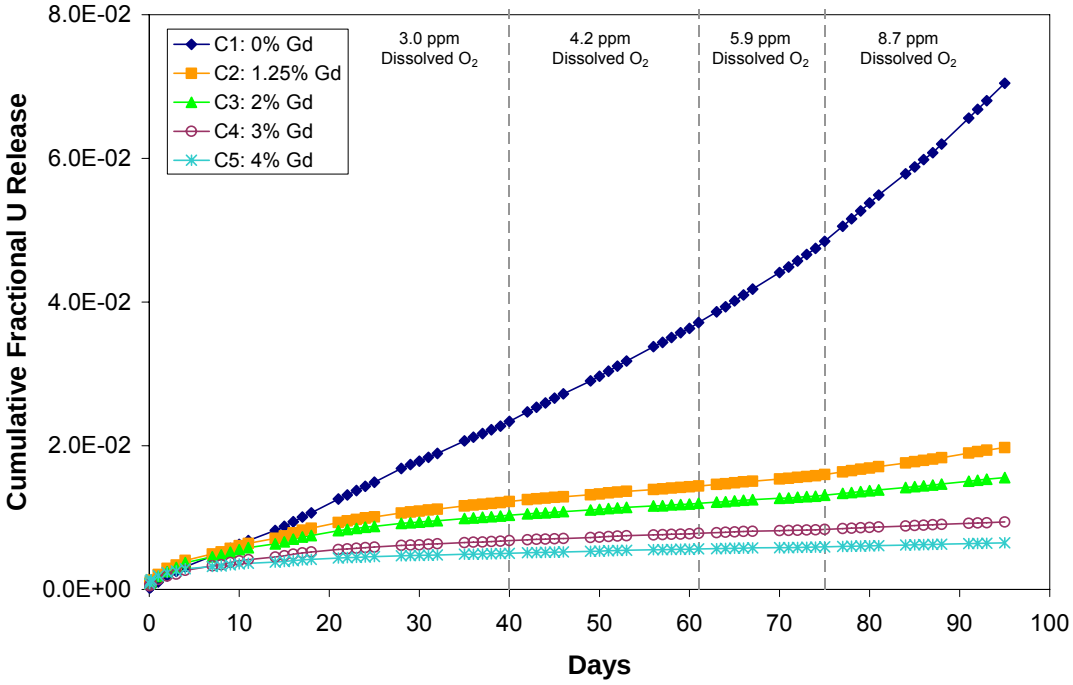

Figure 11.19. Cumulative fraction of uranium released from powder unirradiated UO_2 samples ran at 75ºC with Gd_2O_3 dopant levels ranging from 0-4% over an O_2 range of 3.0 to 8.7 ppm

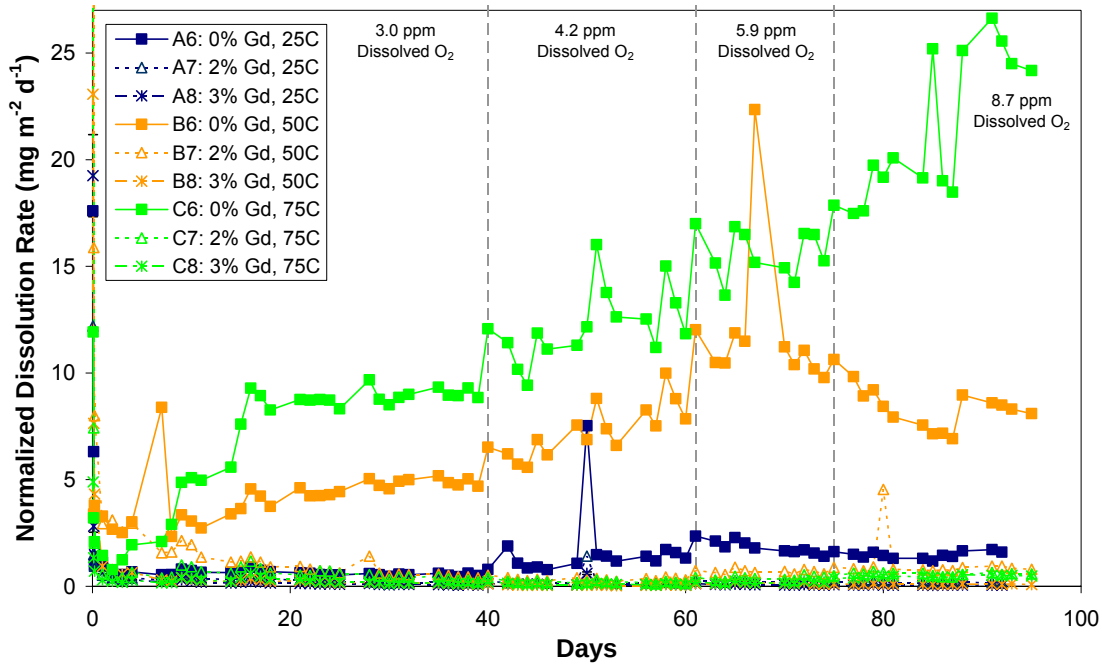

Figure 11.20. Normalized dissolution rate of unirradiated UO_2 fragmented samples with Gd_2O_3 dopant levels ranging from 0-3% over an O_2 range of 3.0 to 8.7 ppm

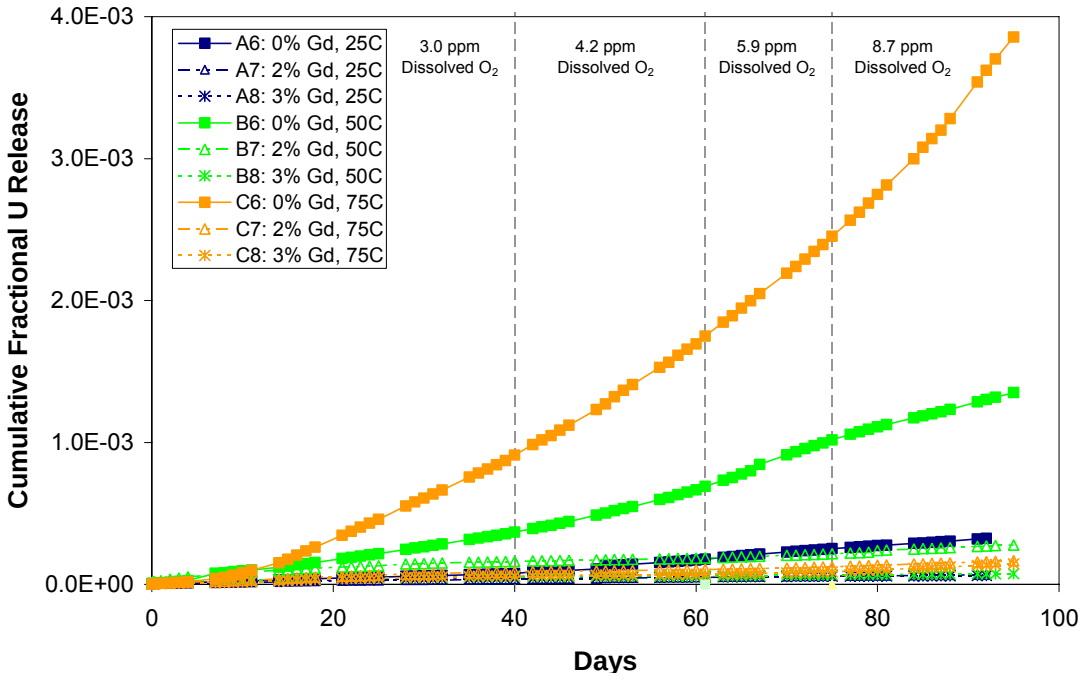

Figure 11.21. Cumulative fraction of uranium released from fragmented unirradiated UO_2 samples with Gd_2O_3 dopant levels ranging from 0-3% over an O_2 range of 3.0 to 8.7 ppm

In these tests, only a few system problems occurred, which are listed in Table 11.2. Two of these occurrences were similar to wall outlet trips in Test 1. The sources of these trips are unknown although they may have been a result of power spikes in the building. The other occurrence was a leak detected on column A1 on day 85 of testing. The leak could not be fixed and the column had to be removed.

Table 11.2. Incidents during Tests 2-5 and affected columns with days measured from the beginning of Test 2

Day	Affected Columns	Incident
49	A set	Wall Outlet Tripped: Pumps to A Columns Down from ~11:30 pm to ~8 am on Day 50
85	A1	Leak on A1 Column, Testing for A1 Ended
93	A set	Wall Outlet Tripped: Pumps to A Columns Down, Testing for all A Ended

This chapter presented the normalized dissolution rates and cumulative fractions of U released over time for all samples. Table 11.1 and 11.2 described incidents that happened during testing that could have impacted the data and should be taken into consideration when evaluating the data. A full comparison of the different parameters tested, such as water chemistry, surface area, fuel chemistry, temperature, and dissolved O_2 will be discussed in the following chapters.

CHAPTER 12: POST-TEST ANALYSIS OF FUEL

Test 1

After the fuels were removed from the single-pass flow-through tests, analysis of the fuel surfaces were performed using SEM. Some results of the fuels from Test 1 are shown in Figures 12.1 through 12.3 below. The fuels examined were run with a flow rate of 0.2 mL/min for the 0 and 8% Gd_2O_3-doped UO_2 powder samples and the 0 and 7% Gd_2O_3-doped UO_2 fragment samples. The powder samples showed most fines had been removed from the fuel surface during testing. It appeared there was minimal change to the fuel surface except for sample A5-b shown in Figure 12.1.c. This sample contained the 0% Gd_2O_3, fragment run at 25ºC. In this image it is clearly seen that the grain boundaries were preferentially attacked during dissolution. This is one property that was discussed in Chapter 6 as changing the surface area of the fuel during testing and thus altering the normalized dissolution rate. However, out of these samples examined, this was the only one that exhibited this property.

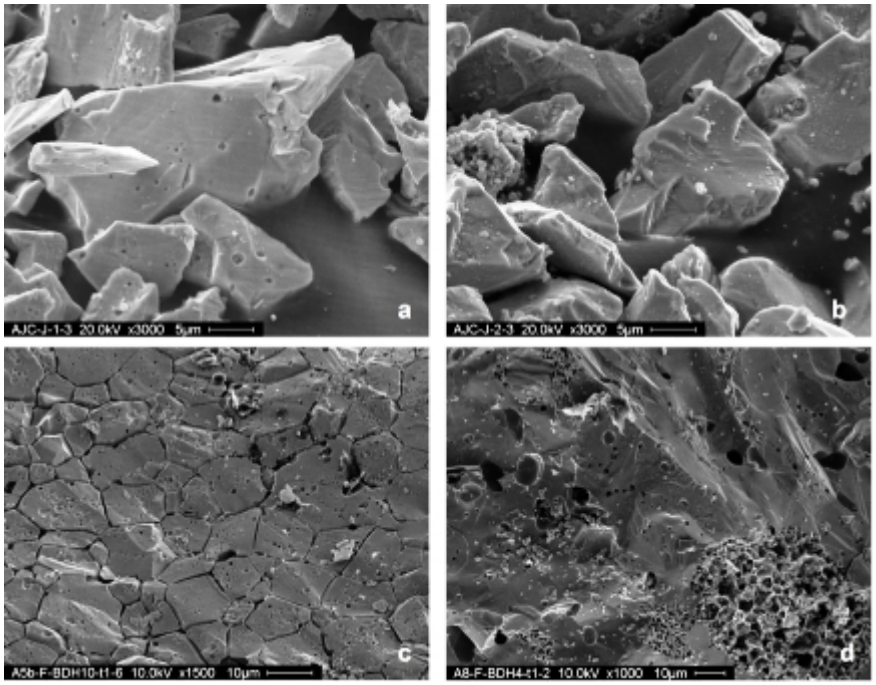

Figure 12.1. SEM images of samples from 25ºC oven in Test 1 taken after SPFT experiment a.) A3: 0% Gd_2O_3-doped UO_2 powder, 0.20 mL/min, b.) A6: 8% Gd_2O_3-doped UO_2 powder, 0.20 mL/min, c.) A5-b: 0% Gd_2O_3-doped UO_2 fragment, 0.20 mL/min, and d.) A8: 7% Gd_2O_3-doped UO_2 fragment, 0.20 mL/min

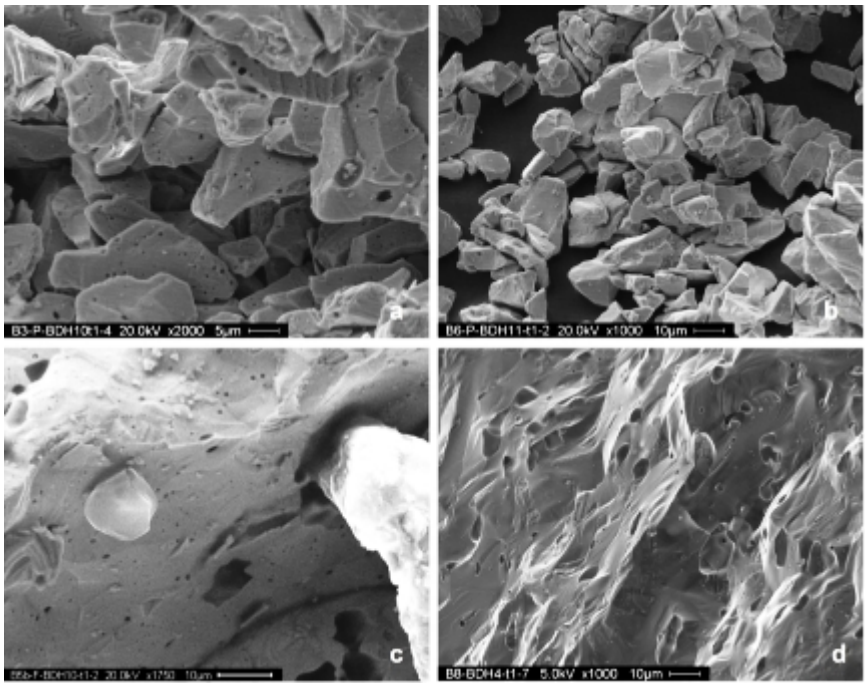

Figure 12.2. SEM images of samples from 50ºC oven in Test 1 taken after SPFT experiment a.) B3: 0% Gd_2O_3-doped UO_2 powder, 0.20 mL/min, b.) B6: 8% Gd_2O_3-doped UO_2 powder, 0.20 mL/min, c.) B5-b: 0% Gd_2O_3-doped UO_2 fragment, 0.20 mL/min, and d.) B8: 7% Gd_2O_3-doped UO_2 fragment, 0.20 mL/min

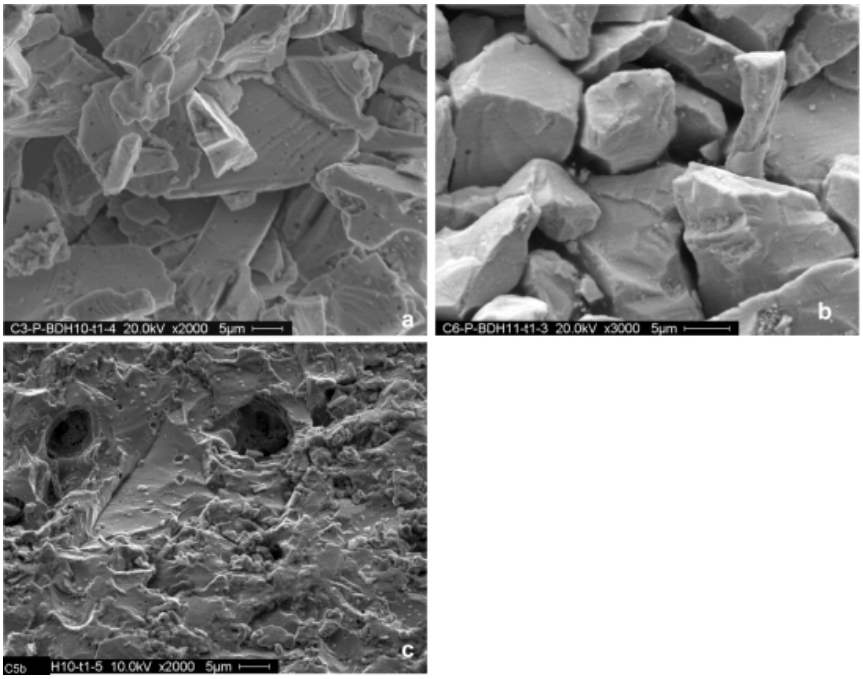

Figure 12.3. SEM images of samples from 75ºC oven in Test 1 taken after SPFT experiment a.) C3: 0% Gd_2O_3-doped UO_2 powder, 0. 20 mL/min, b.) C6: 8% Gd_2O_3-doped UO_2 powder, 0.20 mL/min, and c.) C5-b: 0% Gd_2O_3-doped UO_2 fragment, 0.20 mL/min

These fuels were also analyzed using the EDS system on the SEM. The main constituents observed were C, O, Cu, U, Gd, and Si with their weight percents shown in Table 12.1. The presence of Cu is unexplained, although it was observed and discussed in the analysis of the fuels before testing described in Chapter 10. The occurrence of Si was a result of the feedwater contamination presented in Chapter 11 and will be further discussed in Chapter 13. Along with the above constituents, Al, S, Cl, Ca, Fe, Na, Mg, Cr, Ni, and Zn were observed on samples B5b and B8. These elements were also found with Si to have elevated concentrations in the feedwater due to the DIW system. Only trace levels of these constituents existed on the fuel surface with the exclusions of attached particles such as shown in Figure 12.4. Regions such as 1, 2, and 4 in this figure showed elevated levels with up to 7 wt% of the listed elements.

Table 12.1. SEM-EDS results of surface composition in weight % of samples from Test 1

Element	A3	error ±	A6	error ±	A5b	error ±	A8	error ±
C	11.3	4.3	13.5	7.6	10.7	4.4	13.9	5.3
O	14.6	4.9	19.7	1.7	11.0	4.3	13.8	3.5
Cu	4.5	2.9	0.0	0.0	9.9	4.0	7.7	6.6
U	69.3	7.7	60.9	7.5	68.2	4.7	59.0	8.3
Gd	0.3	0.3	6.0	0.7	0.3	0.3	5.7	0.8
Si	0.0	0.0	0.0	0.0	0.1	0.1	0.0	0.0

Element	B3	error ±	B6	error ±	B5b	error ±	B8	error ±
C	9.9	6.2	15.0	9.1	15.1	5.6	52.6	9.5
O	19.8	3.5	17.3	5.4	19.1	6.4	24.4	6.3
Cu	2.7	2.7	7.8	2.5	2.8	5.6	4.0	6.4
U	64.9	10.1	51.7	13.3	59.0	8.3	15.4	6.1
Gd	0.4	0.3	5.4	1.6	0.3	0.4	0.9	0.4
Si	2.4	0.5	2.6	0.6	3.5	1.7	2.0	1.1

Element	C3	error ±	C6	error ±	C5b	error ±
C	16.1	8.8	13.5	5.5	30.5	1.9
O	21.7	5.9	17.2	5.9	28.9	4.7
Cu	7.9	7.6	8.5	9.1	1.4	3.1
U	51.2	13.2	53.5	9.6	38.5	3.0
Gd	0.4	0.2	5.7	0.3	0.3	0.1
Si	2.5	0.8	1.6	0.4	1.1	1.1

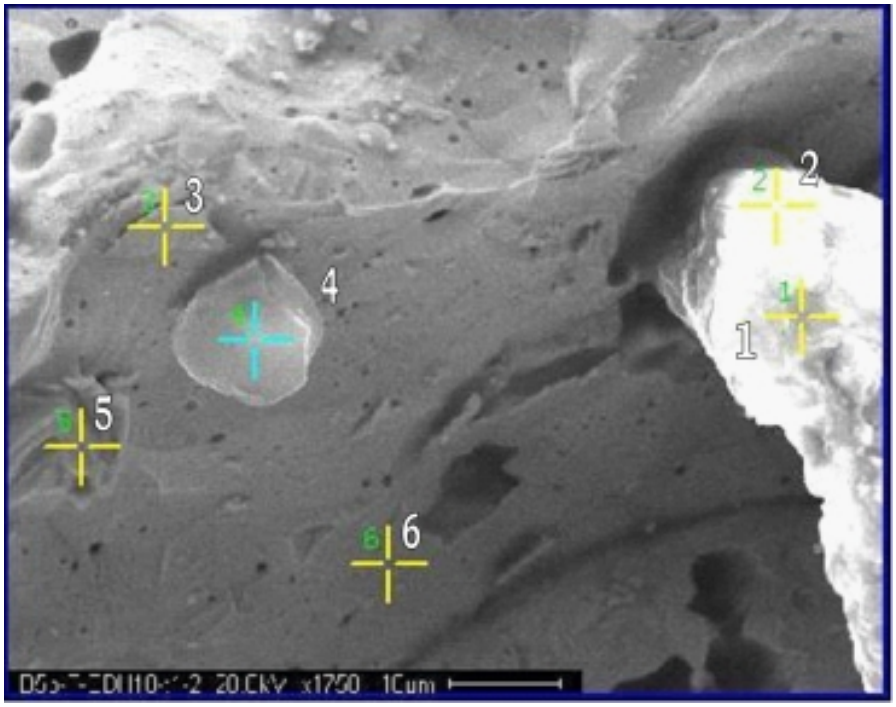

Figure 12.4. SEM-EDS image of sample from 50ºC oven in Test 1 taken after SPFT experiment of B5-b (0% Gd_2O_3 doped-UO_2 fragment)

Tests 2-5

The SEM-EDS images of the powder samples after removal from the single-pass flow-through system are shown in Figures 12.5 through 12.7. In these images, pores on the surface of the fuel were observed, which may have been present before testing although they may not have been visible due to coverage by fines. These samples showed no visible surface alteration products formed during testing, which would interfere with the oxidation and dissolution properties.

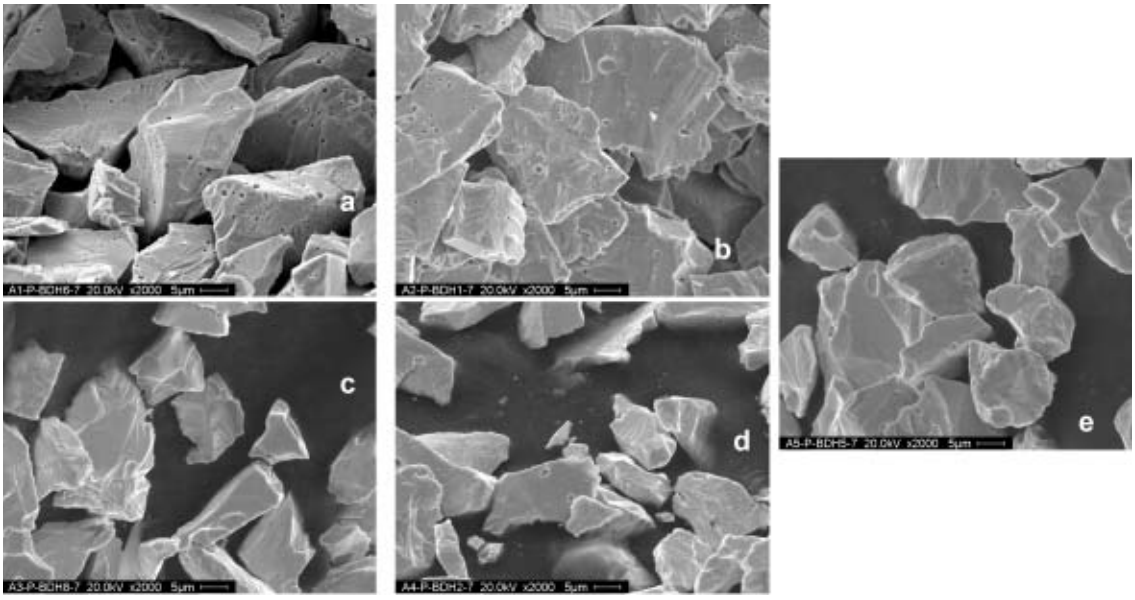

Figure 12.5. SEM images of samples from 25ºC oven in Tests 2-5 taken after SPFT experiment a.) A1: 0% Gd_2O_3-doped UO_2 powder, b.) A2: 1.25% Gd_2O_3-doped UO_2 powder, c.) A3: 2% Gd_2O_3-doped UO_2 powder, d.) A4: 3% Gd_2O_3-doped UO_2 powder, e.) A5: 4% Gd_2O_3-doped UO_2 powder

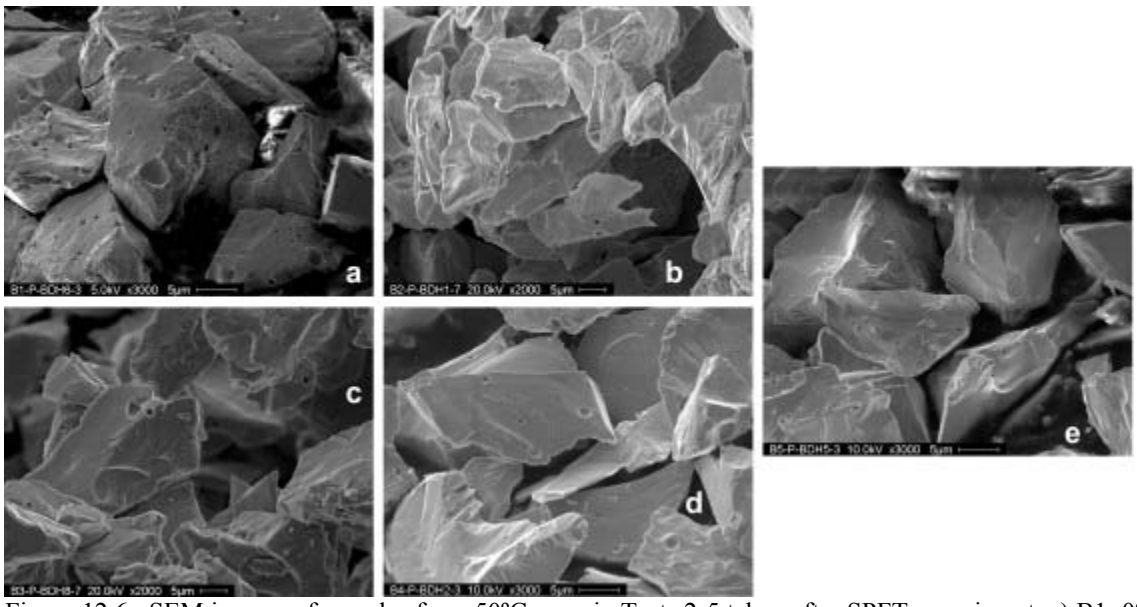

Figure 12.6. SEM images of samples from 50ºC oven in Tests 2-5 taken after SPFT experiment a.) B1: 0% Gd_2O_3-doped UO_2 powder, b.) B2: 1.25% Gd_2O_3-doped UO_2 powder, c.) B3: 2% Gd_2O_3-doped UO_2 powder, d.) B4: 3% Gd_2O_3-doped UO_2 powder, e.) B5: 4% Gd_2O_3-doped UO_2 powder

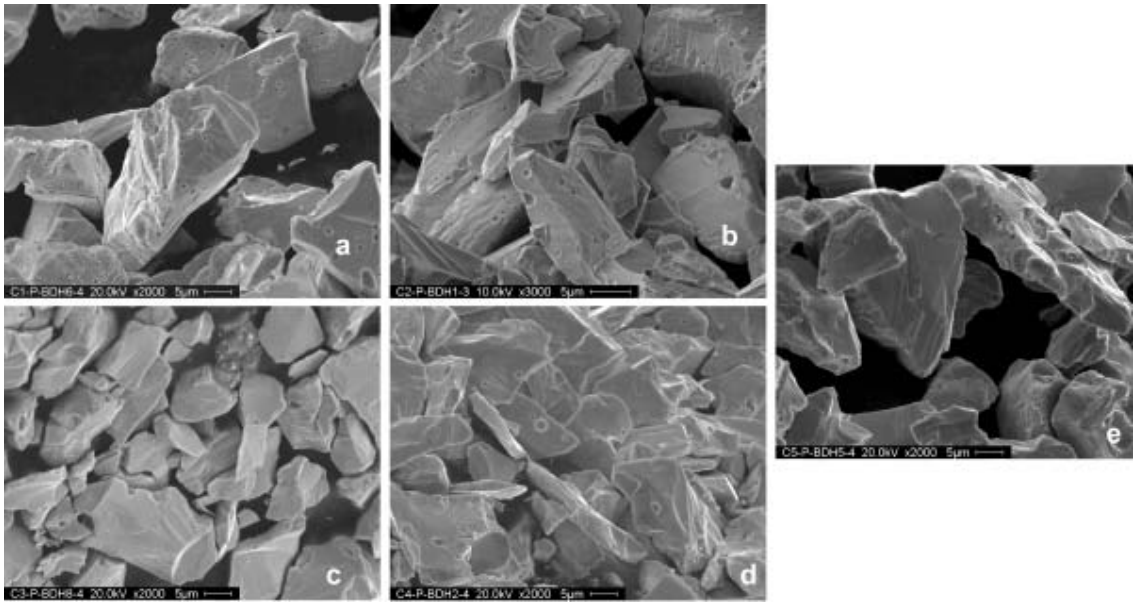

Figure 12.7. SEM images of samples from 75ºC oven in Tests 2-5 taken after SPFT experiment a.) C1: 0% Gd_2O_3-doped UO_2 powder, b.) C2: 1.25% Gd_2O_3-doped UO_2 powder, c.) C3: 2% Gd_2O_3-doped UO_2 powder, d.) C4: 3% Gd_2O_3-doped UO_2 powder, e.) C5: 4% Gd_2O_3-doped UO_2 powder

Along with the SEM analysis, EDS was also run on these fuels with the results shown in Table 12.2. No other constituents other than C, O, Cu, U, and Gd were identified on the surface of the powder samples in Tests 2 through 5. The comparison of

the EDS measurements of the wt% of Gd prior and post testing are displayed in Figure 12.8. The figure shows both the nominal Gd_2O_3 values used to describe the fuels and the actual Gd values that were listed in Table 11.10. It appears that the wt% of Gd on the majority of samples remained statistically equivalent during testing. In some cases there was no Gd observed, although as the samples were highly heterogeneous as discussed in Chapter 10, this may have been a result of the points examined not being entirely representative of the whole.

Table 12.2. SEM-EDS results of surface composition in weight % of powder samples from Tests 2-5

Element	A1	error ±	A2	error ±	A3	error ±	A4	error ±	A5	error ±
C	17.36	7.79	6.74	2.07	11.79	7.83	19.66	4.05	7.00	0.29
O	22.17	0.66	22.92	3.97	19.96	0.73	18.03	0.71	17.16	4.82
Cu	7.51	3.17	2.12	1.86	0.00	0.00	6.53	2.35	3.84	1.95
U	53.23	11.19	68.22	6.26	64.02	7.17	53.41	4.90	67.84	2.09
Gd	0.00	0.00	0.00	0.00	2.43	0.50	2.38	0.48	4.16	1.22

Element	B1	error ±	B2	error ±	B3	error ±	B4	error ±	B5	error ±
C	7.07	0.50	6.86	0.61	12.50	11.13	6.71	1.81	12.13	1.30
O	20.89	3.58	19.46	1.86	20.54	4.03	15.14	5.08	21.66	3.66
Cu	2.58	1.13	4.76	0.22	4.98	4.04	4.55	1.06	3.62	0.34
U	68.54	2.64	68.36	3.22	61.98	18.91	70.04	5.47	59.59	4.72
Gd	0.66	0.34	0.00	0.00	0.00	0.00	3.55	0.41	2.99	0.58

Element	C1	error ±	C2	error ±	C3	error ±	C4	error ±	C5	error ±
C	5.56	0.98	6.65	1.22	22.56	0.61	18.05	3.57	23.19	6.52
O	17.26	1.39	24.90	4.19	38.78	3.16	36.01	3.17	37.46	3.76
Cu	2.23	2.17	0.00	0.00	0.00	0.00	0.00	0.00	0.46	0.79
U	74.32	3.53	66.91	5.04	37.93	4.05	44.48	6.26	37.22	7.21
Gd	0.58	0.51	1.54	0.40	0.74	0.37	1.46	0.23	1.69	0.45

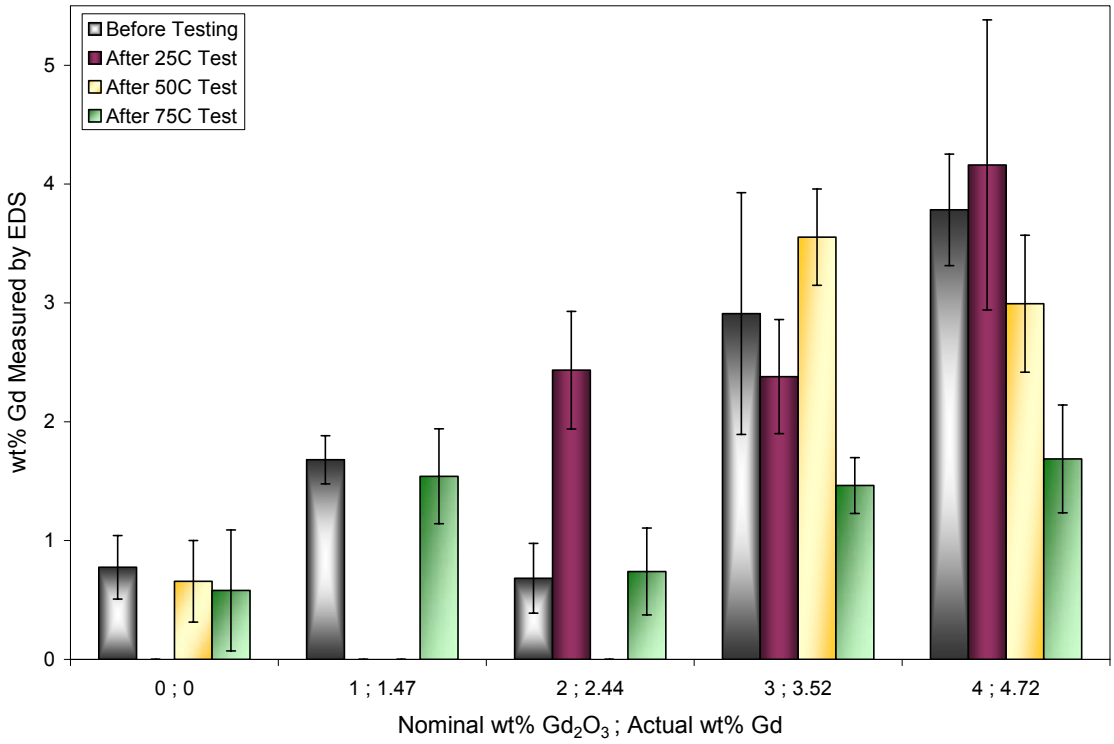

Figure 12.8. Wt% of Gd comparison prior and post testing on UO_2 powders run in Tests 2 through 5 at 25ºC, 50ºC, and 75ºC

Both SEM and EDS were also run on the fragment samples from Tests 2 through 5 and are shown in Figures 12.9 through 12.11 and Table 12.3. In the 2% Gd_2O_3-doped UO_2 fragment in the 75ºC oven (C7) very distinct preferential grain boundary penetration was observed, similar to that seen in the 0% Gd_2O_3-doped UO_2 fragment (A5-b) in Test 1. Some initial penetration of grain boundaries was observed in the 50ºC 0% Gd_2O_3-doped UO_2 fragment (B6), although it was not as pronounced as in the other two samples. There was no clear correlation of temperature or Gd_2O_3-dopant level as the samples occurred at all temperatures and for some, but not all, 0% and 2% Gd_2O_3-doped UO_2 fragment samples.

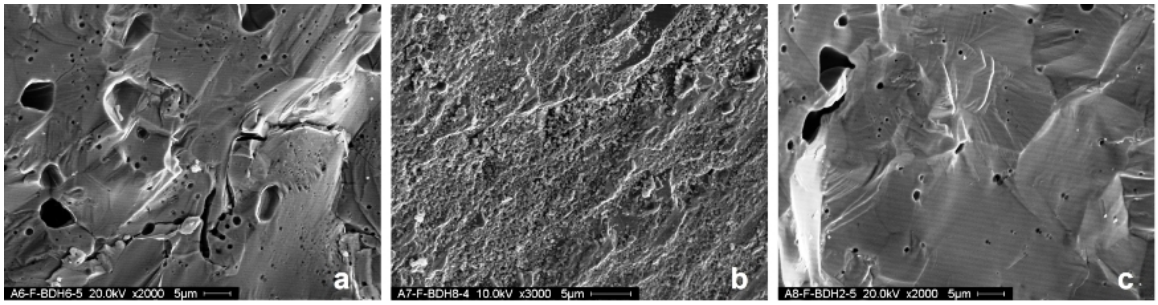

Figure 12.9. SEM images of samples from 25ºC oven in Tests 2-5 taken after SPFT experiment a.) A6: 0% Gd_2O_3-doped UO_2 fragment, b.) A7: 2% Gd_2O_3-doped UO_2 fragment, c.) A8: 3% Gd_2O_3-doped UO_2 fragment

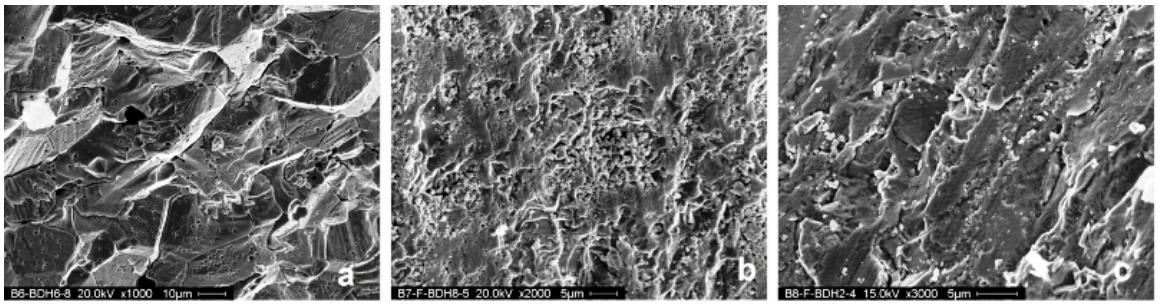

Figure 12.10. SEM images of samples from 50ºC oven in Tests 2-5 taken after SPFT experiment a.) B6: 0% Gd_2O_3-doped UO_2 fragment, b.) B7: 2% Gd_2O_3-doped UO_2 fragment, c.) B8: 3% Gd_2O_3-doped UO_2 fragment

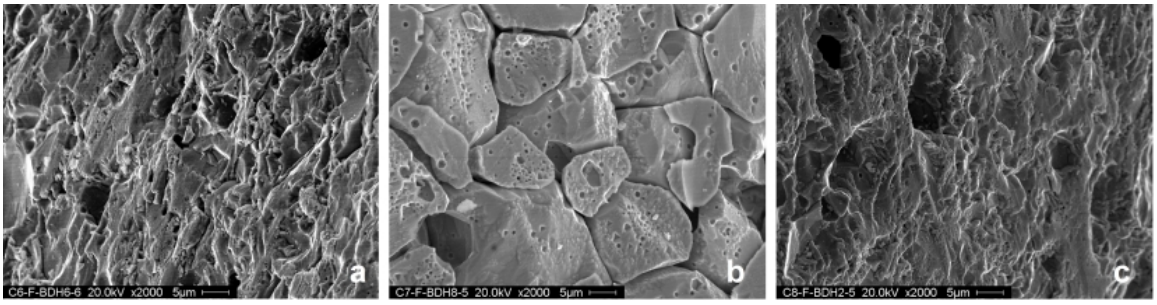

Figure 12.11. SEM images of samples from 75ºC oven in Tests 2-5 taken after SPFT experiment a.) C6: 0% Gd_2O_3-doped UO_2 fragment, b.) C7: 2% Gd_2O_3-doped UO_2 fragment, c.) C8: 3% Gd_2O_3-doped UO_2 fragment

Table 12.3. SEM-EDS results of surface composition in weight % of fragment samples from Tests 2-5

Element	A6	error ±	A7	error ±	A8	error ±
C	23.9	6.3	29.8	2.8	26.9	1.2
O	24.3	11.0	40.8	1.6	31.2	1.5
Cu	7.5	7.1	0.0	0.0	0.1	0.3
U	44.0	10.6	26.1	5.3	40.7	2.4
Gd	0.4	0.1	0.5	0.3	1.1	0.4

Element	B6	error ±	B7	error ±	B8	error ±
C	25.7	6.9	23.4	3.5	28.6	11.9
O	36.3	4.3	39.0	2.8	21.9	5.0
Cu	0.0	0.0	0.1	0.2	3.5	3.8
U	38.0	11.0	37.4	6.5	44.6	8.9
Gd	0.0	0.0	0.1	0.3	1.5	0.1

Element	C6	error ±	C7	error ±	C8	error ±
C	27.7	3.4	29.7	4.3	32.0	3.2
O	30.6	5.4	18.2	2.1	29.6	2.8
Cu	3.1	4.3	11.8	2.9	4.8	4.1
U	37.5	4.8	40.0	4.2	32.9	4.3
Gd	1.0	0.2	0.3	0.1	0.8	0.4

Reference

[1]Grandstaff, D. E., "A Kinetic Study of the Dissolution of Uraninite," *Economic Geology*, **71**, 1493-1506 (1976)

CHAPTER 13: DISCUSSION AND CONCLUSIONS-WATER CHEMISTRY

As described in Chapter 11, there was a disturbance in the water chemistry approximately 30 days into Test 1. It was discovered, upon conclusion of this test, that the DIW system to the building had not been operational the entire time Test 1 was operational, and elevated levels of certain constituents were present in the feedwaters. The system was fixed before Tests 2 through 5 began, therefore they were not affected. Inductively Coupled Plasma Mass Spectrometry (ICP-MS) and Optical Emission Spectroscopy (OES) were run on samples taken from Test 1 on day 17 and day 31 of the 25ºC, 50ºC, and 75ºC tests for both the 0 and 8% Gd_2O_3-doped UO_2 samples, with the results shown in Table 13.1. Only those constituents above the instrument detectability are shown. Some samples were also analyzed around day 50 which showed levels similar to those around day 17. Therefore, the ion capacity was expended within 3 weeks and elevated levels of these constituents persisted.

Table 13.1. Concentrations of constituents in 25ºC, 50ºC, and 75ºC samples for unirradiated UO_2 powder samples with both 0 and 8% doping levels of Gd_2O_3

	Concentration (µg/L)							
Sample*	Al	Ba	Ca	K	Mg	P	Si	S
A2 Day 17	21.68	9.43	914.01	2105.93	215.35	847.92	221.45	245.25
A5 Day 17	26.74	11.14	929.41	2214.16	216.58	851.73	241.74	294.50
B2 Day 17	20.05	10.55	906.70	3179.47	209.39	1150.77	277.27	233.31
B5 Day 17	30.66	15.49	912.97	3181.78	209.23	1177.37	297.87	282.33
C2 Day 17	132.85	11.04	946.26	1768.67	219.60	700.31	963.08	291.88
C5 Day 17	62.37	7.57	891.48	1778.85	216.82	695.57	858.88	330.32
A2 Day 31	16.41	0.88	253.77	665.47	61.23	247.49	105.02	24.94
A5 Day 31	7.67	0.69	264.36	646.21	60.33	271.90	114.15	15.93
B2 Day 31	7.21	0.32	346.36	2305.70	80.21	893.05	217.41	7.48
B5 Day 31	22.46	0.92	355.21	2272.45	80.70	898.17	211.44	83.01
C2 Day 31	27.45	1.78	466.52	705.42	99.25	284.27	761.78	19.65
C5 Day 31	32.02	1.78	463.38	742.81	99.67	254.91	726.62	63.09

*Where A=25ºC, B=50ºC, C=75ºC; 2=0% Gd_2O_3, 5=8% Gd_2O_3

The ratios of the concentrations on day 31 and day 17 are calculated in Table 13.2 and show a decrease in the constituents after the filters were replaced. Two components of particular interest are calcium and silicate. Both of these elements have been shown to decrease the dissolution of fuel[1,2] and are present in J-13 well water, which is the water taken from a well near Yucca Mountain that has similar composition to what might contact fuel within the repository. Figure 13.1 compares the concentration of the Ca and Si in solution over the tested samples. These samples were taken from the leachate after coming into contact with the fuel.

Table 13.2. Factor decrease from day 31 to day 17 of constituent concentrations given in Table 13.1

	Ratio of Day 31/Day 17							
Sample	Al	Ba	Ca	K	Mg	P	Si	S
AJK-A2	1.32	10.69	3.60	3.16	3.52	3.43	2.11	9.83
AJK-A5	3.49	16.17	3.52	3.43	3.59	3.13	2.12	18.49
AJK-B2	2.78	33.45	2.62	1.38	2.61	1.29	1.28	31.20
AJK-B5	1.37	16.77	2.57	1.40	2.59	1.31	1.41	3.40
AJK-C2	4.84	6.18	2.03	2.51	2.21	2.46	1.26	14.85
AJK-C5	1.95	4.25	1.92	2.39	2.18	2.73	1.18	5.24

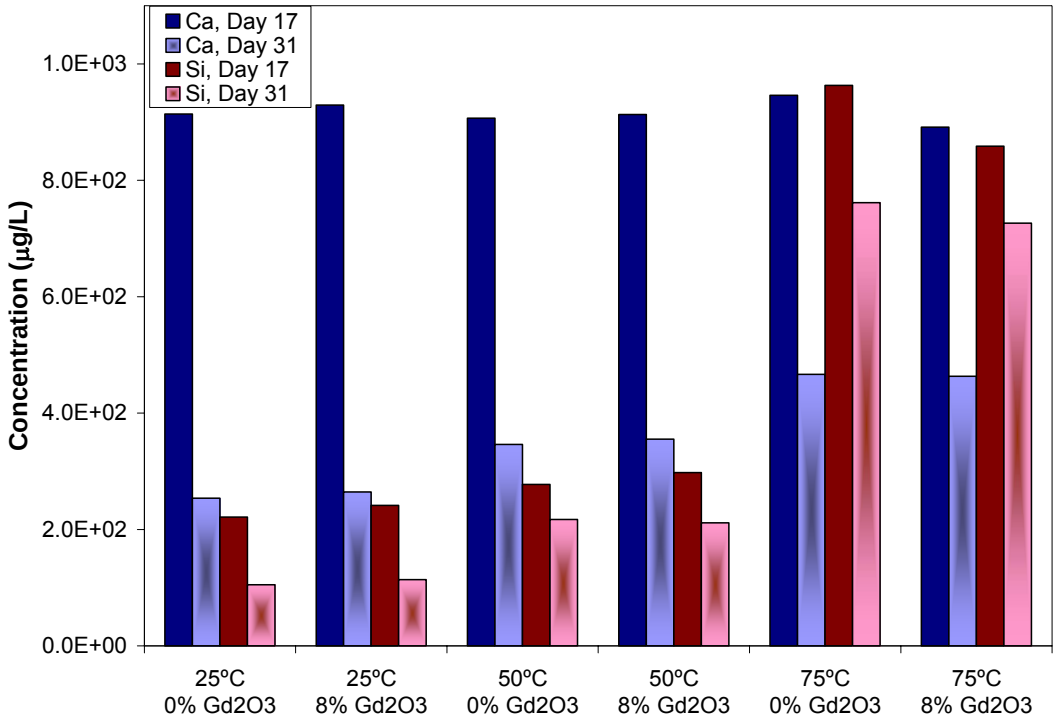

Figure 13.1. Ca and Si concentrations for 25ºC, 50ºC, and 75ºC for unirradiated UO_2 with both 0 and 8% dopings of Gd_2O_3

In Figure 13.1 the Ca concentration was consistent over all samples on day 17. After the filter change on day 31 the Ca concentration in solution was reduced, but increased slightly as the temperature increased. The Si concentration displayed different qualities. On day 17 the 25ºC and 50ºC samples displayed similar Si levels but at 75ºC the concentration was approximately four times higher. On day 31 the Si levels increased with increasing temperature, with the largest jump between the 50ºC and 75ºC samples. In all samples, there was minimal difference between the Ca and Si concentrations in the 0% and 8% Gd_2O_3-doped UO_2 leachate samples. These levels are approximately 3 orders of magnitude below expected Yucca Mountain levels, which are shown in Table 13.3.

Table 13.3. J-13 well water composition[3]

Constituent	µg/mL		Constituent	µg/mL
Ca	13.2		Cl	7.3
Si	33		F	2.3
K	5.3		NO_3	8.1
Na	44		SO_4	18.1
Mg	1.9		HCO_3	124

Analysis of the fuels with SEM-EDS after SPFT testing was complete also yielded results pertaining to the Ca and Si presence. Several areas were analyzed with the average and standard deviation of the readings shown in Table 13.3. There was essentially no Si on any of the 25ºC samples except for one section of A5-b which showed 0.27%, although the other four sections of A5-b showed none. Statistically the 50ºC and 75ºC samples showed similar surface coating of the Si. It should be noted that the data had a large spread and would vary greatly depending upon the area examined, as shown by the standard deviations.

Table 13.4. SEM-EDS analysis of Si concentration on fuel surfaces

Sample*	Si Wt %	St. Dev.	Sample*	Si Wt %	St. Dev.	Sample*	Si Wt %	St. Dev.
A3	0.00		B3	2.45	0.47	C3	2.50	0.82
A6	0.00		B6	2.57	0.58	C6	1.58	0.35
A5-b	0.05	0.12	B5-b	3.50	1.71	C5-b	1.09	1.06
A8	0.00		B8	2.02	1.07			

*Where A=25ºC, B=50ºC, C=75ºC, 3=0% Gd_2O_3 powder, 5-b=0% Gd_2O_3 fragments, 6=8% Gd_2O_3 powder, 8=7% Gd_2O_3 fragments

The SEM-EDS data only picked up the presence of Ca on 3 out of the 11 samples all of which were on fragments. B5-b showed 0.66, 2.71, and 1.24% Ca on 3 out of the 11 areas examined by the EDS, with the rest displaying none. B8 showed 0.17% Ca on 1 out of 13 areas, and C8 exhibited 0.31% Ca on 1 out of 13, although the rest displayed none. Therefore a minimal amount of Ca appeared to be deposited on the fuels, which is consistent with Figure 13.1 having essentially no difference between samples.

As all initial solutions began with the same feedwater, according to Figure 13.1, it would be expected that Si deposition on the surface of the fuel would be greater at lower temperatures than at 75ºC as the deposited amounts would result in less Si in the leachate. This contradicts the SEM-EDS data presented in Table 13.3 which showed essentially no Si on the surface of the fuels at 25ºC. One possibility for this could be a reaction of Si with other constituents in solution that occurs more at low temperatures and the complex is not detected as Si by ICP-MS. If this happened, then there would be more free Si in solution at higher temperatures which could account for the fuel coating displayed by the SEM-EDS.

In Test 1, it was apparent that Si in solution even at low levels had the ability to influence the dissolution rate of unirradiated UO_2. The Si was present on the surface of the 50ºC and 75ºC samples which would block oxidations sites and inhibit dissolution. This would account for the higher temperature samples dissolving at a slower rate than

room temperature samples. The concentrations are 3 orders of magnitude below that of J-13 well water and still effects are seen, therefore in Yucca Mountain higher quantities of Si would be expected on the surface lowering the dissolution rate even further. This appears more advantageous at temperatures above room temperatures as predicted at the fuel surface for over 1,000 years after placement of spent fuel in the mountain.

References

[1]Santos, B.G., Noel, J.J., Shoesmith, D.W., "The Influence of Calcium Ions on the Development of Acidity in Corrosion Product Deposits on SIMFUEL, UO_2," *Journal of Nuclear Materials*, **350**, 320 (2006)

[2]Amme, M., Aldave De Las Heras, L., Betti, M., Stöckl, M., "Effects of Colloidal and Dissolved Silica on the Dissolution of UO_2 Nuclear Fuel in Groundwater Leaching Tests," *Journal of Radioanalytical and Nuclear Chemistry*, **261,** 2, 327 (2004)

[3]Domski, P.S., "In-Package Chemistry Abstraction," ANL-EBS-MD-000037 (2007)

CHAPTER 14: DISCUSSION AND CONCLUSIONS-SURFACE AREA

In Chapter 6, the discrepancies of surface area scaling were discussed. Common practices in previous research have been to normalize the dissolution rate to the surface area of the fuel.[1-7] This method allowed for the comparison of powder, fragment, and pellet data and for scaling to larger sizes. As discussed in Chapter 6, the methods for measuring surface area may give erroneously high or low readings and often surface roughness factors are calculated in larger than grain sized samples.

Figures 14.1 and 14.2 compare the results of the powder and fragment data from Test 1 and Tests 2 through 5, respectively. In these graphs, the factor decrease was calculated by dividing the normalized surface area of the fragment sample by the normalized surface area of its corresponding powder sample. Since the powder samples were obtained from the same original pellet as the fragment, the dissolution rates should display similar dissolution characteristics. In all cases in Figure 14.1, except the 50ºC 8% Gd_2O_3-doped UO_2 case, the fragment data produced much larger dissolution rates than the powder samples. In these powder samples, there were numerous fines, which would have increased the surface area thus producing a lower normalized surface area once they were rinsed away by the leachate. This may have been a contributing factor, but should not have displayed the large discrepancy between the samples shown in Figure 14.1. Another possibility is the changing surface area of the fragment samples during dissolution. Preferentially, oxidation occurs at the grain boundaries first, carving out grooves along the grains. This effect was observed on 3 samples shown in Chapter 12, although no other samples examined displayed this quality.

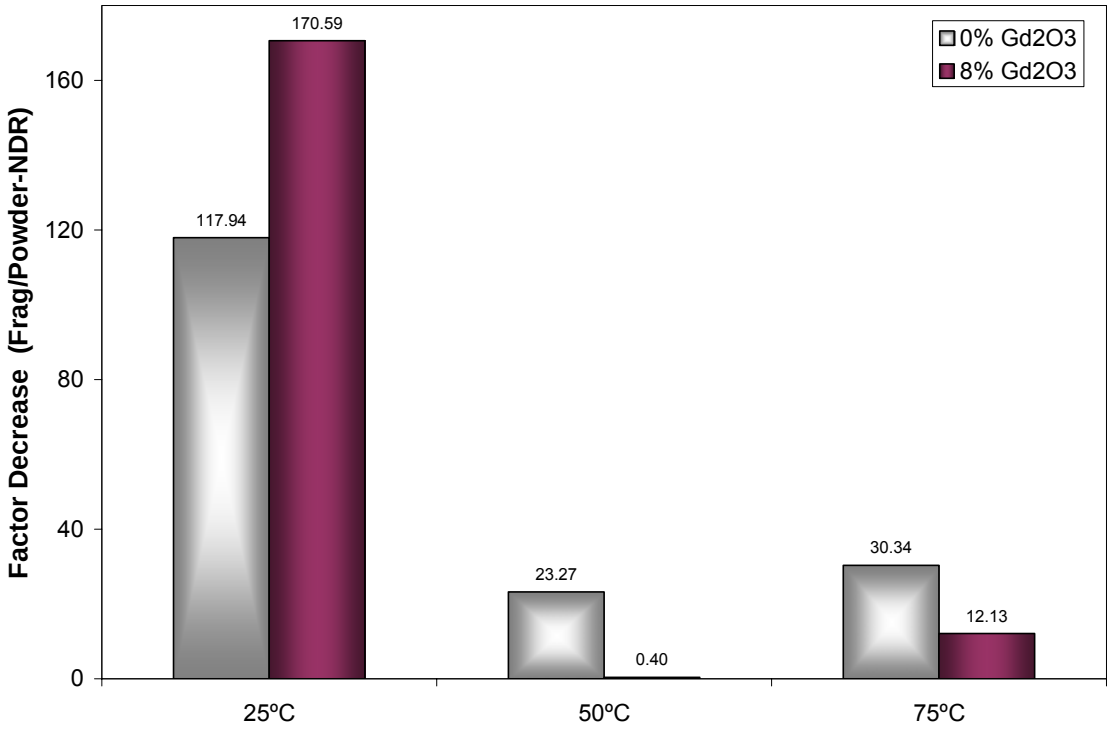

Figure 14.1. Factor decrease in the normalized dissolution rate from Test 1 for both 0 and 8% Gd_2O_3-doped UO_2 at 25ºC, 50ºC, and 75ºC

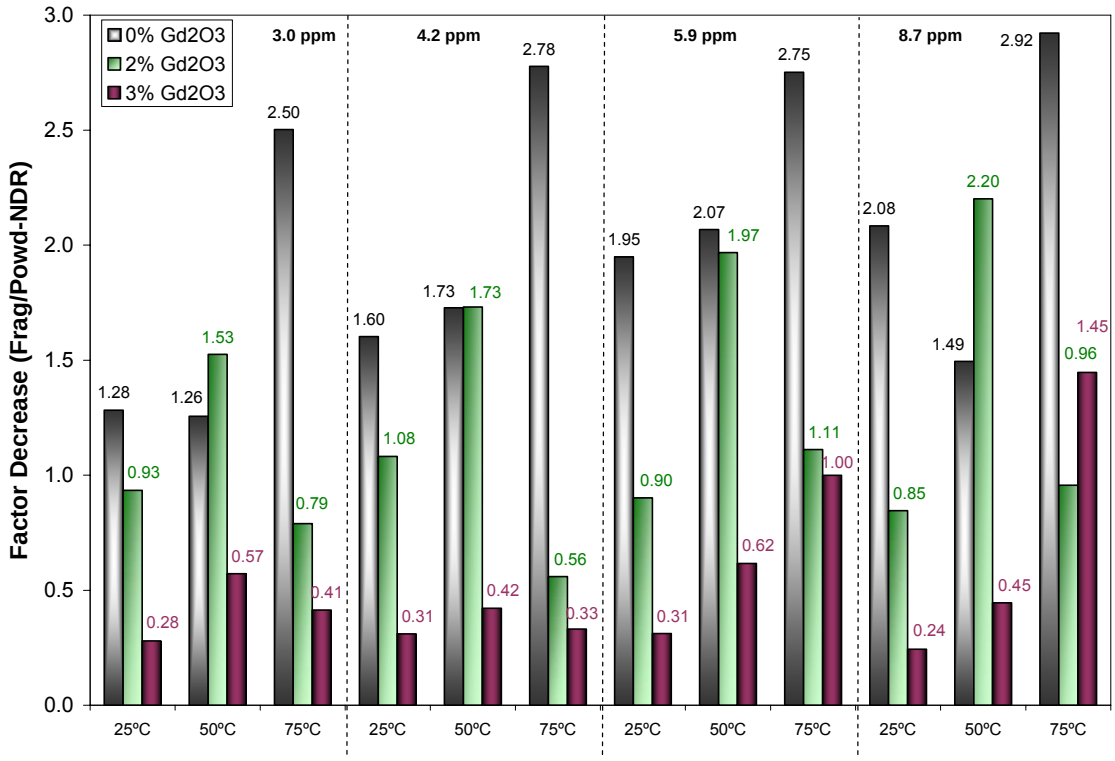

Figure 14.2. Factor decrease in the normalized dissolution rate from Tests 2 through 5 for 0%, 2%, and 3% Gd_2O_3-doped UO_2 at 25ºC, 50ºC, and 75ºC

The total U dissolved as a fraction of the total U in the sample at the end of Test 5 were also compared between the powder and fragment samples. Figure 14.3 compares the factor decrease which is the total fractional release of U of the powder samples divided by that of the fragment samples. In these ratios it is expected that the powder samples would have a much larger fractional release due to the large surface area exposed. These factors ranged from approximately 35 to 125 and no trends were observed for increasing temperature or Gd_2O_3 dopant.

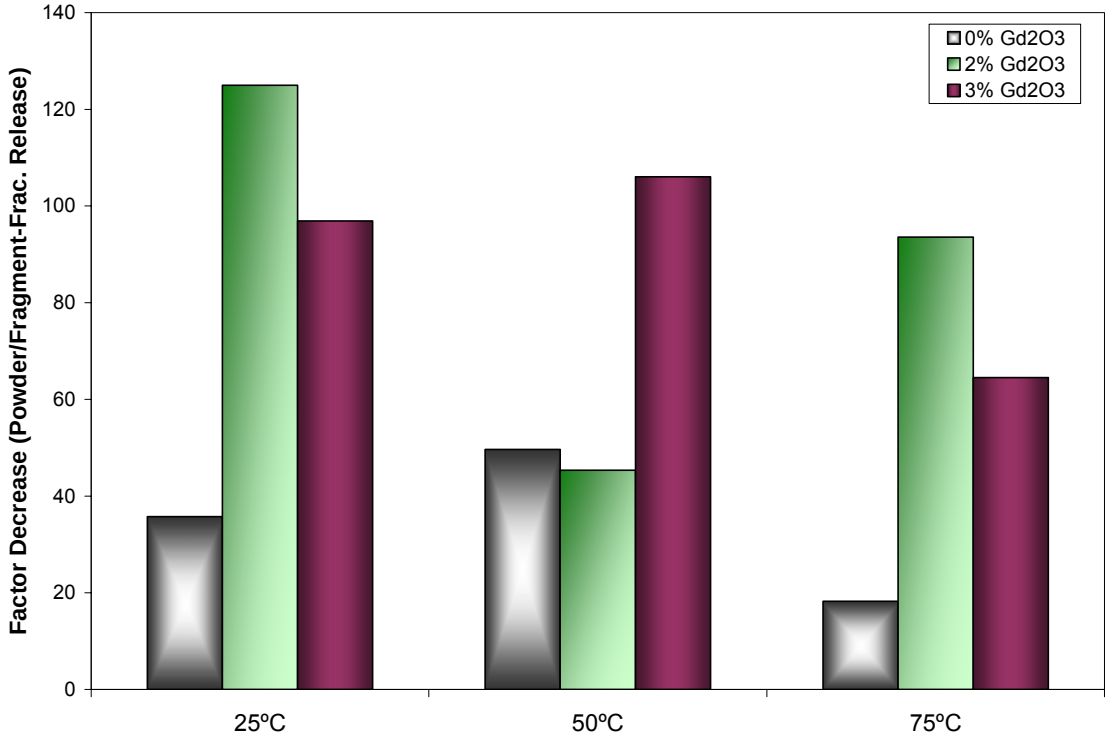

Figure 14.3. Factor decrease in the total fractional release at the end of Test 5 for 0%, 2%, and 3% Gd_2O_3-doped UO_2 at 25ºC, 50ºC, and 75ºC

In Tests 2 through 5 the factor decrease between the fragment and powder samples, as shown in Figure 14.2, was much less than in Test 1. In these tests the ratio

between the samples varied from approximately 0.3 to 3. There appeared to be no clear trends based upon temperature or changes due to the variation of O_2.

No distinct correlation can be made by scaling the fragment and powder samples. In the first test wide variations were observed, although in Tests 2 though 5 all samples fell within a factor of 3 of each other. The normalized dissolution rate is an appropriate comparison for similar samples when measured by the same method, although care should be taken when comparisons are made among diverse samples.

References

[1]Gray, W., Wilson, C., "Spent Fuel Dissolution Studies FY 1991 to 1994," PNL-10540, December (1995)

[2]Tait, J. C., Luht, J. L., "Dissolution Rates of Uranium from Unirradiated UO2 and Uranium and Radionuclides from Used CANDU Fuel Using the Single-Pass Flow-Through Apparatus," Atomic Energy of Canada Ltd., Whiteshell Laboratories, 06819-REP-01200-0006 R00, November (1997)

[3]Shoesmith, D., Sunder, S., "An Electrochemistry-Based Model for the Dissolution of UO2," AECL-10488, Atomic Energy of Canada Limited; also SKB Technical Report 91-63, SKB, Stockholm (1991)

[4]Casas, I., Gimenez, J., Pablo, J., Torrero, M. E., "Dissolution of UO_2(s) in MgCl2-brines under different redox conditions," Scientific Basis for Nuclear Waste Management XVI, *Proceedings of the Materials Research Society Symposium*, **294**, 67-72 (1993)

[5]Steward, S. A., Weed, H. C., "Modeling of UO2 Aqueous Dissolution Over a Wide Range of Conditions," Scientific Basis for Nuclear Waste Management XVII, Proceedings of the Materials Research Society Symposium, **333**, 409-416 (1994)

[6]Gromov, V., "Dissolution of Uranium Oxides in the Gamma-Radiation Field," *Radiation Physics and Chemistry*, **18**, 135-146 (1981)

[7]Christensen, H., Forsyth, R., Lundqvist, R., Werme, L. O., "Radiation Induced Dissolution of UO_2," Studsvik Report NS-90/85, Studsvik Energiteknik AB, Nykoping, Sweden (1990)

CHAPTER 15: DISCUSSION AND CONCLUSIONS-FUEL CHEMISTRY

Commonly, unirradiated UO_2 has been used as a substitute for spent fuel in dissolution studies due it its availability and ease of handling. However, spent fuel placed in Yucca Mountain would contain other elements in the fuel that will influence dissolution properties as was discussed in Chapter 5. In Test 1 samples containing 0, 4, and 8% Gd_2O_3-doped UO_2 were used in order to compare possible changes in the fuel chemistry and their effect on dissolution.

Figures 15.1, 15.2, and 15.3 display the cumulative fraction of U released as a function of the days run. In these figures, the 0% Gd_2O_3-doped UO_2 powders had a higher cumulative release than the 4% and 8% Gd_2O_3-doped UO_2 powders. In Figure 15.2, when comparing the 4% and 8% doped powder cases the groundwater change discussed in Chapter 13 must be taken into account. If the releases from these days and the spike seen around day 60 are excluded, the 4% and 8% Gd_2O_3-doped UO_2 would display similar results. With this taken into consideration, all of the temperatures displayed 0% Gd_2O_3-doped UO_2 with the highest release, but exhibit no distinguishable difference between the 4 and 8% doped cases. Therefore, the matrix appeared to be affected by addition of dopant, but the dependence was not necessarily linear. A drop in the release of U as the % Gd_2O_3-dopant was increased was also observed in the fragment data also shown in Figures 15.1 through 15.3. The fragment samples had a much lower cumulative release overall, which can be attributed to the low surface area to volume ratio. Although there was 5 times as much fuel in the fragments, the cumulative dissolution was an order of magnitude lower.

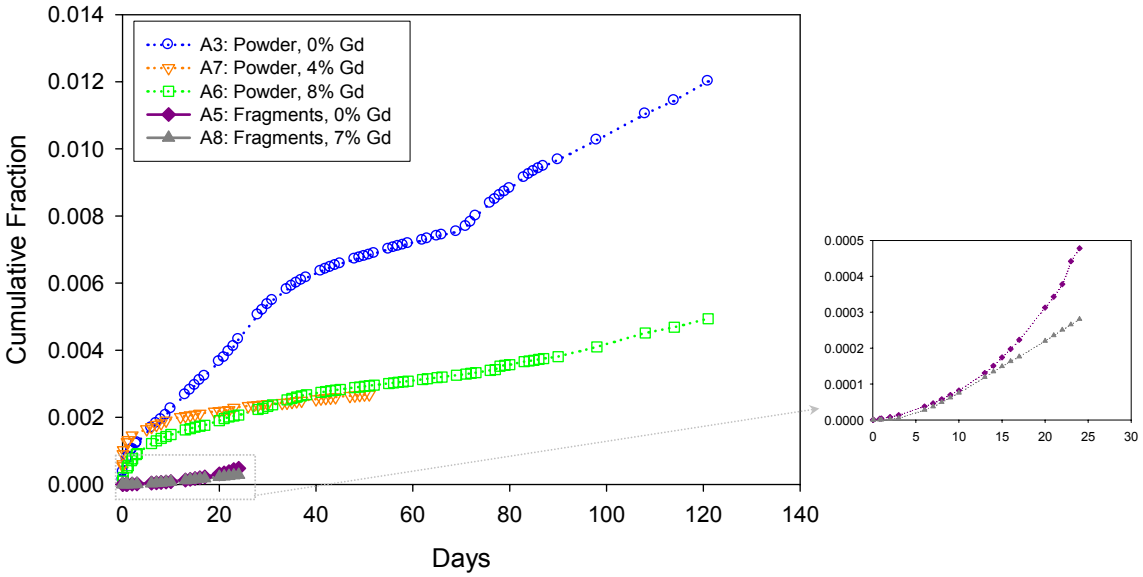

Figure 15.1. Cumulative Fraction of U released from unirradiated UO_2 at 25ºC for powders ranging from 0 to 8% Gd_2O_3-dopant and fragments with 0 and 7% Gd_2O_3-dopant

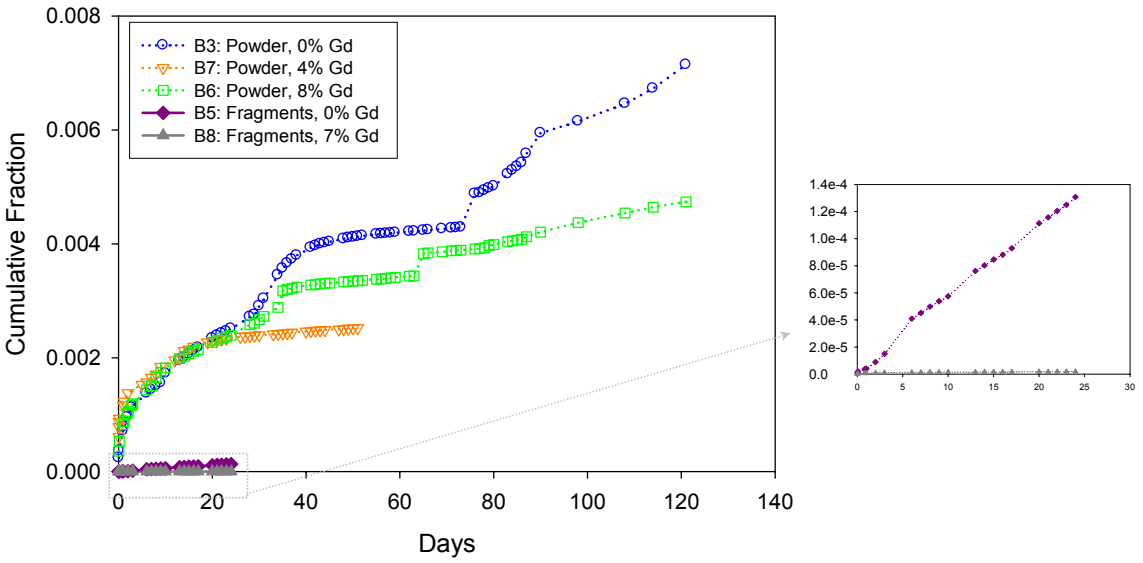

Figure 15.2. Cumulative Fraction of U released from unirradiated UO_2 at 50ºC for powders ranging from 0 to 8% Gd_2O_3-dopant and fragments with 0 and 7% Gd_2O_3-dopant

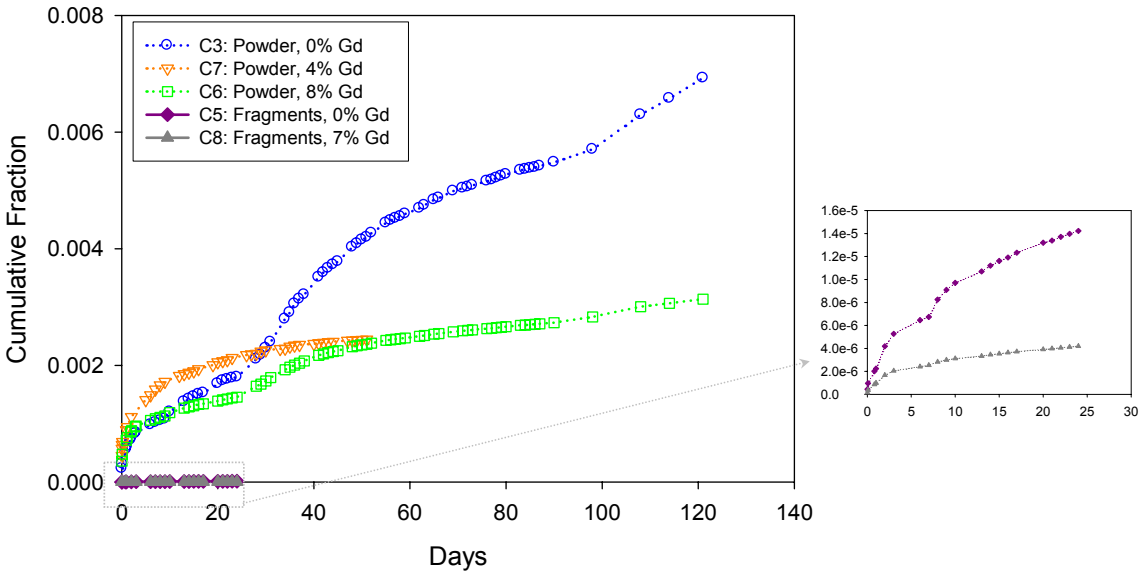

Figure 15.3. Cumulative Fraction of U released from unirradiated UO_2 at 75ºC for powders ranging from 0 to 8% Gd_2O_3-dopant and fragments with 0 and 7% Gd_2O_3-dopant

In Chapter 5, a possible threshold theory was discussed that may begin to be seen around 2 wt% Gd_2O_3, although this theory assumes a homogeneous mixture. As shown by the SEM-EDS data in Chapters 10 and 12, this is not the case for the fuels used in this work. Therefore, this threshold value of wt% Gd_2O_3-doping could shift to a higher percentage due to the sample heterogeneity. Figures 15.4 through 15.7 display the data from Figures 15.1 through 15.3 only they compare the normalized dissolution rates. It was again seen that although there was some variation between the flow rates in general the 4% Gd_2O_3-doped UO_2 sample had approximately the same dissolution rate as the 8% Gd_2O_3-doped UO_2 samples for all three temperatures. Therefore, there may be a threshold effect somewhere lower than 4% Gd_2O_3 doped UO_2, which would agree with the theoretical prediction of Chapter 5.

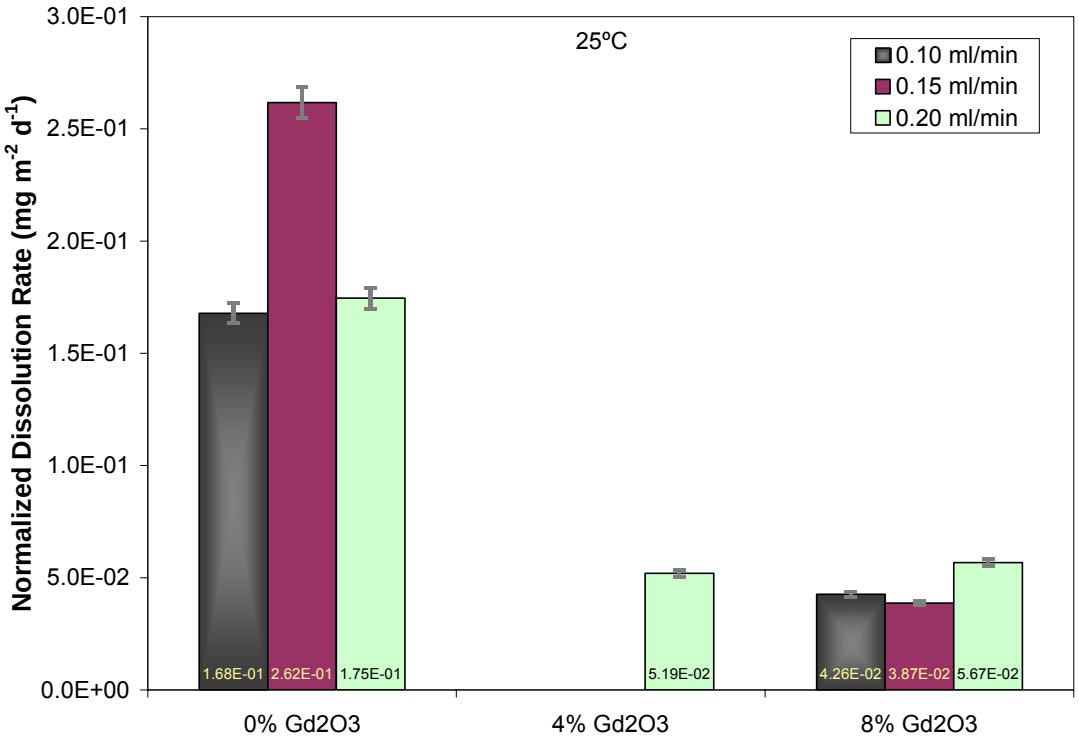

Figure 15.4. Normalized dissolution rate of unirradiated UO_2 at 25ºC for powders with 0, 4, and 8% Gd_2O_3-dopant

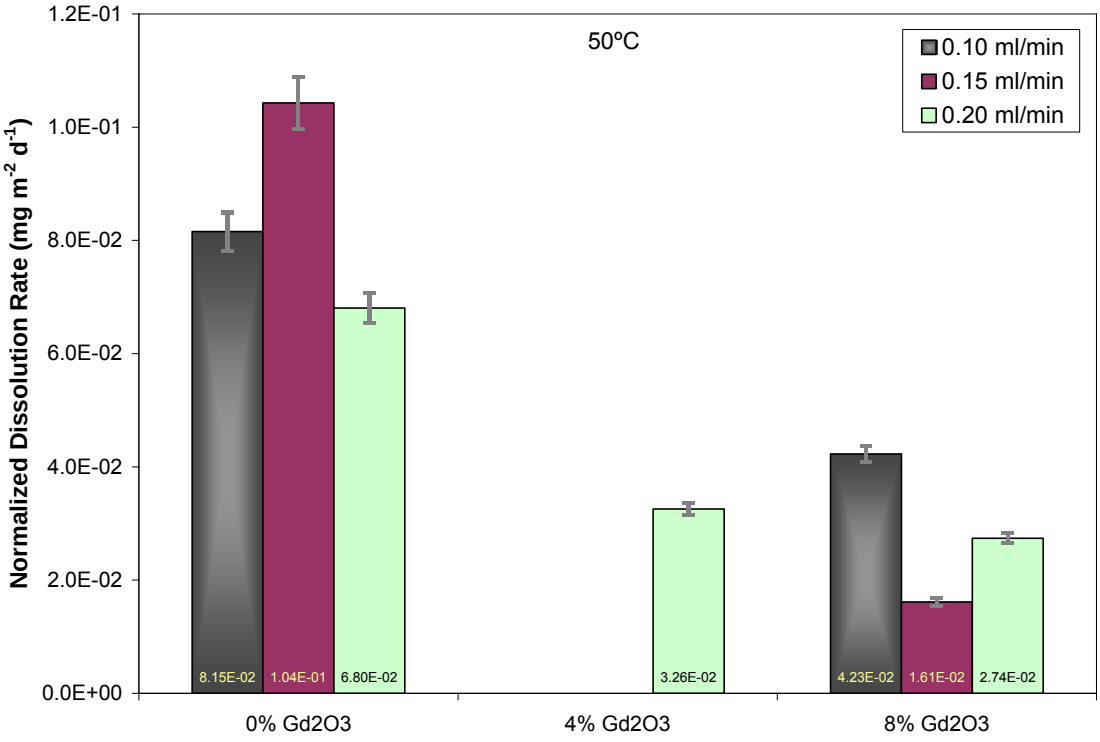

Figure 15.5. Normalized dissolution rate of unirradiated UO_2 at 50ºC for powders with 0, 4, and 8% Gd_2O_3-dopant

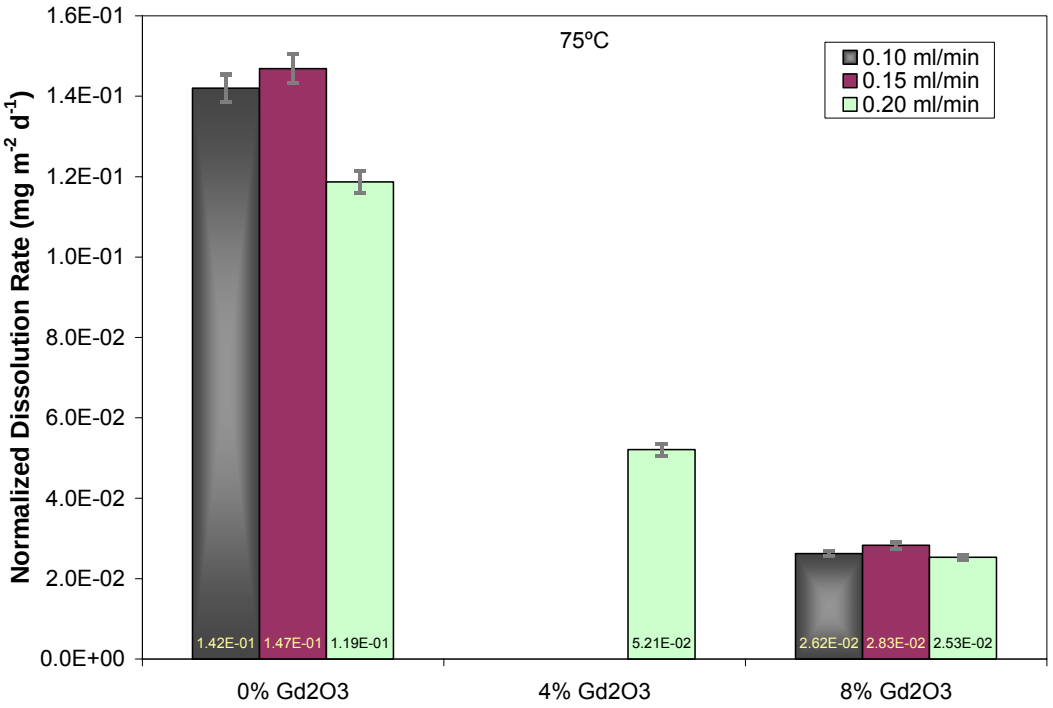

Figure 15.6. Normalized dissolution rate of unirradiated UO_2 at 75ºC for powders with 0, 4, and 8% Gd_2O_3-dopant

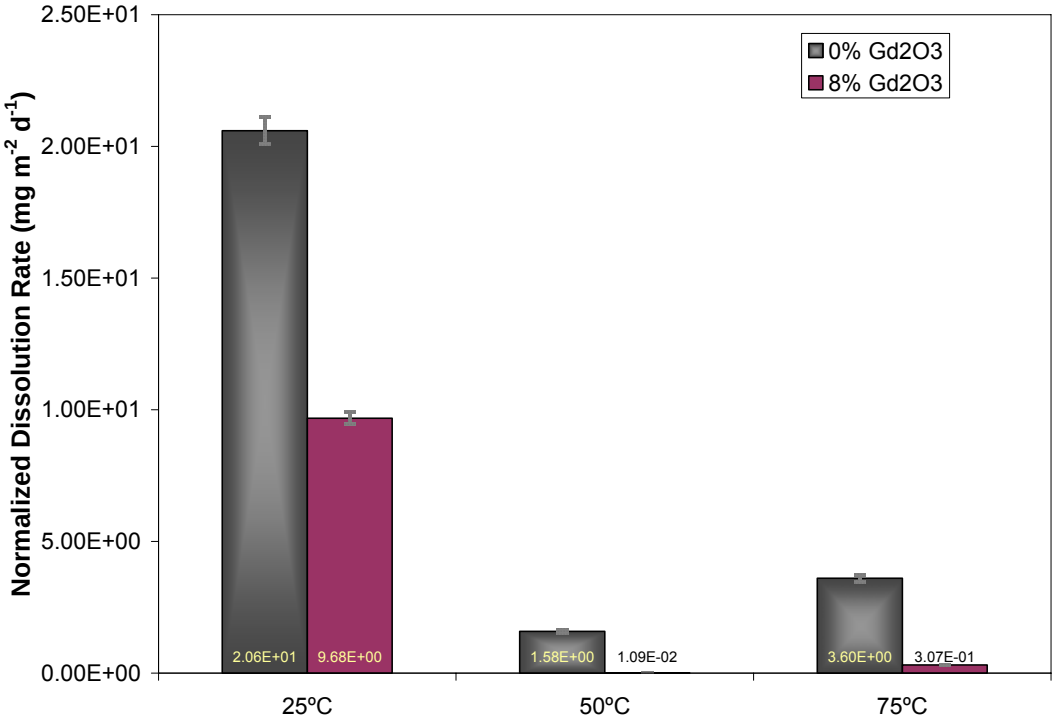

Figure 15.7. Normalized dissolution rate of unirradiated UO_2 at 25, 50, and 75ºC for fragments with 0 and 7% Gd_2O_3-dopant

The dopant levels in Tests 2 through 5 were chosen based upon the results from Test 1 that showed a possible threshold effect for unirradiated UO_2 at less than 4% Gd_2O_3. The results from powder Tests 2 through 5 are shown in Figures 15.8, 15.9, and 15.10. These graphs show the average dissolution rate of the samples for each condition after equilibrium was established. In these graphs, there was a distinct decrease in the normalized dissolution rate over all temperature and dissolved O_2 ranges when Gd_2O_3-dopant was present in the fuel. In all of the cases except the 3% Gd_2O_3-doped UO_2 in the 25ºC test, there was a definite trend of decreasing dissolution as the dopant level was increased. This may have been a result of the excess fines not dissolving as quickly at 25ºC as at the higher temperatures, therefore tailing out the initial drop that was seen in all samples. Another interesting feature was that the decrease in the dissolution rate between the 0% Gd_2O_3 doped UO_2 and 1.25% to 4% Gd_2O_3 doped UO_2 cases becomes much more predominant at 50ºC and 75ºC, which overall have higher dissolution rates. Therefore, Gd_2O_3-doping had a stabilizing effect which lowered the dissolution rate and this effect became more pronounced as the temperature was increased.

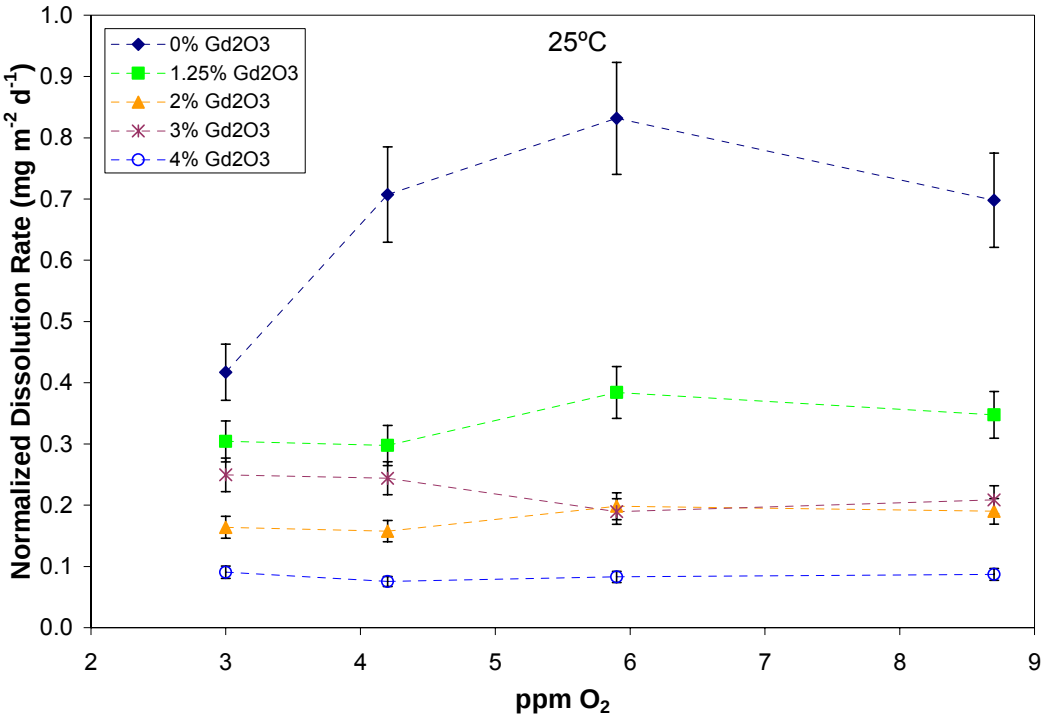

Figure 15.8. Normalized dissolution rate of unirradiated UO_2 at 25ºC for powders ranging from 0 to 4% Gd_2O_3-dopant at 3.0, 4.2, 5.9, and 8.7 ppm O_2

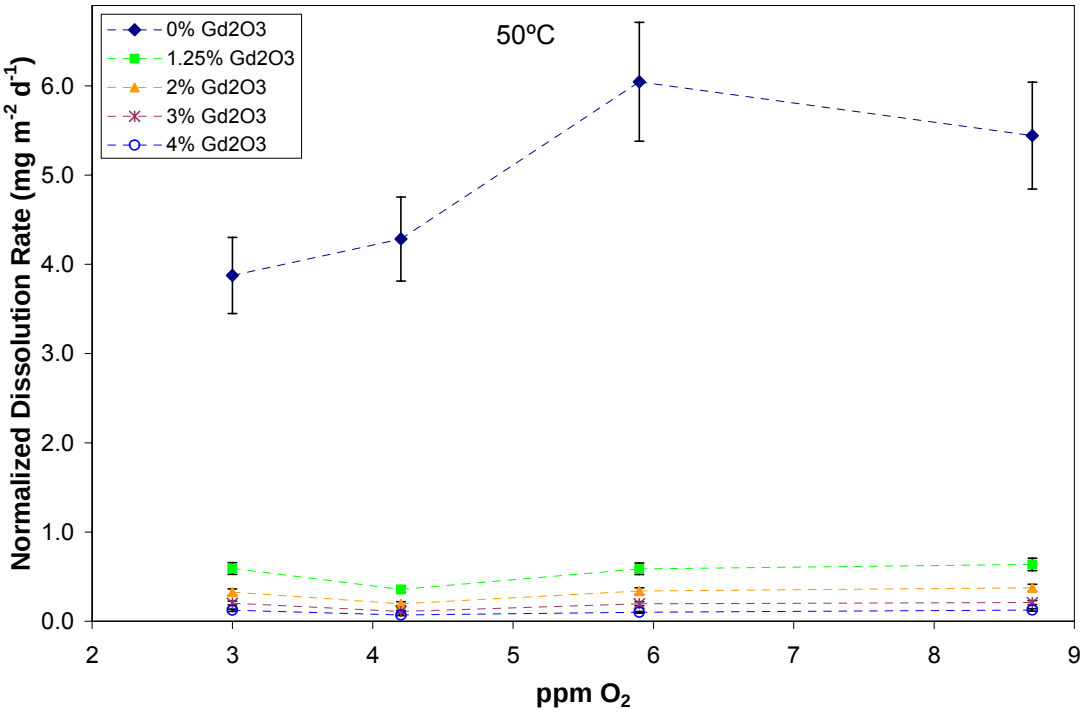

Figure 15.9. Normalized dissolution rate of unirradiated UO_2 at 50ºC for powders ranging from 0 to 4% Gd_2O_3-dopant at 3.0, 4.2, 5.9, and 8.7 ppm O_2

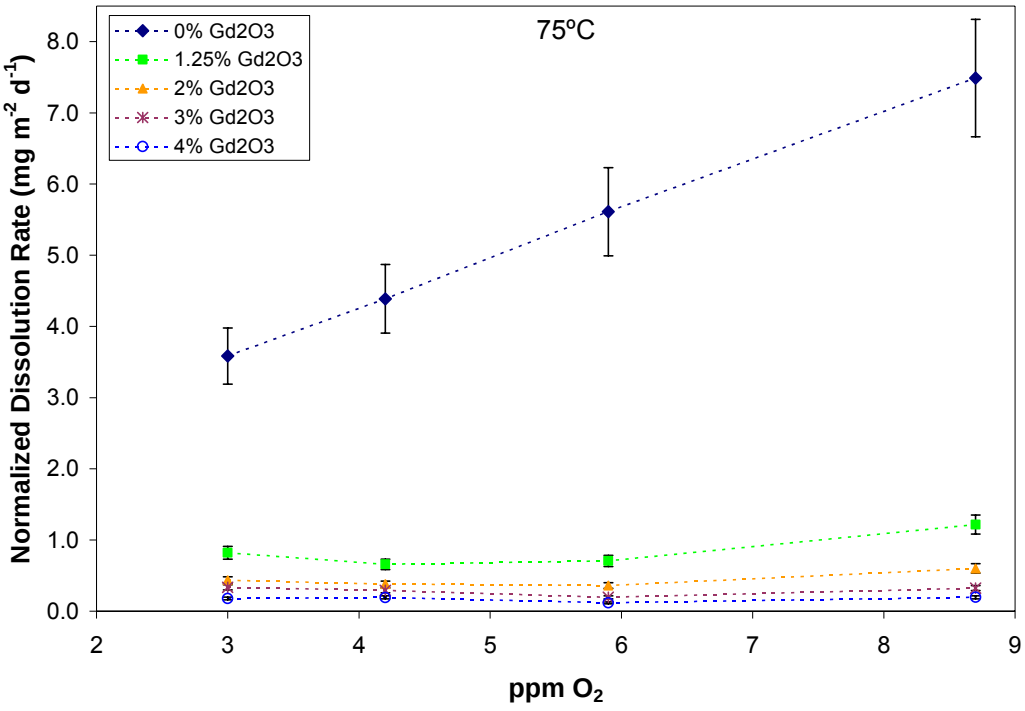

Figure 15.10. Normalized dissolution rate of unirradiated UO_2 at 75ºC for powders ranging from 0 to 4% Gd_2O_3-dopant at 3.0, 4.2, 5.9, and 8.7 ppm O_2

A comparison was made of the normalized dissolution rate relative to the 0% Gd_2O_3-doped UO_2 sample in Figures 15.11 and 15.12. These results were evaluated on a % Gd_2O_3 basis and were calculated according to the equation:

$$\text{Factor Decrease per \% } Gd_2O_3 = \frac{\left(NDR_{0\%\ Gd_2O_3} / NDR_{x\%\ Gd_2O_3}\right)}{x\%\ Gd_2O_3} \qquad (15.1)$$

where NDR is the normalized dissolution rate and x represents the level of Gd_2O_3 dopant in wt%. This allowed investigation into whether or not additional dopant levels were as effective as their quantities were increased.

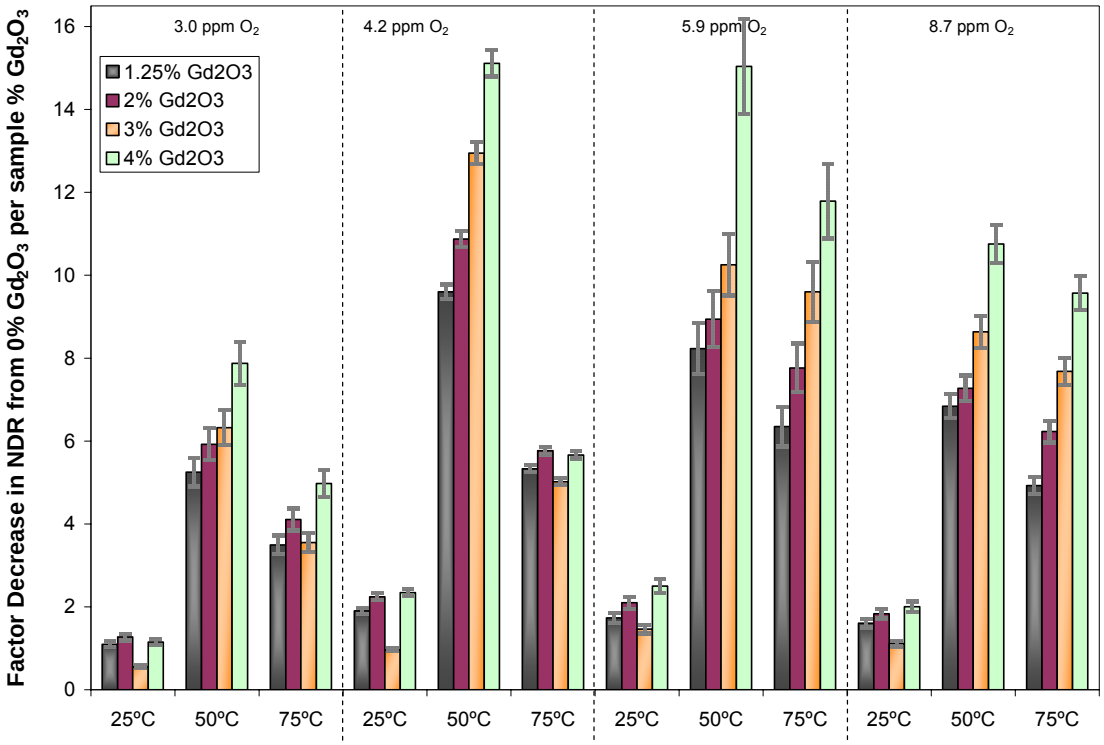

Figure 15.11. Factor decrease in normalized dissolution rate of unirradiated UO_2 at 25ºC, 50ºC, and 75ºC for powders ranging from 0 to 4% Gd_2O_3-dopant at 3.0, 4.2, 5.9, and 8.7 ppm O_2

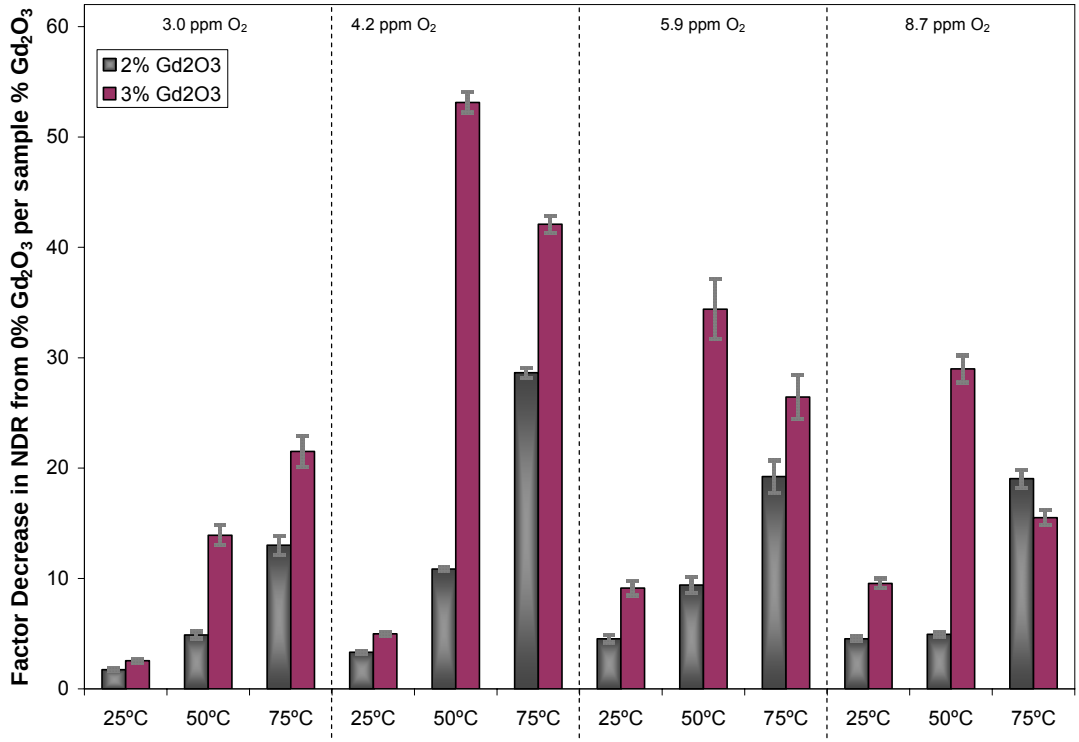

Figure 15.12. Factor decrease in normalized dissolution rate of unirradiated UO_2 at 25ºC, 50ºC, and 75ºC for fragments ranging from 0 to 3% Gd_2O_3-dopant at 3.0, 4.2, 5.9, and 8.7 ppm O_2

In Figures 15.11 and 15.12 in all cases there was a larger decrease in the 50ºC and 75ºC cases relative to the 25ºC case as was previously discussed. Almost all cases showed an added benefit for increasing the dopant level due to the dissolution dropping at a faster rate. Unlike Test 1, no threshold effect was seen in Tests 2 through 5. The threshold may be around 4% Gd_2O_3-dopant or the first test may have been compromised by the altered groundwater chemistry. However, since no coating was seen on the 25ºC sample if this were the case it could be a result of the elevated constituents influencing the O_2 potential relative to oxidation and/or dissolution.

These results show UO_2 may be a conservative substitute for spent fuel after radiolysis is no longer a significant factor. At 75ºC the dissolution rate of the 4 wt% Gd_2O_3-doped UO_2 was a factor of 15 lower for the powder samples and a factor of 50 lower for the fragment samples relative to the pure UO_2. Therefore, the dissolution rate will most likely be lower as a result of added constituents in the UO_2 matrix. The dopants prove even more beneficial in lowering the dissolution rate at higher temperatures where the rates would typically be elevated. Also, a stabilization effect occurs resulting in the fuel being more resistant to changes in solution properties such as elevated temperatures and dissolved O_2 concentrations.

CHAPTER 16: DISCUSSION AND CONCLUSIONS- TEMPERATURE AND DISSOLVED O_2

As discussed in Chapter 3, typically in UO_2 based dissolution tests, higher temperatures produce faster dissolution rates. As was discussed in Chapter 11, upon analyzing Test 1 data, the opposite trend was observed where the lowest temperature had the largest dissolution rate, as shown in Figure 16.1. The undoped samples at 25°C had approximately twice the release of those in the 50°C and 75°C conditions. The Gd_2O_3 doped samples were similar except that the 50°C sample was closer to the 25°C sample and these were approximately double that of the 75°C sample. So although the 50°C sample changed, in both cases the 25°C sample had a higher dissolution than the 75°C sample.

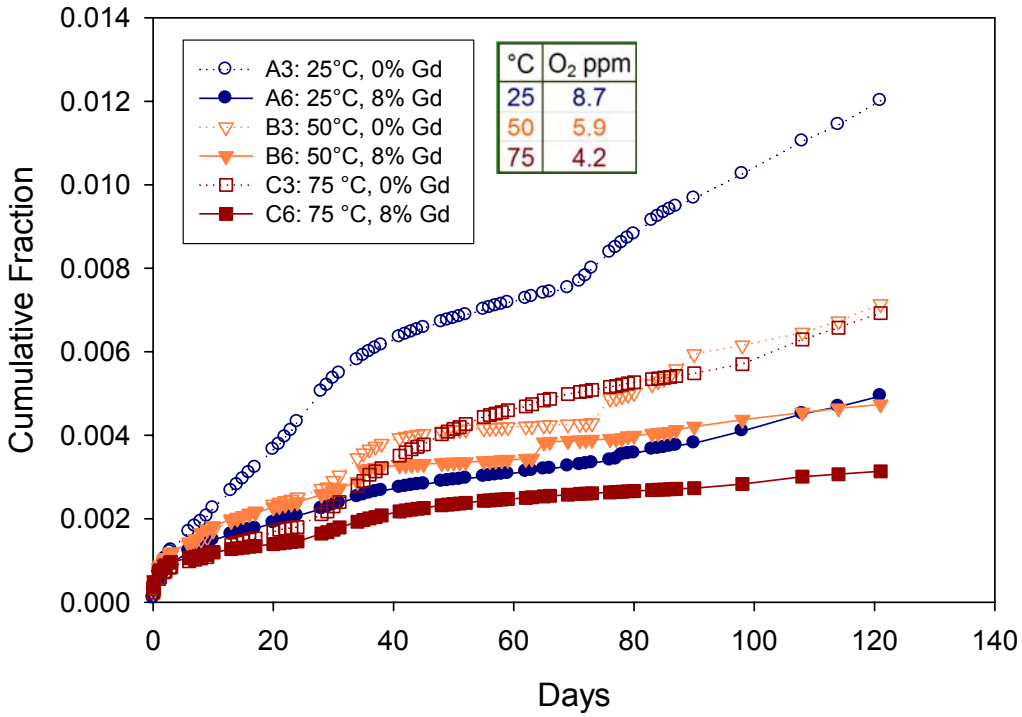

Figure 16.1. Cumulative fraction of U released for both 0 and 8% Gd_2O_3-doped UO_2 at 25ºC, 50ºC, and 75ºC for the 0.20 mL/min samples in Test 1

This temperature trend may have occurred due to the Si coating that was observed on the surface of the 50ºC and 75ºC fuels as was presented in Chapter 13. These coatings would have lowered the dissolution rates by decreasing the sites accessible for oxidation. The dramatic effects seen on the dissolution rates when extra O_2 was added to the system may have been a result of the altered O_2 potential caused by the increased levels of constituents in the water. However these changes may have restabilized if conditions had been held for longer times.

Tests 2 through 5 showed that the inverse temperature effect in Test 1 was a result of more than just differences in the dissolved O_2 levels between 4.2 and 8.7 ppm. The results from Tests 2 through 5 are shown in Figures 16.2 through 16.5. All cases in these tests exhibited the 75ºC test with the lowest O_2 level having a faster dissolution rate than the 25ºC test with the highest O_2 level. If indeed the dissolved O_2 was playing a large role in determining the dissolution rate in Test 1 and the diminished O_2 levels at higher temperatures dictated the dissolution rate to be lower than in the 25ºC test, this would have also been exhibited in tests 2 through 5 with the different O_2 levels.

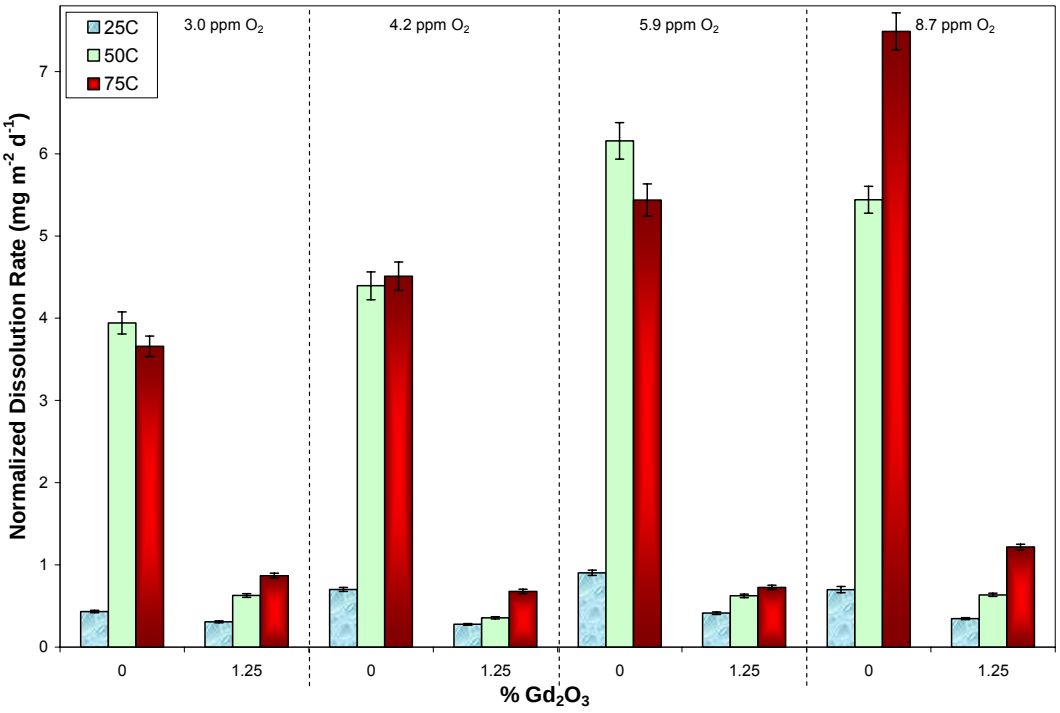

Figure 16.2. Normalized dissolution rate of powder samples with 0 and 1.25% Gd_2O_3-doped UO_2 for 3.0, 4.2, 5.9, and 8.7 ppm dissolved O_2 for tests run at 25ºC, 50ºC, and 75ºC

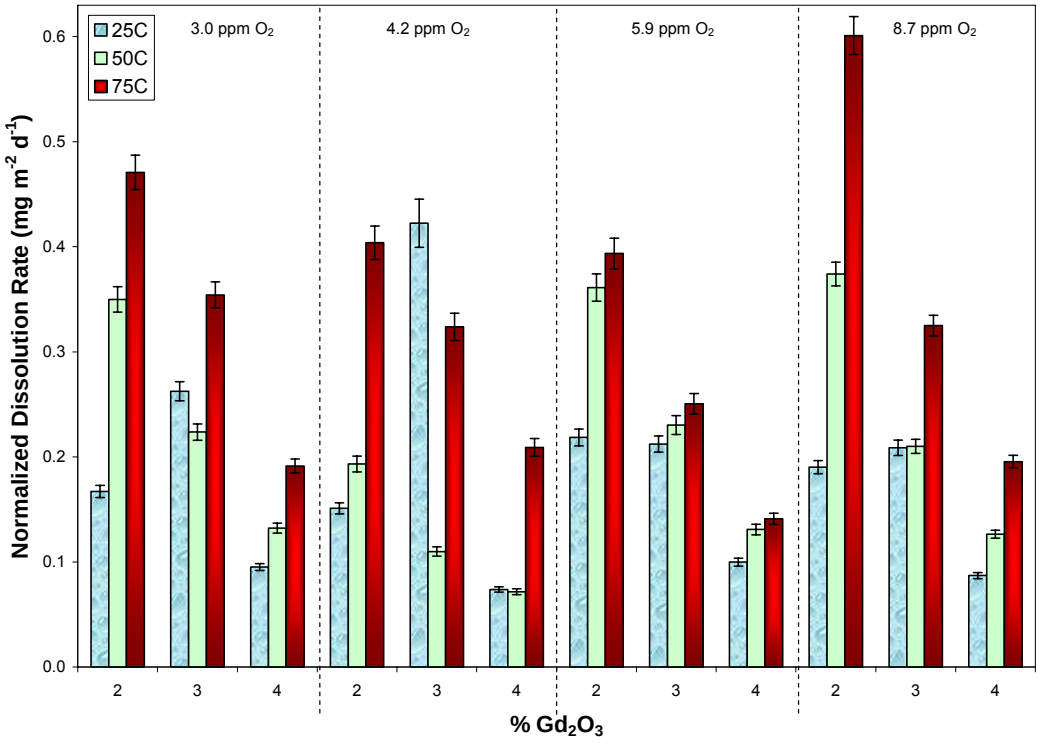

Figure 16.3. Normalized dissolution rate of powder samples with 2, 3, and 4% Gd_2O_3-doped UO_2 for 3.0, 4.2, 5.9, and 8.7 ppm dissolved O_2 for tests run at 25ºC, 50ºC, and 75ºC

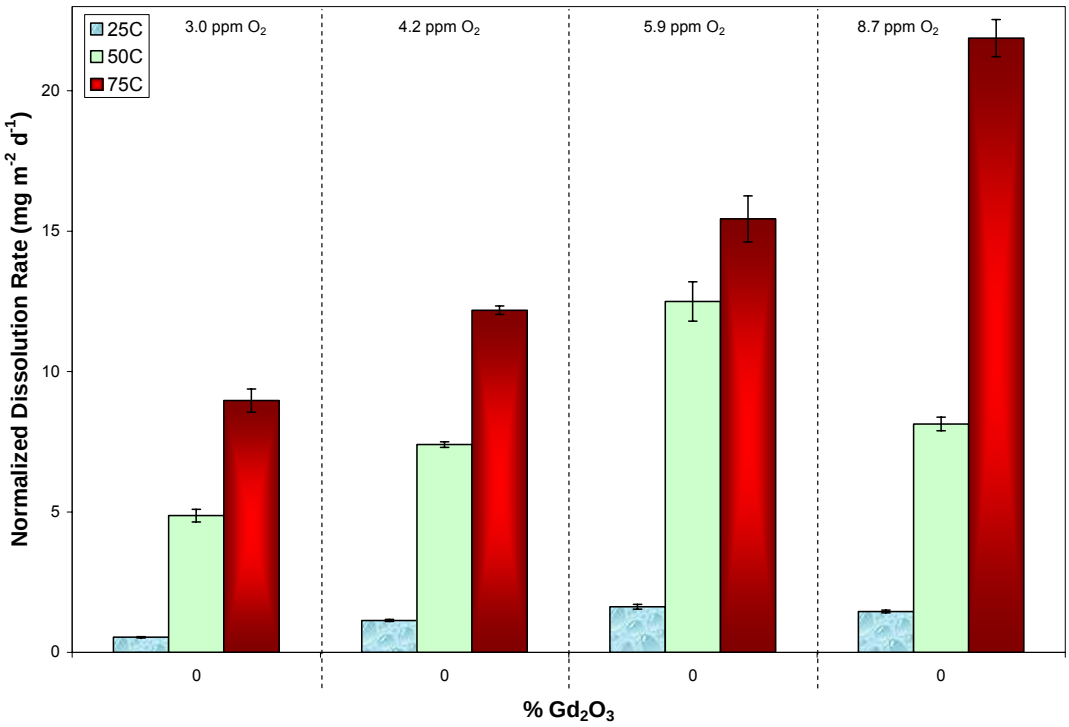

Figure 16.4. Normalized dissolution rate of fragment samples with 0 % Gd_2O_3-doped UO_2 for 3.0, 4.2, 5.9, and 8.7 ppm dissolved O_2 for tests run at 25ºC, 50ºC, and 75ºC

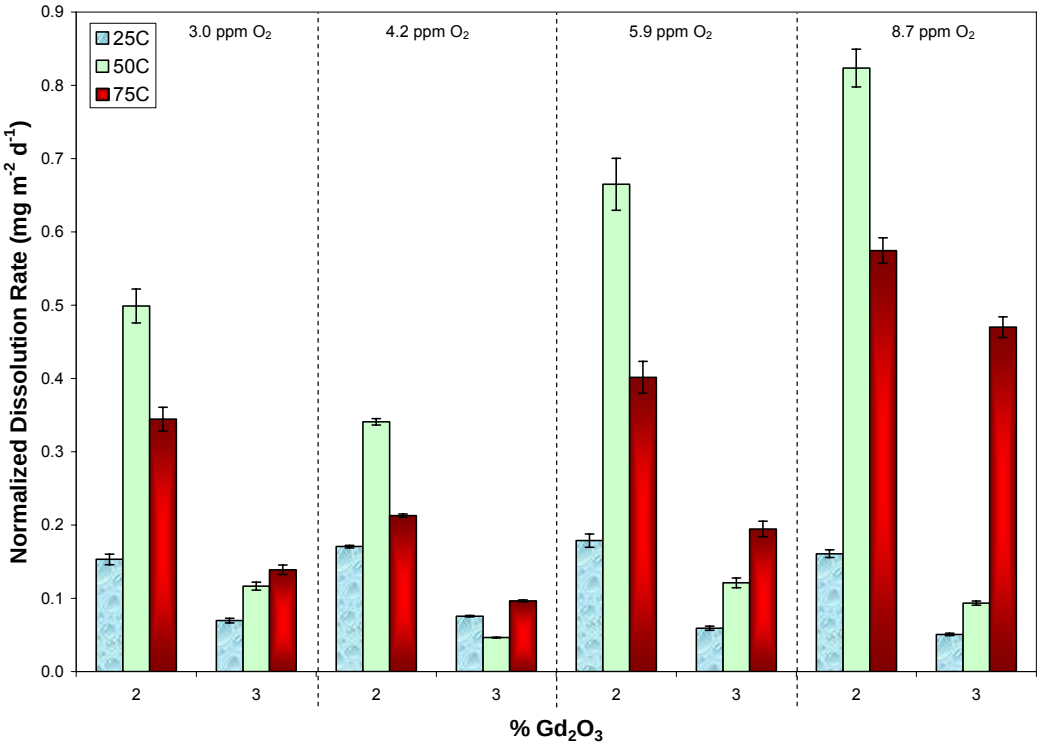

Figure 16.5. Normalized dissolution rate of fragment samples with 2, 3, and 4% Gd_2O_3-doped UO_2 for 3.0, 4.2, 5.9, and 8.7 ppm dissolved O_2 for tests run at 25ºC, 50ºC, and 75ºC

The increases in the normalized dissolution rate relative to the 25ºC test are shown in Table 16.1. For 0% Gd_2O_3-doped UO_2 samples the increase in the dissolution rate at 75ºC over the range of dissolved O_2 levels for powders varied from a factor of 6 to a factor of 10 and for fragments ranged from a factor of 5 to a factor of 17. In most cases in Figures 16.2 through 16.5, the fuels followed the trend of increasing the rate of dissolution as the temperature was raised with a few exceptions. For the 0% Gd_2O_3-doped UO_2 powder, the three lowest O_2 levels displayed statistically similar results for the 50ºC and 75ºC tests, although both were at least a factor of 6 larger than the 25ºC case. Therefore without the stabilization of the Gd_2O_3, any increase in temperature may have a large effect although it is not necessarily linear. This quality was not displayed in the 0% Gd_2O_3 fragment samples as they all increased with further raising the temperature. The ratios of the powder and fragment tests at 50ºC were very similar as shown in Table 16.1. As stated before, the pure UO_2 fragments in the 75ºC test incurred a larger increase than was seen in the powders. Therefore increasing the temperature from 50ºC to 75ºC continued to increase the dissolution rate for the fragment samples but not the powder samples.

Table 16.1. Relative increase of normalized dissolution rate at increased temperatures relative to 25ºC rate for UO_2 samples with Gd_2O_3-dopant levels ranging from 0 to 4% at 3.0, 4.2, 5.9, and 8.7 ppm dissolved O_2 in solution

Temp	% Gd_2O_3	3.0 ppm		4.2 ppm		5.9 ppm		8.7 ppm	
		Powder	Fragments	Powder	Fragments	Powder	Fragments	Powder	Fragments
50°C	0	9.30	9.11	6.06	6.53	7.27	7.71	7.80	5.59
	1.25	1.42		0.50		0.71		0.91	
	2	0.78	0.93	0.28	0.30	0.41	0.41	0.54	0.57
	3	0.49	0.22	0.16	0.04	0.24	0.07	0.30	0.06
	4	0.30		0.10		0.12		0.18	
75°C	0	8.59	16.76	6.20	10.75	6.74	9.52	10.73	15.05
	1.25	1.97		0.93		0.85		1.74	
	2	1.05	0.64	0.54	0.19	0.43	0.25	0.86	0.40
	3	0.81	0.26	0.41	0.09	0.23	0.12	0.47	0.32
	4	0.43		0.27		0.14		0.28	

Another sample that did not increase with rising temperature was the 3% Gd_2O_3 doped UO_2 powders. At 50ºC the sample had the lowest dissolution rate at 3.0 ppm and 4.2 ppm while at 8.7 ppm the 25ºC and 50ºC samples exhibited statistically equal rates. For the case of the 2% Gd_2O_3-doped UO_2 fragments, all O_2 levels displayed 25ºC tests having the lowest dissolution rate, followed by 75ºC and then 50ºC having the highest rate. The explanation for these results is not intuitive. However, in the 2% Gd_2O_3-doped UO_2 fragment case the relative rate increase for the 50ºC was similar for both the powders and fragments, while the 75ºC showed much lower ratios with respect to the fragments.

The O_2 dependence for Tests 2 through 5 can be seen in Figure 16.6. This dependence was determined by the slope of the best fit line in the normalized dissolution rate as a function of the dissolved O_2 concentration graph. The O_2 dependence is the reaction order of O_2 in the rate equation

$$NDR = a \times [O_2]^b \tag{16.1}$$

where NDR is the normalized dissolution rate, a is a constant, and b is the O_2 dependence. In Figure 16.6 the samples with Gd_2O_3-doping have minimal if any dependence on O_2. However, both the powder and fragment samples of pure UO_2 show clear dependence that increases with temperature. Steward and Gray[1] ran similar studies which exhibited O_2 dependences shown in Table 16.2. In both the cases of spent fuel and unirradiated UO_2 they also observed an increase in O_2 dependence as the temperature increased. Although their UO_2, at 75ºC, was similar to the value in Figure 16.6, the 25ºC case in this research displayed a much lower dependence on O_2.

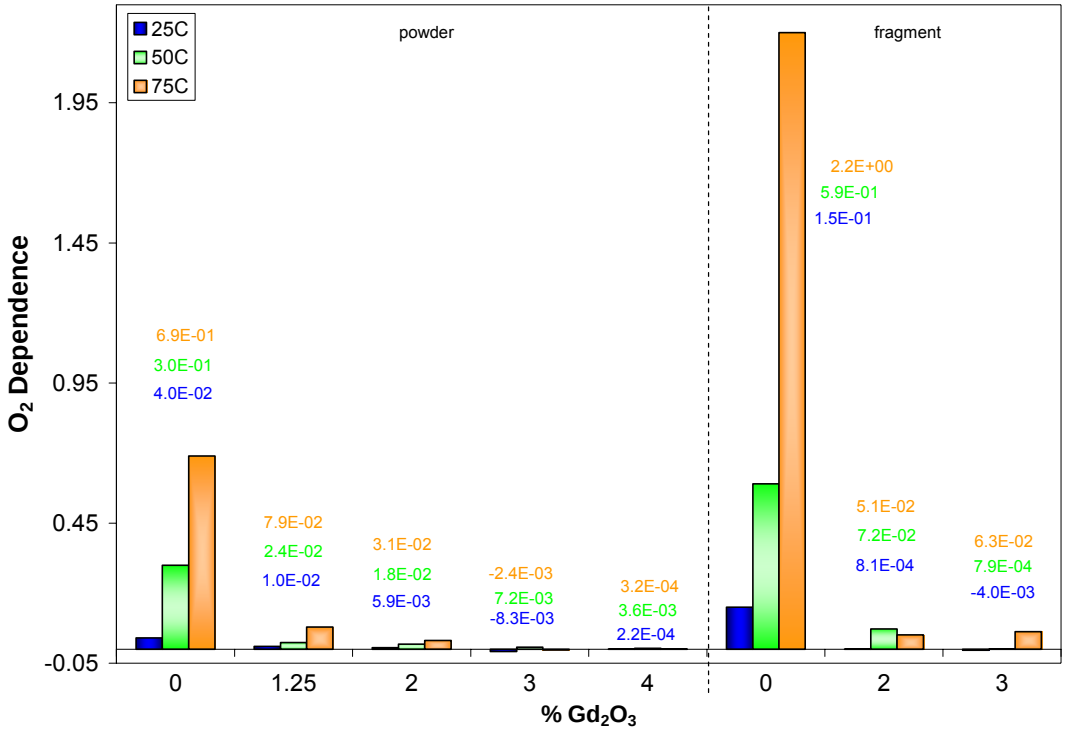

Figure 16.6. O_2 dependence over the range of 3.0 to 8.7 ppm of UO_2 samples with Gd_2O_3-dopant levels ranging from 0 to 4% at 25ºC, 50ºC, and 75ºC

Table 16.2. Steward and Gray's O_2 dependence for 25ºC and 75ºC for both unirradiated UO_2 and spent fuel samples[1]

Unirradiated UO_2		Spent Fuel	
25ºC	75ºC	25ºC	75ºC
0.53	0.62	0.047	0.73
0.52	0.66	0.051	0.35

In general, a rise in temperature increased the dissolution rate of UO_2. The rate was increased between 1.5 to over 10 times depending on the conditions. The increase in temperature had a larger effect on pure UO_2 than on those doped with Gd_2O_3. Oxygen dependence was observed in the pure UO_2 case and increased as the temperature rose, although in the doped cases minimal dependence was observed.

Reference

[1]Steward, S.A. and Gray, W.J., "Comparison of Uranium Dissolution Rates from Spent Fuel and Uranium Dioxide," *High Level Radioactive Waste Management 5th Annual International Conference*, pp. 2602–2608 (1994)

CHAPTER 17: YUCCA MOUNTAIN MODEL COMPARISON AND FINAL CONCLUSIONS

The current model for Yucca Mountain predicts the values that were calculated and tabulated in Chapter 8. These values are graphed with the experimental data measured in this research in Figures 17.1, 17.2, and 17.3. In Figure 17.1, it can be seen that all three models overestimate the dissolution rate at 25ºC by a minimum of a factor of 2 for the fragment samples and 3.5 for the powder samples. As the temperature was increased to 50ºC, the powder sample was similar to the CSNF model and the combined model, but it was approximately 1.5 times lower than the UO_2 model. The fragment data on the other hand displayed a broader range and was below the UO_2 model at 3.0 ppm and 8.7 ppm O_2, but either similar to or above it at 4.2 ppm and 5.9 ppm dissolved O_2. At 75ºC, the powder data was slightly lower than the spent fuel and combined models, but approximately 3.5 times lower than the UO_2 model. The fragment data was higher than the CSNF and combined models although it was approximately 1.5 times less than the UO_2 model.

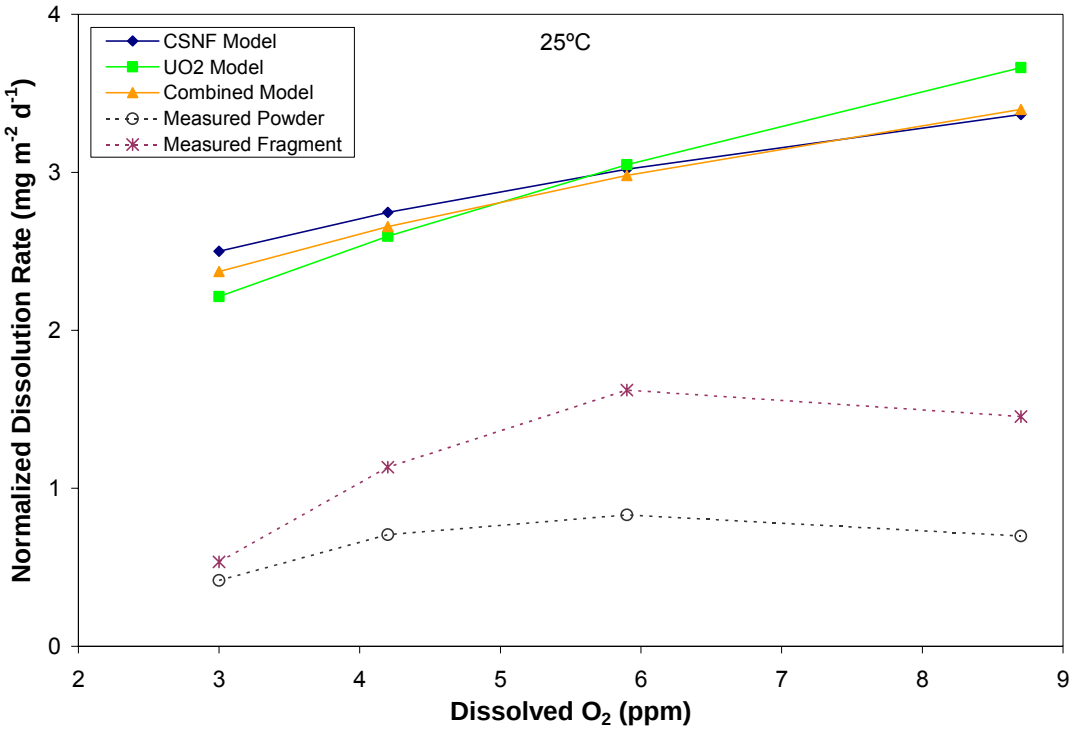

Figure 17.1. Data comparison of measured results to Yucca Mountain models at 25ºC for both powder and fragment samples of pure UO_2 over the dissolved O_2 range of 3.0 to 4.2 ppm

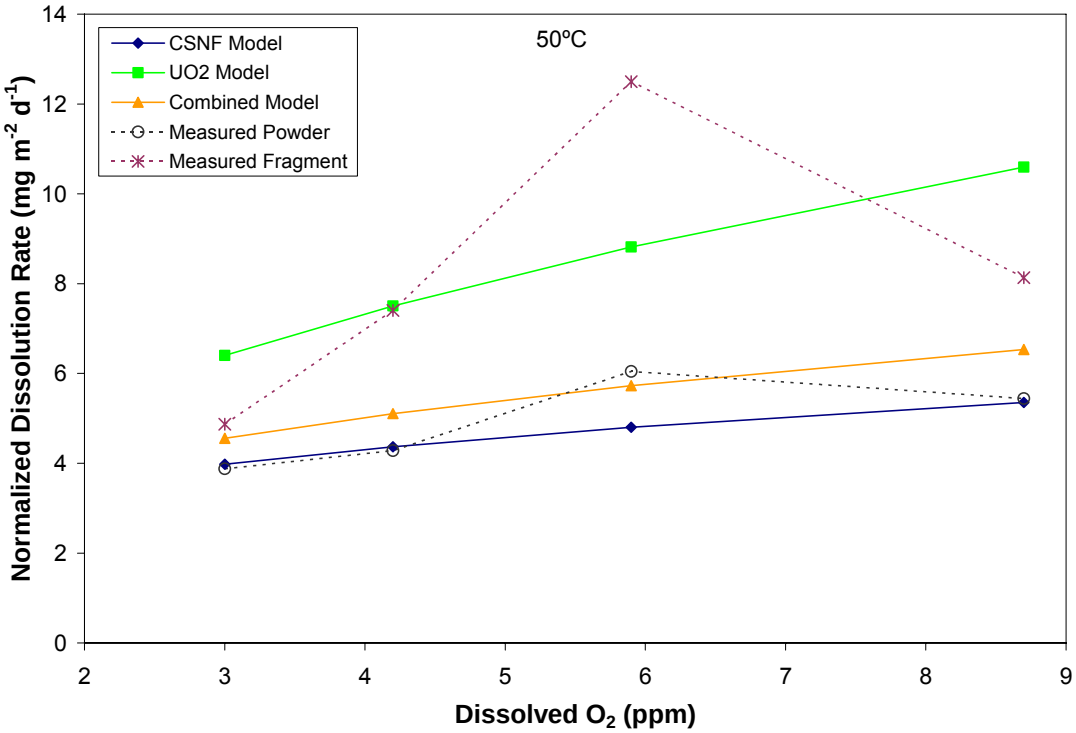

Figure 17.2. Data comparison of measured results to Yucca Mountain models at 50ºC for both powder and fragment samples of pure UO_2 over the dissolved O_2 range of 3.0 to 4.2 ppm

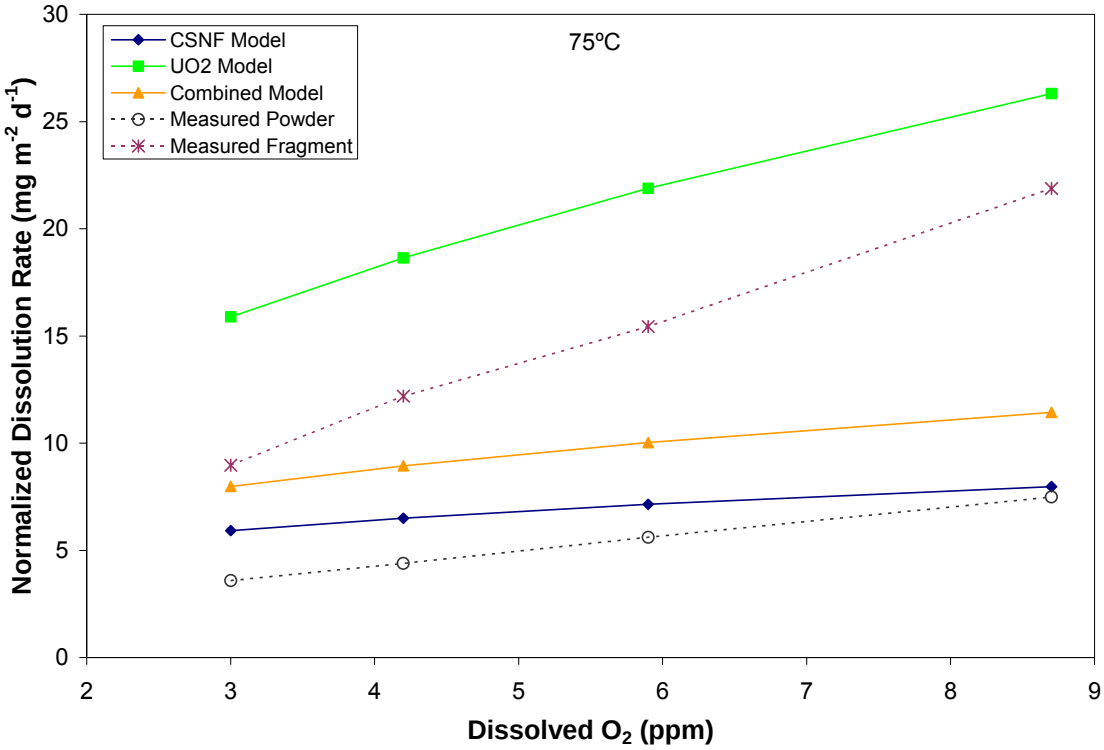

Figure 17.3. Data comparison of measured results to Yucca Mountain models at 75ºC for both powder and fragment samples of pure UO_2 over the dissolved O_2 range of 3.0 to 4.2 ppm

Based upon this research the current models for Yucca Mountain overestimate the normalized dissolution rate of UO_2 at 25ºC by at least a factor of 2, but became more accurate as the temperature was increased. The powder test results from this research tended to agree more with the CSNF model than the UO_2 model at higher temperatures and the fragment test results in most cases were lower than the UO_2 model but higher than the combined model.

Other factors examined in this research proved beneficial in decreasing the dissolution rate of fuel predicted for Yucca Mountain. The presence of Si in groundwater solutions, which may drip on the fuel in the repository, would coat the fuel at higher temperatures blocking oxidation sites, thus lowering the dissolution rate. Even though

the concentrations were approximately 3 orders of magnitude below those in J-13 well water, an effect was still observed. This proves even more valuable due to the increased dissolution rates at higher temperatures observed in Tests 2 through 5.

Another advantageous property of fuel entering Yucca Mountain is the presence of dopants which stabilize the matrix and lower the dissolution rate relative to pure UO_2. The powders containing 4 wt% Gd_2O_3-doped UO_2 reduced the normalized dissolution rate by up to a factor of approximately 15 relative to non-doped UO_2 and the fragments reduced the dissolution rate by up to a factor around 50. These effects were most pronounced at higher temperatures.

The Gd_2O_3 had an additional benefit which added a stabilization property to the fuel in which it was less sensitive to changes in either temperature or dissolved O_2 concentrations. Therefore as these parameters were increased less of an effect was observed in the dissolution rate. This is consistent with literature data that shows the dissolution rate dependence on temperature and oxygen for commercial spent fuel to be smaller than for UO_2. While it has often been assumed that these differences are due to the effects of water radiolysis for spent fuel, it appears that fuel chemistry is also an important factor.

VITA

Amanda (Kline) Casella was born on August 19th, 1980 in St. Joseph, Missouri to Ed and Linda Kline. After graduating from Mid-Buchanan R-V High School in 1998, she enrolled at the University of Missouri in Columbia (MU). Amanda majored in Chemical Engineering and performed undergraduate research on polymer resins for Dr. Sunggyu Lee. She received her B.S. in Chemical Engineering with an emphasis in waste management in December of 2002 and applied as a graduate student in Nuclear Engineering at MU. Amanda opted for the medical physics emphasis of the Nuclear Engineering department and based her Masters research on the nuclear localization of an α–MSH peptide complexed with In-111 under the supervision of Dr. Thomas Quinn. In 2004, Amanda was given the opportunity to perform a summer internship at the Paul Scherrer Institut (PSI) in Switzerland. While at PSI, Amanda developed a model to simulate metal surface precipitation and polymerization on colloids while under the guidance of Dr. Claude Degueldre. She received her Masters degree in Nuclear Engineering in 2005 and decided to pursue a PhD with an energy emphasis in Nuclear Engineering. Amanda was awarded an Office of Civilian Radioactive Waste Management fellowship to perform the research for this thesis under the supervision of Dr. William Miller and Dr. Brady Hanson. In 2006, Amanda completed her PhD classes at MU and moved to Richland, Washington to perform her thesis research at Pacific

Northwest National Laboratory (PNNL). In December of 2007, Amanda married Andy Casella and in 2008 she accepted a full time position as a member of the Radiochemical Engineering Team at PNNL.

APPENDIX

Modeling of UO_2 Radiolytic Products

Model Development

A model was developed to help understand and predict the conditions that lead to oxidative dissolution of spent fuel. The model was written in FORTRAN and incorporated ODEPACK, a differential equation solver produced by Lawrence Livermore National Laboratory. Initial conditions were taken into account in the program, such as species like dissolved O_2 and CO_2, carbonate/bicarbonate accumulated by water dripping through the rock in Yucca Mountain, and uranium. G-values for alpha, beta, and gamma radiation were used as the generation term and the initial dose given off by the fuel was a variable parameter.

Dose to the water was obtained from the model developed by Miller et al.[1], which takes into account burn-up of the fuel and self-shielding of the radiation by the fuel itself. This dose, along with the G-values, determines the initial radiolytic yields. A generalized description of how the program works is given below:

$$A + B \rightarrow C + D \qquad \text{k=x} \qquad \text{(A.1)}$$

$$A \rightarrow C + B \qquad \text{k=y} \qquad \text{(A.2)}$$

$$D \rightarrow C + A \qquad \text{k=z} \qquad \text{(A.3)}$$

where k is the rate constant and A, B, C, and D represent different species created by radiolysis. The differential equations (defined as Reaction Zones (RZ) in the program) are then set up by:

$$RZ(9.1) = x[A][B] \qquad \text{(A.4)}$$

$$RZ(9.2) = y[A] \qquad \text{(A.5)}$$

$$RZ(9.3) = x[D] \tag{A.6}$$

$$\frac{\partial[A]}{\partial t} = [A]^o - RZ(9.1) - RZ(9.2) + RZ(9.3) \tag{A.7}$$

$$\frac{\partial[B]}{\partial t} = [B]^o - RZ(9.1) + RZ(9.2) \tag{A.8}$$

$$\frac{\partial[C]}{\partial t} = [C]^o + RZ(9.1) + RZ(9.2) + RZ(9.3) \tag{A.9}$$

$$\frac{\partial[D]}{\partial t} = [D]^o + RZ(9.1) - RZ(9.3) \tag{A.10}$$

where the $[\ ]^o$ takes into account both the initial concentration and the amount produced by radiolysis. Equations A.7 through A.10 are then solved simultaneously to give the concentration of the species over time.

The initial species in the water that are modeled are: H^+, OH^-, H_2O, H_2O_2, HO_2^-, e_{aq}^-, H, OH, O^-, HO_2, O_2^-, O_2, H_2, O_3^-, O_3, and HO_3. A set of differential equations were set up based on the interaction of these species and their rate constant, which were taken from Pastina and LaVerne's work.[2] This resulted in a set of 16 differential equations to be solved simultaneously. Initial tests were run with identical parameters as Pastina and LaVerne to verify the model, which produced similar results.

For the scenario where groundwater has seeped through the rock and dripped into the cask additional carbonate interactions must be taken into account. Using a set of reactions published by Cai, et. al.[3], reactions involving CO_3^{2-}, HCO_3^-, CO_2, CO_2^-, CO_3^-, $C_2O_6^{2-}$, $HCOO^-$, $C_2O_4^{2-}$, $C_2O_4^-$, and $C_2O_4^{3-}$ were added to the model. The carbonate reactions introduced 28 new reactions into the model with 10 new species, resulting in 10 additional differential equations.

In order to add UO_2 into the model an adaptation had to be made. The model dealt only with aqueous species and UO_2 is a solid. One way to overcome this was discussed by Christensen and Sunder[4] in their model which incorporated UO_2. They assumed that the monolayer on the UO_2 surface was dissolved in a water layer of approximately 25 μm thickness. They then use a diffusion term to replenish the UO_2 as in the real circumstance where new reaction sites would become available as the UO_2 dissolved. The model developed here utilizes the same basis and incorporates 21 of these reactions given in Christensen and Sunder's publication.[4] This incorporated UO_2, UO_3H (which represents the oxidized form of UO_2, $UO_{2.33}$), UO_3, UO_3^-, UO_2D (the replenishing term), and UO_3D (a diffusion term) in the model, thus adding 5 additional differential equations. The reactions not accounted for in this model are reactions of uranium with carbonate and any uranium dissolution reactions. The rate constants of these reactions have not been definitively determined and therefore could not be incorporated.

Applications of the Model

The model takes into account water chemistry reactions surrounding the fuel and generation terms due to G-values which are a result of 15 μm diameter fuel grains. Three of the variables that can be adjusted are: the radiation level, bicarbonate in the solution, and the initial equilibrium of dissolved O_2 as predicted in Chapter 4. For the first set of graphs (Figures A.1-A.4) comparisons use either spent fuel that has been out of the reactor for 23 years, which is the age of much of the spent fuel that has been available for testing, or unirradiated UO_2. However, these graphs do not take into account any reactions of the radiolytic species with the UO_2. Two scenarios have been considered:

water that has filtered through the rock containing bicarbonate dripping onto the fuel and humid air condensing onto the fuel which has no bicarbonate. The third variable will look at the influence that an oxidizing environment has on the concentration of the key oxidants, since Yucca Mountain is expected to have an oxidizing environment while other repositories such as those in Europe are expected to be reducing.

Figure A.1 looks at the effect of an oxidizing environment. As applicable, the solution is considered to be in equilibrium with air containing 21% O_2, which results in a dissolved O_2 concentration of 8.7 ppm at 25ºC (as described in Chapter 4). For reducing conditions, the air is assumed to be O_2 deficient with no initial dissolved O_2 in solution. Figure A.1 shows the calculated concentration of the main oxidizers of UO_2, which are H_2O_2, OH, and O_2^- as a function of time. The conditions used for the calculations simulate the simplified scenario with no initial bicarbonate involved. Peroxide shows a 2 order of magnitude increase, when initial dissolved O_2 is present, at times greater than 10^3 seconds, and O_2^- shows a less significant change, but still has a notable increase. OH concentration decreases, but as this oxidizer has concentrations approximately 4 orders of magnitude less than H_2O_2 the effect would be much smaller.

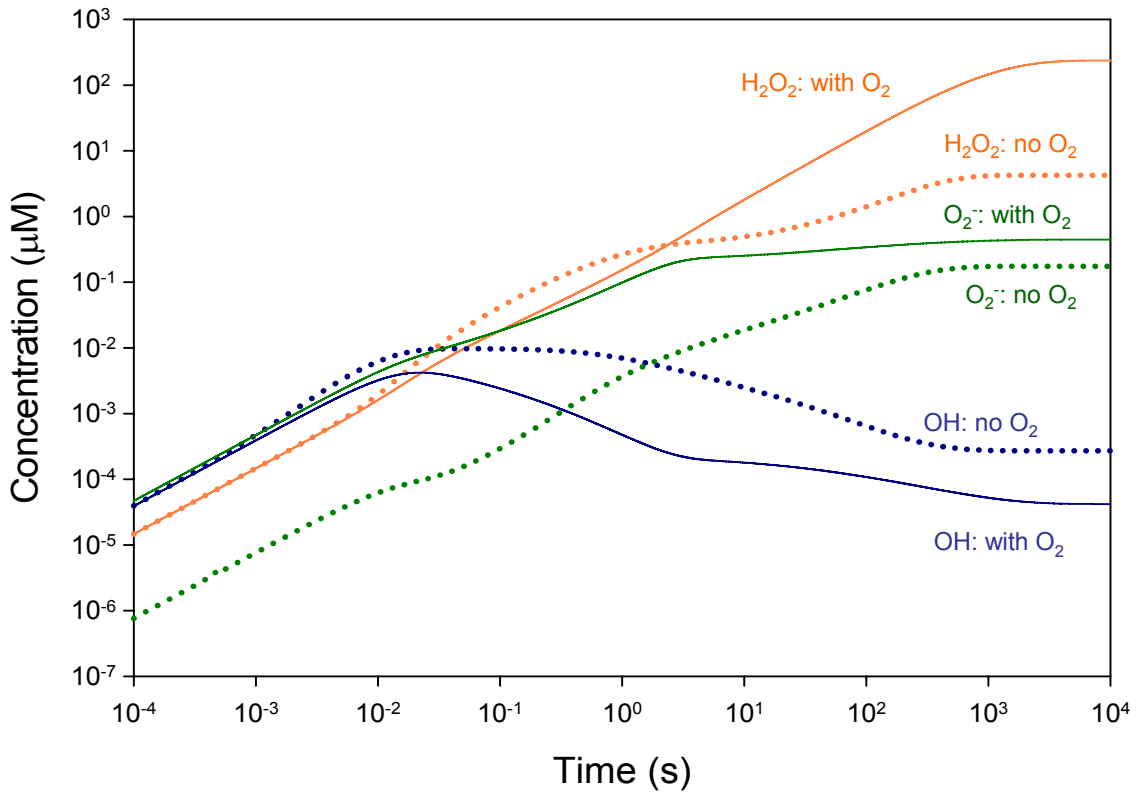

Figure A.1. Effect of an oxidizing environment: Radiation field produced by 23 year old spent fuel and when applicable in equilibrium with air containing 21% O_2

Figure A.2 has all of the same conditions as Figure A.1 except that there is an initial bicarbonate concentration of 2×10^{-3} M. The carbonate masks the effect of the oxygenated environment, but after 10^3 seconds there is an increase in the H_2O_2 and O_2^- concentrations such that their concentration is now greater than the scenario with no carbonate. This jump is most likely due to the carbonate species moving towards equilibrium. If the initial bicarbonate concentration is increased, this jump shifts to the right, and when looking at the full plot of all species there is a corresponding drop in some of the carbonate species, which appears to level off at the same time as the H_2O_2 and O_2^-. There was essentially no difference in oxidizer concentrations specified between

the cases with and without initial dissolved O_2. Although it should be noted that O_2 is itself an oxidizer and this would have a significant effect on UO_2 oxidation.

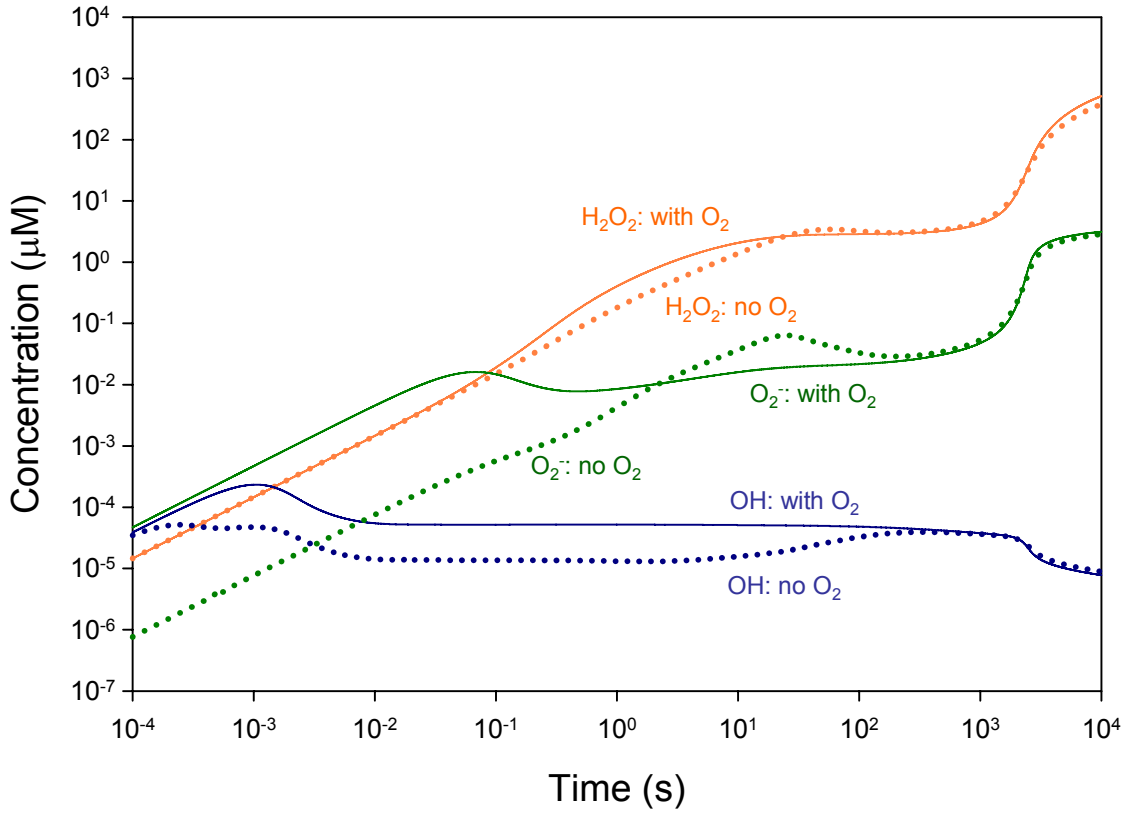

Figure A.2. Effect of an oxidizing environment: Radiation field produced by 23 year old spent fuel, an initial HCO_3^- concentration of 2×10^{-3} M, and when applicable in equilibrium with air containing 21% O_2

Figure A.3 looks at the effect radiation has on UO_2 oxidizers. The concentration of the main UO_2 oxidizers in 23 year old spent fuel and unirradiated UO_2 in an oxidizing environment are compared without bicarbonate in solution. It can be clearly seen that radiation dose has a large effect on the concentration of the oxidizers in solution. Peroxide shows approximately a 4 order of magnitude increase and O_2^- and OH show approximately a 2 order of magnitude increase. Therefore, it is expected that with the

increase in oxidizers spent fuel should dissolve faster when the radiolytic field is stronger than at extended time periods when the radiation has decayed.

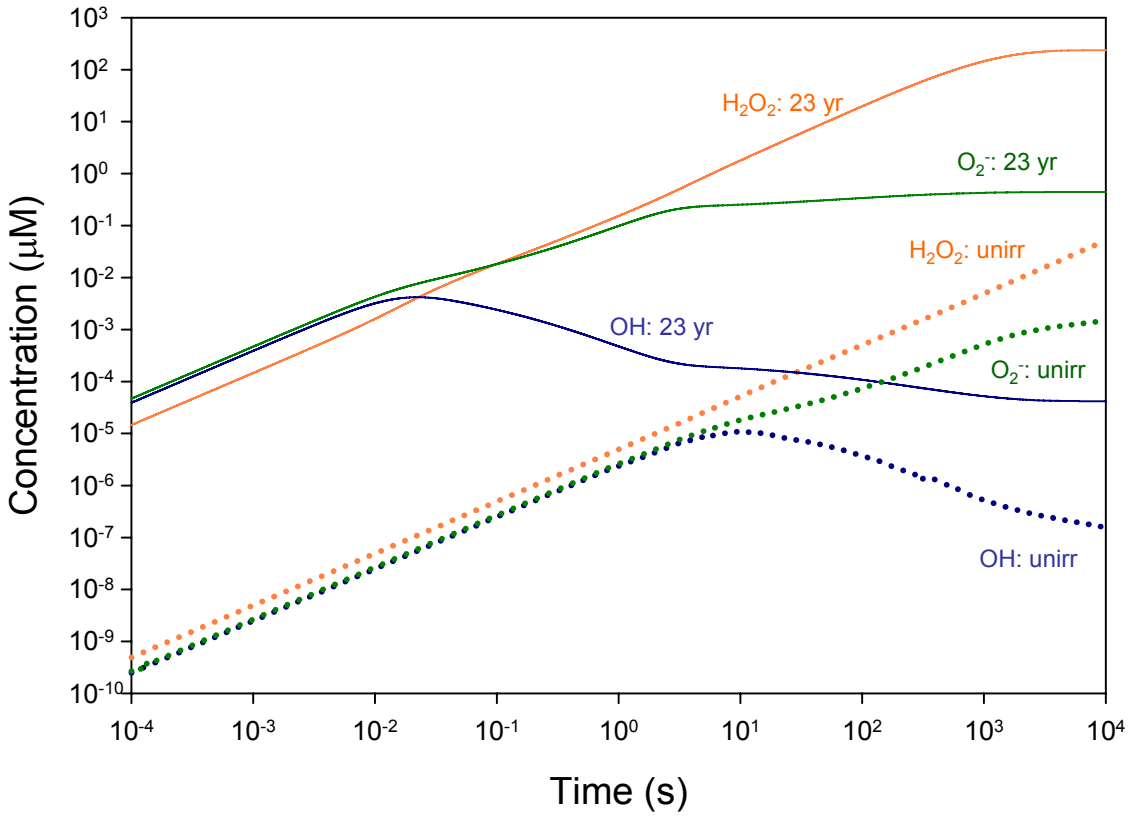

Figure A.3. Effect of Radiation: Radiation field produced by either 23 year old spent fuel or unirradiated UO_2 and with the solution in equilibrium with air containing 21% O_2

Figure A.4 is for the same conditions as Figure A.3 except that there is 2×10^{-3} M bicarbonate added to the solution. As before the jump of oxidants, at approximately 10^{-2} seconds for the spent fuel and 10^{1} second for unirradiated fuel, may be a result of the excess bicarbonate in solution being consumed. Also as previously shown, there is at least a 2 order of magnitude increase for each oxidizer for the fresh fuel case compared to the unirradiated UO_2 case. This shows that for either scenario, when doing dissolution tests, fresh spent fuel may be a poor substitute for accurate dissolution rates expected

over geologic times by providing overly conservative rates that are much greater due to these radiolytic effects.

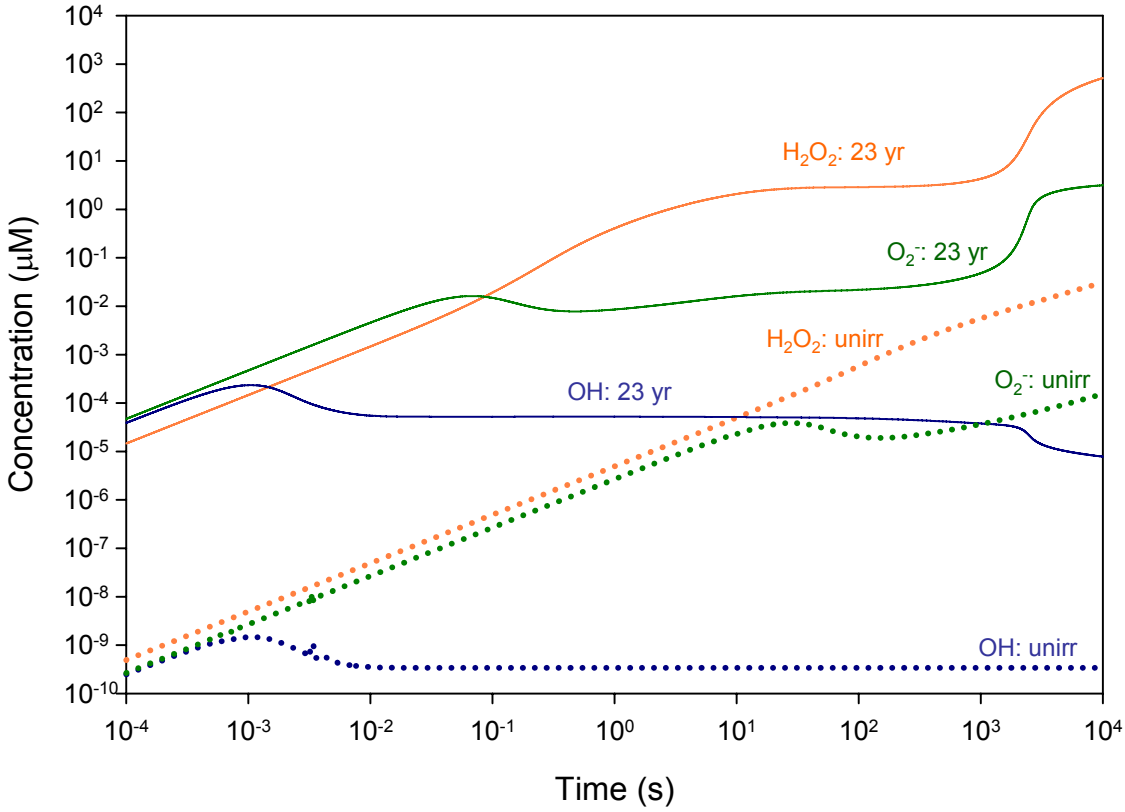

Figure A.4. Effect of Radiation: Radiation field produced by either 23 year old spent fuel or unirradiated UO_2, an initial HCO_3^- concentration of 2×10^{-3} M, and with the solution in equilibrium with air containing 21% O_2

In Figure A.5 the oxidation of UO_2 and its corresponding uranium reactions have been added. All scenarios: radiation field, bicarbonate, and an oxidizing environment are shown. It can be seen that the radiation field still plays the largest role in the amount of oxidation taking place. The level of carbonate does not appear to affect the amount of oxidation occurring, but as the model does not include U reactions with carbonate this may be misleading. At the high radiation level an oxygenated environment also seems to be insignificant, which can greatly alter the expectation of a repository with a reducing

environment at least in short term scenarios. This is a result of the high level of radiolytic products masking the influence of the dissolved O_2. At an unirradiated UO_2 radiation level there was approximately two orders of magnitude more UO_2 oxidization in an oxidizing environment than in an anoxic environment. This trend showed that an oxidizing environment may play a larger role when spent fuel has decayed to unirradiated UO_2 dose levels.

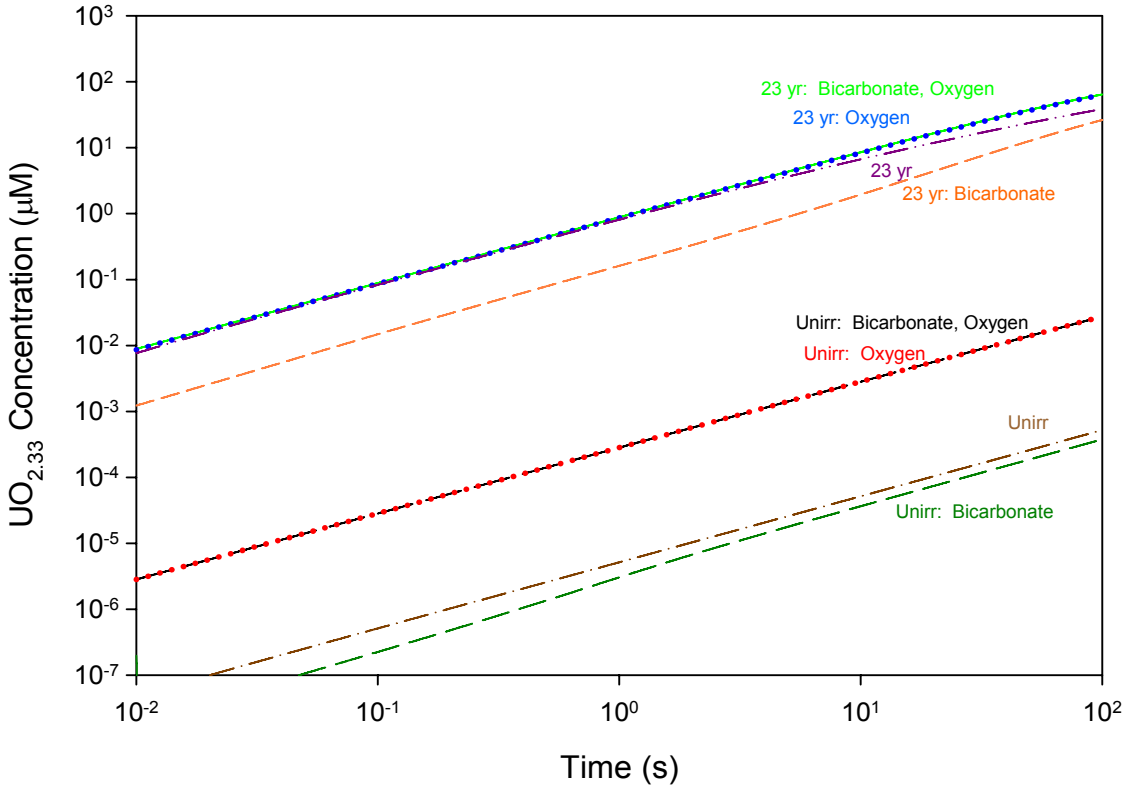

Figure A.5. UO_2 Oxidation: Radiation field produced by either 23 year old spent fuel or unirradiated UO_2, and when applicable an initial HCO_3^- concentration of 2×10^{-3} M and with the solution in equilibrium with air containing 21% O_2

Currently the model only applies to the oxidation of UO_2 and not the dissolution. Further work that would enhance this model, when available, is the addition of the uranium-carbonate reactions and the uranium dissolution. Other groundwater

constituents such as calcium and silicate may inhibit the dissolution and those reactions could also be incorporated. The model is based upon batch conditions and advancing the work for a flow system would also prove beneficial. With these additions a more detailed simulation of conditions in Yucca Mountain would be obtained.

References

[1]Miller, W.H., Kline, A.J., Hanson, B.D., "Dosimetry Modeling for Predicting Radiolytic Production at the Spent Fuel - Water Interface," *Proceedings of the 11th International High-Level Radioactive Waste Management Conference (IHLWM),* Las Vegas, NV, American Nuclear Society (2006)

[2]Pastina, B., LaVerne, J., "Effect of Molecular Hydrogen on Hydrogen Peroxide in Water Radiolysis," *Journal of Physical Chemistry A*, **105**, 9316-9322 (2001)

[3]Cai, Z., Li, X., Katsumura, Y., Urabe, O., "Radiolysis of Bicarbonate and Carbonate Aqueous Solutions: Product Analysis and Simulation of Radiolytic Processes," *Nuclear Technology*, **136**, 231-240 (2001)

[4]Christensen, H., Sunder, S., "Current State of Knowledge of Water Radiolysis Effects on Spent Nuclear Fuel Corrosion," *Nuclear Technology*, **131**, 102-123 (2000)

Equilibrium and Rate Constants from References 2-4

Equilibria 10^(-pKa)

```
RKeq(2) = 10.d0**(-13.999d0)   ! H2O  <--> H+  +  OH-
RKeq(3) = 10.d0**(-11.65d0)    ! H2O2 <--> H+  +  HO2-
RKeq(4) = 10.d0**(-11.9d0)     ! OH   <--> H+  +  O-
RKeq(5) = 10.d0**(- 4.57d0)    ! HO2  <--> H+  +  O2-
RKeq(6) = 10.d0**(- 9.77d0)    ! H    <--> H+  +  e-
```

Rate coefficients (M-1 s-1 or s-1)

```
rk( 7) =   1.4d11                        ! H+   + OH-        --> H2O
rk( 8) =   rk( 7)*RKeq(2)/H2O            ! H2O               --> H+   +  OH-
rk(10) =   5.0d10                        ! H2O2              --> H+   +  HO2-
rk( 9) =   rk(10)*RKeq(3)                ! H+   + HO2-       --> H2O2
rk(11) =   1.3d10                        ! H2O2 + OH-        --> HO2- +  H2O
rk(12) =   rk(11)*RKeq(2)/(RKeq(3)*H2O)  ! HO2- + H2O        --> H2O2 +  OH-
rk(13) =   1.9d1 * H2Oact                ! e-   + H2O        --> H    +  OH-
rk(14) =   2.2d7                         ! H    + OH-        --> e-   +  H2O
rk(16) =   2.3d10                        ! H                 --> e-   +  H+
rk(15) =   rk(16)*RKeq(6)                ! e-   + H+         --> H
rk(17) =   1.3d10                        ! OH   + OH-        --> O-   +  H2O
rk(18) =   rk(17)*RKeq(2)/(RKeq(4)*H2O)  ! O-   + H2O        --> OH   +  OH-
rk(20) =   1.0d11                        ! OH                --> O-   +  H+
rk(19) =   rk(20)*RKeq(4)                ! O-   + H+         --> OH
rk(22) =   5.0d10                        ! HO2               --> O2-  +  H+
rk(21) =   rk(22)*RKeq(5)                ! O2-  + H+         --> HO2
rk(23) =   5.0d10                        ! HO2  + OH-        --> O2-  +  H2O
rk(24) =   rk(23)*RKeq(2)/(RKeq(5)*H2O)  ! O2-  + H2O        --> HO2  +  OH-
rk(25) =   3.0d10                        ! e-   + OH         --> OH-
rk(26) =   1.1d10                        ! e-   + H2O2       --> OH   +  OH-
rk(27) =   1.3d10/H2O                    ! e-   + O2-  +  H2O --> HO2- +  OH-
rk(28) =   2.0d10                        ! e-   + HO2        --> HO2-
rk(29) =   1.9d10                        ! e-   + O2         --> O2-
rk(30) =   5.5d9*H2Oact/H2O              ! e-   + e-   + 2H2O --> H2   + 2OH-
rk(31) =   2.5d10/H2O                    ! e-   + H    +  H2O --> H2   +  OH-
rk(32) =   3.5d9                         ! e-   + HO2-       --> O-   +  OH-
rk(33) =   2.2d10/H2O                    ! e-   + O-   +  H2O --> OH-  +  OH-
rk(34) =   1.6d10/H2O                    ! e-   + O3-  +  H2O --> O2   +  OH-   + OH-
rk(35) =   3.6d10                        ! e-   + O3         --> O3-
rk(36) =   1.1d1   * H2Oact              ! H    + H2O        --> H2   +  OH
rk(37) =   1.0d10                        ! H    + O-         --> OH-
rk(38) =   9.0d7                         ! H    + HO2-       --> OH   +  OH-
rk(39) =   1.0d10                        ! H    + O3-        --> OH-  +  O2
rk(40) =   7.8d9                         ! H    + H          --> H2
```

```
rk(41) =   7.0d9                          ! H   + OH        --> H2O
rk(42) =   9.0d7                          ! H   + H2O2      --> OH  + H2O
rk(43) =   2.1d10                         ! H   + O2        --> HO2
rk(44) =   1.8d10                         ! H   + HO2       --> H2O2
rk(45) =   1.8d10                         ! H   + O2-       --> HO2-
rk(46) =   3.8d10                         ! H   + O3        --> HO3
rk(47) =   3.6d9                          ! OH  + OH        --> H2O2
rk(48) =   6.0d9                          ! OH  + HO2       --> H2O + O2
rk(49) =   8.2d9                          ! OH  + O2-       --> OH- + O2
rk(50) =   4.3d7                          ! OH  + H2        --> H   + H2O
rk(51) =   2.7d7                          ! OH  + H2O2      --> HO2 + H2O
rk(52) =   2.5d10                         ! OH  + O-        --> HO2-
rk(53) =   7.5d9                          ! OH  + HO2-      --> HO2 + OH-
rk(54) =   2.6d9                          ! OH  + O3-       --> O3  + OH-
rk(55) =   6.0d9                          ! OH  + O3-       --> O2- + O2- + H+
rk(56) =   1.1d8                          ! OH  + O3        --> HO2 + O2
rk(57) =   8.0d7                          ! HO2 + O2-       --> HO2- + O2
rk(58) =   7.0d5                          ! HO2 + HO2       --> H2O2 + O2
rk(59) =   6.0d9                          ! HO2 + O-        --> O2  + OH-
rk(60) =   5.0d-1                         ! HO2 + H2O2      --> OH  + O2  + H2O
rk(61) =   5.0d-1                         ! HO2 + HO2-      --> OH  + O2  + OH-
rk(62) =   6.0d9                          ! HO2 + O3-       --> O2  + O2  + OH-
rk(63) =   5.0d8                          ! HO2 + O3        --> HO3 + O2
rk(64) =   1.0d2 * H2Oact/(2.0 * H2O)     ! O2- + O2- + 2H2O --> H2O2 +O2 + 2OH-
rk(65) =   6.0d8/H2O                      ! O2- + O-  + H2O --> O2  + 2OH-
rk(66) =   1.3d-1                         ! O2- + H2O2      --> OH  + O2  + OH-
rk(67) =   1.3d-1                         ! O2- + HO2-      --> O-  + O2  + OH-
rk(68) =   1.0d4/H2O                      ! O2- + O3- + H2O --> O2  + O2  + 2OH-
rk(69) =   1.5d9                          ! O2- + O3        --> O3- + O2
rk(70) =   1.0d9/H2O                      ! O-  + O-  + H2O --> HO2- + OH-
rk(71) =   3.6d9                          ! O-  + O2        --> O3-
rk(72) =   8.0d7                          ! O-  + H2        --> H   + OH-
rk(73) =   5.0d8                          ! O-  + H2O2      --> O2- + H2O
rk(74) =   4.0d8                          ! O-  + HO2-      --> O2- + OH-
rk(75) =   7.0d8                          ! O-  + O3-       --> O2- + O2-
rk(76) =   5.0d9                          ! O-  + O3        --> O2- + O2
rk(77) =   3.3d3                          ! O3-             --> O2  + O-
rk(78) =   9.0d10                         ! O3- + H+        --> O2  + OH
rk(79) =   1.1d5                          ! HO3             --> O2  + OH
rk(80) =   4.0d8                          ! UO2 + OH        --> UO3H
rk(81) =   2.0d-1                         ! UO2 + H2O2      --> U3OH + OH
rk(82) =   2.0d8                          ! UO2 + HO2       --> UO3H + H2O2 - H2O
rk(83) =   2.0d8                          ! UO2 + O2-       --> UO3H + HO2- - H2O
rk(84) =   1.0d-1                         ! UO3H + UO3H     --> UO3 + UO2 + H2O
rk(85) =   8.0d8                          ! UO3H + OH       --> UO3 + H2O
rk(86) =   5.0d8                          ! UO3H + e-       --> UO2 + OH-
```

```
rk(87) =   2.0d-1                  ! UO3H + H2O2      --> UO3  +  H2O   + OH
rk(88) =   4.0d8                   ! UO3H + O2-       --> UO3  +  HO2-
rk(89) =   4.0d8                   ! UO3H + HO2       --> UO3  +  H2O2
rk(90) =   5.0d8                   ! UO3  + e-        -->UO3H +  OH-   - H2O
rk(91) =   4.0d7                   ! UO3  + O2-       --> UO3- +  O2
rk(92) =   1.0d1                   ! UO3- + H2O       --> UO3H +  OH-
rk(93) =   4.5d6                   ! UO3H + H         --> UO2  +  H2O
rk(94) =   4.5d6                   ! UO3  + H         --> UO3H
rk(95) =   4.0d7                   ! UO3  + HO2       --> UO3H +  O2
rk(96) =   7.0d-4                  ! UO2              --> UO2D
rk(97) =   3.5d-7                  ! UO2D             --> UO2
rk(98) =   4.0d-4                  ! UO3              --> UO3D
rk(99) =   1.0d-3                  ! UO2  + O2        --> UO3H + HO2  -H2O
rk(100) =  1.0d-3                  ! UO3H + O2        --> UO3  + HO2
rk(101) =  5.0d10                  ! H+   + CO3,2-    --> HCO3-
rk(102) =  2.0d4                   ! CO2  + H2O       --> H+   + HCO3-
rk(103) =  5.0d10                  ! H+   + HCO3-     --> CO2  + H2O
rk(104) =  2.0d0                   ! HCO3-            --> H+   + CO3,2-
rk(105) =  7.7d9                   ! CO2  + e-        --> CO2-
rk(106) =  8.5d6                   ! HCO3-  + OH      --> CO3- + H2O
rk(107) =  3.9d8                   ! CO3,2- + OH      --> CO3- + OH-
rk(108) =  4.4d4                   ! HCO3-  + H       --> H2   + CO3-
rk(109) =  3.9d5                   ! CO3,2- + e-      --> CO2- + 2OH- - H2O
rk(110) =  1.4d7                   ! CO3-   + CO3-    --> C2O6,2-
rk(111) =  9.8d5                   ! CO3-   + H2O2    --> CO3,2- + O2- + 2H+
rk(112) =  1.0d7                   ! CO3-   + HO2-    --> CO3,2- + O2- +  H+
rk(113) =  4.0d8                   ! CO3-   + O2-     --> CO3,2- + O2
rk(114) =  3.0d8                   ! CO3-   + CO2-    --> CO3,2- + CO2
rk(115) =  1.0d9                   ! CO2-   + e-      --> HCOO-  + OH- - H2O
rk(116) =  6.5d8                   ! CO2-   + CO2-    --> C2O4,2-
rk(117) =  2.0d9                   ! CO2-   + O2      --> CO2    + O2-
rk(118) =  7.3d5                   ! CO2-   + H2O2    --> CO2    + OH- + OH
rk(119) =  1.0d3                   ! CO2-   + HCO3-   --> HCOO-  + CO3-
rk(120) =  1.0d0                   ! C2O6,2-     --> C2O4,2- + O2
rk(121) =  2.0d2                   ! C2O6,2-     --> HO2-   + 2CO2 - H2O
rk(122) =  3.0d3                   ! CO3-   + C2O4,2-  --> C2O4-  + CO3,2-
rk(123) =  3.1d7                   ! C2O4,2- + e-     --> C2O4,3-
rk(124) =  7.7d6                   ! C2O4,2- + OH     --> C2O4-  + OH-
rk(125) =  1.5d5                   ! CO3-   + HCOO-   --> HCO3-  + CO2-
rk(126) =  3.2d9                   ! HCOO-  + OH      --> H2O    + CO2-
rk(127) =  2.1d8                   ! HCOO-  + H       --> H2     + CO2-
rk(128) =  8.0d3                   ! HCOO-  + e- + H+  --> H2     + CO2-
rk(129) =  4.0d8                   ! UO2    + CO3-    --> UO3H   + HCO3-  -H2O
rk(130) =  8.0d8                   ! UO3H   + CO3-    --> UO3    + HCO3-
rk(131) =  (6.5d5)*dexp((-8.5398d3)/temp)  !  H2O2--> OH    + OH  thermal decomp
```